University of Southampton
Faculty of Engineering, Science & Mathematics
School of Engineering Sciences

A New Solar Energetic Particle Event Modelling Methodology Incorporating System Memory

by

Piers Jiggens

Thesis for the degree of Doctor of Philosophy

April 2010

UNIVERSITY OF SOUTHAMPTON

ABSTRACT

FACULTY OF ENGINEERING, SCIENCE & MATHEMATICS
SCHOOL OF ENGINEERING SCIENCES

Doctor of Philosophy

A NEW SOLAR ENERGETIC PARTICLE EVENT MODELLING METHODOLOGY INCORPORATING SYSTEM MEMORY

by Piers Thomas Arthur Jiggens

This PhD thesis begins with an investigation into the state of the art of Solar Energetic Particle Event (SEPE) modelling. This is followed by an update of this modelling through introduction of new time distributions, an incorporation of system memory (required due to the finding of an inter-dependence of SEPEs) and the development of a new modelling methodology based on virtual timelines which is different from the methodologies of previous models.

Solar Energetic Particles (SEPs) can result in effects on spacecraft including displacement damage and single event effects. As such, modelling the SEP environment to be able to derive the likely extent of these effects is important for efficient design of future spacecraft. The SARG (Southampton Astronautic Research Group) modelling methodology can be applied to data for predicting the worst-case peak flux, worst-case event fluence and cumulative mission fluences for various time periods at different confidence level across a range of energies from 5 - 200 MeV.

This thesis includes data processing tools for 'cleaning' SEP flux data prior to the extraction of SEPEs from the time series. There is a review of the time distributions applied to SEPEs and Poissonian assumptions of existing models with the finding that the SEPE environment appears to be less constant in time with more variation with a greater level of 'memory' in the process indicating that the events are less random than was previously thought. The new modelling methodology incorporates SEPE durations to create realistic timelines for modelling the environment. Finally, there is a comparison of results using the SARG methodology and other well-known methods for producing solar proton models at 1 AU namely the JPL and ESP methods. Also included are some concluding remarks and ideas for extension of this work.

Contents

List of Figures

List of Tables

Acknowledgements

When you're working on a PhD in an engineering faculty you're going to need some help; much of it psychological but some of it emotional, a significant amount of it technical and a decent chunk of it financial. Of course, the most useful people on this last point were Rosemary and Martin (my mum and dad) by offering free rent and food whenever I needed it. However, their generosity didn't end there and they have always been massively supportive and taken an interest even when they had no idea what it was all about beyond "He does something to do with space and the Sun". I'm sure they'll dine out on: "My son's a doctor but I wouldn't trust him with a scalpel!" for the rest of time just as they have with: "It's not rocket science and he'd know!" (followed by some pointing) over the past 8 years. I'd like to thank my brother Giles and his lovely wife Kathryn for all their love and support, the light relief including their wedding which was one of my happiest days (even if it did ruin my Canadian holiday plans) and their (possibly misplaced) confidence that I'm going to be very rich and successful after all this.

I'd like to thank my housemates (especially Christine and Michelle) and all the friends I met through them who accepted me just like a young person while I was doing my PhD for all the tea, the chats, the parties, the memories, the missing memories and for not quite derailing the whole show but providing me with plenty of diversions. Also, I want to thank Rosanna and Max (my final year housemates) for the wine and chat and mental support at the toughest of times.

I must thank my longest-standing friends Rennike, Ed, Mo, James, Max, Dave and Chris who were always there for a beer and some banter which I never grow tired of even if nobody else would have a clue what we are on about most of the time. Additionally, I want to thank my friends who I met in Southampton during my undergraduate days especially Freya (and Tom), Jon, Miller, Asher and Sam who

give me that non-geek balance that all of us geeks can use to anchor us to reality. Big thanks to Fatmore for being the only one to stick around in Southampton from my early days there and allowing for me to sit on his couch and take some abuse when I frankly had no other friends.

I'd like to thank everyone in the office for all the tea, chat about sports and spaceships, beer festivals, help with code, tequila and empathy which were utterly essential even if it often seemed like complete madness. The fact that John, Punch Nick, Jaye, Rebecca, Sam, Stefano, Tony, Tarek, Riaz and Charlotte were dragging themselves through it as well seemed to help justify the whole debacle. I'm just sorry the printer didn't really work out, that Nick still doesn't completely understand the number zero and that John and I didn't get to go and support Northern Ireland in the Euros in 2008. Especially I have to thank Nick Lincoln (and Katie) for the absurdly cheap rent, the stiff drinks and the bike rides. I need to thank the other lot from upstairs and elsewhere in Tizard including Scotty, Dave, John, Max, Kon, Nico, Koen, Phil and the rest for the cricket and football and Hugh for some fine advice. I had few breaks in my three years but a massive thanks to everyone that I went to Glastonbury, Morocco and Edinburgh with for the help getting some R&R and 'streamlining' my mind.

I need to thank the good people at ESA's European Space Research and Technology Centre (ESTEC) for part-sponsoring my work. I'd also like to thank all my colleagues on the ESA Solar Energetic Particle Environment Modelling (SEPEM) Project for the meetings and dinners and especially Daniel Heynderickx for all the interesting discussions we've had about related work. I need to thank Mike Xapsos for passing me his full list of particle events and answering my many queries regarding it. I'd like to thank Eamonn Daly and Adrian Tatnall for an interesting viva defence and for the advice on the minor adjustments for final version of this thesis. Finally, I must thank my supervisor Steve Gabriel mainly because I'll be in trouble if I don't but also for all the opportunities, helping me to produce a fine journal article and all the money for trips to Brussels and around the World!

Declaration of Authorship

I, Piers Thomas Arthur Jiggens, declare that the thesis entitled "A New Solar Energetic Particle Event Modelling Methodology Incorporating System Memory" and the work presented in the thesis are both my own, and have been generated by me as the result of my own original research.

I confirm that:

- This work was done wholly or mainly while in candidature for a research degree at this University;
- Where any part of this thesis has previously been submitted for a degree or any other qualification at this University or any other institution, this has been clearly stated;
- Where I have consulted the published work of others, this is always clearly attributed;
- Where I have quoted from the work of others, the source is always given. With the exception of such quotations, this thesis is entirely my own work;
- I have acknowledged all main sources of help;
- Where the thesis is based on work done by myself jointly with others, I have made clear exactly what was done by others and what I have contributed myself;
- Parts of this work have been published as:

  Jiggens, P. T. A. and S. B. Gabriel (2009). Time distributions of solar energetic particle events: Are SEPEs really random? *Journal of Geophysical Research 114(A10)*, A10105

Nomenclature

Acronyms

cdf - cumulative density function (or distribution function)

CME - Coronal Mass Ejection

CRÈME - Cosmic Ray Effects on MicroElectronics

ECSS - European Cooperation on Space Standardization

ESA - European Space Agency

ESP - Emission of Solar Protons

EVA - Extra-Vehicular Activity

GLE - Ground Level Enhancement

GCR - Galactic Cosmic Ray

ICME - Interplanetary CME

IDS - Integrated Data Set (from PSYCHIC model)

IMF - Interplanetary Magnetic Field

IP - Interplanetary

JPL - Jet Propulsion Laboratory

MATLAB - MATrix LABoratory (computing environment and programming language)

MSU - Moscow State University

NASA - National Aeronautics and Space Administration

NOAA - National Oceanic & Atmospheric Administration

pdf - probability density function

PSYCHIC - Prediction of Solar particles Yields for CHaracterising Integrated Circuits

SARG - Southampton Astronautics Research Group

SEP - Solar Energetic Particle

SEPE - Solar Energetic Particle Event

SEU - Single Event Upset

SIDC - Solar Influences Data Analysis Center

SPE - Solar Proton Event

SOLPRO - computer code for King Model of SOLar PROtons

SWPC - Space Weather Prediction Center

SXR - Soft X-rays

UH - Ultra-Heavy (particles)

Other Important Terms

Coronal Hole - Solar surface region of low density with an open magnetic field structure

Ejecta - Mass of material ejected from the Sun

Fluence - The flux integrated over time

Flux - The number of particles arriving at a cross-section every second

Heliosphere - Covers the solar system, solar wind, and the entire solar magnetic field

Solar Flare - An intense variation in brightness on the surface of the Sun
(X-class are large, M-class and medium-sized, C-class are small)

Solar Wind - Ionized atoms from the Sun permeating across the IP medium

Units and constants

AU - Astronomical unit (the mean distance between the Earth and the Sun)

c - The speed of light ($\approx 3 \times 10^8 \mathrm{ms}^{-1}$)

eV - electron-Volt (keV = $\times 10^3$; MeV = $\times 10^6$; GeV = $\times 10^9$)

nuc. - nucleon (either a proton or a neutron)

pfu - particle flux unit (particles $\mathrm{cm}^{-2}\mathrm{sr}^{-1}\mathrm{s}^{-1}$)

sr - steradian (the SI unit of solid angle)

W - yearly sunspot number

Z - atomic number (number of protons found in the nucleus of an atom)

Spacecraft and Instruments/Experiments

ACE - Advanced Composition Explorer

- ULEIS - Ultra Low Energy Isotope Spectrometer
- EPAM - Electron, Proton, and Alpha Monitor
- SIS - Solar Isotope Spectrometer

GOES - Geostationary Operational Environmental Satellite

- MEPAD - Medium Energy Proton and Alpha Detector
- SEM - Space Environment Monitor

IMP - Interplanetary Monitoring Platform

- CPME - Charged Particle Measurement Experiment
- CRNE - Cosmic Ray Nuclei Experiment
- CRT - Cosmic Ray Telescope
- GME - Goddard Medium Energy experiment
- LED - Low Energy Detector
- MED - High Energy Detector

OGO - Orbiting Geophysical Observatory

SAMPEX - Solar Anomalous and Magnetospheric Particle Explorer

- PET - Proton/Electron Telescope

SOHO - Solar and Heliospheric Observatory

- ERNE - Energetic and Relativistic Nuclei and Electron experiment

STEREO - Solar TErrestrial RElations Observatory

Wind

- LEMT - Low Energy Matrix Telescope

Chapter 1

Introduction

Solar Energetic Particles (SEPs) are high energy particles originating from the Sun. They arrive in bursts known as SEPEs (Solar Energetic Particle Events). Effects on spacecraft due to SEPEs include ionisation, displacement damage, sensor background noise, and single event effects. They can also pose a serious hazard to humans especially those on interplanetary space missions in the future (Feynman and Gabriel, 2000). Cases of SEPEs having noticeable negative effects on spacecraft include the 'Halloween Events' during October and November 2003 (Dyer et al., 2004).

To aid spacecraft designers in mitigating against the effects of SEPEs it is necessary to have accurate long-term models (from months to years) for the prediction of the SEP environment. This work investigates several aspects of modelling this environment at 1 AU (Astronomical Unit - the distance from the Earth to the Sun) in doing so questioning previous assumptions and including new aspects to modelling with consideration of factors such as system memory and the non-point-like nature of SEPEs. By considering the inter-dependence of SEPEs and their non-point-like nature a new dimension to SEPE modelling is presented.

There are several models of the solar particle environment for spacecraft at 1 AU most of which focus upon the cumulative mission fluence (the flux integrated over the total time of the mission) of protons. These models are based on data from various instruments, available at different energies and employ a variety of approaches to attain predictions. The most important models are the King model (King, 1974), the JPL model (Feynman et al., 1990, 1993, 2002), the MSU model (Nymmik, 1999), the ESP model (Xapsos et al., 2000) and the PSYCHIC model (Xapsos et al., 2004).

A study into the effects of cross-calibrating the data input into the JPL model by Rosenqvist et al. (2005) produced a new model while the extension of the JPL method to include heavy ion species by Tylka et al. (1997) produced models for Helium(He), Carbon, Nitrogen and Oxygen (CNO), and Iron (Fe). The MSU model (Nymmik, 1999) includes an extension to heavy ions with atomic number $Z = 2 - 28$ and an extension to heavy ions have also been produced for the PSYCHIC model (Xapsos et al., 2007). Earlier ESP models covered the worst-case peak flux (Xapsos et al., 1998b) and worst-case event fluence (Xapsos et al., 1999).

This PhD thesis describes the development of a new modelling methodology for solar protons at 1 AU considering all facets of modelling the SEP environment. This provides an update to existing models with careful consideration given to past assumptions which are re-evaluated where necessary including the distributions which are fitted to the various characteristics of SEPEs.

Chapter 2 gives a review of the phenomenology of SEPEs (Section 2.1), an introduction to available data and inherent problems or caveats which appear (Section 2.2) and an appraisal of the state of the art of the statistical modelling of SEPEs (Section 2.3).

Chapter 3 covers the various data which are used in this work. First, in Section 3.1 three existing lists of SEPEs are introduced along with the data and input parameters used to form them. Next, in Sections 3.2 and 3.3 methods for processing the raw data (the flux time series for SEPEs) are introduced, this is key for confidence in the model outputs and includes de-spiking the data and filling gaps in the data. Finally, in Section 3.4 the creation of a new event list is described incorporating these processing methods and cross-calibration of data where there are long-term instrument data inaccuracies. This list includes the fluences, peak fluxes and start and end times of the SEPEs. This chapter also covers the definition used to extract relevant events from the time series across an energy spectra from $5 - 200$ MeV (using standardised differential energy bins).

Chapter 4 covers modelling techniques including both statistical distributions and modelling methodology. A methodology for combining SEPE characteristics by creating realistic virtual timelines which include the SEPE waiting times (the time between SEPEs), durations, fluences and peak fluxes for modelling the environment is intro-

duced in Section 4.2. This method consists of interspersed waiting times and events which have characteristics which are interlinked through regressions. In Section 4.3 the time distributions of the time between SEPEs (the waiting times) and the durations of SEPEs are studied. Previously all authors had used some form of Poisson distribution but it is found that a Lévy distribution provides a more accurate and robust fit to the data. Following this, in Section 4.4 the idea of system memory between event waiting times (a dependency of one waiting time on the previous waiting time) is tackled. As it is found that there is significant system memory for the waiting times of SEPEs a method is introduced to build this into the model by a numerical method linking consecutive waiting times. Next, in Section 4.5 the distribution fits to the fluences and peak fluxes of SEPEs are investigated.

Chapter 5 covers the results of the new modelling methodology applied to the new event list generated. These results include predictions of cumulative mission fluence, worst case event fluence and worst case peak flux across ten energy channels for six time periods against confidence level. Finally, spectral plots at selected, different confidence levels are created allowing the calculation of parameters over integral energy ranges (for example > 10 MeV).

Chapter 6 covers the conclusions of this work as well as work which might follow on to further improve the statistical modelling of SEPEs.

Chapter 2

Literature Review

This chapter contains an up-to-date review of the literature in relevant areas of study. This includes the particles that make up the SEP (Solar Energetic Particle) environment, sources of SEPs, existing statistical models for predicting the environment, a review of existing SEP data and caveats with that data and a review of statistical distributions and modelling methodologies which have been applied in the past.

2.1 The SEP Environment

This section contains a review of the available literature as regards the physical processes associated with producing SEPs. This includes the definition of an SEPE, particle acceleration mechanisms which produce SEPs, the propagation of particles through the interplanetary (IP) medium, ion abundance ratios, energy spectra and flux profiles. There are many factors affecting SEP flux levels (or intensities) both at a single point in time and integrated over the duration of the SEPE (known as the event fluence) and the processes involved are not fully understood.

2.1.1 Solar Energetic Particle Events

SEPs are energetic particles originating from the Sun contained in relatively short bursts called Solar Energetic Particle Events (SEPEs). The largest of these SEPEs are characterised by a large enhancement in the flux of protons of energies from a few MeV to GeV levels at 1 AU and are therefore sometimes known as solar proton events (SPEs). These events are easily detected as the flux increases from a background level

less than 1 particle $cm^{-2}sr^{-1}s^{-1}$ (or pfu - particle flux units) in the > 10 MeV energy range to tens, hundreds, thousands and even tens of thousands of pfu. Prior to arrival at the Earth particles must first propagate through the IP medium, the first protons may arrive within hours (Krucker and Lin, 2000) although some high energy particles have been measured within 15 minutes of an event being observed (Mewaldt et al., 2005).

In the literature there have been various definitions of events using different parameters to extract the events from the time series (Feynman et al., 1990; Xapsos et al., 1999; Jun et al., 2007; Xapsos et al., 2004). Definitions must consider the energy level, the flux threshold, the time after the event drops below the threshold before it is said to have ended (hereafter referred to as the lagtime), the sampling time (i.e. the time binning of the flux time series) and the minimum event characteristics (such as the lowest fluence of event considered (Feynman et al., 1993; Xapsos et al., 1999) or the lowest peak flux of event considered (Xapsos et al., 2004)).

The flux thresholds are chosen to distinguish the events from the background and are varied with the energy channel selected (the starting and ending thresholds are most commonly chosen to be the same). Combined with the lagtime these thresholds also serve to link connected events where there may be a causal link between consecutive CMEs (Coronal Mass Ejections) which are the main producers of SEPEs (Tylka et al., 1997).

The size and rise time to the peak flux of an event depend on the position of the source phenomenon on the solar surface with a tendency for those events resulting from activity on the Sun's western hemisphere to be larger and have faster rise times reflecting the connection of the magnetic field line from the Earth to a point on the Sun in this region (Lario et al., 2006). SEPEs extending to the highest energies result in Ground-Level Enhancements (GLEs) and are caused by CMEs which are usually faster and wider than those causing smaller events (Wang and Wang, 2005). However, although it is known that the CME speed and SEP intensity are correlated, for a given CME speed SEP intensity can vary over four orders of magnitude (Gopalswamy et al., 2003). Following the peak there is the decay phase of the event as the flux returns to the background level. Events caused by a single CME can have durations from several hours to several days (Reames, 2004).

Figure 2.1 from Shea and Smart (1990) shows a typical SEPE with the propagation delay (the time taken for the particles to traverse the IP medium), the time for the the flux to rise to the peak (or rise time) and then the decay stage of the event. The use of 'solar flare' as the event on the solar surface accelerating particles is reflective of the time when the paper was written as it is now thought that CMEs are the main cause of SEPEs. This is a simple single enhancement event but SEPEs may consist of more than one enhancement caused by multiple phenomena before a return to the background flux level. The shape of the SEPE may also vary due to the relative positions of the 'footprint' on the solar surface and the position of the observer. Shea and Smart (1995) gives a history of solar proton event observations.

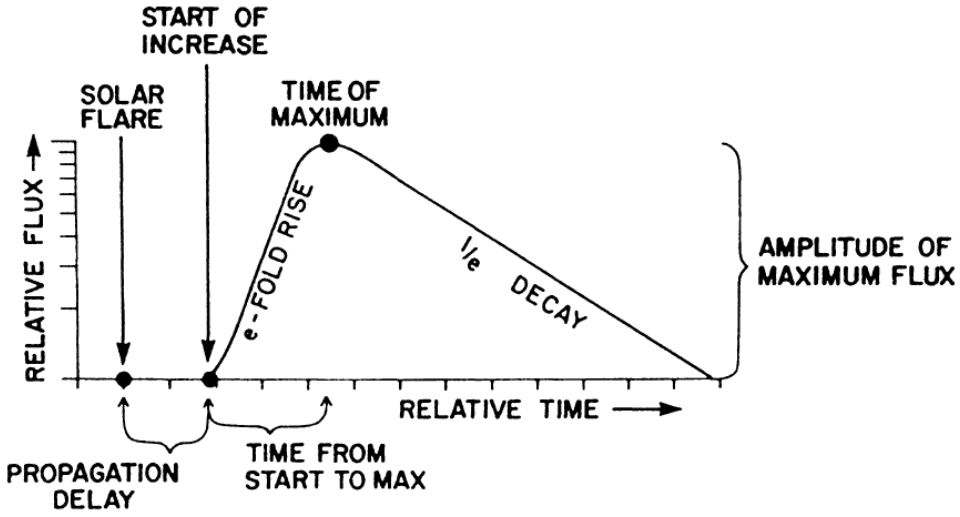

Figure 2.1: Typical flux profile for an SEPE taken from Shea and Smart (1990).

2.1.2 SEPE Effects

There are a variety of effects on spacecraft resulting from the environment of space. SEPEs are not the only cause of such effects but are dominant in some cases. Space weather includes effects from the Van Allen radiation belts and ionospheric disturbances but also Solar Energetic Particles (SEPs). NASA's Space Weather Prediction Center (SWPC) web page at:

`http://www.swpc.noaa.gov/info/Satellites.html`

states that one major spacecraft insurance company estimated that over $\$500,000,000$ in insurance claims were disbursed during the period 1994-1999 due to on-orbit failures

due to space weather. The SWPC has performed assessments of over 300 spacecraft anomalies and approximately one third of these were attributed to variations in the space environment.

Of these effects those that are caused predominantly by SEPs are displacement damage, Single Event Upsets (SEUs) and total dose effects. SEUs occur when a high energy particle ($>\sim$ 50 MeV) penetrates spacecraft shielding impacting an electrical component resulting in an upset which can be a tripping of the component, latch-up of the component which may require it to be re-set or component failure. The higher the flux levels the greater the likelihood of SEUs and, as previously stated, these flux levels can increase over 4 orders of magnitude. A good example of total dose effects is the degradation of power panels which are physically and permanently damaged by particles of energy high enough to penetrate their surfaces. In the worst case, a single SEPE can result in the loss of several percent of power panel output. This shortens the overall lifetime of the spacecraft or at least entails power management problems as the spacecraft nears its end of life. Feynman and Gabriel (2000) cite displacement damage as occurring due to the movement of silicon atoms from their usual lattice positions to interstitial sites leaving behind a vacancy. This in turn has a negative effect on the component properties and requires a prediction of fluence of SEPs along with energy spectra.

At a Round Table Meeting of Experts in Southampton, February 2007 it was decided that the baseline energy range for engineering purposes was 5-200 MeV. Higher energy particles in the $\sim$ GeV range may produce significant numbers of secondary particles upon impact with spacecraft which could be relevant for future manned missions. Lower energies may be important for the effects on newer thinner solar cells, X-ray CCDs and other modern and future technologies due to the miniaturisation of spacecraft components. However, as a result of geomagnetic shielding low energy particles are incapable of reaching spacecraft in orbits close to the Earth. This means that detection for modelling is difficult and SEPs at these energies only need to be considered for missions away from the Earth. Additionally, the dominant sources of low energy particles for Earth orbit are the Van Allen radiation belts (Feynman and Gabriel, 2000).

2.1.3 Major Historical SEP Events

There have been several notable major historical SEPEs recorded. Due to differences in their spectra the energy at which the events can be thought of as extraordinary varies. Possibly the best known event is the 'Carrington Event' of September 1859 (Carrington, 1860) which is recognised as the largest event of the past 450 years with a proton fluence of 1.88×10^{10} cm^{-2} in the $>$ 30MeV energy range estimated from the nitrate deposition in ice cores (Shea et al., 2006) as there were no direct measurements taken at this time.

The August 1972 event dominated solar cycle 20 so much so that it produced 69%, 84%, 84% and 83% of the $>$ 10, $>$ 30, $>$ 60 and $>$ 100 MeV proton fluxes for the cycle (King, 1974). The fluence of 9.7×10^9 cm^{-2} in the $>$ 30 MeV energy range for the August 1972 event was approximately half the estimated fluence of the Carrington event.

The October 1989 event was noted by Kallenrode and Cliver (2001) as the largest well-recorded particle event so far and was of similar magnitude to the August 1972 event with a proton fluence of 4.26×10^9 cm^{-2} in the $>$ 30 MeV energy range and 1.93×10^{10} cm^{-2} in the $>$ 10 MeV energy range calculated from GOES-7/SEM data. The flux profile for both of these channels is shown in Figure 2.2.

It can clearly be seen that there are multiple increases caused by multiple CMEs but for the remainder of this work such sequences (which can last as long as a month) will be considered a single event. In this study connected enhancements are considered to be a single SEPE. Defining events in this way mitigates factors such as the effect of a seed population in the IP medium resulting from one CME then being accelerated by a shock from a future CME (Reinard and Andrews, 2006) and CME interaction (Gopalswamy et al., 2002) both of which can affect the size (peak flux, fluence, etc.) of the SEPE. Failure to link connected enhancements will result in a systematic under-prediction of the likelihood of such a sequence when modelling the environment (Tylka et al., 1997).

Belov et al. (2005) investigated using data collected by neutron monitors as a possible way to include additional data especially for very large events. Effects of protons of energies below 500 MeV will not register on any neutron monitor, therefore, the methods used by the authors consider the neutron counts from the 1 GeV deduced

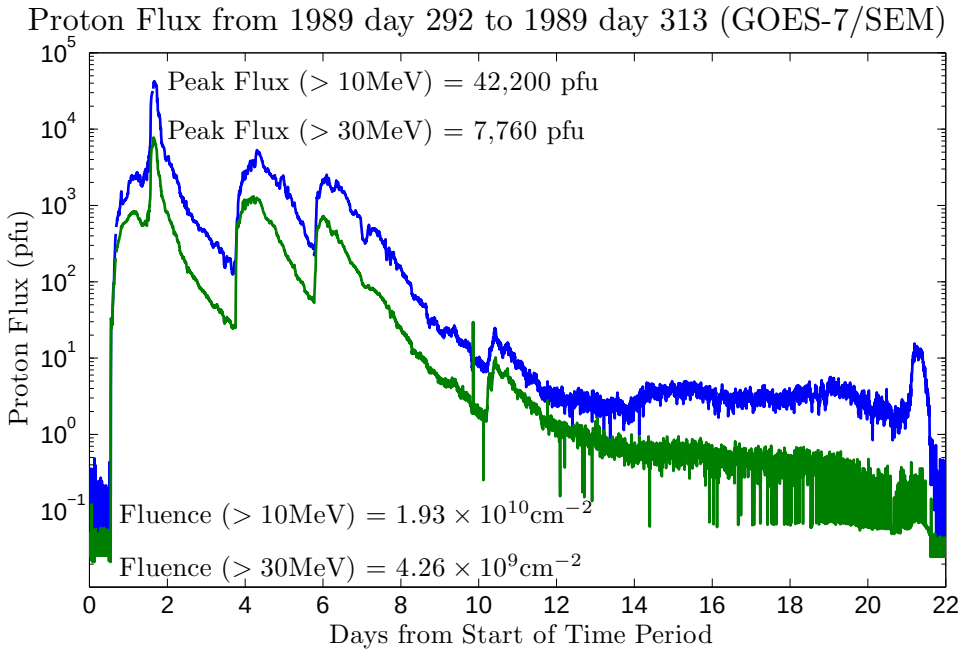

Figure 2.2: Event flux profile from GOES-7/SEM for the large October 1989 event resulting from multiple CMEs showing the > 10 MeV energy channel (blue) and the > 30 MeV energy channel (green).

measurements and from these they have extrapolated the likely proton fluxes in the > 300 MeV and > 100 MeV energy ranges. It was found that the event on 23rd February 1956 had a higher peak flux in the > 100 MeV energy range than any event since but that it was only in excess of twice the values observed during the satellite epoch and therefore is not outside current distributions (although the neutron monitor enhancement was one order of magnitude higher than anything seen since). Data extrapolation for > 10 MeV particles indicates that, although the February 1956 event would have been one of the largest seen, there are similar events (Belov et al., 2005).

The event of February 1956 was particularly notable for its intensity at energies > 100 MeV due to it having a very hard spectrum (Mewaldt et al., 2005) and although the fluence in the lower energy range was significantly less than the August 1972 event it was significantly greater at the highest energies. An event on 20th January 2005 studied by Mewaldt et al. (2005), which was the largest GLE measured in neutron monitors since 1956 and the most intense SEP event measured by GOES satellites at high energies in their 29-year history (1976-2005), was similar in terms of the hardness of its spectrum as well as having a very fast rise time, faster than any other event within the last 30 years (for proton intensity > 100 pfu in the > 100 MeV energy

range). The possibility of such events has ramifications for EVAs (Extra-Vehicular Activities) as the > 1 GeV protons must have been accelerated very low in the solar corona. Figure 2.3 shows the fluence spectra of some of the largest SEPEs of the last 55 years (Mewaldt et al., 2005).

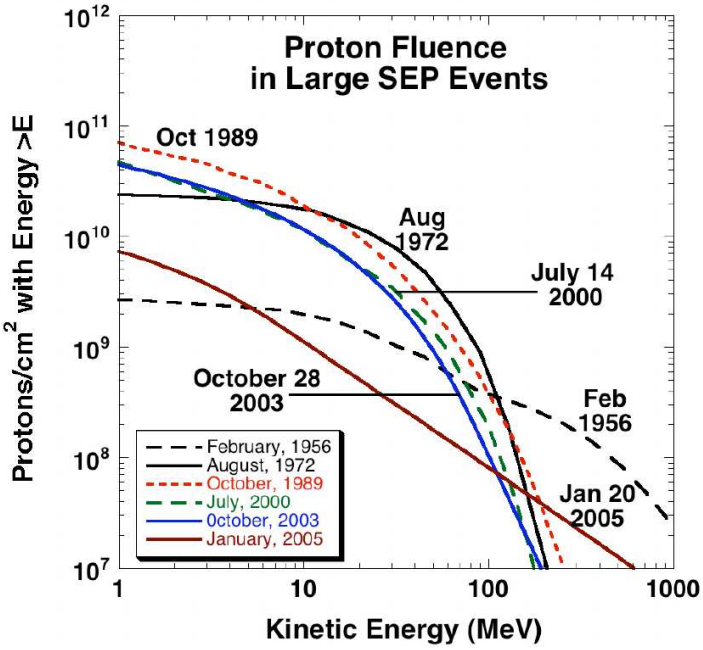

Figure 2.3: Fluence spectra of some of the largest SEPEs of the last 55 years (Mewaldt et al., 2005).

It has been suggested that it is feasible to consider the identification of solar proton events extending many thousands of years into the past through the measuring of nitrate layer thicknesses in ice cores in places such as Greenland and Antarctica (McCracken et al., 2001) which could therefore include such events as the Carrington event of 1859. There are several issues with using these derived fluxes to augment current data sets for the modelling of SEPEs especially the difficulty of comparing it with current spacecraft data:

- Comparison is difficult between recent in-space data and the ice core data as man-made components of the nitrate signal in the ice core used for the indication of events has been on the increase resulting in significant noise.
- We must wait ~ 30 years for the packing of ice before good data can be obtained
- There is also a short-term meteorological influence occurring since the 1950s making events difficult to identify.

The time period from which useful data for SEPEs can be taken is limited by the time over which humans have been taking measurements. Homogeneous, space-based measurements are only available from the 1960s onwards. This leaves a shortage of very large events for statistical analysis especially in higher energy bands where significant enhancements are less frequent. Although it would be very useful to use neutron monitors or ice cores to extend the data time range for SEPE modelling purposes it is hard to be sure of the accuracy of the estimates made for solar proton fluxes with these data.

2.1.4 Solar Activity and the Solar Cycle

It was found by Wolf (1852) that the Sun follows a cycle with a period of approximately 11 years (although this can vary between 9 and 14 years). The solar activity is often stated as the Sunspot (or Wolf) number although it should be remembered that this is just one proxy for solar activity. In the past there have been periods of inactivity the most famous of which is the Maunder minimum which lasted from 1645 to 1715 (Maunder, 1922). Solar cycle 1 is taken to be that which started in March 1755 while the maxima for the past 4 cycles have been in 1968, 1979, 1989 and 2000 (cycles 20, 21, 22 and 23 respectively).

Hathaway et al. (1994) showed that with knowledge of the maximum sunspot number and the cycle start time it is possible to make good predictions for the shape of a solar cycle. These predictions can normally be made to 10% accuracy within 30 months and 20% accuracy within 42 months of the start of a solar cycle however it would be very useful for modellers to have better prediction techniques for a solar cycle before the onset. It should be noted that cycles overlap by about 3 years with new cycle sunspots appearing at high latitudes while old cycle spots can still be seen at low latitudes (Hathaway et al., 1994).

Modelling the Sun as a dynamo and employing a flux-transport dynamo-based tool and using multiple previous solar cycles, Dikpati et al. (2006) predicted that solar cycle 24 would be $\sim 50\%$ stronger than cycle 23 with a maximum sunspot number of ~ 140. However, Svalgaard et al. (2005), using a polar field precursor method, predicted that the cycle 24 peak will be 40% below that of cycle 23 at ~ 75 giving it possibly the smallest amplitude of a cycle in last 100 years.

Hathaway et al. (1999) presented a synthesis of prediction methods using both precursor and regression methods to predict the coming solar cycle activity. Geomagnetic precursors work well near solar minimum to give an estimate of the cycle amplitude which regression techniques work well as solar activity approaches a maximum (Hathaway et al., 1999). Studying the drift rate of sunspots, which are known to migrate from high latitudes towards the solar equator reflected in 'butterfly diagrams', Hathaway et al. (2003) found a correlation between the drift rate and the amplitude of the following cycle.

Illustrating the difficulties in prediction of the nature of future solar cycles, the international prediction panel are still split concerning the amplitude of cycle 24. The continued delay in the onset of the new cycle might indicate that it will be of small amplitude as generally small amplitude cycles rise to maximum more slowly than those with larger amplitude (Hathaway et al., 1999).

Some authors have suggested a correlation of SEPE occurrence on sunspot number (Nymmik, 1999; Kuznetsov et al., 2005), however, the strength of this correlation has been questioned (Feynman et al., 2002).

2.1.5 Sources of SEPs: Flares and CMEs

For over 40 years it was believed that solar flares were the sole cause of SEPEs but it is now accepted that this is not the case. This outdated paradigm was termed 'the solar flare myth' by Gosling (1993). The current paradigm is that there are two types of SEPEs: smaller, low fluence, short duration (or impulsive) events caused by solar flares and larger, high fluence, longer duration (or gradual) events accelerated in coronal/IP shocks driven by Coronal Mass Ejections (CMEs) (Kahler, 2003). Two differences between impulsive and gradual events are the height in the corona at which the particles can be said to be initiated and the respective volumes. Impulsive events occur in the corona at a height of $< 10^4$ km and have a total volume generally in the region of $10^{26} - 10^{28}$ cm^3 while gradual events occur in the corona at a height of $\sim 5 \times 10^4$ km and have a total volume generally in the region of $10^{28} - 10^{29}$ cm^3 (Kallenrode, 2003). A review of the different particle acceleration mechanisms and resulting particle compositions from CME-driven shocks and solar flares is given by Reames (1999) and references therein. Recent observations of mixed events suggest

that this two-class division of SEPEs needs to be modified (Kallenrode, 2003).

Impulsive events tend to have higher Iron (Fe) charge states than gradual events which are more similar to the solar wind (Boberg et al., 1996). In general, large gradual events have element abundances similar to the corona while impulsive SEP events have high ratio of ^{3}He to ^{4}He Helium isotopes (sometimes 1000 times) and enhancements in heavier elements (Reames and Ng, 2004).

It is known that the CME speed and SEP intensity are well correlated (Kahler, 2001) but for a given CME speed, intensity can vary over four orders of magnitude (Gopalswamy et al., 2003). Gopalswamy et al. (2002) found that 4500 CMEs were observed from January 1996 to November 2001 but only ~ 100 SEPEs with intensity of > 10 MeV protons exceeding 1 pfu were recorded. The authors also point out that huge angular widths of some CMEs producing SEPs ensures that they intersect the ecliptic consequently resulting in SEP events at the Earth.

The largest SEPEs may result in Ground-Level Enhancements (GLEs). In a study of events between 1977-2003 Wang and Wang (2005) found that CMEs resulting in GLEs had an average speed of $1,762$ kms^{-1} and width of 317°, moderate SEPEs ($10 - 100$ pfu, E > 10 MeV) had CMEs with an average speed of $1,077$ kms^{-1} and minor SEP events (1-10 pfu, E > 10 MeV) had CMEs with an average speed of 887 kms^{-1}. The study also found that all SEP-related CMEs came from between S30 and N40 latitude and 85% of GLE-related CMEs originated in the Western hemisphere.

A study by Reinard and Andrews (2006) compared those CMEs that do result in events and those that do not, more specifically investigating the differences in CME/flare combinations including the importance of CME velocity, flare duration and CME-flare time delays. The study took a list of SEPEs (using the NOAA event definition) and a list of times when no SEPE occurred but there were similar observations such as comparable numbers with X-, M- and C-class flares. Flares were considered to be associated with a CME if they peak one hour before or after the CME launch time. The flare durations and difference in onset time from the CME launch time were not found to be different to a statistically significant level. However, it was found that the SEPE CMEs had a mean speed of $1,225$ kms^{-1} and median speed of $1,300$ kms^{-1} (± 145 kms^{-1}) while the non-SEP CMEs had a mean speed of 926 kms^{-1} and median speed of 884 kms^{-1} (± 110 kms^{-1}). The difference here is

about 30%. A theoretical Alfvén speed in the corona above which a shock may form (thus potentially creating SEPs) is 800 kms^{-1}. 82% of SEP-related events had higher velocities than this while only 54% of non-SEP-related events did. The conclusions of the study were that the speeds of the CME are a determining factor but probably in addition to the seed population. The Alfvén speed, V_a, is given by:

$$\frac{\mathrm{d}V_a}{V_a} = \frac{\mathrm{d}B}{B} - \frac{1}{2}\frac{\mathrm{d}n}{n} \tag{2.1}$$

where n is the plasma density and B is the magnetic field. These Alfvén waves accompanying shocks cause SEPs to resonate allowing rapid particle acceleration to high energies. However, waves generated as particles stream outward can be absorbed if those particles subsequently scatter and stream inward. When intensities of resonant waves become large, scattering limits the intensities of particles that can stream away (Reames, 1999). This 'streaming limit' could result in a reduction of the peak fluxes and fluences seen in the largest SEPEs.

Zurbuchen and Richardson (2006) state that ICMEs (the name given to the interplanetary counterpart of a CME as it propagates though the interplanetary (IP) medium) can be identified in situ based on a number of magnetic field, plasma, compositional and energetic particle signatures and combinations thereof. McKenna-Lawlor et al. (2002) state that CMEs will usually not produce significant geomagnetic storms when the southward magnetic field component perpendicular to the ecliptic plane is small, if the component is directed northward or if the ICME source on the Sun is unfavourably far from the Central Meridian.

Kallenrode (2003) suggests that the current paradigm of two distinct particle populations, those accelerated by flares and those accelerated at CME Shocks, which are mutually exclusive is not necessarily accurate and that mixed events need to be taken into account. Re-acceleration from remnant particles from earlier CMEs and other interplanetary disturbances means that the properties of an SEPE are not only determined by the properties of the acceleration mechanism(s) but also by earlier CMEs and remnant SEPs from previous flares or shocks. Therefore SEPEs may contain particles contributed from various processes (Reames and Ng, 2004). CMEs create shocks and reconnection processes due to changes in the magnetic field topology and this can allow connectivity to the IP medium (i.e. open field lines) but the particles exploiting this connectivity could be produced by flares or CMEs. The possibility

that particles accelerated during the flare process contribute in large SEP events is supported by charge state and abundance measurements but the presence of a CME is the distinguishing feature between the two classes of events. This indicates that in the largest events both acceleration processes could be taking place and that the sharp division separating SEP events is likely to be misleading (Cane and Lario, 2006).

Torsti et al. (2001) used an event on 9^{th} May 1999 to highlight a combination of processes including coronal and interplanetary acceleration associated with both a flare and a CME which resulted in unexpected increases in abundances of particles, such as heavy ions. Kahler et al. (2001) noted that while solar flares cause impulsive events and CMEs tend to be the cause of gradual events there are many variables for each type of event and events can be combined. This can result in some narrow CMEs (10-40°) being associated with impulsive SEP events.

Gopalswamy et al. (2002) investigated occurrences of CME interaction in the IP medium and concluded that the vast majority (80%+) of major SEPEs occur at times of CME interaction. Gopalswamy et al. (2003) found that CME interaction and the extent of that interaction seem to discriminate SEP-poor and SEP-associated as a density enhancement represented by the preceding CME can lower the Alfvén speed resulting in a strong shock. Combined occurrence of mixed events at the solar source and the re-acceleration of remnant particles indicates that attempting to define SEPEs with physical processes on a one-to-one basis is not only very difficult but unwise due to the possible inter-dependence of the characteristics. This justifies linking enhancements by using relatively low flux threshold values.

2.1.6 Radial Variations and Magnetic Connection

Intuitively, one might expect that the further the observer's position is from the Sun, the lower the flux of SEPs they would see. One might also think that it would be logical that this would fall away following an inverse square law in the same way that energy from a point source appears to. This is not strictly the case with SEPs and there are a variety of factors that can affect radial variations, such as the acceleration of particles at varying heliospheric distances. Powers for adjusting flux values are nonetheless useful for modelling although authors have found slightly different values for these indices.

Recommendations by the working group on solar particle events of a workshop on Interplanetary Charged Particle Environment held at JPL in March 1987 were to use the scaling values for radial dependence shown in Table 2.1. These values gives conservative estimates for points closer to Sun with greater variation for peak fluxes than for fluences.

Table 2.1: Recommended indices for helioradial variation from 1987 workshop.

Parameter	Functional form	Variation Range
Proton fluxes (R> 1 AU)	$R^{-3.3}$	R^{-4} to R^{-3}
Proton fluxes (R< 1 AU)	R^{-3}	R^{-3} to R^{-2}
Proton fluences (R< 1 AU or R> 1 AU)	$R^{-2.5}$	R^{-3} to R^{-2}

Hamilton et al. (1990), excluding anisotropies, shocks and the focussing effect of energetic particles (using data mostly beyond 1 AU), deduced values shown in Table 2.2. Ng and Reames (1994), taking into account the propagation effects of Alfvén waves amplified by the streaming particles, deduced a $\sim R^{-3}$ dependence. Later, Reames and Ng (1998) found data from Helios 1 & 2 and GOES spacecraft to support the earlier conclusion with the inclusion of streaming limit intensities. This study only included the first part of events and therefore did not look at the effects of shocks also known as energetic storm particle (ESP) events. Smart and Shea (1985) noted that the peak intensities seen in events as a result of shocks do not scale with radial distance as suggested by recommended power laws or those deduced from transport models.

Table 2.2: Indices for radial dependence suggested by Hamilton et al. (1990).

Parameter	$10 - 20$ MeV protons
Peak fluxes	$R^{-3.3\pm0.4}$
Fluences	$R^{-2.1\pm0.3}$

Lario et al. (2006) investigated the dependence on radial and longitudinal variations for proton peak intensities and fluences in depth studying a time period from 1976 to 1982. Data were used from IMP-8 at $\sim$ 1 AU and Helios 1 & 2 (which had elliptic orbits with perigee 0.3 and apogee 0.98 AU about the Sun) to study variations in both proton peak intensities and fluences. It was concluded that radial

distance was not as important as the longitudinal angular distance when determining variations shown in the plotting of both peak intensity and fluence data but it is worth considering that for cumulative fluence models it is expected that different longitudinal positions will all see approximately equal fluences as it averages out over time.

There was no systematic increase of peak fluxes and fluences with Radial distance found although there were intensities for several events seen by Helios -1 & -2 that were in excess of anything ever experienced by IMP-8. Thus the conclusions were to recommend the values given in Table 2.3.

Table 2.3: Indices for radial dependence suggested by Lario et al. (2006).

Characteristic	$4-13$ MeV protons	$27-37$ MeV protons
Peak Intensities	$R^{-2.7}$	$R^{-1.9}$
Event fluences	$R^{-2.1}$	$R^{-1.0}$

Presently the European Cooperation on Space Standardization (ECSS) recommends scaling factors for helioradial distances other than 1 AU of R^2 for less than 1 AU and 1 for greater than 1 AU (section 9.2.2 ECSS Standard (2008)).

The radial dependency clearly does not strictly obey an inverse square law, one reason behind why this is not the case is the acceleration of particles at different heliospheric distances rather than the acceleration occurring solely at the solar surface. More data from new spacecraft, such as the two STEREO spacecraft, will facilitate a greater understanding of the processes and more sophisticated physical models.

Lario et al. (2006) state that the tendency for large events to result from activity on the Sun's Western hemisphere reflects the connection of the magnetic field line for the Earth to a point on the Sun in this region (the footpoint). Computing the Parker Spiral (Parker, 1958) for the Interplanetary Magnetic Field (IMF) and assuming a constant solar wind of 450 kms^{-1} gives a footpoint of W52 for 1 AU. Gradual SEPE profiles vary depending on the particle energy considered and the position of the observer with respect to the propagating CME-driven shock. This would be footpoint of W58 if a solar wind speed of 400 kms^{-1} were used. These magnetic field lines are affected by the presence of CMEs and other solar physical structures and this can affect which particles have good magnetic connection to the Earth.

Mewaldt et al. (2005) highlight the event on 20th January 2005 as having a fast onset in part due to good magnetic connection (W61) but particles must also have been accelerated quickly and experienced less scattering than in most SEPEs. Leske et al. (2005) state that high energy measurements show that many large western events have high charge states ($\sim \pm 20$ for Fe) just like in smaller events which supports the idea that, due to some alteration in the magnetic field caused by the CME, flare accelerated particles gained access to open field lines and were therefore detected at the Earth.

The helioradial variations of SEP flux and the impact of the longitudinal position of the observer are important for adapting a SEPE environment model from the Earth to other points in the heliosphere, e.g. predictions of the environment for interplanetary missions.

2.1.7 Energy Spectra and Elemental Abundances in SEPEs

SEPs arrive from the Sun at a wide range of energies from less than 0.1 MeV to GeV particles. The quantity of particles seen at different energies is dependent upon the initial processes and the particles' propagation through the IP medium.

Daibog et al. (2003) state that IP space is a scene for propagation of previously accelerated particles but also interactions with magnetic field inhomogeneities that affect the particle energies, this shows up in the energy spectra of SEPEs. There are two factors contributing to the variance of the energy spectra with time, one is diffusion which follows a power-law relationship which is more important for high energies (> 100 MeV) and the other is convection which follows an exponential function which is more important for lower energies (< 10 MeV). This is complicated further by different processes of acceleration such as IP shocks associated with CMEs. Additionally, the average values of characteristic decay time and energy spectral index change with the solar activity phase.

In a study by Mewaldt et al. (2005) using data from ACE/ULEIS, EPAM & SIS, SAMPEX/PET and GOES-11 to measure the energetic spectra of H, He, O, and electrons, a wide energy interval ($\sim$ 0.1 to 100 MeV/nuc for ions and $\sim$ 0.04 to 8 MeV for electrons) was observed for the large SEPEs from solar cycle 23 including the October-November 2003 ('Halloween') and January 2005 events. It was found

that the five enhancements from the October-November 2003 SEPE and the January 2005 SEPE spectra fit well with the double-power-law formalism of Band et al. (1993) at energies > 5 MeV.

Changes in spectra between different events and during the same events indicate that it is dangerous to extrapolate to different energies using analytical spectral fits and where possible real data should be used although if not then some extrapolation must be used.

It is expected that approximately coronal abundances will be seen in large gradual events while increased heavy elements can be seen in impulsive events. The composition of SEPEs varies greatly depending on the type of event, but can also vary from the expected abundances for gradual and impulsive events as a result of other factors.

A preliminary study by Leske et al. (2005) using data from the LEMT instrument onboard the Wind spacecraft and the ULEIS instrument on the ACE spacecraft shows that elements heavier than Zn ($Z = 30$) can be enhanced by factors of 100 to 10,000 in impulsive SEPEs at energies below several MeV/nuc. However, using ACE/SIS it was found that even large gradual SEPEs at energies of ~ 10 to > 100 MeV/nuc are often very iron rich and may appear similar in composition to impulsive events. In one small event on 23 July 2004 the $(33 < Z < 50)/O$ enhancement was $\sim 400 - 500$. This demonstrates that large UH (ultraheavy - Z$>$ 30) enhancements can exist in SEP events at energies > 10 MeV/nuc. These increased UH element abundances in gradual events might be expected if there is direct access from the flare site or there is re-acceleration of flare suprathermals at quasi-perpendicular shocks.

Further to earlier comments in Section 2.1.5 regarding mixed events, it was suggested by Gopalswamy et al. (2002) that the charge state composition of SEPs should rarely reflect the quiet solar wind conditions as the CME shock has to accelerate the SEPs from the solar wind 'contaminated' by the preceding CMEs, rather than from the quiet solar wind and is based upon the discovery by the authors of the importance of CME interaction as an SEP event discriminator. These factors would indicate that using standard abundance tables to extend a solar proton model to heavy ions would be ill-advised without a thorough investigation of heavy ion data available from spacecraft such as ACE.

2.2 Data Available

Models of the SEPE environment are dependent upon the raw data collected and the way in which it is manipulated in terms to the methods of extracting events from the flux time series. In this section possible problems with the raw data and issues of manipulation are discussed. The raw data used for analysis is in the form of flux time series, the number of particles which impact the detector are recorded and translated into standard units. For a given energy bin the units are usually particles.cm^{-2}.s^{-1}.sr^{-1}.MeV^{-1}. To find the number of particles incident across one square centimeter this value is multiplied by the energy bin width (in MeV), the time period (in seconds) and 4π (to account for the solid angle steradians). Instruments will bin the particles by energy and it is normally assumed that the mean energy of the particles is the geometric mean of the upper and lower bins limits. Past data giving proton fluxes can be used to predict the probably SEPE environment for future space missions.

SEP data used includes that from the IMP series of spacecraft, the longest data set coming from IMP-8 (1973-2001). One IMP-8 instrument is the Charged Particle Measurement Experiment (CPME) built by the Johns Hopkins University Applied Physics Laboratory which has 10 proton channels ranging from 0.29 - 440.0 MeV and data is recorded in sampling periods of 5.5 minutes (this is called the time resolution):
`http://sd-www.jhuapl.edu/IMP/cpme_handbook.pdf`
A second instrument onboard IMP-8 is the Goddard Medium Energy (GME) instrument which has 30 channels for differential fluxes from 0.5 - 500 MeV and a time resolution of 30 minutes:
`http://spdf.gsfc.nasa.gov/imp8_GME/GME_instrument.html`
Another widely used instrument for SEP data are the Space Environment Monitor (SEM) instruments onboard the GOES spacecraft covering a time period from 1986 to the present day which have 7 proton channels ranging from $\sim$ 1 - 500 MeV (depending on version of the SEM) and have a sampling time of 5 minutes:
`http://goes.gsfc.nasa.gov/text/databook/section05.pdf`
More recent data from spacecraft at L1, the first Lagrangian Point, are available from the Electron, Proton, and Alpha Monitor (EPAM) (Gold et al., 1998) and the Solar Isotope Spectrometer (SIS) (Stone et al., 1998) onboard the ACE spacecraft (from

1997 to the present day) and the Energetic and Relativistic Nuclei and Electron experiment (ERNE) instrument onboard the SOHO spacecraft (from 1996 to the present day):
`http://www.srl.utu.fi/projects/erne/index_english.html`

2.2.1 Data Gaps and Errors

Many issues with data sets were raised by Rosenqvist et al. (2005); these included small gaps in data from GOES -6, -7, -8 & -10 while GOES -10 also showed intermittent high noise levels in high energy channels. IMP-8/GME (Goddard Medium Energy detector) had large data gaps which were filled with values found using exponential interpolation with an e-folding time of 2 hours. IMP-8/CPME (Charged Particle Measurement Experiment) had large data gaps which were filled by taking the average of existing data for the day. There were also significant saturation and dead-time (in which the instrument fails to record flux data) effects especially for large events and high intrinsic background levels which would affect the detection of small events. Tylka et al. (1997) found an issue with IMP-8/CRT (University of Chicago's Cosmic Ray Telescope) resulting from the anti-coincidence shield sometimes causing the count rate to be suppressed during peak rates of very large particle events resulting in dead-time. This problem was also present on IMP-8/CPME which was an instrument used in the JPL-91 analysis and this could explain, in part, the departure from a lognormal distribution of the experimental data at highest daily proton rates.

Data gaps close to the maximum intensity prevent the computing of the fluence of events without using data from another instrument, while data gaps in the decay phase of an event can be filled by a linear or parabolic interpolation or a 5-point Newton-Cotes method (Lario et al., 2006).

In the construction of their integrated data set (IDS), Xapsos et al. (2004) cited saturation effects on the IMP-8/GME instrument as reason for supplanting GOES/SEM data during periods of high flux. However, due to the orbit of the GOES satellite at geostationary Earth orbit ($\sim$ 6 Earth radii) and possible magnetospheric effects the authors reasoned to use IMP-8/GME data where it wasn't saturated as the orbit of the IMP-8 spacecraft was further out at 35 Earth radii. It should be noted that the impact of geomagnetic shielding is only significant at energies $>$ 5 MeV due to

magnetic rigidity being the particles momentum divided by its charge. Additionally, data from GOES spacecraft tended to disagree with one another due to calibration errors and may need to be adjusted (Rosenqvist et al., 2005).

All of the above issues highlight the importance of considering carefully the reliability of data being used and, where possible, cross-referencing fluxes with other instruments.

2.2.2 Limitations of data set size

Studying $>$ 10 MeV protons SEPEs Rosenqvist and Hilgers (2003) found that the data sets used by models are not necessarily large enough to provide accurate results. To test the stability of models Rosenqvist and Hilgers (2003) created 1,000 artificial data sets by random generation of event fluences using the lognormal distributions with the JPL-91 model parameters (Feynman et al., 1993). These data sets each included 200 events (some of which would not exceed the minimum fluence threshold), from these new lognormal fitted parameters were found in each case (which would vary due to statistical scatter for a limited number of events) and the JPl-91 modelling method was run on each one to generate fluence predictions (shown in Figure 2.4). The authors took these results and used the uncertainty of the prediction of Q90 and Q95 (the 0.90 and 0.95 confidence levels) as a benchmark for the robustness of the prediction model by studying the stability of the fitting parameters (their fluctuation when new data is added) with respect to the size of the sample. Rosenqvist and Hilgers (2003) also tested adding events from 4.7 active years with the theoretical average of 6.75 events per year to see the impact on data sets of adding just a short time period of flux data. The results were a wide spread on the probability distributions as the probability of exceeding a certain fluence decreases (increasing confidence level), this result was checked by expanding the artificial data sets to 10,000 with no noticeable change in results.

Using the spread of predictions generated by the artificial data sets upper and lower boundaries F_U and F_L containing 95% of the values were established. The authors found that to reduce the ratio between these values to less than 1.5 for Q90 and Q95 would require approximately 1,200 events. Assuming an average of 6.75 events each active year (Feynman et al., 1993) this corresponds to several hundred years of data.

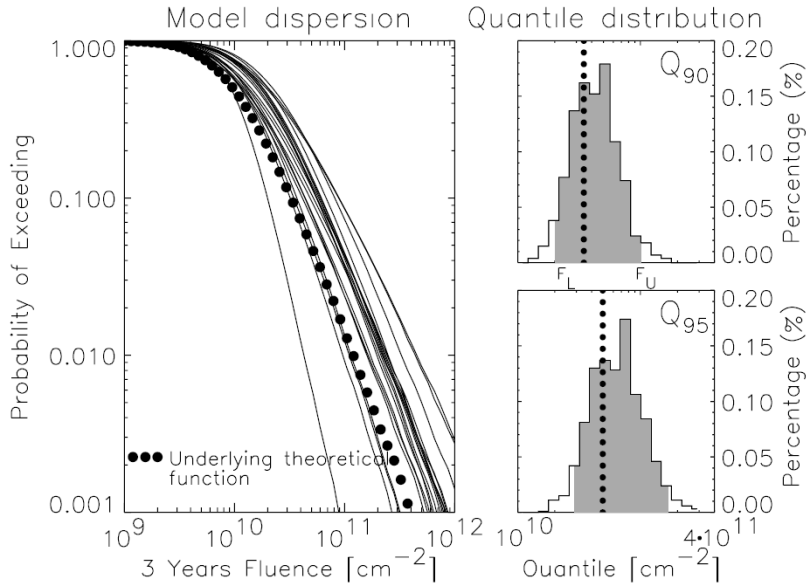

Figure 2.4: Effect on fluence results generating artificial data sets (Rosenqvist and Hilgers, 2003).

This work shows how the limited data set can strongly impact predictions due to the fluence fitting parameters. However, seeing as there is only $\sim$ 45 years of data available there doesn't appear to be a solution other than to investigate the use of other records of historical SEPEs such as those covered in Section 2.1.3 where the problem of accurately determining the intensity of the SEPEs is a problem.

2.2.3 Energy Ranges Considered by Models

The JPL model (Feynman et al., 1993) uses a narrow proton range ($>$ 1 to $>$ 60 MeV) and thus disregards the high-energy proton fluxes. The JPL model is based purely on the data that has been collected and doesn't make the attempt to extrapolate to higher energies. There is no reason that the JPL model might not be extended to higher energies other than limitations of the data available. The earlier King Model (King, 1974) used 4 energy proton channels of $>$ 10, $>$ 30, $>$ 60 and $>$ 100 MeV but there are a limited number of SEPEs at the highest energies.

Rosenqvist et al. (2005) performed their update using only the $>$ 10 MeV proton channel. The extension of the JPL method to heavy ions (Tylka et al., 1997) is limited by available data to 11-20 MeV/nuc and 25-95 MeV/nuc for He, 21-43 MeV/nuc and 45-211 MeV/nuc for CNO (Carbon, Nitrogen and Oxygen combined), and 45-79

MeV/nuc and 97-432 MeV/nuc for Fe.

The MSU model (Nymmik, 1999) extends the results from > 30 MeV using analytical formulae. The MSU model is based on the > 30 MeV energy range but allows for extrapolation to other energies based on observations with an analytical expression of an adjusted power law of particle momentum.

The ESP worst-case peak flux model (Xapsos et al., 1998b) uses only the > 10 MeV proton channel (although there is no reason why the method may not be applied to an event list at other energies). The ESP worst-case event fluence model and cumulative fluence models extend to > 100 MeV with an analytical method for allowing a further extension up to 300 MeV. The PSYCHIC model (Xapsos et al., 2004) which is an evolution of the ESP cumulative fluence model uses real data to extend this energy range to > 327 MeV. The extension of the PSYCHIC model to heavy ions (Xapsos et al., 2007) used various modern data to extend the proton model to similar energies for all significant ion species.

Due to the differences in the spectra of events due to differences in their production and propagation through the IP medium covered in Section 2.1.5 it is dangerous to make spectral fits to results. However, it might be reasonable to say that although on an event-to-event basis there is significant variance that this will even out over time. A major problem for producing models at higher energies are the lack of events in these energy ranges making it difficult to fit distributions to the data or validate spectral extrapolations from results at lower energies.

2.2.4 Event definition selection

As introduced in Section 2.1.1 SEPEs are extracted from a flux time series by use of threshold parameters dependent upon the energy being investigated. The SEPE is said to begin when the flux rises above the start threshold and finish when it drops below the end threshold. Different threshold parameters or caveats in the underlying data can result in identifying a sequence of flux data as one or more than one SEPE. To ensure that all interdependent enhancements were treated as single events Feynman et al. (1990) utilised a lagtime (of 2 days) such that the flux needed to remain below the threshold for the stated time and if it did not then the sequence was treated as a single SEPE. Kuznetsov et al. (2005) suggested that each event

should be linked to a single phenomenon occurring on the solar surface. Tylka et al. (1997) used the example of the episode from $19^{th} - 27^{th}$ October 1989 (shown in Figure 2.2 in Section 2.1.3), this was a grouping of physical 'events' comprising of three distinct CMEs from the same active region considered as a singular statistical 'episode'. It is pointed out that if we did not do this we would systematically under-predict the probability of such a sequence of events (as there is clearly both a time and size dependence). The issues raised in Section 2.1.5 explain why the philosophy of Kuznetsov et al. (2005) is dangerous. Beyond a physical interaction at the solar source or in the IP medium during propagation CMEs enhancements may be interdependent due to being generated by the same active region. Choosing not to ensure that enhancements whose fluxes are interdependent are defined as a single SEPE means that any time dependency as well as possible flux dependencies must be accounted for in any model. This adds a level of complexity to the modelling that is unnecessary.

Another important aspect of event definition are minimum event parameters (duration, fluence and peak flux). It is key to apply these so that the distributions are well fit to the data. Lower fluence (or peak flux) events are not always detected due to the presence or larger events, insufficient instrument sensitivity and background radiation and this reduction in event numbers will skew the distribution fit. These small events do not contribute significantly to the total flux as the largest events are several orders of magnitude larger in terms of both fluence and peak flux (depending on energy). Feynman et al. (1993) used a minimum fluence parameter where Xapsos et al. (2004) used two minimum flux parameters (each event had to exceed at least one to remain in the list). Minimum durations are more likely to be used to exclude data spikes and should be set at a value less than the shortest true SEPEs. Table 2.4 shows the event definition parameters for the best known models (where known) along with the energy ranges and elements covered, data sources and distributions used.

The minimum sampling time is the time resolution of the instrument being used, using this gives the most accurate measurements of event peak flux, start and end times and consequently event fluence. However, in order to mitigate for errors in the data often the sampling time is increased (so the effects of spikes, gaps, etc. are reduced). Feynman et al. (1990, 1993) and Jun et al. (2007) used a flux threshold of 1 pfu averaged over one day. The event list published by Jun et al. (2007) applied

Table 2.4: Comparison of statistical models.

	Data Sets Used	Time Period	Event Definition Criteria	Event Frequency Distribution	Flux/Fluence Distribution	Energy Range	Elements Covered
The King Model	IMP-4, -5, -6	1966 - 1972	weekly >10 MeV fluence $>25\times10^7$ cm^2	Burrell extension Poisson statistics	Lognormal (OR) + separate (AL)	>10 - >100 MeV	Protons only
JPL-85 Fluence model	Mixture of data	1956 - 1985	↑ | >10 pfu (>1 MeV)	↑ |	↑ |	>10, >30 MeV	↑ |
JPL-91 Fluence model	IMP -1, -2, -3, -5, -6,	1963 - 1991	>5 pfu (>4 MeV), >1 pfu (>10 MeV,	Poisson Distribution	Lognormal Distribution	↑ >1, >4,	Protons only
The JPL model update	-7 & -8, OGO -1	1963 - 1998	>30 MeV, >60 MeV) ↓	| ↓	| ↓	>10, >30, >60 MeV	| ↓
MSU model	IMP, OGO & MIR data	1960s - 1990s	None Given	$W(t)^{0.75}$	Power Law	>30 MeV (ext. to all)	all
ESP peak flux model	Mixture of data	1967 - 1996	>10 pfu (>10 MeV)	↑ |	↑ | Truncated	>10 MeV ↓	↑ |
Worst-case fluence model	IMP-3, -4, -5, -7 & -8,	↑ 1963 -	Various ↓	Poisson Distribution	Power Law ↓	↑ >1 to	Protons only
Cumulative fluence model	GOES -5, -6 & -7	1996 ↓	Not Applicable	| ↓	Lognormal Distribution	>300 MeV ↓	| ↓
Extension to Heavy Ions	IMP-8, GOES-7	1973 - 1996	>1 pfu >10 MeV (protons)	Poisson Distribution	Lognormal Distribution	11 - 432 MeV/nuc	He, CNO and Fe
Toolkit Models	GOES -6, -7, -8 & -10	1956 1991	>1 pfu (>10 MeV)	Poisson Distribution	Lognormal Distribution	>10 MeV, >30 MeV	Protons only
PSYCHIC model	IMP-3, -4, -5, & 8, GOES	1966 - 2001	>4 cm^{-2}s^{-1}sr^{-1}MeV^{-1} ($1.15-1.43$ MeV) or $>10^{-3}$ cm^{-2}s^{-1}sr^{-1}MeV^{-1} ($42.9-51.0$ MeV)	Poisson Distribution	Lognormal Distribution	>1 MeV to >327 MeV	all

this threshold to the > 11.1 MeV channel which is similar to Feynman et al. (1993) which used > 10 MeV integral channel but Jun et al. (2007) did not apply a lagtime where Feynman et al. (1993) applied a lagtime of 2 days. The data was taken from different instruments onboard the IMP-8 spacecraft, namely from the Goddard Low Energy Detector (LED) and Medium Energy Detector (MED) and the University of Chicago's Cosmic Ray Nuclei Experiment (CRNE) where Feynman et al. (1993) used data from the CPME instrument onboard IMP-8. The time range was from 1973 to 1997 and the list includes 135 solar proton events from the 14 solar active years in this time period.

A minimum duration, peak flux or fluence can be applied to the list of events to neglect small events which might be of little consequence, more greatly affected by data errors or erroneous due to poor data. It should be noted that while these events may be excluded due to their negligible contribution to fluence or low peak flux they may be important in terms of the understanding of event inter-dependence.

The current NOAA (National Oceanic and Atmospheric Administration) event definition for > 10 MeV solar proton events takes the beginning of a proton event to be the first of 3 consecutive data points (equal to 15 minutes) with fluxes greater than or equal to 10 pfu. The end of an event is taken to be the last time the flux was greater than or equal to 10 pfu. There is a danger in the NOAA definition of not grouping linked enhancements close together in time.

2.2.5 SEPE Fluence and Peak Flux Distributions

Once the algorithm for extracting an SEPE is defined a list of SEPEs is formed, this includes the start and end times of all the SEPEs. From this the time integrated flux (or fluence) and peak flux of each SEPE can be deduced from the time series. These two characteristics along with the duration of the SEPE and delay between events will be used in this work to model the SEPE environment. A key aspect of this modelling are the distribution fits made to the SEPE fluences and peak fluxes. Models of the SEPE environment use two distributions to model these SEPE characteristics: the lognormal distribution and the power law (often adjusted).

2.2.5.1 The Lognormal Distribution

The distribution of fluences of SEPEs has been fitted with a lognormal distribution for all models using the JPL method (Feynman et al., 1990, 1993, 2002) as were the 'ordinary events' in the King model (King, 1974). The probability density function (pdf) of the lognormal distribution is given by:

$$P(\phi) = \frac{1}{\phi\sigma\sqrt{2\pi}} \exp\left(-\frac{(\ln(\phi) - \mu)^2}{2\sigma^2}\right) \tag{2.2}$$

where ϕ is the event fluence, μ is the mean value and σ the standard deviation of the natural logarithms of the event fluences. The distribution function (cdf) is then given by:

$$F(\phi) = 1 - \frac{1}{2}\left(1 + \text{erf}\left[\frac{\ln(\phi) - \mu}{\sigma\sqrt{2}}\right]\right) \tag{2.3}$$

where $F(\phi)$ gives the likelihood of a single SEPE having a fluence in excess of ϕ. In modelling, this distribution would be randomly sampled using the cdf to get a fluence value for each event. Often in models the $\log_{10}$ of the event fluences were used which is not the standard form of the distribution but makes no difference as the opposite operation (either 10 raised to the power or the exponential) must later be performed.

It is well known that this distribution does not fit the entire range of the data as it is poorly fit at the lowest fluences as there are an increasing number of smaller events below the mean value (of the natural logarithms) while the distribution predicts a reducing number of smaller events. If this continually increasing numbers of smaller events is ignored and the fit only applied to the top half of the distribution a reasonable fit can be achieved. As the contribution from these smaller events is negligible in comparison to the large events the resulting under-prediction of the size of the smaller events is not significant. Changes in the minimum SEPE fluence parameter (see Section 2.2.4) will alter the distribution parameters (μ and σ). However, this should be balanced by an adjustment in the event frequency distribution (Feynman et al., 1990).

2.2.5.2 The Power Law

Power laws have been found to fit impulsive solar phenomena such as radio wave (Fitzerreiter et al., 1976), X-ray (Crosby et al., 1993) and gamma-ray (Lu et al., 1993)

flares. The cdf of this distribution is:

$$F(\phi) = 1 - \phi^{-b} \tag{2.4}$$

which gives the likelihood of a random event exceeding a value of ϕ, the integral of which gives the pdf:

$$P(\phi) = b\phi^{-(b+1)} \tag{2.5}$$

So the exponent is simply increased by 1 for the pdf compared to the cdf so both forms gives straight lines on double logarithmic axes.

A power law has been suggested for the frequency-size distribution for the proton events (Cliver, 1991; Gabriel and Feynman, 1996; Kurt and Nymmik, 1997), with the exponent of the pdf found to be between $1.15 - 1.45$. Belov et al. (2001) presented a catalogue of solar proton events in the energy channels > 10 MeV, > 30 MeV, > 60 MeV and > 100 MeV and GLEs (Ground-Level Enhancements) for the period 1976-2000. Values of 1.41 ± 0.04 (for > 10 MeV), 1.34 ± 0.05 (for > 30 MeV), 1.2 ± 0.03 (for > 60 MeV) and 1.12 ± 0.12 (for > 100 MeV) were found, thus indicating the slope values are dependent on the energy being considered.

The MSU model (Nymmik, 1999) uses a power law to model the fluence of events in the > 30 MeV energy range but it is noted that there is a shortage of low fluence events. This was attributed to an inability to detect these events resulting completely from the threshold effect of solar cosmic ray detection. The function quoted in Equation 2.11 in Section 2.3.3 is the pdf and quotes the exponent to be 1.41. If we integrate this function to find the cdf this is reduced to 0.41.

2.2.5.3 The Truncated Power Law

Feynman et al. (2002) noted that while a power law might fit the data well for the most part that there are fewer high fluence events from what a standard power law would predict and therefore that an arbitrary cut-off would be needed. A physical justification for the reduction in the fluences of the largest SEPEs is the streaming limit as discussed in Section 2.1.5. This makes power laws less favourable especially if a fluence higher than the maximum decided upon was possible but simply hadn't been observed as yet. The lognormal distribution has no similar issues. These largest events have a big impact on the overall fluence.

A solution proposed by Xapsos et al. (1998b, 1999) is to declare a maximum event size as a parameter to be found as part of a 'truncated' power law which would give a smoother tailing off than a sharp cut-off, this distribution was applied to both the peak flux and fluence of events. The maximum event size is strongly dependent on the maximum size of events in the data set. The exponent by Xapsos et al. (1999) found of 0.36 for the event fluence fit in the $>$ 30MeV range is comparable to that found by Nymmik (1999).

Xapsos et al. (1998b) fit the peak fluxes of events with a truncated power law and later applied this to event fluences (Xapsos et al., 1999). As a result, a maximum event size was found which defined the 'design limit' for spacecraft which it is predicted would not be exceeded by any single event's fluence (peak flux). The distribution function of the truncated power law is given by:

$$F(\phi) = 1 - \frac{\phi_{\min}^{-b} - \phi^{-b}}{\phi_{\min}^{-b} - \phi_{\max}^{-b}} \tag{2.6}$$

which gives the likelihood that a single event fluence (peak flux) will exceed the value ϕ. $\phi_{\min}$ is the minimum event fluence (peak flux) which is an input parameter when defining the event list while $\phi_{\max}$ is the maximum event fluence (peak flux) which along with b is to be determined. Using a maximum statistical entropy technique given by (Kapur, 1989) the truncated power law was found to be the distribution best suited to solar proton data.

2.3 Statistical Modelling

Statistical modelling in this sense refers to models of the Solar Energetic Particle Event (SEPE) environment for use in long-term predictions based upon statistical techniques and data recorded in the past especially since the mid-1960s when space-based instruments have been in operation to record particle fluxes. The results of models predicting the SEPE environment can be of particular use to the designers of spacecraft and spacecraft instruments. These models differ from physical modelling of SEPEs which employs physical theory to describe aspects of the environment such as the propagation of SEPs from their source at the Sun to their arrival at the observer using suitable approximations. An evaluation of solar proton models for ESA missions is given in Tranquille and Daly (1992).

Key outputs of models of the SEPE environment include: The cumulative mission fluence; the worst case peak flux; and the worst case event fluence. These outputs are dependent upon other factors such as particle species and energy range and can be displayed graphically in a variety of ways.

For modelling the statistics of the SEP environment it is standard to link consecutive enhancements where the flux does not return to the background level between events. Tylka et al. (1997) termed these 'episodes' and highlighted that a modelling technique which ignored an obvious correlation between enhancements would systematically under-predict the probability of such a sequence of events. Those studying the physics and creating physical models of SEPEs often refer to such a sequence as compound events while a single enhancement would be referred to as an isolated event (one example use of this terminology is Ho et al. (2003)). Kuznetsov et al. (2005) opposed the view that multiple enhancements should be considered a single event stating that each of the occurrences must be regarded as resulting from a certain single process originating on the Sun.

2.3.1 The King Model

The King solar proton model (King, 1974) was constructed using data obtained exclusively during the active years of solar cycle 20 (1966-1972). The stated aim of the model is to provide likely mission fluences for space missions from 1977-1983. The activity in solar cycle 20 was considerably less than that in solar cycle 19 and, in taking data from only one solar cycle (as a result of the lack of good data being available), King split the events into anomalously large events (of which there was only 1; the August 1972 event) and ordinary events (of which there were 24). This division was due to the massive difference in the fluence of the August 1972 event compared to the remaining events which made it hard to fit a single distribution to the complete list of events. The ordinary events were fit with a lognormal distribution. This is a problem caused by a limited amount of data.

The anomalously large events were taken to follow a Burrell distribution (Burrell, 1972) which is adapted from a Poisson distribution considering the issue of having only a single solar cycle's worth of data. The $\log_{10}$ of the fluence was taken to follow a normal distribution. SOLPRO is computer code based on the King Model and doc-

umented by Stassinopoulos (1975). In other regards the King modelling methodology is similar to that of the JPL fluence model which is covered in the next section.

2.3.2 The JPL Fluence Model

The JPL Fluence Model is a model predicting the mission cumulative fluence of solar protons which dominate the interplanetary proton fluence below 100 MeV; this is due, in the main, to a small number of very large events. The model is the result of a progression of work beginning with the JPL-85 model (Feynman et al., 1990), before the JPL-91 model (Feynman et al., 1993) and the update of this model by Feynman et al. (2002).

The method followed is similar to that of the earlier model by King with a key difference that it does not distinguish between anomalously large and ordinary events. Again, the model takes the event frequency as being Poissonian and assumes the $\log_{10}$ of the fluence to be distributed normally.

The JPL-85 model included data from cycles 19, 20 & 21 with the data from 1956 to 1963 (solar cycle 19) taken from instruments on weather balloons and rocket experiments, whereas the data from cycles 20 & 21 was taken from space-based measurements. The data used by JPL-91 was collected by closely related instruments on the IMP-1, -2, and -3, OGO 1 and IMP-5, -6, -7 and -8 spacecraft between 1963 and 1991 and did not include earlier rocket and balloon data, this was seen an improvement in terms of the homogeneity of the data set. The update uses data from day 126 of 1991, where the JPL-91 data ends, to day 365 of 1993 and therefore covers 3 complete solar cycles (20, 21 and 22). The update used only data in the $>$ 10 MeV energy range.

An 'event' is defined as the total fluence occurring over a number of days during which the daily proton fluence exceeds a selected threshold and it is said to have ended when the daily flux has fallen below the threshold for two consecutive days. The threshold values used in the JPL models in terms of the average flux for the integral flux channels are shown in Table 2.5. In the $>$ 10 MeV proton channel the flux threshold of 1 pfu corresponds to a daily fluences of 1.08×10^6 cm^{-2} (Feynman et al., 2002).

An important assumption was that the 11 year solar cycle can be partitioned into

Table 2.5: JPL Flux threshold values (Feynman et al., 1990).

> 1 MeV	> 4 MeV	> 10 MeV	> 30 MeV	> 60 MeV
10 pfu	5 pfu	1 pfu	1 pfu	1 pfu

pfu = particle flux unit = $\mathrm{cm}^{-2}\mathrm{s}^{-1}\mathrm{sr}^{-1}$

a 7 year solar maximum (active years) and a 4 year solar minimum (quiet years) and that the quiet years can be ignored for the purpose of modelling the cumulative mission fluence as the contribution from those years is negligible compared to that from the active years (Feynman et al., 1990). The contribution of SEPEs at solar minimum would be important if the spacecraft designer knew that the mission was to be launched and operate only during a time of solar minimum. Solar maximum is determined to 0.1 years, with the active period beginning 2.5 years before solar maximum and ending 4.5 years after it.

The Poisson distribution used in the JPL models (Feynman et al., 1990, 1993) to model the event frequency distribution is a discrete probability distribution that expresses the probability of a number of events occurring in a fixed period of time if these events occur with a known average rate, and are independent of the time since the previous event. The form of the Poisson distribution given by (Feynman et al., 2002) is:

$$p_k(t) = \frac{(wt)^k}{k!} e^{-wt} \tag{2.7}$$

where w is the average number of events per year (e.g. taken as 6.75 for the > 10 MeV energy range), t is the time period (or mission length) being considered in years and $p_k(t)$ is the probability of seeing k events in that time period.

Another important component of the JPL fluence model is the use of a lognormal distribution to fit the ranked event fluences; from this mission integrated fluences are given which won't be exceeded with a given degree of confidence for that particular energy level. The probability density function is given by:

$$p(F) = \frac{1}{\sigma\sqrt{2\pi}} \exp[-(F-\mu)^2/2\sigma^2] \tag{2.8}$$

where σ is the standard deviation of the log distribution, μ is the mean $\log_{10}$ fluence and F is given by $f_p = 10^F$ where f_p is the proton fluence associated with a particular event.

The use of a normal fit implies that there will be a peak at some value but in fact the number of events keeps growing with reducing fluence. The justification is that when concerned with the total fluence for a long enough period of time, the smaller event fluences will not be significant in any case. A lognormal distribution fitted to the $>$ 60 MeV solar event fluences for the time period 1963-1991 is shown in Figure 2.5.

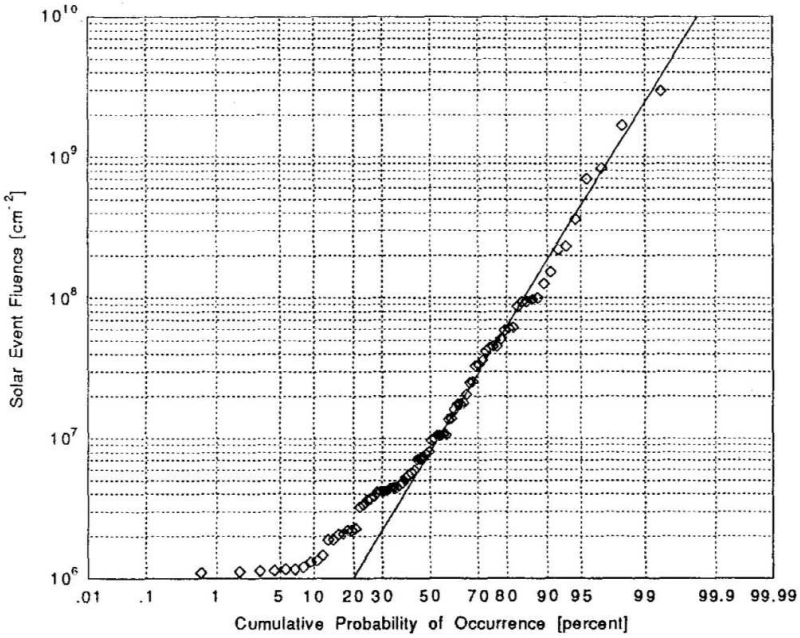

Figure 2.5: Lognormal distribution fitted to $>$ 60MeV event fluences (Feynman et al., 1990).

The total mission fluence may then be calculated using:

$$P(> F, \tau) = \sum_{k=1}^{\infty} p_k(t) Q(F, k) \tag{2.9}$$

where $Q(F, k)$ is the probability that the sum of fluences due to k events will exceed 10^F and is calculated by summing fluences from SEPEs generated by a large number of Monte-Carlo simulations with that number of events. $P(> F, \tau)$ can then be calculated as the proportion of the total number of simulations for all numbers of events where the summed fluences were greater than F with the proportion of the total number of simulations for k events being equal to p_k.

Curves are produced for different integral energy ranges ($>$ 1, $>$ 4, $>$ 10, $>$ 30 & $>$ 60 MeV) for finding the likelihood that a certain fluence will not be exceeded

for a set time period (1, 2, 3, 5 & 7 years). When using the model to calculate a mission fluence for a given confidence level any mission length between 7 and 11 years can be taken at the 7 year fluence level as at least 4 from the 11 years will be at solar minimum and the fluences in these years are not seen as significant. The fluence probability curves for each of these time periods again for the > 60 MeV channel are displayed (see Figure 2.6).

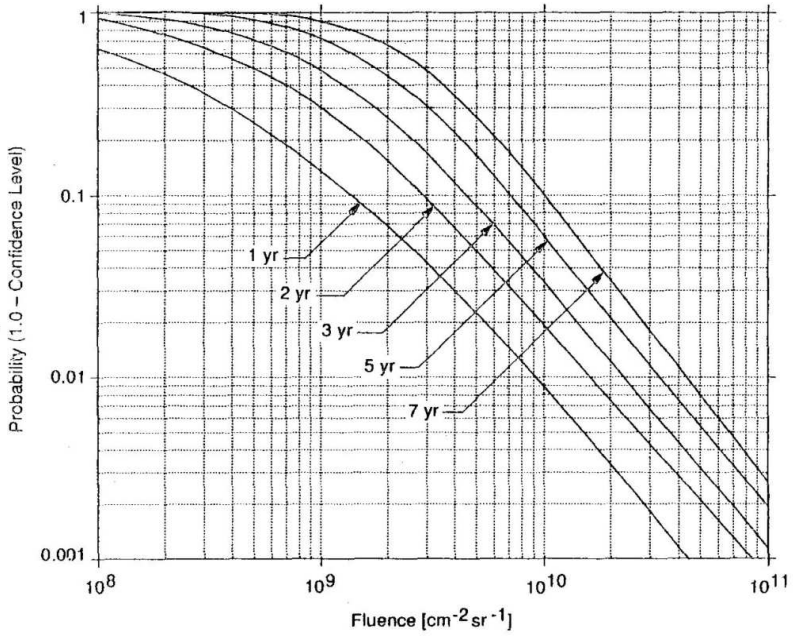

Figure 2.6: JPL-91 predicted mission integrated fluences for $>$ 60MeV energy range (Feynman et al., 1990).

The JPL-91 model predicts lower fluences than the JPL-85 model, these differences between the outcomes must be down to the data. This could mean either the calibration of the data, a time variation of the intrinsic properties of the underlying distribution function of solar particle events or possibly normal statistical fluctuations due to the small size of the data set (Rosenqvist and Hilgers, 2003).

The JPL model update (Feynman et al., 2002) uses IMP-8 data to expand the data set from day 126 of 1991 where the JPL-91 data ends to day 365 of 1993 bringing the number of events from 114 to 202 for the $>$ 10 MeV range and concludes that the results produced by the JPL-91 model are still valid verified by the more recent data and that there is no significant change to the fitting parameters.

2.3.2.1 Extension to Heavy Ions

In 1997 using data from 1973 to 1996 a model was created for heavy ions including Helium (He) nuclei, grouped Carbon Nitrogen and Oxygen nuclei (CNO) and Iron (Fe) nuclei which were considered as important causers of displacement damage and SEEs (Single Event Effects). This can be found in 'Probability distributions of high-energy solar-heavy-iron fluxes from IMP-8: 1973-1996' (Tylka et al., 1997). The method used follows closely that used in the JPL-91 proton fluence model (Feynman et al., 1993). Alpha particles can cause much more displacement damage ($\sim \times 40$) than protons of the same energy but the average ratio of protons to alpha particles in a Solar Particle Event is only 3.6%. Still, this makes their impact significant and additionally they can also be significant for SEEs. There is some discussion by Tylka et al. (1997) about the relevance of heavy ions and what range of ions atomic number (Z) needs to be considered for the solar energetic particle environment.

The data were taken from the IMP-8/CRT (University of Chicago's Cosmic Ray Telescope) from between 30$^{\text{th}}$ October 1973 and 18$^{\text{th}}$ September 1996. Data from GOES-7/MEPAD were used to correct for 'dead-time' errors, typically the corrections were for a factor of ~ 1.5 although the peak was a factor of ~ 7 for the 20$^{\text{th}}$ October 1989 event. Selected events had an accumulated fluence of > 10 MeV protons exceeding 10^7 protons/cm^2, this corresponds to roughly an order of magnitude increase over the typical GCR proton fluence.

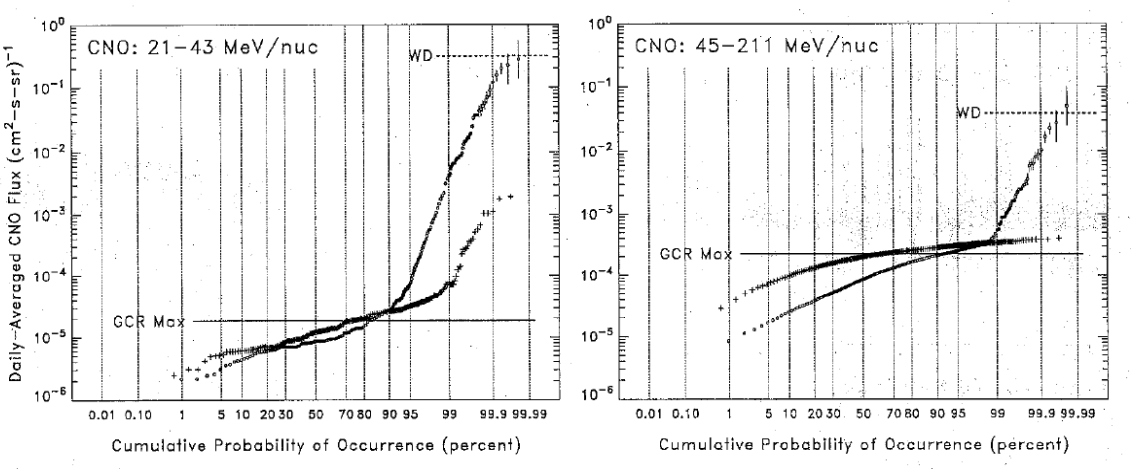

Figure 2.7: Cumulative probability of daily averaged fluxes for CNO at 2 energy levels (Tylka et al., 1997).

The cumulative probability distributions of daily averaged fluxes show steep increases above the 90^{th} quantile. This highlights that if only 90% certainty were needed then the prediction of fluxes would be a lot lower - the extent to which this is true is dependent both on the species and the energy level. This is illustrated in the diagrams for the CNO nuclei in the two bins taken from the paper by Tylka et al. (1997) in Figure 2.7. This method being based on the JPL method will have many similar drawbacks but additionally the results have been deduced from only 2 solar cycles with only 95 events and therefore might not be representative of the whole.

2.3.3 The MSU Model

The Moscow State University (MSU) Model (Nymmik, 1999) takes a different approach to modelling and attempts to resolve the event statistics with what are perceived to be the fundamental physical statistics. Kuznetsov et al. (2005) states that statistical models should reflect the physical reality of the underlying processes at work and that:

- Any statistical event should correspond to a single physical event.
- SEPE occurrence frequency linked to solar activity as a smooth function.
- The fitting function for SEPE size should be a power law (albeit truncated).
- The particle flux is required to be expressed as a function of energy and that there should be a continuous SEP energy spectra.
- A model must include all solar heavy ions.
- Ion flux prediction must be based upon the limited data and relative compositions.
- We must confirm the reliability of data with that from different instruments.

These guidelines appear to form the basic premise of the MSU model. The MSU model (Nymmik, 1999) describes the probability of event fluences and peak fluxes to occur in the near-Earth space beyond the Earth's magnetosphere under varying solar activity levels from protons to heavy ions ($Z = 2 - 28$) with energy $\geq$ 10

MeV/nucleon. The data used to generate these models mixed IMP and OGO data with data from instruments on MIR (information from personal communication featured in Feynman et al. (2002)).

The SEP size (initially taken to be the > 30 MeV proton fluence size) distribution is described by a power-law function within a $10^5 - 10^{11}$ proton/cm^2 range. This can then be extended to other energies using the described energy spectral form.

By linking the event frequency to sunspot number the MSU model considers events during solar minimum as well as solar maximum. It also takes the solar activity dictated by sunspot number upon which is based the distribution governed by a power law. The mean occurrence frequency for ≥ 30 MeV proton fluences $\Phi_{30} \geq 10^6$ protons/cm^2 is given by:

$$\langle \nu(t) \rangle = 0.18 \cdot W(t)^{0.75} \text{events/year} \tag{2.10}$$

where $W(t)$ is the yearly sunspot number. The frequency-size variation for ≥ 30 MeV proton fluence is given by:

$$\psi(\phi) = \frac{1}{N} \frac{\mathrm{d}N(\phi)}{\mathrm{d}} = C \cdot \phi^{-1.41} \tag{2.11}$$

where N is the number of events and ϕ is the fluence of the events. The MSU model also employs the Poisson distribution with the input for the mean rate for the total time period (or mission length) coming from the relationship given in Equation 2.10. So an estimate of the solar activity, determined by the sunspot number, is required. Belov et al. (2001) showed that the correlation between proton events occurrence and sunspot number was found to be 0.76 while the correlation between proton events and SXR (Soft X-ray) flares of class 4M or above was found to be 0.94, using yearly values in both instances. This highlights that perhaps sunspot number is not the most appropriate measure of solar activity as regards a link to solar proton events. Additionally, the necessity to predict the sunspot number for the years of the mission lifetime is non-trivial and cannot currently be done reliably (as explained in Section 2.1.4); this makes any model dependent upon a known sunspot number as an input less reliable.

As a further justification for this method beyond the postulated requirement for a power law Nymmik (1999) gives an illustration of the better correlation (by least

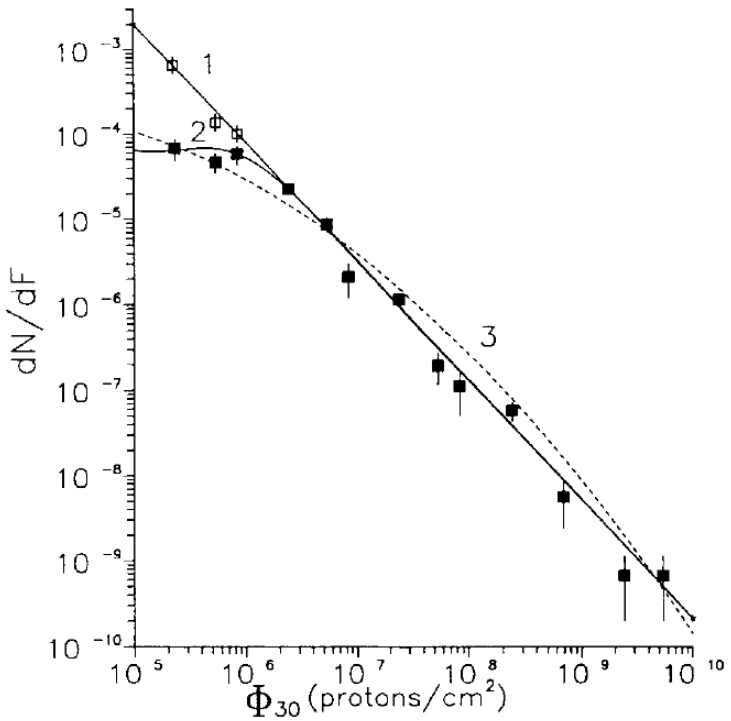

Figure 2.8: Plot of event fluence against occurrence frequency (Nymmik, 1999).

squares) for observed ≥ 30 MeV proton fluence events using a power law than a log-normal distribution with data provided by Gabriel and Feynman (1996). The graph is shown here with curve (1) being the power law, curve (2) being the power law accounting for minimum threshold effect and curve (3) being the lognormal distribution (see Figure 2.8). The light squares are experimental data corrected for the threshold effect.

The paper explains that the SEP energy spectra at E > 30 MeV are mostly power law functions of particle momentum rather than exponential functions of energy or rigidity. The equation given to describe this spectral relationship is:

$$F(E)\mathrm{d}E = F(p)\frac{\mathrm{d}p}{\mathrm{d}E}\mathrm{d}E = C \cdot \left(\frac{p}{p_0}\right)^{-\gamma} \cdot \frac{\mathrm{d}E}{\beta} \tag{2.12}$$

where E is the energy, β is the relative particle velocity, γ is the spectral index and p is the particle momentum; $p_0 = 239$ MeV/c. The heavy-ion-to-proton flux ratio is not treated as constant as assumed by the CRÈME model and instead it is taken as being dependent on energy.

There is a need to apply a 'droop' factor to the spectral index for higher energy particles as the power law overestimates the number of events at this end of the scale.

The correction factors that are applied as part of the model appear a little arbitrary and additional data at high energies would be needed to verify these findings. Using a power law for proton fluences has been shown to over-predict the number of large events that are seen, this problem can be solved by introducing a maximum event size resulting in a truncated power law but what to choose for this value is debatable.

The definition of an event in the MSU model is unclear but if it follows the guidelines set out by Kuznetsov et al. (2005) then the definition differs markedly from that used in other models and for the rest of this work. The danger in using such an event definition is that consecutive enhancements may be in linked both in clusters of enhancements (in time) and the inter-dependence of the intensities of consecutive enhancements. At other times it may be impossible to connect an enhancement to a single physical phenomena, these issues were discussed in Section 2.1.5. Any model using this event definition would need to overcome all of these problems.

2.3.4 The Emission of Solar Proton (ESP) Models

One set of models that utilises truncated power laws are the ESP models. These use maximum entropy theory (Kapur, 1989) to select the least biased distribution in the face of missing information. There are three models; the probability models for: peak fluxes of solar protons (Xapsos et al., 1998b), worst case solar proton event fluences (Xapsos et al., 1999) and cumulative solar proton event fluences (Xapsos et al., 2000). The first two of these models use a truncated power law, the third uses a lognormal distribution and the event frequency is taken to be Poissonian.

The data used for the peak flux model was the >10 MeV values published for solar cycles 20 and 21 by Shea and Smart (1990) including data from the GOES spacecraft and polar riometer extrapolated to find fluxes augmented with data from the IMP-7 and IMP-8 spacecraft and the >10 MeV values for cycle 22 published by NOAA in Solar Geophysical Data Reports (1994) which also uses GOES data. The peak flux model considers a minimum event flux of 1 pfu.

The data used for the fluence models was from IMP-3, -4, -5, -7 & -8 (cycle 20), IMP-8 (cycle 21) and GOES-5, -6 & -7 (cycle 22) which extends up to much higher energies. By using the available GOES data from cycle 22 and comparing them to the results for >1 MeV to >100 MeV an empirical formula was drawn up to extrapolate

the data beyond 100 MeV allowing extension of energy range for predictions from > 1 MeV to > 300 MeV as shown for 90% confidence level compared with The JPL Model at lower energies (see Figure 2.9), taken from the ESP cumulative solar proton fluence model.

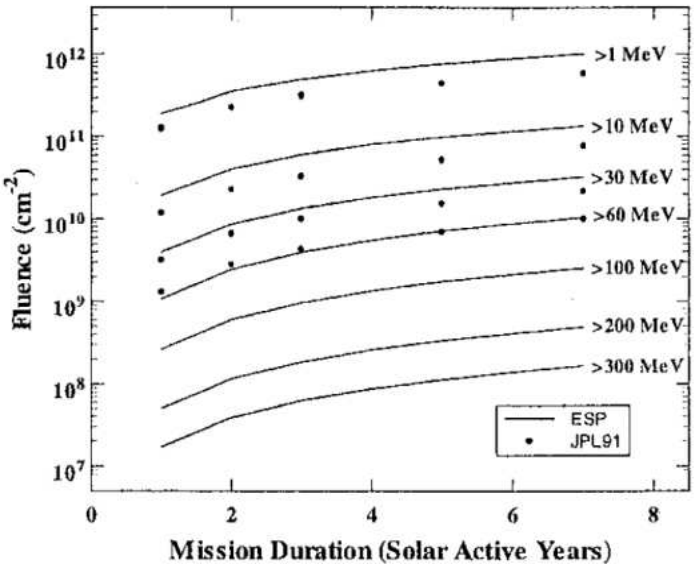

Figure 2.9: Predictions of cumulative fluence for various mission lengths and various energies for the ESP model (lines) compared with the JPL-91 model (points) (Xapsos et al., 2000).

The beginning and end of an event are identified by a threshold proton flux so that successive rises and falls in flux may be combined into one event where appropriate in the same way as the JPL models did. Additionally there are minimum event fluences considered for the whole range of energies, a sample of this is given (see Table 2.6).

> 1MeV	> 10MeV	> 30MeV	> 60MeV	> 100MeV
$5.0 \times 10^{8}\text{cm}^{-2}$	$2.5 \times 10^{7}\text{cm}^{-2}$	$3.0 \times 10^{6}\text{cm}^{-2}$	$3.0 \times 10^{5}\text{cm}^{-2}$	$1.0 \times 10^{5}\text{cm}^{-2}$

Table 2.6: Sample of minimum event fluences used in ESP model (Xapsos et al., 1999)

These models also use only data from active years of the solar cycle; the 7-year period beginning 2.5 years before and ending 4.5 years after the point of solar maximum. The 3 solar maxima for the time period considered are taken to be 1968.9, 1979.9 and 1989.9. This is the same as the JPL approach and differs from that of Kuznetsov et al. (2005).

The assumption is that the occurrence of solar proton events is a Poisson process with a constant mean rate but an actual rate varying about that mean value. The maximum entropy technique (Kapur, 1989) dictates that the statistical entropy, S, is maximised, S is given by:

$$S = -\int p(M)\ln[p(M)]\mathrm{d}M \tag{2.13}$$

where $p(M)$ is the probability density function, ϕ is either the event peak flux or the event fluence depending on the model and $M = \log_{10}(\phi)$.

For this technique it is necessary that there is a defined minimum (which are illustrated above), a well defined mean, that the probability distribution can be normalised and crucially that there is an upper limit the value of which can be found later. Some processing using the Lagrange multiplier technique is required until ultimately

$$N = N_{\mathrm{tot}}\frac{\phi^{-b} - \phi_{\mathrm{max}}^{-b}}{\phi_{\mathrm{min}}^{-b} - \phi_{\mathrm{max}}^{-b}} \tag{2.14}$$

and

$$P(\phi) = \frac{\phi^{-b} - \phi_{\mathrm{max}}^{-b}}{\phi_{\mathrm{min}}^{-b} - \phi_{\mathrm{max}}^{-b}} \tag{2.15}$$

are arrived at for the peak flux and worst case fluence models. Here, ϕ_{min} is the minimum peak flux (fluence) considered (note that this is 1 for the peak flux model which is considering > 10 MeV proton flux events of 1 pfu or more only but varies for the fluence model with different energies as stated above), $P(\phi)$ is the cumulative distribution in terms of ϕ, N_{tot} is the total number of events with peak flux (fluence) above 1 pfu, ϕ_{max} is the maximum peak flux (fluence) and ϕ is the peak flux (fluence) which is being exceeded by the number of events N. Where $\phi \ll \phi_{\mathrm{max}}$ this simplifies to the power law:

$$N = N_{\mathrm{tot}} \cdot \phi^{-b} \tag{2.16}$$

A double logartihmic plot of the data and a least squares regression fit between 10 and 10^3 pfu facilitates the calculation of N_{tot} and b from the intercepts for ϕ_{min} and the slope respectively and a further least squares regression fit was carried out to find a values for ϕ_{max}. The > 30 MeV fluence graph from worst case solar proton event fluences model (Xapsos et al., 1998b) fitted using this truncated power law is shown (see Figure 2.10). A power law is a straight line on a double logarithmic axes and the deviation from the straight line in the figure is the effect of the truncation.

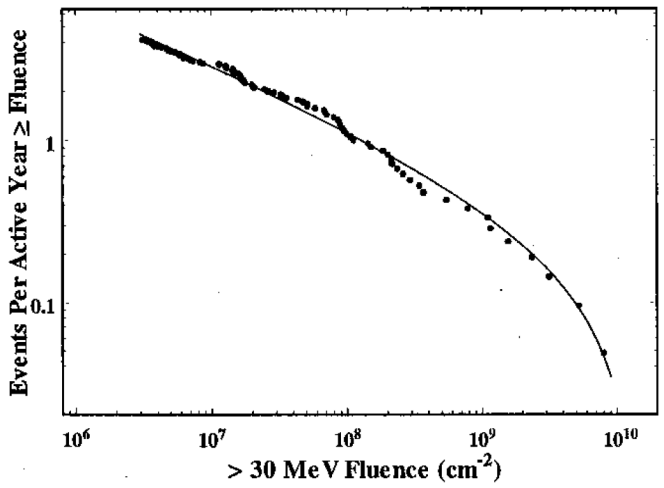

Figure 2.10: $>$ 30MeV event fluence fitted by truncated power law (Xapsos et al., 1999).

Extreme value theory gives the worst case peak flux (fluence distributions) over T active years to be given by:

$$F_T(M) = \exp\{-N_{\text{tot}}T[1 - P(M)]\} \tag{2.17}$$

where $F_T(M)$ is the confidence level and $P(M)$ is the cumulative distribution which can be taken from $P(\phi)$ given in Equation 2.15.

The value of $\phi_{\max}$ for the fluence model was found to be 1.32×10^{10} cm^{-2} denoted as the 'Design Limit'. This is approximately 1.5 times the largest observed fluence for the $>$ 30 MeV data. The model essentially predicts that this design limit will never be exceeded. A similar method is followed for the peak flux giving a value of 1.78×10^5 pfu for $\phi_{\max}$. The graph of probability of exceeding a fluence for $>$ 30 MeV protons after 1, 3, 5 & 10 year active year periods from the worst case solar proton event fluences model (Xapsos et al., 1999) is given and includes the 'Design Limit' (see Figure 2.11).

The maximum entropy technique applied for the cumulative fluence model in contrast shows that the best choice of a probability distribution is the lognormal distribution fitted to the yearly fluences. This is despite the initial distribution - the distribution of solar proton event magnitudes (either event fluences or event maximum fluxes, depending on application) - being found to be a truncated power law. It can be shown that the use of these 2 distributions in this fashion is completely consistent

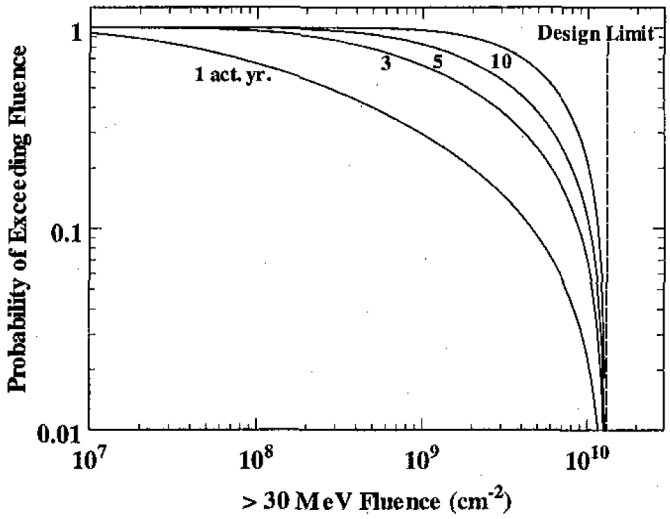

Figure 2.11: Probability of exceeding event fluence for various time periods (Xapsos et al., 1999).

(M. Xapsos, personal communication, 2007). The fit to yearly fluences may then be extended to other time periods analytically by use of Poisson assumptions.

The resulting lognormal cumulative fluence distribution is given by:

$$F_{\mathrm{CUM}}(\phi') = \frac{1}{\sigma\sqrt{2\pi}} \int_0^{\Phi} \frac{1}{\phi'} \exp\{-\frac{1}{2\sigma^2}[ln(\phi') - \mu]^2\} \mathrm{d}\phi' \tag{2.18}$$

where F_{CUM} is the confidence level of observing a total proton fluence no greater than ϕ over a time period of T active years, σ and μ are the standard deviation and mean parameters. The mean fluence for T years is $T \times \phi_{mean}$ where ϕ_{mean} is the mean 1-year fluence given by:

$$\phi_{mean} = \exp\left(\mu + \frac{\sigma^2}{2}\right) \tag{2.19}$$

The relative variance for T years is ϕ_{RV}/T where ϕ_{RV} is the relative variance for 1 year given by:

$$\phi_{RV} = \exp(\sigma^2) - 1 \tag{2.20}$$

where μ and σ are the normal characteristic mean and standard deviation for the natural logarithm of the yearly fluences.

For an extension to different energies away from > 30 MeV, the empirically derived fluence-energy spectrum is given by:

$$\phi = \phi_0 \exp(-kE_{\mathrm{th}}^a) \tag{2.21}$$

where E_{th}^{a} is the threshold energy in MeV and ϕ_0, k and a are fitted constants.

The truncated power law has a similar index to that Gabriel and Feynman (1996) reported for an ordinary power law, the truncation is seen as necessary due to the tail off in event frequency seen above fluences of 10^9 cm^{-2} as shown in Figure 2.10.

The ESP model follows a thorough technique using modern statistical methods including maximum entropy and the above equations to predict fluences and peak fluxes. As with the JPL model a Poisson distribution for modelling the event frequency is used and this assumption is to be investigated in this work. The ESP cumulative fluence model is currently the ECSS Standard (2008) (section 9.2.2).

2.3.5 Toolkit for Updating Interplanetary Proton-Cumulated Fluence Models

In a study of the various decisions and assumptions made when creating statistical models by Rosenqvist et al. (2005), it was found that by changing the fitting parameters only a small amount model outputs can be drastically altered. The authors made a series of recommendations for how any proton fluence model might be updated to mitigate certain issues that can modify model prediction. They used the JPL-91 model to exemplify this. The effects that can modify model prediction were identified as the following:

1. Event selection criteria
2. Choice of flux threshold
3. Choice of fluence threshold
4. Identification of high activity part of the solar cycle
5. Parameter fitting procedure of event intensity distribution
6. Size of data set
7. Calibration uncertainty
8. Data gaps
9. Data errors

One aspect investigated by the authors is the possibility of cross-calibrating data to correct errors in data sets. 4 main factors were identified as producing the differences between models following the same procedure. These were: the cross-calibration of the sources, data errors and missed events, and the division of events into multiple or single events. Additionally, the data used came from GOES-7, GOES-8, and IMP-8/GME rather than IMP-8/CPME as the data was seen as being of higher quality due to caveats such as saturation known to exist in the IMP-8/CPME data set.

By carrying out some processing on the data prior to following the method laid out by Feynman et al. (1993) and using the updated data set the authors present a new model for the >10 MeV proton range the results of which vary from the original JPL-91 Model. Rosenqvist et al. (2005) also altered the threshold used for event definition in the >10 MeV energy range to 1, 2, 5 and 10 pfu noting little direct impact as the total fluence is dominated by the higher fluence events. There can be indirect impact seen through the event selection criteria, by varying the threshold it may alter the number of flux enhancements registered in a single SEPE (events may be split using higher flux thresholds).

A comparison was carried out between JPL-91 and JPL-85 models and fitting procedures. It was shown that there are greater differences seen at the higher quantiles for the models (more than factor 2 for the 95^{th} quantile (1-year fluence in the $>$ 10 MeV energy range)) caused exclusively by differences in the fitting parameters. Rosenqvist et al. (2005) created two new data sets generated for the same time period as the JPL-91 and JPL-85 models using IMP-8/CPME, IMP-8/GME and GOES data correcting for dead-time and data gaps. These new data sets produced different fitting parameters to the original JPL-91 and JPL-85 models. Despite a greater deduced difference between the mean of the $\log_{10}$ fluences (for the two new data sets) there were closer deduced values for the average number of events per year and the standard deviation of the $\log_{10}$ fluences and this resulted in closer model outputs (about 25% discrepancy on the 95^{th} quantiles (1-year fluence in the >10 MeV energy range)). It was concluded that the remaining differences can be as a result of natural statistical variation related to the finite size of the data sets or uncertainty in ground-based measurements used for the JPL-85 model compared to the more homogeneous JPL-91 data. This highlights the importance of choosing fitting parameters for data and

the impact small changes in this can have. It is noted in the study that small changes in the parameters for the data sets used and those from the JPL-85 and JPL-91 models are possibly due to a change in the dates of solar maximum used which were derived from the 13-month running mean international sunspot number from the World Data Center for the Sunspot Index (SIDC) by Rosenqvist et al. (2005).

One of the most interesting facets of the paper by Rosenqvist et al. (2005) involves discrepancies and cross calibration between data sets. For this study, events for which there is disagreement between the data sets for event grouping were excluded (where periods in the time series were treated as a single event in one case or multiple events in another due to discrepancies in the data). The data sets compared were IMP-8/GME, IMP-8/CPME, GOES-6, GOES-7, GOES-8 and GOES-10 for time periods where they overlapped. A linear fitting was done using the log values of the fluence for the two data sets being compared; this gives the possibility of calibrating one data set using another. Particular caveats in the data included:

- Large discrepancies between GOES-6 and GOES -7 (GOES-7 returning an average of about twice the fluence).
- GOES-8 results are in general about twice the fluence of those measured by GOES-10.
- Comparing IMP-8/GME and IMP-8/CPME with GOES data shows that GOES-6 and GOES-10 have lower fluences while GOES-7 and GOES-8 data compares well.
- The IMP-8/CPME data measures lower fluences in the largest events which is likely a saturation problem with the instrument that has been reported.
- By cross-calibrating between GOES-8 and IMP-8/CPME there is a far closer agreement between the two sets than previous to the calibration.

The suggestion for using current data due to issues (caveats) with the GOES-12 and GOES-10 data is to cross-calibrate the GOES-10 data with the GOES-8 data which was shown to be well correlated with data from the IMP-8 and GOES-7 data and is therefore assumed to be reliable.

The method of calibration is to take the log fluences from two data sets and plot them finding the intercept, l, and the slope, d, as per:

$$\log(F_1) = l + d \cdot \log(F_2) \tag{2.22}$$

where F_1 and F_2 are the two data set fluence values. It is important to gather which data set is the most accurate and which needs to be calibrated. As there is no direct way of testing the instruments in space it is assumed that those data sets which have the greatest agreement with others are the most accurate. Samples of the comparisons are shown in Figure 2.12.

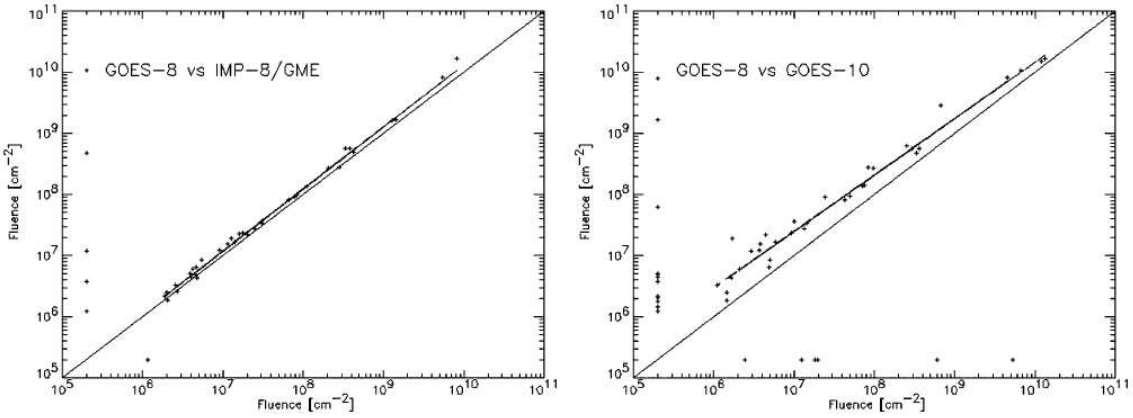

Figure 2.12: Cross-calibration plots of SEPE fluences from GOES-8 vs IMP-8/GME (left) and GOES-8 vs GOES-10 (right) (Rosenqvist et al., 2005).

By cross-calibrating the data used in the models prior to producing those models as per the methodology of Feynman et al. (1993) different fitting parameters were found which resulted in noticeable differences in mission integrated fluences. The work done by Rosenqvist et al. (2005) can be seen to represent an upgrade of the JPL-91 solar proton fluence model (in the the > 10 MeV energy range) based on calibrated data from a number of sources.

2.3.6 PSYCHIC Model

The PSYCHIC (Prediction of Solar particle Yields for CHaracterizing Integrated Circuits) model (Xapsos et al., 2004) for cumulative solar proton fluences is an expansion of the work done on the ESP models (Section 2.3.4) and the improvements can be identified under three main headings:

1. The improvement of the underlying database through the integration of IMP and GOES data to exploit the strong points of each data set.

2. The extension of the energy range of cumulative proton fluences being modelled for out to energies of 327 MeV.

3. The modelling of the solar minimum phase in addition to the solar maximum phase of the solar cycle.

The first of these was achieved in the creation of an Integrated Data Set (IDS) combining IMP-8/GME and GOES/SEM data to capture the best qualities of both. It uses the IMP-8/GME data as a baseline as that data set contains data from a long time period with 30 energy bins ranging from 0.88 to 485 MeV with sufficiently fine increments. This is supplemented with GOES data as the SEM instrument onboard performs very well during high flux rates unlike the GME instrument which has a tendency to saturate. The GOES data is not available in such fine energy increments nor is the orbit as good for measuring interplanetary fluxes at the lowest energies due to geomagnetic shielding, there is also discrepancy between GOES instruments. Due to these factors the GOES data replaces the IMP-8/GME data only when the GME instrument is saturated. To extend the time range to before 1986 which was the limit of available GME data set when the model was created, data from IMP-8/CPME (from 1973-1986) and from IMP-3, -4 & -5 satellites (1966-1972) taken from analysis done by King (1974) was used. To include a wide range of events significant at both high and low energies the whole time series was analysed manually and enhancements where included in the event list where the peak differential flux was > 4 cm^{-2}s^{-1}sr^{-1}MeV^{-1} in the 1.15 to 1.43 MeV range or > 0.001 cm^{-2}s^{-1}sr^{-1}MeV^{-1} in the 42.9 to 51.0 MeV range.

The second improvement is enabled by use of all of the differential channels available on IMP-8/GME supplemented with GOES/SEM data and represents a significant improvement on previous models including the ESP model which, although it extends to a > 300 MeV energy range, provides a true statistical model is only from > 1 to > 100 MeV and an extrapolation is performed to extend this to > 300 MeV. The PSYCHIC model is based on actual data for the whole range and is therefore seen as more reliable. Good agreement is found for overlapping energy ranges of

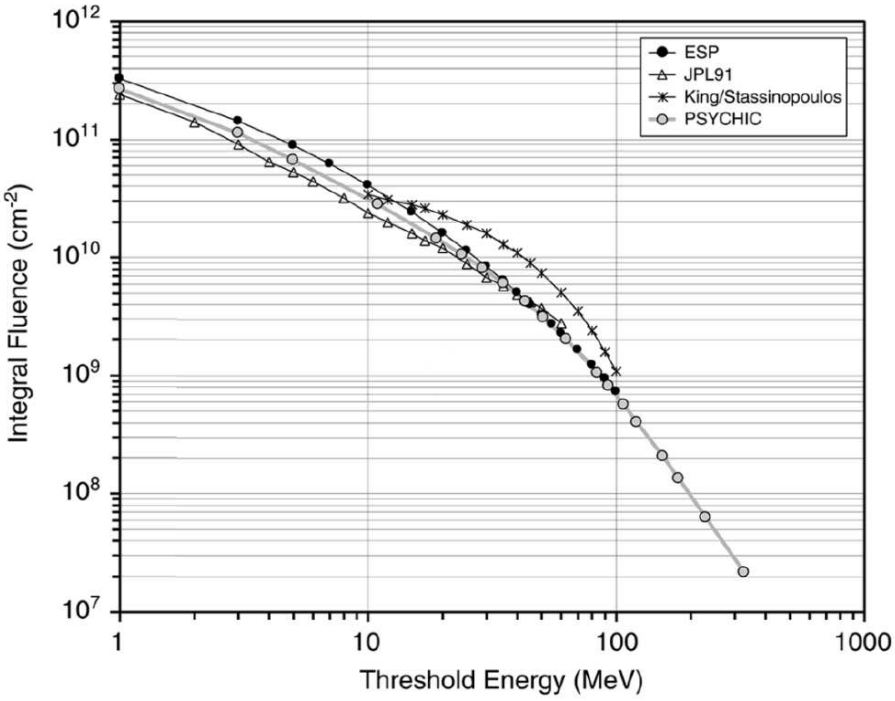

Figure 2.13: Comparison of solar proton cumulative fluence models for a 2-year mission during solar maximum at the 90% confidence level (Xapsos et al., 2007).

ESP (Xapsos et al., 2000), JPL-91 (Feynman et al., 1993) and PSYCHIC and shown in Figure 2.13 taken from Xapsos et al. (2004), the different energy spectrum of the King Model (King, 1974) is due to its being based purely upon the August 1972 event.

The third change is to analyse the solar minimum period by taking yearly averages of the fluxes at solar minimum. Taking the most conservative estimate of fluence at solar minimum (so as to avoid possibly dangerous under-prediction) the fluences were obtained by summing the fluences from the solar minimum period at the end of cycle 20 and beginning of cycle 21 and dividing by the total time, the harshest seen outside solar maximum in the data set (Xapsos et al., 2004). It was found that the fluence was significantly smaller at solar minimum than at solar maximum but that the difference was more exaggerated at high energies indicating that the spectrum was harder during the solar active years. The cumulative fluence for an 11-year mission taken from Xapsos et al. (2004) is shown in Figure 2.14. To summarise these points it is stated in the conclusion that during solar minimum, the event frequencies are smaller, the event magnitudes are smaller, and the energy spectra are softer (Xapsos et al., 2004).

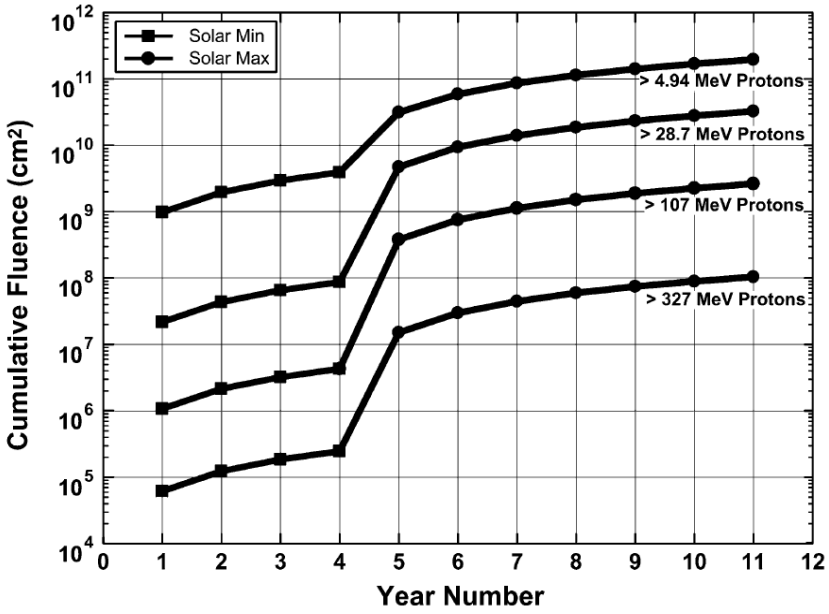

Figure 2.14: Cumulative fluence for protons of different energy ranges over the course of an 11-year mission. The first four years are during solar minimum (using the worst solar minimum period) and the last seven are during solar maximum using the original ESP technique (at the 90% confidence level.) (Xapsos et al., 2004).

The extension of the PSYCHIC model to heavy ions (Xapsos et al., 2007) makes use of the IDS constructed for PSYCHIC and compares the alpha particle spectrum to that of the solar proton spectrum for the solar maximum periods between 1973 and 2001 meaning an alpha particle spectrum can then be deduced from the proton spectrum. The spectra of the major heavy elements (C, N, O, Ne, Mg, Si, S & Fe) from the ACE/SIS instrument taken from 1998 through 2004 are compared to the alpha particle summed over the 7 years giving a relationship between these elements and the alpha particles on which the model is then based. Finally, the spectra for the minor heavy elements (excluding atomic numbers Z = 43, 61, 84 - 89 & 91) are calculated by comparison to the closest major heavy element in the Periodic Table using data from the International Sun-Earth Explorer (ISEE-3) spacecraft and an abundance model. This allows fluence values to be calculated for different elements at different energies as shown in Figure 2.15.

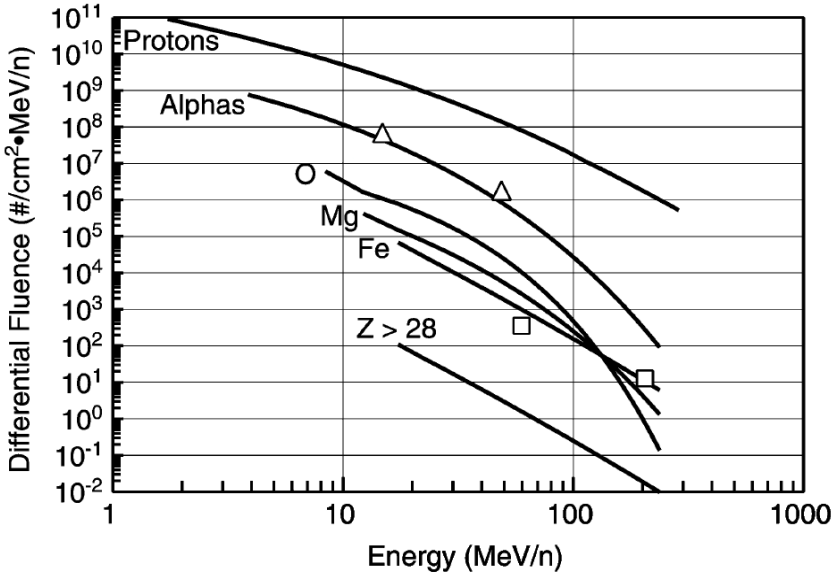

Figure 2.15: Differential fluence-energy spectra from protons, alpha particles, oxygen, magnesium, iron and summed for Z > 28 elements for a 2-year mission during solar maximum at the 90% confidence level (Xapsos et al., 2007). The triangles and squares in the figure are taken from the analysis by Tylka et al. (1997)

Chapter 3

The Background Data

This chapter contains a review of three Solar Energetic Particle Event (SEPE) lists which were used in this research, methods of processing or 'cleaning' data and a new list which is hereafter referred to as 'The SARG (Southampton Astronautics Research Group) Event List'.

The process of creation of a new event list would ideally be to first create a continuous time series spanning the time for when data is available by processing all the raw data to be used and then choosing instruments for different periods of time (this choice would be dependent upon the quality of the various available data). Only after this would SEPEs be identified in the time series and statistics would then be performed on this data. However, there is a great deal of data which would need to be processed, so, in the creation of the SARG Event List the time periods of greatest importance were focussed upon by first identifying the SEPEs and then the flux time series for each event was then processed. A manual check was introduced to visually inspect all events identified and another check was done against other event lists to ensure that no SEPEs were missed during the time period.

3.1 Existing Event Lists

The list of SEPEs depends on the data set used (see section 2.2) and the event definition used (see section 2.2.4). Here three event lists are introduced, one using the JPL event definition, another used for the PSYCHIC solar proton model and the last produced by the National Oceanic and Atmospheric Administration (NOAA).

3.1.1 JPL Event List

One model which is widely used and has seen various incarnations over the past 2 decades is the JPL model (Feynman et al., 1990, 1993, 2002). The events were defined separately in the > 10 MeV energy channel using a threshold of 1 pfu, a lagtime of 2 days, a sampling time of 24 hours and a minimum event fluence of 10^6 cm^2 (Feynman et al., 1993). In addition to the event list published in the JPL-85 model for the time prior to January 1986 which used IMP and OGO data (Feynman et al., 1990), data from GOES/SEM instruments was used (as shown in Table 3.1) to extend the event list (the JPL-91 event list was not published). For the time period from 1986 each of the event flux time series plots were checked and those entries that were data errors rather than real events were removed.

Table 3.1: Instruments used for extension of JPL event list.

Spacecraft/Instrument	Time Period		
GOES-6/SEM	01/01/1986	-	28/02/1987
GOES-7/SEM	01/03/1987	-	31/12/1995
GOES-8/SEM	01/01/1996	-	31/12/2002
GOES-10/SEM	01/01/2003	-	13/06/2003
GOES-11/SEM	14/06/2003	-	31/12/2005

Where two or more spacecraft instruments were operating simultaneously a choice was made based on the comparative reliability Rosenqvist et al. (2005) and others have previously reported; this meant using GOES-7 and GOES-8 data as much as possible. Often at the ends of the data set there are a greatly increased number of data gaps so the time series were analysed and using data from time periods when the portion of gaps was above $\sim 10\%$ was avoided. The list was also also cross-checked with the NOAA list (see below) to ensure that no major events had been missed. It includes 276 events over a 41 year time period (1965-2005) at an average of 6.73 per year. This event list used is included in Appendix Section A.1.

3.1.2 PSYCHIC Event List

The event list used for the recent PSYCHIC model (Xapsos et al., 2004) contains many more events (481) over a shorter time period of 28 years (11/1973 - 11/2001)

than the list generated using the JPL model event definition. This is an average of 17.18 events per year. It uses IMP-8/GME data supplemented with GOES/SEM data during periods of high flux to counter saturation effects and IMP-8/CPME data prior to 1986 as earlier GME data was not available at the time the model was created. Extensive analysis has been undertaken to calibrate and combine all this data to get the best features from the different instruments (Xapsos et al., 2004). Events detected are said to begin when the flux first goes above the background and end when the flux first returns to the background. This event identification procedure was done manually. Events were then excluded if the peak differential flux in the 1.15 to 1.43 MeV channel did not exceed > 4 cm^{-2}s^{-1}sr^{-1}MeV^{-1} and the peak flux in the 42.9 to 51.0 MeV channel did not exceed > 0.001 cm^{-2}s^{-1}sr^{-1}MeV^{-1} (Xapsos et al., 2004). This event definition resulted in the inclusion of a larger number of events significant at low and high energies.

3.1.3 NOAA Event List

NOAA publish an online event list at:

`http://www.swpc.noaa.gov/ftpdir/indices/SPE.txt`

This list uses the > 10 MeV channel with data taken from the GOES spacecraft and defines the start of a SEP event to be when the flux rises above 10 pfu and the end of an event being the last time the flux was greater than or equal to 10 pfu. There is no lagtime, a high temporal resolution of 5 minutes and a requirement of 3 consecutive at the start of the event points serves to exclude 'non-events' detected by data errors. There is no minimum event size although the high threshold filters out a significant number of smaller events. The list contains 224 events over a period of 31 years from 1976 to 2006 (which is the date of the occurrence of the last event by this definition) which is an average of 7.23 events per year.

The NOAA event list sometimes excludes smaller events included in the JPL list due to the higher thresholds such as in 1980, close to solar maximum, where it includes only 2 events compared to 8 in the JPL list. Conversely, due to the higher threshold, the NOAA list can have a greater number of events by splitting sequences where the flux drops below its 10 pfu threshold but not the JPL list's 1 pfu threshold. An example of this is seen in March 1989 where the JPL list has only a single event of 17

days while in that time the NOAA list has 3 separate events.

3.2 Data Processing: De-Spiking

Data processing or 'cleaning' is a vital precursor to accurate model creation as all models are based on raw data. Two key aspects of cleaning are discussed in this section and the next: de-spiking and gap filling. A third data processing algorithm is the cross-calibration of data sets which is discussed in the following section which covers creation of The SARG Event List.

Data spikes occur in solar particle data, possible causes are technical glitches on the detector, misinterpretation of multiple particles of lower energies arriving at the same point in time for one of a higher energy (pulse pile-up) and faulty memory recording the data. They manifest themselves as large sudden increases in flux but last only for one or two data points. Here the aim is to find a method for the automatic detection of data spikes by comparison of individual flux points with the points surrounding them without any erroneous detection of true data points as spikes. The existence of spikes in data will have an effect on the peak fluxes of SEPEs if they exceed the true peak flux value (this can be a difference of orders of magnitude). With a high concentration of large spikes there can also be a significant impact on the fluence of SEPEs. An example of a spike from the > 10 MeV integral channel on the GOES-7/SEM instrument just before 29^{th} July 1989 is shown in Figure 3.1. This spike is almost an order of magnitude higher than the peak of the preceding SEPE.

The first and most obvious method of finding data spikes automatically is to compare each point with the two points either side of it and where the point is significantly greater than both the surrounding points it would classified as a spike. This ratio depends on the sampling time of the detector channel but for 5-minute gaps between data points a flux value of ~ 3 times surrounding points would denote a spike. This simple method may eliminate the majority of spikes but difficulties arise where there are consecutive spikes or data gaps. Where there are consecutive spikes one or more will not be detected as a spike and where there are gaps there is no point of reference for comparing the points either side of the gap. Another method for dealing with data spikes is to smooth the time series by using a median filtering

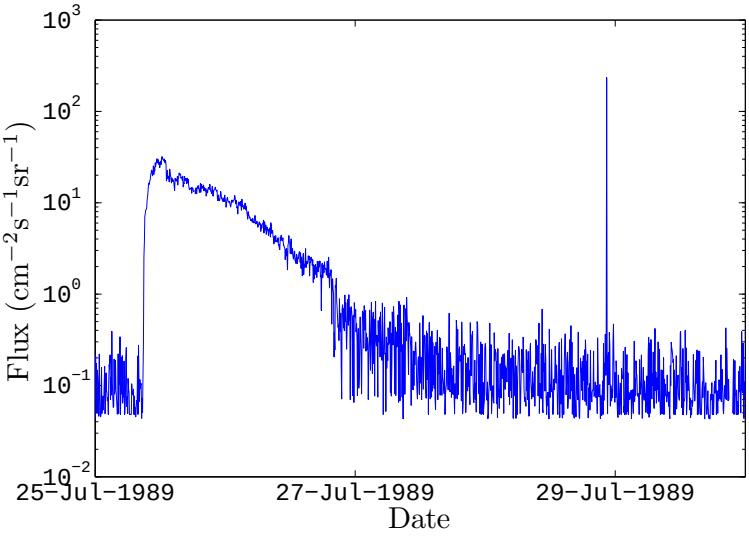

Figure 3.1: Example of a spike in GOES-7/SEM particle data.

method (Stamper and Hapgood, 2001). Median filtering methods take a window of flux values about each point in time (approximately 5 points either side plus the original point) and replace the original value with the median of the window of surrounding points points producing a 'smoothed' time series. The problem with the method is that it will necessarily reduce the peak values from SEPEs. The extent to which these peak fluxes are reduced is dictated by a combination of the sharpness of the peak and the time length of the window chosen for the median filtering. However, any reduction is negative for SEPE modelling as it artificially reduces the peak flux and to a lesser extent fluence of the SEPEs. The changes to these values will affect the distributions of these values which in turn will result in a prediction of a less harsh SEPE environment. The method introduced here combines these techniques by comparison of flux values with a window of flux values surrounding them in such a way that spikes are not missed but that peak values are not replaced unless they are erroneous.

3.2.1 Methodology

The de-spiking algorithm tested here compares the six out of the ten closest points in the flux time series to the point of interest. The six chosen exclude the two lowest and two highest points allowing so points are not compared to other possible spikes or gaps. The flux value is removed only if it exceeds the average of these six points

by more than a threshold named *spikeratio*. Two values for this threshold are tested here: *spikeratio* = 1.5 and *spikeratio* = 3.0. The lower of the two threshold values is more sensitive and will remove more points as spikes. The algorithm is included in Appendix Section A.2. Spikes due to instrument errors are usually seen in only a single channel so another approach to spike detection may be to compare channels although it should be noted that spectra change from event to event and even over the course of the events with onset often having a harder spectra than the decay phase.

3.2.2 Data

The flux time series used in this report is from the CPME instrument on board the IMP-8 spacecraft. These data have been used in the production of the JPL model (Feynman et al., 1990, 1993, 2002). Here the raw data from the 15.0-25.0 MeV and 25.0-48.0 MeV proton channels over 4 SEPEs between 1998 and 2001 have been used. These data includes a high density of spikes and gaps possibly due to the degradation of instrument which had been operational since 1973. This makes a challenging test scenario for determining spikes, therefore successful detection on these data would give a good indication that the algorithm is performing well and will work on other data. This energy range is seen as very significant for the users of SEPE models and these events have many spikes over a range of magnitudes but also many smaller spikes providing a good test for the de-spiking algorithm.

3.2.3 Results of De-Spiking

3.2.3.1 Event of 20^{th} Apr 1998

The event on the 20^{th} April 1998 had a duration of 6 days with a peak flux of 1,700 pfu and a fluence of 1.62×10^9 cm^{-2} in the > 10 MeV proton channel as measured by GOES-8.

Figure 3.2 shows the de-spiking algorithm with a *spikeratio* value of 1.5; this makes it quite sensitive. In the lower energy channel (top) there are 18 points detected as spikes many of which appear to be small amounts of noise in the data and not significant enough to require being removed. In the higher energy channel (bottom) there are again 18 detected spikes but it is arguable as to whether any of these points

are true spikes and need to be removed.

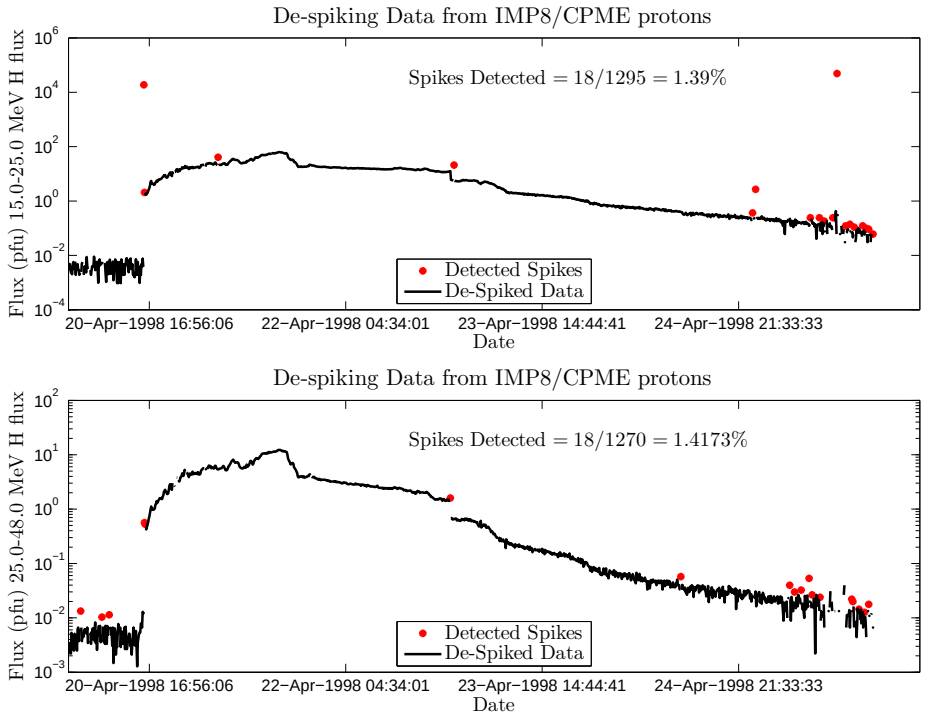

Figure 3.2: IMP-8 data de-spiked for an event on the 20$^{\text{th}}$ April 1998 (*spikeratio* = 1.5).

When the value of *spikeratio* is increased to 3 (reducing the sensitivity) a greatly reduced number of spikes are detected in both channels as shown in Figure 3.3. In general this appears to give a more sensible result but there is one point which is not removed and looks as if it might be a spike. This is the 3$^{\text{rd}}$ spike detected in the lower energy channel using the lower value of *spikeratio* (approximately 1/5 of the way through the event). Here this value is probably not significant but were it to be nearer the peak it might be.

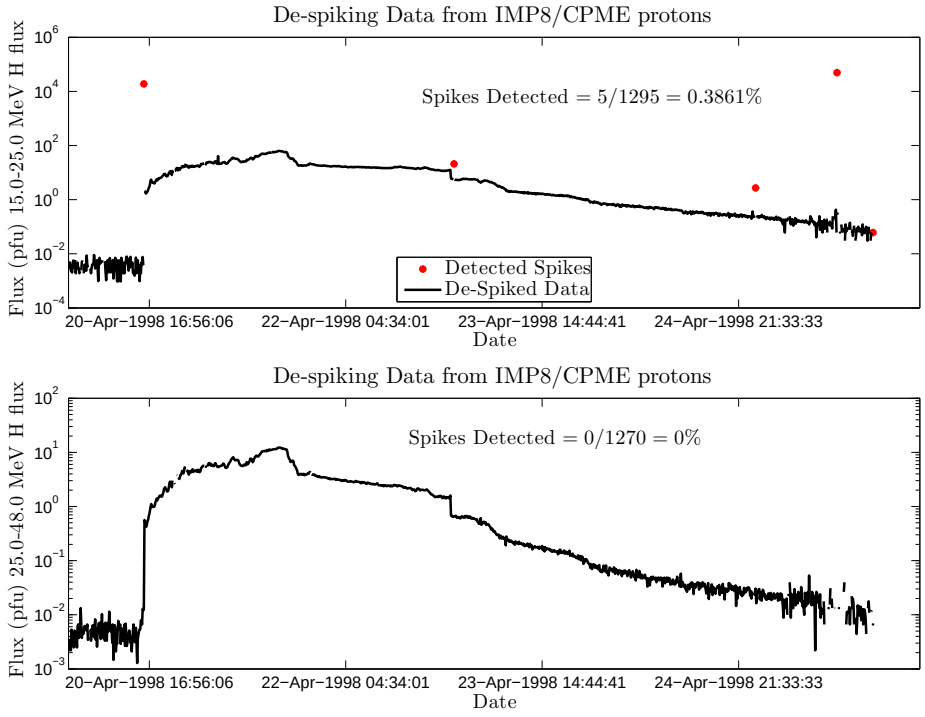

Figure 3.3: IMP-8 data de-spiked for an event on the 20$^{\text{th}}$ April 1998 (*spikeratio* = 3.0).

3.2.3.2 Event of 14$^{\text{th}}$ July 2000

This event on the 14$^{\text{th}}$ July 2000 had a duration of 11 days with a peak flux of 24,000 pfu and a fluence of 1.65×10^{10} cm^{-2} (from inspection of integral GOES-8/SEM data) in the $>$ 10 MeV proton channel. This large SEPE is known as the 'Bastille Day' event.

Figure 3.4 shows the flux time series from this event de-spiked in the 15-25 MeV energy channel (top) and the 25-48 MeV energy channel (below) using a value of *spikeratio* of 1.5. There were 15 spikes detected in the lower energy channel and 12 in the higher energy channel. Again many of these might not have been spikes and could have remained in the time series.

Figure 3.5 shows the flux time series de-spiked using the higher value of *spikeratio* of 3. As expected far fewer spikes are detected in both cases and this is probably a fairer representation of the number of spikes in the time series for this event. There is one contentious spike in the lower energy channel which is the first detected using the lower value of *spikeratio*. With the higher value of *spikeratio* this point is left in the time series and is in fact the peak value of the event. Eliminating this value

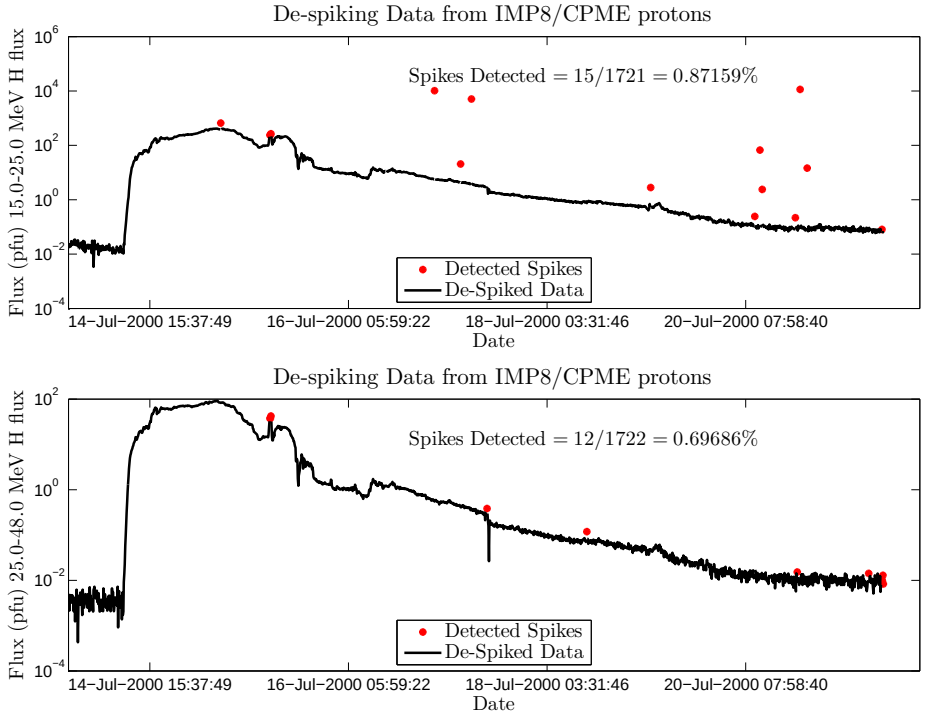

Figure 3.4: IMP-8 data de-spiked for an event on the 14$^{\text{th}}$ July 2000 (*spikeratio* = 1.5).

reduces the peak flux from 658 cm^{-2}s^{-1}sr^{-1}MeV^{-1} to 416 cm^{-2}s^{-1}sr^{-1}MeV^{-1} but this could either be a spike or part of the physical phenomenon. This illustrates the difficulty of de-spiking solar proton data as this sudden increase could be caused by the CME-driven shock passing the observing instrument or a minor instrument glitch. The best that can be hoped for with a de-spiking algorithm is to remove the points that a human would remove doing it by eye but no others. As there is uncertainty over this point and it is possibly 'real' it is best that it remains in the time series.

It should be noted that during this event the lower energy channel was saturated (when compared to the GOES data and the higher energy channels) therefore this is a mute point. However, similar circumstances may arise in non-saturated events and other data sets for which a decision must be made.

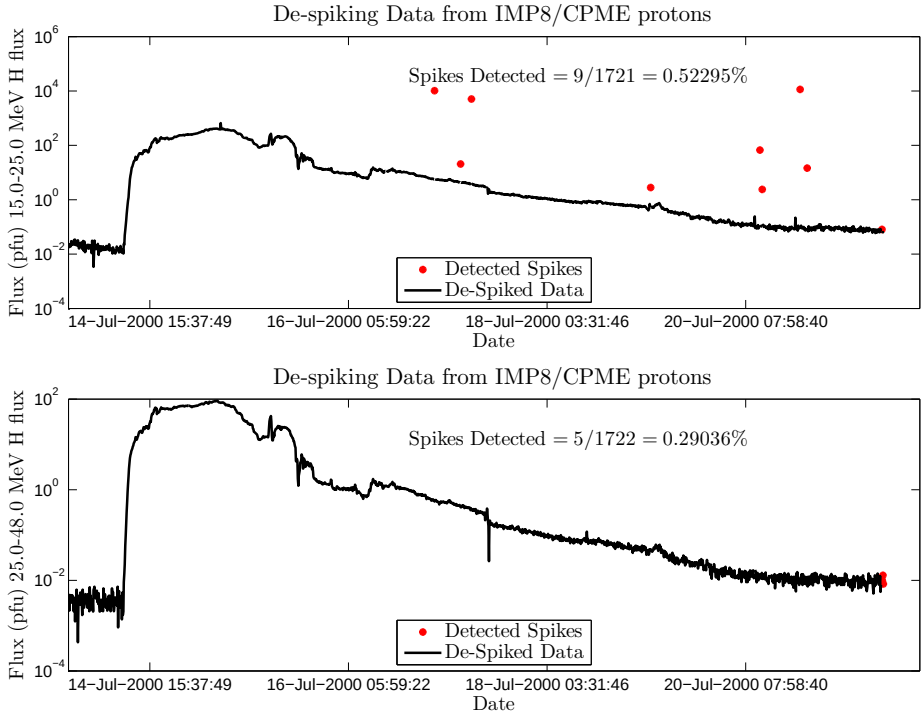

Figure 3.5: IMP-8 data de-spiked for an event on the 14$^{\text{th}}$ July 2000 (*spikeratio* = 3.0).

3.2.3.3 Event of 8$^{\text{th}}$ November 2000

This event on the 8$^{\text{th}}$ November 2000 had a duration of 11 days with a peak flux of 14,800 pfu and a fluence of 1.08×10^{10} cm^{-2} using the $>$ 10 MeV proton channel as measured by GOES-8.

Figure 3.6 shows the data de-spiked in the lower energy channel (top) and the higher energy channel (bottom) for the lower value of *spikeratio* of 1.5. The lower energy data was very spikey for this event and the algorithm removed 36 points which is 1.359% of the total. Most of these do appear to be spikes although one in the rise phase does give cause for alarm as it does not appear to be a spike. The higher energy channel has a greater number of spikes detected but only 1 of them appears to be a genuine spike, the remainder could be left in the time series.

Figure 3.7 shows the de-spiked time series for the higher value of *spikeratio* of 3. There are still 23 spikes detected in the event in the lower energy channel (top), however, here all but those at the very end of the plotted data are undeniably genuine spikes. In the higher energy channel (bottom) the single definite spike is found and only 3 more erroneously detected at the tail of the event.

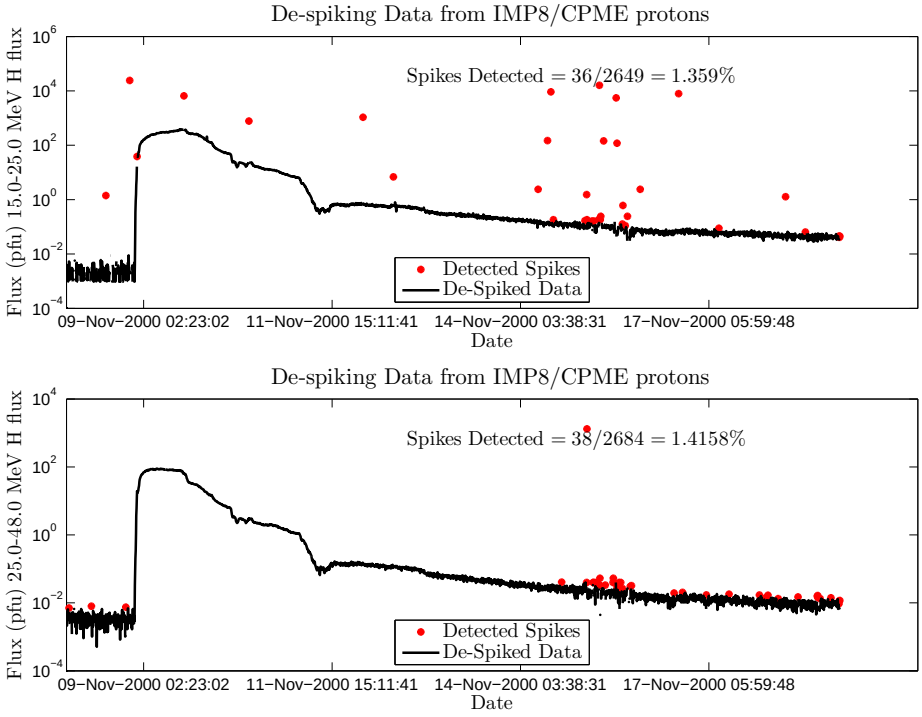

Figure 3.6: IMP-8 data de-spiked for an event on the 8$^{\text{th}}$ November 2000 (*spikeratio* = 1.5).

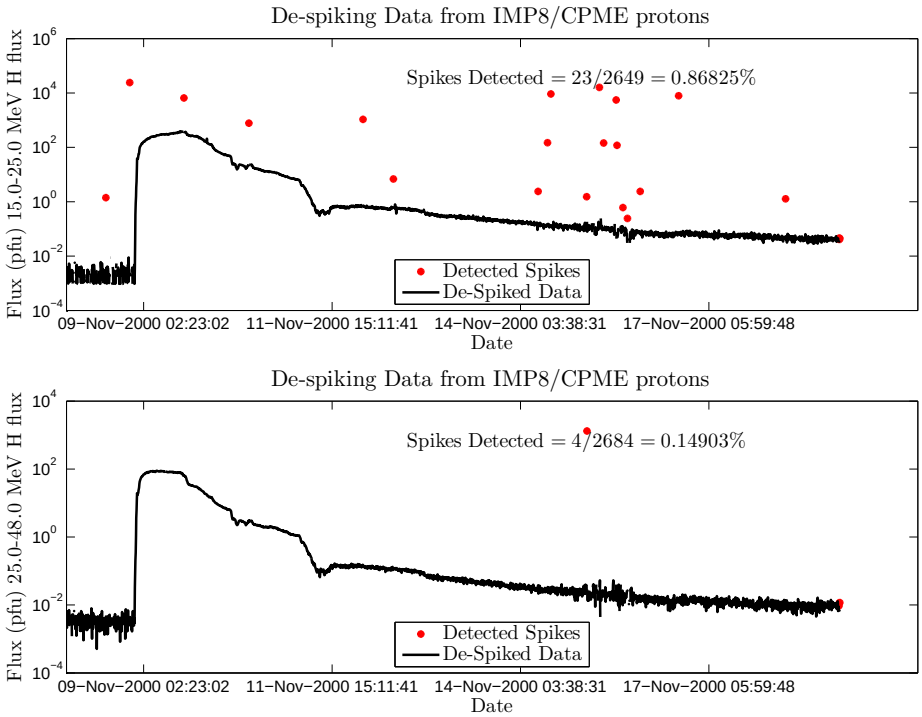

Figure 3.7: IMP-8 data de-spiked for an event on the 8$^{\text{th}}$ November 2000 (*spikeratio* = 3.0).

3.2.3.4 Event of 24th September 2001

This event on the 24th September 2001 had a duration of 18 days with a peak flux of 12,900 pfu and a fluence of 8.41×10^9 cm^{-2} in the $>$ 10 MeV proton channel as measured by GOES-8.

This event has two enhancements which have been included in the same event as a result of the event definition used. Figure 3.8 shows the results of the de-spiking algorithm using a *spikeratio* of 1.5 for the higher energy channel (top) and the lower energy channel (bottom). Again the lower energy channel shows a far greater number of real spikes whereas the higher energy channel has more spikes detected due to higher noise at lower fluxes. Many of these points did not need to be removed but all the true spikes have definitely been found.

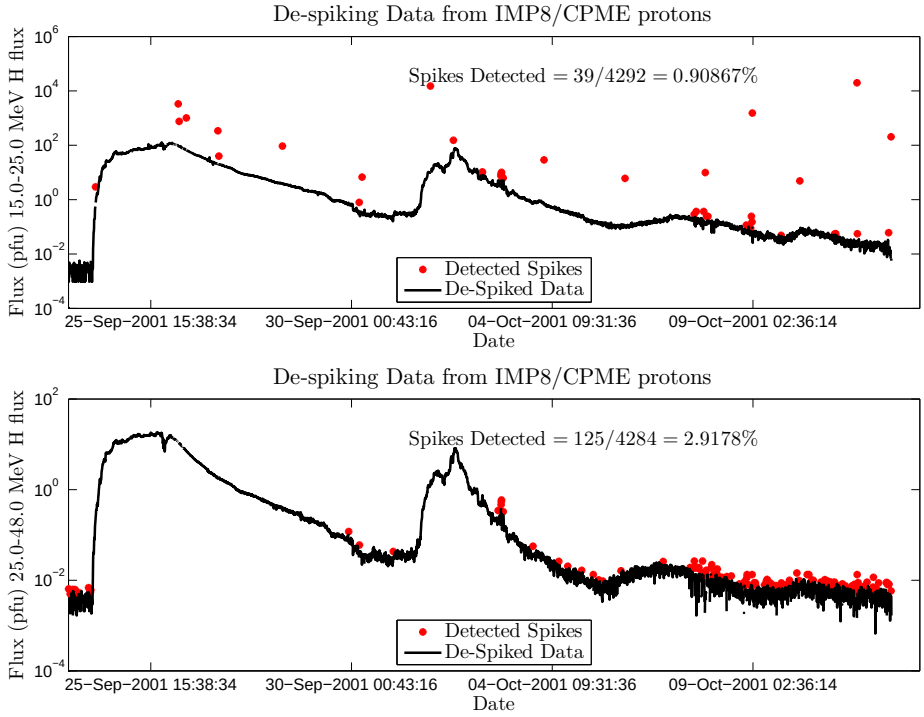

Figure 3.8: IMP-8 data de-spiked for an event on the 24th September 2001 (*spikeratio* = 1.5).

Figure 3.9 shows the data de-spiked using the higher *spikeratio* value of 3 and again there is an issue with the peak of the event in the lower energy channel (top). The highest point on the 2nd enhancement in this case is 152 cm^{-2}s^{-1}sr^{-1}MeV^{-1} but this is possibly a spike and was removed when using the lower value for *spikeratio* which resulted in the peak flux for this event being the peak of 124 cm^{-2}s^{-1}sr^{-1}MeV^{-1} in

the first enhancement of the event. As it is not possible to be certain by eye whether this is a spike or part of physical phenomenon it is best to leave the value in the time series. The higher energy channel again performs better with the higher value of *spikeratio* as there appear to be no spikes in the time series and only 3 (as opposed to 125) have been detected erroneously.

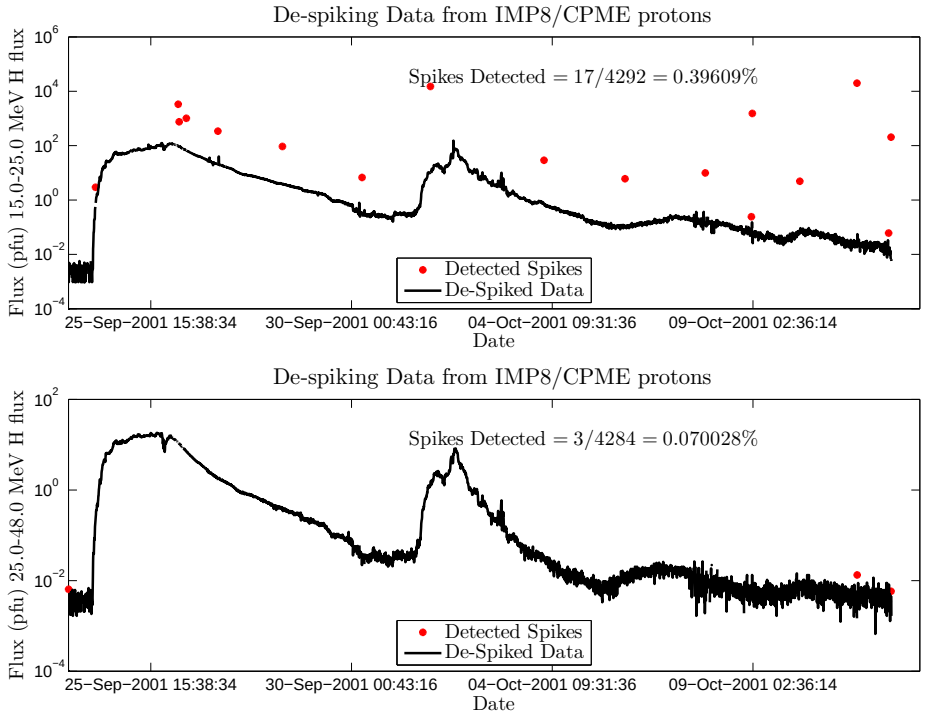

Figure 3.9: IMP-8 data de-spiked for an event on the 24$^{\text{th}}$ September 2001 ($spikeratio = 3.0$).

3.2.4 Conclusions

A automatic de-spiking algorithm has been created by using small time windows of surrounding points to compare to each point in the time series. As the philosophy must be to remove only the points that it is certain are spikes it appears that using a value for *spikeratio* of 3.0 is preferable to a lower value which may remove points which may not be spikes. It should be noted that values *spikeratio* other than 1.5 and 3.0 were tested but that these two values were chosen to illustrate differences in the way the algorithm performs. The value of 3.0 is that which will be used in the cleaning of the SEPE data to create the SARG event list. Much higher values were found to leave points which were spikes. However, this parameter is quite robust in that a value

anywhere between 2.5 and 3.5 could have been used with little noticeable impact. This is encouraging for confidence in this parameter and therefore the algorithm as a whole. The benefit of leaving in possible spikes rather than removing those which are possibly not spikes is that these points may always be removed later upon visual inspection of the SEPEs.

3.3 Data Processing: Gap Filling

Gaps are found regularly in SEP (Solar Energetic Particle) data caused by instrument malfunction or a failure in transmission of the data. Data gaps can have a significant impact on the peak flux and fluence of SEPEs if they occur during times of high flux. They may also have a significant indirect effect if they occur when the flux is lower by splitting SEPEs, the start and end times of which are determined based on exceeding some threshold parameter. Here a variety of methods for filling such data gaps using raw and scaled secondary data (data from another instrument) and a 3rd order polynomial interpolation are presented. To test these methods, gaps are created in the flux time series and the deduced fluxes found using various methods are compared with the original (primary) data which had been removed.

To find what the most commonly occurring gap sizes are (and therefore what should be tested using artificial gaps), the $>$ 10 MeV proton channel for the SEM instrument onboard GOES-7 was studied for the time period from 3/1987 to 11/1994. It was found that there were:

- A total of 1620 data gaps
- An average gap length of 59.5 minutes
- A standard deviation of 159 minutes
- A maximum gap size of 5,545 minutes (3.85 days)
- The 2nd largest gap was 1,015 minutes (0.705 days)
- Only 7 gaps were over 5 hours (0.43%)
- 1,198 of the gaps were less than an hour in length (73.95%)

3.3.1 Data

To test the various methods for filling data gaps artificial gaps were created in events from the GOES-7 > 10 MeV proton channel and then filled with a variety of methods. Where a method made use of secondary data to fill data gaps the GOES-6 data set was used. These two data sets were used due to the long time period which they overlapped (from 03/1987 to 12/1994) and the same time resolution. The > 10 MeV channel was used as this includes the majority of the 5-200 MeV energy range that will be used for the SARG Event List. Data from SEPEs was used to test the various algorithms because these are the times when the impact of data gaps will be most greatly felt. The artificial gaps were at evenly spaced points in the events so as to avoid any possible bias that might be introduced by manual selection. The gaps taken were:

- 9 gaps of 2 hours in 10 events (a total of 90 gaps)
- 9 gaps of 5 hours in 5 events (a total of 45 gaps)

these were centered about points 10%, 20%, 30%, ..., 90% through each of the events selected. The events chosen are shown in Table 3.2, they were chosen as they are of different lengths and of various intensity (peak flux and fluence). A total of 135 artificial data gaps gives a large sample to test gap filling algorithms.

Table 3.2: Dates of events used: Start day - End day (inclusive); Format: year/dayofyear.

2 hour gaps				5 hour gaps	
1	1988/313 - 1988/316	6	1991/238 - 1991/243	1	1989/224 - 1989/249
2	1988/350 - 1988/355	7	1992/177 - 1992/184	2	1989/331 - 1989/339
3	1989/331 - 1989/339	8	1992/304 - 1992/313	3	1990/136 - 1990/152
4	1990/097 - 1990/103	9	1993/071 - 1993/074	4	1992/177 - 1992/184
5	1991/130 - 1991/135	10	1994/051 - 1994/054	5	1992/304 - 1992/313

Figure 3.10 shows artificial gaps (in red) formed in the event commencing on the 20th February 1994. There are 9 gaps each 2 hours in length and the flux produced by the various gap filling methods will be compared to the original data which has been removed.

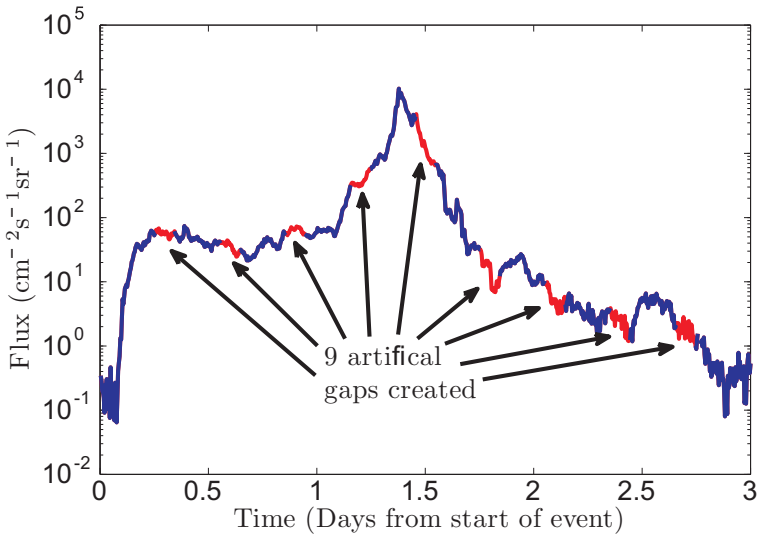

Figure 3.10: Artificial gaps created in event commencing day 51 in 1994.

3.3.2 Methodology

In total nine methods were tested for filling data gaps. The first method is named the Local Mean Fitting Method and uses secondary (in this case GOES-6) data to fill the data gap scaling it using only points (from both the primary and secondary data sets) very close to the data gap. The second method is the Medium-term Calibration method which performs a calibration of data from the secondary data set to the primary data set using data from one day either side of the gap and scales the secondary data using this calibration to fill the gap. The third method is the Long-term Calibration method which performs a calibration of data from the secondary data set to the primary data set using data from ten days either side of the gap and scales the secondary data using this calibration to fill the gap. The fourth method is the Complete Data Set Calibration method which performs a calibration of data from the secondary data set to the primary data set using all points for which there is a flux value in both data set and scales the secondary data using this calibration to fill the gap. The fifth method is the average of the two closest agreeing from the first four methods. The sixth method is the average of three of the first four methods excluding the method in poorest agreement with the others. The seventh method is the average of all four of the first four methods. The eighth method tested was to use the secondary data without altering (scaling) it. The final method is a 3rd Order Polynomial fit which does not use secondary data.

Figure 3.11 shows 2 artificial gaps created the event commencing on the 20th February 1994. The red sections shows the unaltered secondary data with the red arrows indicating the effect of scaling this secondary data to fill the gap. The purple sections show the polynomial fit not using secondary data.

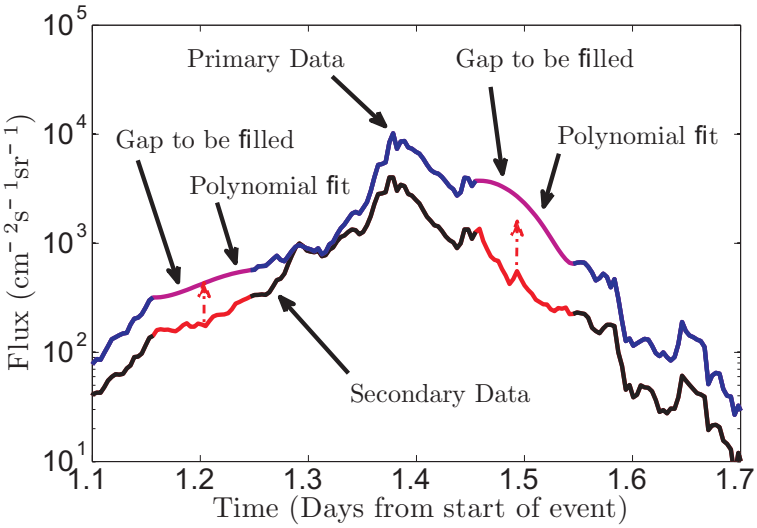

Figure 3.11: Filling artificial data gaps.

3.3.2.1 Local Mean Fitting Method

This method allows a data gap to be filled in one (primary) data set with data from another (secondary) data set; both time series are assumed to have the same time step and begin at the same point in time. Firstly the mean values of the 5 points before the start and after the end of the data gap for both the primary and secondary data are found:

$$Mean_{start}^{primary} = \frac{\sum Flux^{primary}([s-4:s])}{5} \quad (3.1)$$

$$Mean_{end}^{primary} = \frac{\sum Flux^{primary}([e:e+4])}{5} \quad (3.2)$$

$$Mean_{start}^{secondary} = \frac{\sum Flux^{secondary}([s-4:s])}{5} \quad (3.3)$$

$$Mean_{end}^{secondary} = \frac{\sum Flux^{secondary}([e:e+4])}{5} \quad (3.4)$$

where s is the position of the last point where there is data before the data gap and e is the first point where there is data after the gap in the primary data. $[a:b]$ is a uniform integer vector from a to b of step 1 used here to establish a vector of 5 points before and after the data gap in the time series. If there is a data gap in the vectors

for either the primary or secondary data being used to find the mean values the next point along (either backwards or forwards in time) is used so that exactly 5 points are always used. Next the mean values from the primary data before and after the data gap are divided by those from the secondary data:

$$S.F._{start} = \frac{Mean_{start}^{primary}}{Mean_{start}^{secondary}} \tag{3.5}$$

$$S.F._{end} = \frac{Mean_{end}^{primary}}{Mean_{end}^{secondary}} \tag{3.6}$$

this gives the scaling factors, $S.F_{start}$ and $S.F_{end}$, for modifying the secondary data to fit in the primary data time series. However, any possible change in these scaling factors over the course of the data gap must also be accounted for. To do this a straight line weighting factor for both the scaling factors over the course of the gap is used to give a combined scaling vector, $S.V.$, which varies over the gap:

$$S.V. = \left(S.F._{start} \frac{(l - [1:l]) + 0.5}{l} + S.F._{end} \frac{[1:l] - 0.5}{l} \right) \tag{3.7}$$

This is then multiplied by the secondary flux for the points over the gap to produce an adjusted flux to fit into the primary data time series:

$$Flux^{adjusted}([s+1:e-1]) = Flux^{secondary}([s+1:e-1]). \times S.V. \tag{3.8}$$

where l is number of missing data points and $.\times$ is an element-by-element multiplication of two vectors of equal dimensions. At the start of the gap the contribution comes entirely from $S.F._{start}$ with no contribution from $S.F._{end}$, half way through the gap the contributions are equal and at the end there is no contribution from $S.F._{start}$ with the entire contribution from $S.F._{end}$. Note, because the gap is considered to start (end) half way between the data point at s (e) just before (after) the gap and the first (last) missing data point, by the time the first (last) point is scaled it is already (still) a small way through (from the end of) the gap so there is a small contribution from $S.F_{end}$ ($S.F._{start}$).

3.3.2.2 Inter-Calibration Methods

Inter-calibration methods are based on a linear regression between the two time series (the primary and secondary data). The regression is inspired by that carried out by Rosenqvist et al. (2005) using the fluences of SEPEs. Here the regression is performed

using the individual data points as it is not desirable that the method be dependent upon any event definition. Furthermore, the straight line regression is performed with the intercept fixed at zero; a non-zero intercept made little difference to results other than at very low fluxes where negative values of deduced flux became possible. Where there was a gap in the primary data set it was replaced using the re-calibrated secondary flux data:

$$Flux^{adjusted}([s+1:e-1]) = \frac{Flux^{secondary}([s+1:e-1])}{slope} \tag{3.9}$$

where *slope* is the gradient deduced from the regression. 3 varieties of the inter-calibration method for filling data gaps were tested: Medium-term, Long-term and Complete Data Set calibration. The Medium-term Calibration used only data from 1 day either side of the data gap for the regression, this fit will be reflective of the relative performance of the instruments in the small time frame about the gap but if there is any erroneous data this will have a more pronounced effect. 'Medium-term' is an indication that the a calibration uses data from over a longer time span than that used for the Local Mean Fitting Method. The Long-term Calibration used 10 days either side of the data gap for the regression which is less particular to the specific timing of the data gap but less susceptible to bad data close to the data gap. The Complete Data Set Calibration uses all the data points for which there are flux values for both data sets. However, this technique does not account for any temporal changes there might be in the calibration between data sets. Figure 3.12 shows the complete data set calibration for GOES-6 to the GOES-7 data set. The same method is used for the Medium-term Calibration and the Long-term Calibration but with fewer data points from closer to the gap being considered.

3.3.2.3 Averaging Methods

Three methods of averaging the results of the Local Mean Fitting Method and the inter-calibration methods were also applied. The first of these methods took an average for each gap of the two methods that were in closest agreement. The fluxes were compared point-by-point with the sum of the absolute differences, D, found for the six combinations of the four different scaling methods:

$$D_{j,k} = \sum \left| Flux_j^{adjusted} - Flux_k^{adjusted} \right| \tag{3.10}$$

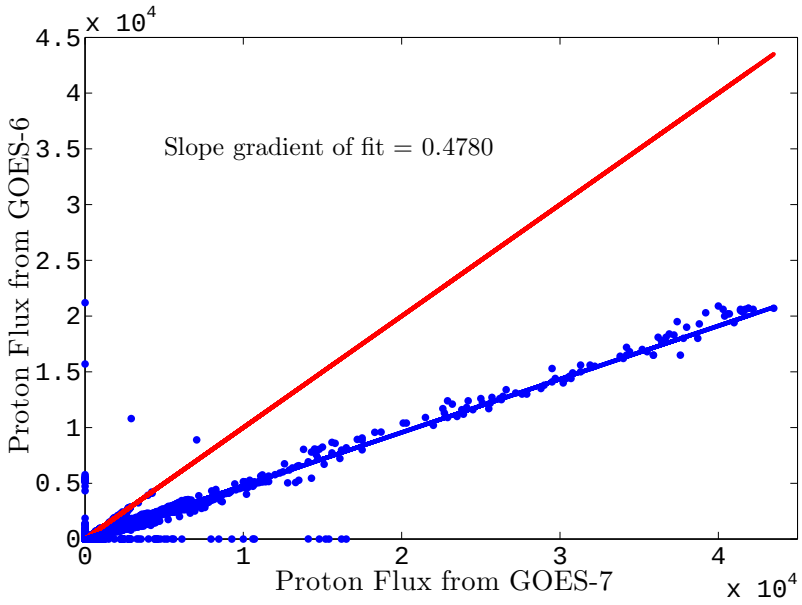

Figure 3.12: Complete data set calibration of GOES-6 to GOES-7, blue line shows the best fit of all the flux data points while the red line shows $x = y$ where the data would lie if the instruments were in agreement.

where $k < j$. $k = 1$ denotes the Local Mean Fitting Method, $k = 2$ denotes the Medium-Term Calibration, $k = 3$ denotes the Long-Term Calibration and $k = 4$ denotes the Complete Data Set Calibration. If k were equal to j a method would be compared with itself giving a value of D of zero and if j were less than k this would repeat the results of $k < j$. The average for the two methods which D was smallest was used to form the replacement flux profile:

$$Flux^{adj.avr.2} = \frac{\sum Flux^{adjusted}_{j,k\min(D)}}{2} \tag{3.11}$$

The methods for which the average was taken could be different for data gap.

The second averaging method was to take an average of three methods excluding only that method which was in poorest agreement with the others (the outlier). The outlier method was found by taking the flux from each of the four original methods from the average of the remaining three methods:

$$O_j = \sum \left| \frac{\sum Flux^{adjusted}_{\neq j}}{3} - Flux^{adjusted}_{j} \right| \tag{3.12}$$

here the value of j for which maximum value for O is found is established as the

outlier and the average of the three remaining methods is used, i.e.:

$$Flux^{adj.avr.3} = \sum \frac{Flux^{adjusted}_{\neq j\max(O)}}{3} \tag{3.13}$$

The final combination was the average of all four of the original methods (the Local Mean Fitting Method and the three inter-calibration methods):

$$Flux^{adj.avr.4} = \sum_{j=1}^{4} \frac{Flux^{adjusted}_{j}}{4} \tag{3.14}$$

It was felt that these averaging methods may exclude or minimise the impact of a flaw in the gap filling methods seen in special cases.

3.3.2.4 Unaltered Secondary Data

Another method tested was to fill the data gaps with raw secondary data without scaling it. This is the red line sections in Figure 3.11. It is clear that this would not form a realistic flux time series over the data gap unless the raw secondary data was well calibrated. The raw secondary data allows a good point of comparison for the remainder of the methods, a failure to substantially improve upon the use of raw secondary data would indicate that the gap filling method was poor.

3.3.2.5 3rd Order Polynomial

The final method for filling data gaps did not use data from another time series but used a simple 3rd order polynomial. To perform an interpolation using a 3rd order polynomial first estimates are required for the gradients at the start and end of the data gap:

$$\mathrm{Gr}_{start} = \frac{\sum(Flux^{primary}([s-3:s]) - Flux^{primary}([s-4:s-1]))}{l} \tag{3.15}$$

$$\mathrm{Gr}_{end} = \frac{\sum(Flux^{primary}([e+1:e+4]) - Flux^{primary}([e:e+3]))}{l} \tag{3.16}$$

here s is the point just previous to the start of the data gap, e is the first point after the end of the data gap and l is 1 less than the number of points being considered (typically 4) and normally the equations will reduce to the difference between the first and last of the 5 flux values either side of the gap divided by 4. However, if either one of these points is itself a gap the time over which the gradients are calculated may be

reduced. The polynomial to fit the gap can now be calculated in the usual way:

$$\begin{aligned} D &= Flux^{primary}(s) \\ C &= \mathrm{Gr}_{start} \\ A &= 2D + 3C + \mathrm{Gr}_{end} - 2Flux^{primary}(e) \\ B &= Flux^{primary}(e) - A - C - D \\ Flux^{polyfit} &= At^3 + Bt^2 + Ct + D; \end{aligned} \tag{3.17}$$

where t is the time over the data gap scaled to lie between 0 and 1 (0 being the start of the gap and 1 the end).

3.3.3 Results of Gap Filling

Once the events had been selected, artificial gaps created and filled using the 9 possible methods the resulting fluxes were then compared to the real fluxes from the primary data. Two parameters created used to measure the difference between the fluxes: The Average Fluence Error (AFE) and the Average Percentage Error (APE). The AFE is:

$$\mathrm{AFE} = \frac{\sum_{i=1}^{n_g \times n_e} |Flu_i^{primary} - Flu_i^{filled}|}{n_e n_g l} \tag{3.18}$$

where $Flu^{primary}$ is the fluence of the primary data over a gap, Flu^{filled} is the fluence over the gap given by the particular gap filling method, n_e is the number of events investigated, n_g is the number of gaps created in each event (which is fixed at 9) and l is the length of each data gap (in minutes). Before summing, the absolute value is taken over each data gap, this means that the total fluence error per minute is being considered on a gap-by-gap basis. Additionally it means that the AFE parameter is heavily weighted towards those gaps created at points of high flux over the event. These are the most important in terms of peak flux and fluence contribution but as the suitability of the different methods should also be tested at lower fluxes a second value, the APE, was also measured:

$$\mathrm{APE} = \frac{\sum_{i=1}^{n_g \times n_e} PE_i}{n_e n_g} \tag{3.19}$$

where PE is the percentage error over each gap as given by:

$$PE_i = \frac{|Flu_i^{primary} - Flu_i^{filled}|}{Flu_i^{primary}} \tag{3.20}$$

By using the percentage errors far greater weight is given to the gaps created at smaller flux levels.

Table 3.3: Results of various fitting methods applied to artificial gaps created in SEPEs.

	2 hour gaps		5 hour gaps	
Fitting Method	AFE*	APE†	AFE*	APE†
Local Mean Weighted	0.2081	11.62	0.3773	8.68
Medium-term Calibration	0.7177	52.55	0.7532	20.11
Long-term Calibration	0.7828	31.07	0.7054	16.80
Complete Data Set Calibration	1.1159	27.40	1.0065	20.06
Average of 2 ($Flux^{adj.avr.2}$)	0.6719	27.35	0.6218	13.96
Average of 3 ($Flux^{adj.avr.3}$)	0.6951	27.40	0.6644	16.98
Average of all ($Flux^{adj.avr.4}$)	0.6650	24.91	0.7110	15.22
3rd order polynomial Interpolation	1.2436	23.44	1.2508	13.57
Raw Secondary Data	4.1957	61.17	6.7511	55.29

* AFE = Average Fluence Error (10^4.cm^{-2}.min^{-1})

† APE = Average Percentage Error (%)

Table 3.3 shows the AFE and APE values calculated over the 10 events for the 2 hour data gaps and the 5 events for the 5 hour data gaps. The first thing to notice is that the Local Mean Fitting Method has the lowest errors for both the 2 hour and 5 hours gaps measured with either the AFE or the APE. By far the worst was the unaltered secondary data with percentage errors over 50%.

The average methods were an improvement on all the methods other than the Local Mean Fitting Method when measured using the AFE for the 2 hour gaps and to all but the Long-term Calibration method for the 5 hour gaps. However, the results were still largely inferior to the Local Mean Fitting Method. The 3rd order polynomial compared favourably to the other fits when measured using the APE but it was worse when measured with the AFE. This indicates that it was better at fitting the data gaps at the lower flux levels but poorer at the higher flux levels.

3.3.3.1 Potential Problems for the Local Mean Fitting Method

Some possible problems with using the Local Mean Fitting Method should not be ignored. Firstly there is the issue of the positions of two separate spacecraft carrying the detectors used for the primary and secondary data sets. The example here is a small enhancement in March 1988. It can be seen in Figure 3.13 that the secondary instrument (onboard GOES-6) is seeing the event marginally before the primary instrument (on board GOES-7). As a result of this and the rapid rise time in this event the filling of the artificial data gap using the Local Mean Fitting Method results in an under-prediction of the peak flux for the event. The under-prediction of a peak flux can have a significant impact on the event fluence. This problem is very rare but visual inspection of flux time series near data gaps should indicate where it may arise. The method remains far better than using raw secondary data or an interpolation method.

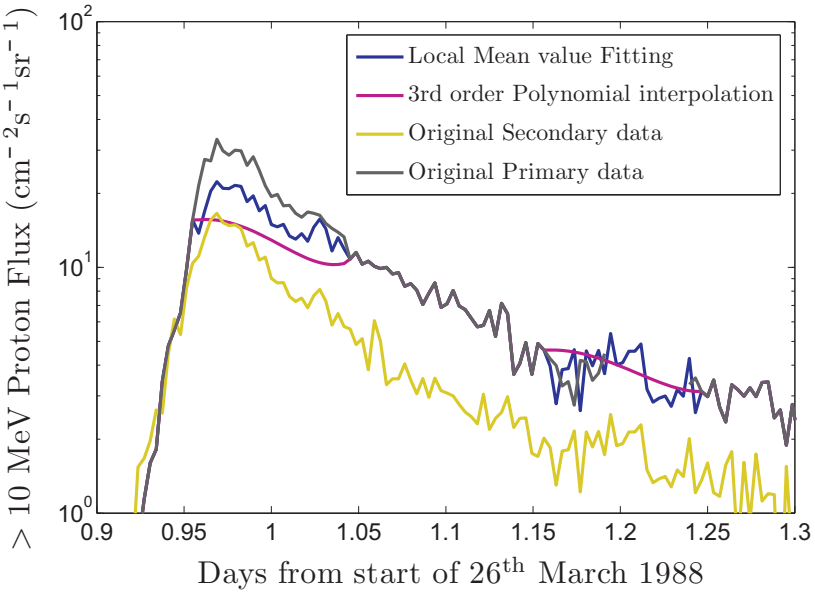

Figure 3.13: Example showing possible issues for the Local Mean Fitting Method being applied during event onset.

The second problem with the Local Mean Fitting Method is that it is very sensitive to the few points being used (10 in total for each gap) from each time series. An example of this can be seen in Figure 3.14. If there is a data spike in the time immediately before or after the gap it is very likely that a poor result will be given. It is therefore very important that a de-spiking algorithm (see Section 3.2) is run on

the data prior to using this gap filling algorithm.

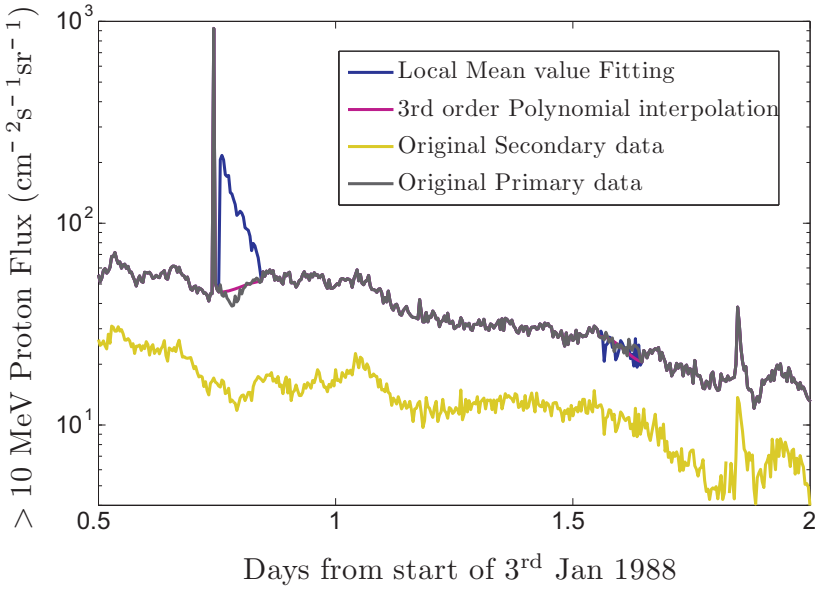

Figure 3.14: Example showing the need to de-spike data before applying the Local Mean Fitting Method.

3.3.3.2 Advantages for the Local Mean Fitting Method

There are significant advantages that the Local Mean Fitting Method has over its rivals. The second best fit when looking at the lower flux gaps was a 3rd order polynomial fit (as shown by the APE). However, the APE measure does not consider the errors on a point-by-point basis but rather the average percentage fluence error measured over the entire gap. Figure 3.15 shows the failure of the interpolation method to capture the shape of the flux profile in comparison with the other fitting methods. As a combination of this failure and the poor AFE results in comparison with the other fittings an interpolation should only be used when there is no secondary data.

While the Local Mean Fitting Method is susceptible to the effects of erroneous data near to data gaps this sensitivity is usually a great advantage. The suitability of the various calibration methods can vary greatly over the course of a single event. This is shown in Figure 3.16 where the 3 calibration methods give a very high result for the data gap due to a local change in the ratio between the two flux time series. The Local Mean fitting Method performs very well in this case adjusting for this local gain change in the secondary data and matching well the original primary data.

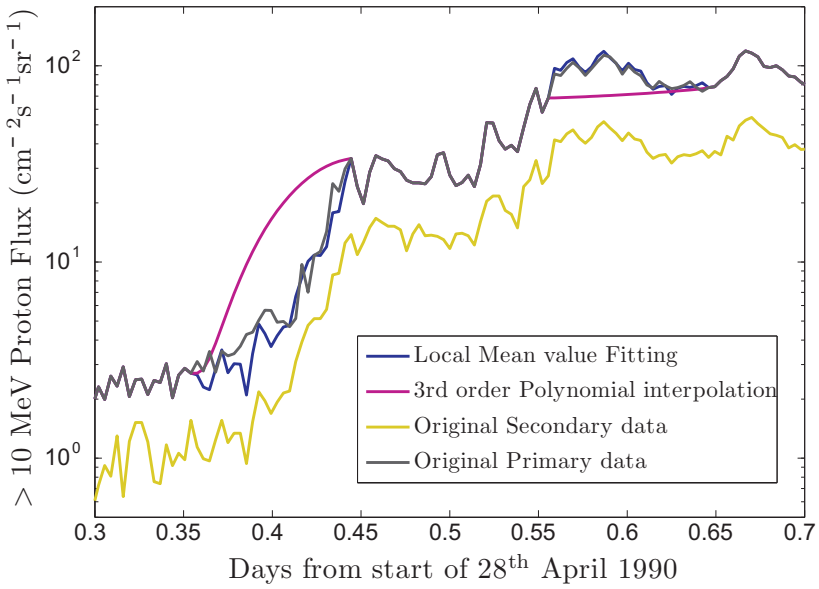

Figure 3.15: Example of the problems using a polynomial fit rather than using secondary data.

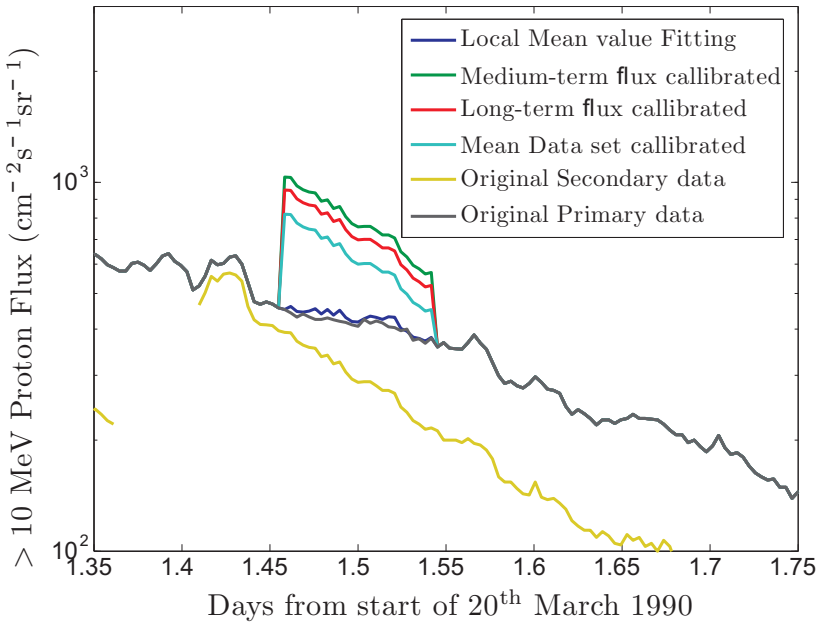

Figure 3.16: Example of the improved performance of the Local Mean Fitting Method.

3.3.3.3 A Real Data Gap: 8th - 25th March 1989

Having looked at the differences between the gap filling methods by creating artificial gaps and then comparing them to the real data now a gap in a real SEPE at the peak of an event in March 1989 is studied. Figure 3.17 shows the flux profiles provided by each of the 6 main methods including the secondary data. It can be seen that the secondary data would give a far lower peak value than the likely true value. The

interpolation fails to capture the peak of the event at all. The calibration methods all give a similar shape and without knowing what the true flux was we cannot discern which profile is the best. It can only be assumed that based upon previous results that the Local Mean Fitting Method gives a good result and in which case so does the Medium-term Flux Calibration Method as they agree very closely. The next best would be the Complete Data Set Calibrated Method and then the Long-term Flux Calibration Method.

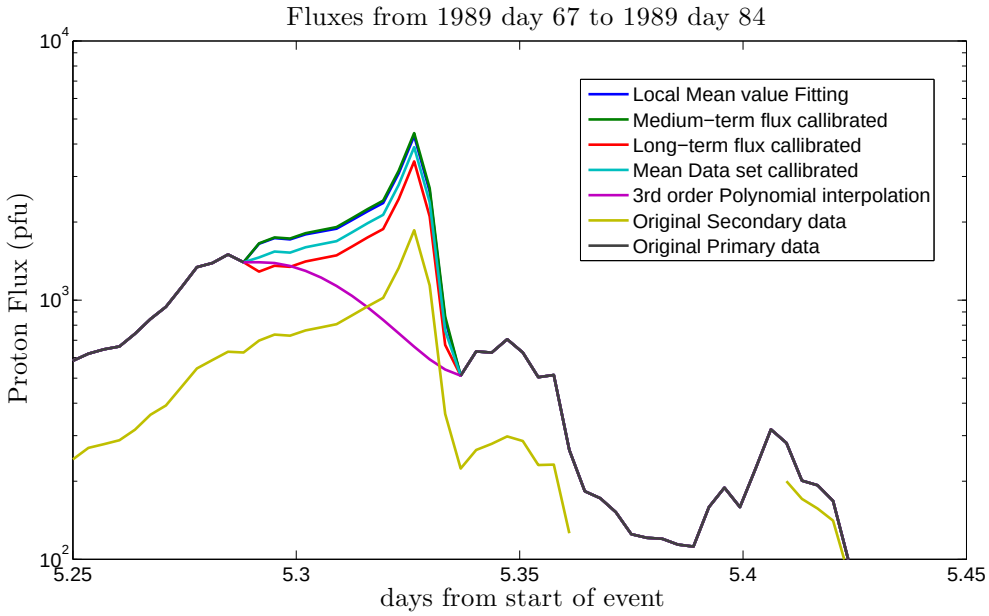

Figure 3.17: Various Methods of Filling a Real Data Gap in March 1989.

The results for the peak flux values given by each method and the fluence difference for the event are given in Table 3.4. Clearly there is a significant impact on the peak flux for this event making the use of a good gap filling method very important but there is also a very significant contribution to the overall fluence from this short time period of $\sim 12\%$.

3.3.4 Conclusions on Gap Filling Methods

From the results it can be concluded that the Local Mean Fitting Method is the best way of fitting data gaps from those investigated. It should be ensured that all data spikes are removed from the data prior to applying this gap filling technique and care should be taken in fitting data to gaps where there is a rapid increase in the

Table 3.4: Effect on using different techniques to fill a real gap at the peak of an event from day 67 to day 84 in 1989.

	Fluence		Peak Flux	
Method Used	$\times 10^9 \mathrm{cm}^{-2}$	% diff.	$\mathrm{cm}^{-2}.\mathrm{s}^{-1}\mathrm{sr}^{-1}$	% diff.
Local Mean Weighted	1.2065	12.77	4,300	186.66
Medium-term Calibration	1.1987	12.05	4,415	194.31
Long-term Calibration	1.1761	9.93	3,446	129.74
Complete Data Set Calibration	1.1898	11.22	3,891	159.42
Average of 2 ($Flux^{adj.avr.2}$)	1.1928	11.49	4,013	167.53
Average of 3 ($Flux^{adj.avr.3}$)	1.2016	12.32	4,357	190.49
Average of all ($Flux^{adj.avr.4}$)	1.1961	11.80	4,202	180.13
Interpolation	1.1514	7.62	1,500	0.00
Raw Secondary Data	1.1272	5.36	1,860	24.00
Primary Data	1.0698	0.00	1,500	0.00

flux level due to possible effects of spatial differences of instruments onboard different spacecraft. Although laborious it is necessary to be confident that the gap filling method has been affective to visually inspect the original and resulting flux profiles for SEPEs. Where there is no other data set to scale and fit to a gap the 3$^{\mathrm{rd}}$ order polynomial fitting method will be used.

The analysis carried out here over 135 generated artificial data gaps provides good evidence of the relative strength of the Local Mean Fitting Method in comparison to other possible techniques of filling data gaps. It is known that the > 10 MeV channel on GOES-6/SEM has a gain problem resulting in low flux level (Rosenqvist et al., 2005) as such it provided a good test for the algorithms. Other than the requirement that data is binned in the same energy and time there is no reason why the Local Mean Fitting Method cannot be applied to other gaps in solar particle data where there is a secondary data source available.

3.4 Creating A New SEPE List

The JPL event list uses daily averaged fluxes which limits the precision at which the start and end times of the SEPEs are calculated. The SEPEs in the PSYCHIC event list are manually detected which makes the list difficult to reproduce. The NOAA event list does not give durations or end times for the SEPEs. A new list presented here named 'The SARG Event List' makes use of the data processing tools introduced in Sections 3.2 and 3.3 meaning that the start and end times can be automatically and accurately calculated without fear that the characteristics will be erroneous. This accuracy in turn will allow more precise distribution fits to the SEPE waiting times and durations. The peak flux and fluence data is stored in standard differential energy bins and all the data is 5-minute average for a consistent time series. SEPEs significant at any of the ten energies used were included but events not significant in terms of peak flux or fluence at any of the energies were excluded (justification for these exclusions were given in Section 2.2.4). Automation of the process makes it faster, eliminates any bias which might be introduced by the creator of the list and makes the list more easily reproducible and extendable with new data. However, a manual check was performed to ensure that the algorithms were performing as expected and changes made where necessary.

3.4.1 Choice of Raw Data

It was decided to use the GOES/SEM differential data to form the data set. This data stretches from the beginning of 1986 to the present day. One major positive aspect of this data is that it doesn't saturate unlike the data available from the IMP-8 spacecraft. Saturation of the CPME instrument at high fluxes was noted by Tylka et al. (1997) while the GME instrument had similar issues reported by Xapsos et al. (2004) forcing the authors of the PSYCHIC model to use data from GOES at times of high flux. Saturation affects the flux time series at the most important point, i.e. the peak of SEPEs, which has a significant impact on both the peak flux and the fluence value for the events. Another advantage of using the GOES/SEM data is that for the entire time period there is redundancy because there are always 2 or 3 spacecraft operating. This means that no events are missed due to instrument malfunction and that the

time series can be compared to validate the data and calibrated if necessary. The time ranges for data available from the GOES spacecraft used are shown in Table 3.5.

Table 3.5: Time ranges for GOES spacecraft.

GOES-5 (1986-01-01 1987-03-31)	GOES-8 (1995-03-01 2003-06-17)
GOES-6 (1986-01-01 1994-12-31)	GOES-10 (1998-07-01 2009-06-30)
GOES-7 (1987-03-01 1996-08-31)	GOES-11 (2000-07-01 2009-06-30)

The GOES/SEM instruments also have the same time resolution of 5 minutes which users of SEPE models have stated is the desired time resolution at a Round Table Meeting of Experts in Southampton, February 2007. At that meeting it was also decided that the energy range of interest for users of SEPE models was 5-200 MeV. There are two sets of 6 energy channels that have been used on the GOES/SEM instruments (see Table 3.6), the lowest channels (not listed) were not used as they are outside the range of interest and heavily contaminated by trapped particles. The energy resolution is not as good as that provided by the IMP-8 instruments but is sufficient to calculate energy spectra and therefore convert the data into standard energy bins.

Table 3.6: Raw data energy bins with geometric mean values.

GOES-5/-6/-7	Bin 1	Bin 2	Bin 3	Bin 4	Bin 5	Bin 6
Energy (MeV)	4.2 - 8.7	8.7 - 14.5	14.5 - 44	39 - 82	82 - 200	110 - 500
Geo. Mean (MeV)	6.04	11.23	25.26	56.55	128.06	234.52
GOES-8/-10/-11	Bin 1	Bin 2	Bin 3	Bin 4	Bin 5	Bin 6
Energy (MeV)	4.0 - 9.0	9.0 - 15	15 - 40	40 - 80	80 - 165	165 - 500
Geo. Mean (MeV)	6.00	11.62	24.49	56.57	114.89	287.23

It would be desirable to extend this data set further into the past but the data from prior to 1986 would need to be processed not just for spikes and data gaps but also for saturation effects which are widely reported (Tylka et al., 1997). As such this list is used in this work to illustrate a modelling methodology with the hope that the data set may be extended to produce an improved model.

3.4.2 Initial Event Detection Parameters

The event recognition algorithm detects events from the flux time series between two dates for a specific particle and a specified energy using four user input parameters; the flux start threshold (the flux value above which an event is said to have begun, this should be significantly higher than the background level), the flux end threshold (the flux value signifying the end of the event, often chosen to be the same as the start threshold) and the time after the event drops below and remains below the threshold before it is said to have ended (the lagtime).

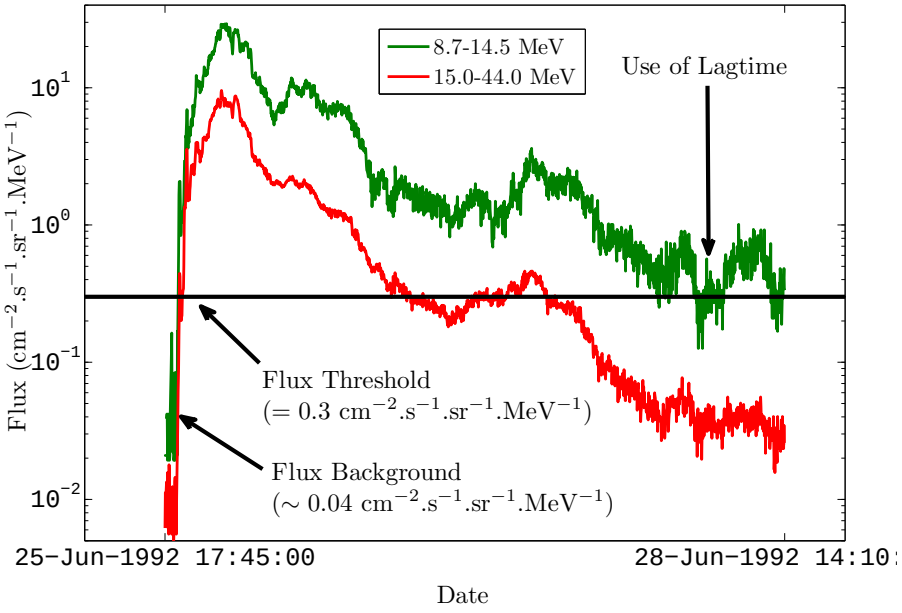

Figure 3.18: Event definition parameters as applied to SEPE beginning 25$^{\text{th}}$ June 1992.

The initial detection of events used the second energy bins from Table 3.6 and a flux threshold of 0.3 cm^{-2}sr^{-1}s^{-1}MeV^{-1} for both the start and end of the events. This threshold value is almost an order of magnitude above the background level as shown in Figure 3.18. By comparison of the GOES-7 8.7-14.5 MeV differential channel and integral data for $>$ 10 MeV for September 1989 (see Figure 3.19) it can be seen that this threshold is equivalent to a value between 1 pfu (used for the $>$ 10 MeV channel for the JPL series of solar proton models) and 10 pfu (used in the creation of the NOAA event list) although it is nearer to the former.

A minimum event duration is included in the event recognition to eliminate anomalies detected as events, this is an easy way of avoiding a large initial event list full of

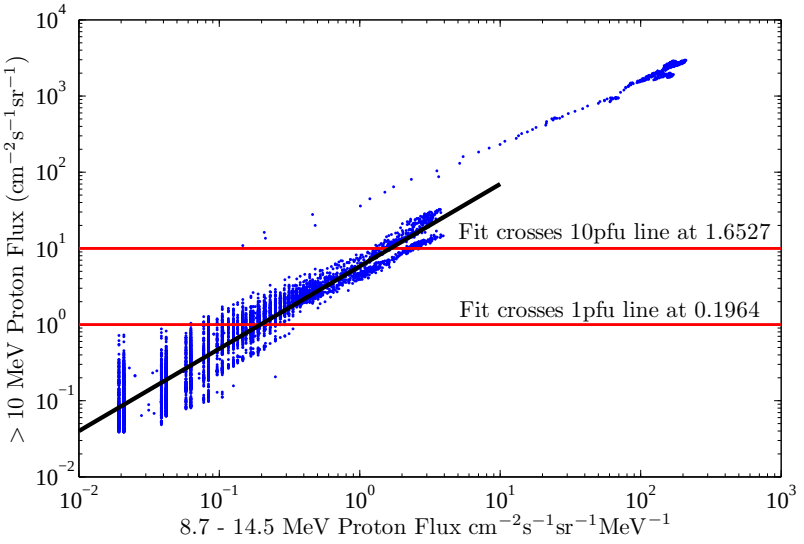

Figure 3.19: Comparison of differential 8.7-14.5 MeV proton flux data and > 10 MeV proton flux data from GOES-7/SEM for September 1989

erroneous 'non-events'. This value was chosen to be 1 hour since it avoids elimination of significant SEPEs which are known to last from days to weeks. The fluences and peak fluxes of any small impulsive events which may be eliminated would not make a significant contribution compared to larger events and therefore not considering them does not affect the model's accuracy.

Lastly a lagtime of 12 hours is used to ensure that events which are close in time but were separated due to a drop below the flux threshold were linked together. The effect of the lagtime can be seen in Figure 3.18 where the flux drops below the threshold level but does not remain there for 12 hours so the event continues. This is important as an earlier CME may leave seed particles which are re-accelerated by the next and therefore the fluxes of the enhancements are not independent (see Section 2.1.5). A lagtime of 2 days was used for the JPL event list but there is no such lagtime for the NOAA event list and by visual inspection of the SEPEs found a value of 12 hours appears suitable to achieve the goal. For more background on event definition see Section 2.2.4.

For the complete time range from 1986 to 2009 this event definition gave an initial list of 201 events at a rate of 8.739 per year.

3.4.3 Manual Start/End Time Extensions

As this list was defined only in one (relatively low) energy channel each event was plotted and the duration extended where the enhancements in other energy channels extended outside the original start and end time limits. This was especially important for the event onset in the higher energy channels, due to a larger portion of higher energy particles arriving at 1AU sooner than the lower energy particles, failure to account for this would result in lower fluences (and sometimes peak fluxes) for these energy channels which would result in erroneously predicting a less harsh environment at higher energies. This process was done manually by eye for each of the 201 events.

3.4.4 Cross-Calibration

It is important to calibrate the data as it has been shown by Rosenqvist et al. (2005) that there are significant differences in the fluence values given for the same events using different instruments. It was noted in the work of these authors that the data from GOES-7 and GOES-8 were reliable (the event fluences were in good agreement and thought to accurately reflect the incident particles). GOES-7 and GOES-8 data was used as the primary (or baseline) data set where possible. A secondary data set would be used only to fill data gaps (as described in Section 3.3). Data from GOES-6 and GOES-10 instruments needed to be scaled as the agreement with other instruments was poor. The authors showed that the impact on the JPL-91 model in the > 10 MeV channel is significant (Rosenqvist et al., 2005).

3.4.4.1 Methodology

The method used by Rosenqvist et al. (2005) was to take the event fluences, to plot them against one another and then apply a straight line fit, the parameters of which produce a factor for scaling each of the fluences of events in the time series.

This method has been adapted to be applied to the instantaneous flux values for 8 events to compare GOES-6 data to GOES-7 data and 7 events to compare GOES-10 data to GOES-8 data and GOES-11 data to GOES-8 data. As GOES-7 and GOES-8 data are seen as reliable the idea is to find scaling factors for the remaining three data sets. The calibration is the same as that applied for the inter-calibration gap filling methods introduced in Section 3.3.2.2 with the straight line fit illustrated in Figure

3.12. The slope of the straight line fit is calculated for each SEPE and the average of the slope gradients for each channel across the selection of events is then used to scale the data set. All points within the events where data was available in both of the two time series being compared were used to find this gradient. This slope is termed the comparison of fluence values as it uses all available points for the SEPE. The ratio of peak fluxes were also calculated for each channel for each SEPE to investigate any variation between this and the fluence values (these used only the single highest flux points).

3.4.4.2 Results

There were significant differences in the parameters found for calibration of the same instruments with different SEPEs but the trends were clear. Firstly the calibration of GOES-6 using GOES-7 is investigated. It was noted by Rosenqvist et al. (2005) that the $>$ 10 MeV integral energy channel on GOES-6 systematically under-estimated the size of events. The results of the comparison done here show that there is a small contribution to this from the 8.7 - 14.5 MeV energy channel but that the main contribution to this comes from the 14.5 - 44.0 MeV energy channel with a mean peak flux 5.337 times lower (see Table 3.7) and a mean fluence 5.539 times lower (see Table 3.8) than that of GOES-7. The 4.2 - 8.7 MeV and 110 - 500 MeV channels were in good agreement overall and the 39.0 - 82.0 MeV and 82.0 - 200 MeV channels gave higher values for GOES-6 than GOES-7.

Table 3.7: Ratios of Peak Flux Values for 8 Events for GOES-6 and GOES-7.

Channel No.	Ev. 1	Ev. 2	Ev. 3	Ev. 4	Ev. 5	Ev. 6	Ev. 7	Ev. 8	Mean
1	0.360	1.039	0.878	0.786	0.995	0.866	0.991	0.907	0.853
2	0.618	1.410	1.259	1.284	1.394	1.165	1.154	1.172	1.182
3	1.504	3.307	3.457	6.098	7.567	4.662	7.556	8.545	5.337
4	0.255	0.843	0.723	0.662	0.694	0.771	0.919	0.826	0.712
5	0.863	0.934	0.782	0.884	0.793	0.955	0.869	0.823	0.863
6	0.918	1.013	1.198	1.333	0.882	1.480	0.987	0.931	1.093

Figure 3.20 shows the effects of applying the calibration values from the last column of Table 3.8 to the GOES-6 data for an event prior to the start of the GOES-7 data set.

Table 3.8: Ratios of Fluence Values for 8 Events for GOES-6 and GOES-7.

Channel No.	Ev. 1	Ev. 2	Ev. 3	Ev. 4	Ev. 5	Ev. 6	Ev. 7	Ev. 8	Mean
1	0.988	0.997	0.895	0.833	0.999	0.868	1.012	0.954	0.943
2	1.619	1.249	1.242	1.270	1.245	1.186	1.333	1.238	1.298
3	2.651	3.548	4.871	6.422	6.173	4.385	7.682	8.577	5.539
4	0.813	0.827	0.690	0.661	0.780	0.764	0.867	0.847	0.781
5	0.826	0.871	0.733	0.732	0.836	0.895	0.899	0.842	0.829
6	0.901	1.024	1.050	0.791	0.938	1.355	1.041	0.964	1.008

Figure 3.20 (top) gives the unaltered flux profiles in which the 14.5 - 44.0 MeV energy channel is clearly lower than would be expected lying very close to the higher 39.0 - 82.0 MeV energy channel. Figure 3.20 (bottom) shows the corrected flux profiles. Here the separation between energy channels appears to be what would be expected.

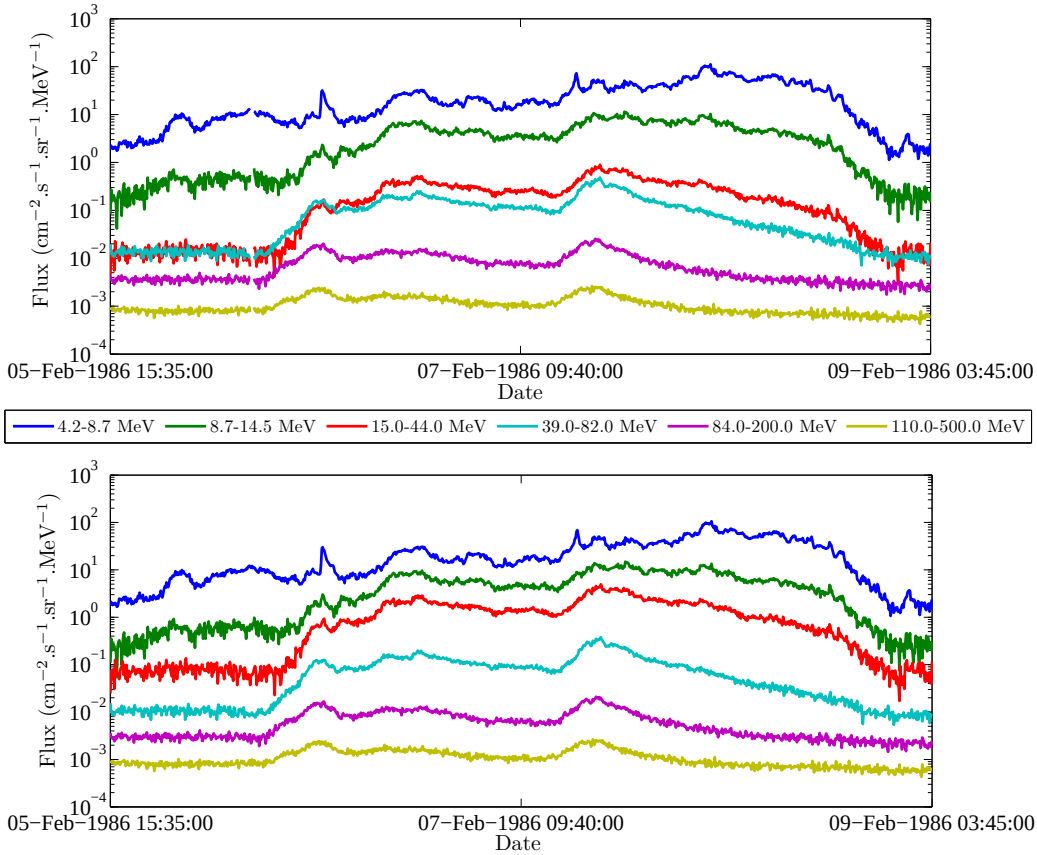

Figure 3.20: GOES-6/SEM data for SEPE on 5th February 1986 before calibration (top) after calibration (bottom).

Next, the calibration of GOES-10 using GOES-8 is studied. Each of the GOES-10

channels give peak flux values (see Table 3.9) and fluence values (see Table 3.10) lower than those given by GOES-8 for the same time periods. The greatest difference is seen in the 9.0 - 15.0 MeV and 15.0 - 40.0 MeV energy channels. This is similar to the results reported by Rosenqvist et al. (2005). There some differences between the results from the fluence and peak flux comparisons and while this is to be expected due to the different positions of satellites they are more pronounced here than in the other cases. This is because the GOES-10/SEM instrument gives significant periodic fluctuations. It is therefore deemed a poor instrument compared to GOES-8 and GOES-11 and is only used where there is no other viable alternative.

Table 3.9: Ratios of Peak Flux Values for 7 Events for GOES-10 and GOES-8.

Channel No.	Ev. 1	Ev. 2	Ev. 3	Ev. 4	Ev. 5	Ev. 6	Ev. 7	Mean
1	1.110	1.399	1.118	0.874	0.648	2.027	0.978	1.165
2	1.148	1.887	1.382	1.136	0.986	2.139	2.739	1.631
3	1.259	1.215	1.233	1.038	0.925	2.598	4.902	1.881
4	1.136	0.979	1.443	1.311	1.340	1.144	2.152	1.358
5	1.113	0.968	1.095	1.123	1.175	0.967	1.270	1.102
6	1.130	1.061	1.218	0.926	1.145	1.140	1.272	1.127

Table 3.10: Ratios of Fluence Values for 7 Events for GOES-10 and GOES-8.

Channel No.	Ev. 1	Ev. 2	Ev. 3	Ev. 4	Ev. 5	Ev. 6	Ev. 7	Mean
1	1.012	1.915	1.375	0.978	0.959	2.318	1.514	1.439
2	1.218	2.288	1.676	1.394	1.351	2.440	2.690	1.865
3	1.196	1.470	1.446	1.078	1.243	2.053	3.217	1.672
4	1.128	1.207	1.395	1.193	1.454	1.220	2.093	1.384
5	1.040	0.983	1.036	0.957	1.068	1.008	1.274	1.052
6	1.105	1.039	1.175	1.012	1.075	1.084	1.248	1.106

Lastly, the calibration of GOES-11 using GOES-8 shows a $\sim 25\%$ error in the 9.0 - 15.0 MeV and 15.0 - 40.0 MeV energy channels although elsewhere there was good agreement. There was good agreement between the fluence (see Table 3.11) and peak flux (see Table 3.12) comparisons. As a result of this the scaled GOES-11 data was used preferentially over GOES-10 after 2003 when GOES-8 stopped being operational.

It was not always possible to use GOES-11 as there is a large data gap in the data set which extends until after GOES-8 stopped being operational. As a result, GOES-10 had to be used as the primary spacecraft for one event in June 2003. The GOES-11 data gap ends part way through this event and was therefore used as the secondary spacecraft (it could be used to fill data gaps using the method given in Section 3.3 for the latter part of the event).

Table 3.11: Ratios of Peak Flux Values for 7 Events for GOES-11 and GOES-8.

Channel No.	Ev. 1	Ev. 2	Ev. 3	Ev. 4	Ev. 5	Ev. 6	Ev. 7	Mean
1	0.982	0.960	0.849	0.876	0.722	0.870	1.286	0.935
2	1.140	1.469	1.105	1.301	1.203	1.344	1.240	1.257
3	1.217	1.221	1.347	1.143	0.999	1.345	1.402	1.239
4	1.029	0.858	0.958	1.028	0.962	0.925	1.053	0.973
5	1.053	0.964	0.987	1.158	1.028	0.955	1.049	1.028
6	1.130	0.968	1.098	1.029	0.998	1.043	1.103	1.053

Table 3.12: Ratios of Fluence Values for 7 Events for GOES-11 and GOES-8.

Channel No.	Ev. 1	Ev. 2	Ev. 3	Ev. 4	Ev. 5	Ev. 6	Ev. 7	Mean
1	0.882	1.028	0.902	0.922	0.995	1.240	1.159	1.019
2	1.064	1.506	1.102	1.350	1.438	1.394	1.284	1.305
3	1.204	1.170	1.232	1.098	1.203	1.382	1.455	1.249
4	0.963	0.901	0.987	0.975	0.957	0.911	0.985	0.954
5	1.049	1.022	1.028	1.001	1.001	0.990	1.062	1.022
6	1.106	1.019	1.113	1.013	1.010	1.035	1.080	1.054

3.4.4.3 Implementation

The scaling factors for the fluences were used to scale GOES-6 to GOES-7, GOES-10 to GOES-8 and GOES-11 to GOES-8 where it was not possible to use either GOES-7 or GOES-8 as the primary data set. The peak flux scaling factors were calculated to check that there was no significant differences at higher flux values. Any difference would imply a difference in the behaviour of instruments with increasing flux. In all but the GOES-10 to GOES-8 comparison differences between the two were small. The

Table 3.13: Standard energy bins with geometric mean values.

	Bin 1	Bin 2	Bin 3	Bin 4	Bin 5
Energy (MeV)	5.0 - 7.2	7.2 - 10.5	10.5 - 15.1	15.1 - 21.9	21.9 - 31.6
Geo. Mean (MeV)	6.01	8.70	12.58	18.18	26.30
	Bin 6	Bin 7	Bin 8	Bin 9	Bin 10
Energy (MeV)	31.6 - 45.7	45.7 - 66.1	66.1 - 95.6	95.6 - 138	138- 200
Geo. Mean (MeV)	38.03	54.99	79.53	115.01	166.31

peak flux scaling factors were not used in the model but were calculated for validation purposes (these use only a single flux point as opposed to the fluence values which use all in the event). The scaling factors were calculated after the removal of spikes (as described in Section 3.2) but before the filling of gaps with secondary data or a polynomial fit (as described in Section 3.3). However, in the creation of the SARG event list the scaling factors were applied to the SEPE time series after the data gaps had been filled.

3.4.5 Re-Binning into Standard Energies

At this juncture there are 6 different energy channels for events found using GOES-6 and GOES-7 and those found using GOES-8, GOES-10 and GOES-11. To standardise these energy bins a set of 10 energy bins were established with the boundaries distributed linearly on a logarithmic scale between 5 and 200 MeV. These are shown in Table 3.13. For each event spectra were produced for both the fluence and the peak flux using the geometric mean values for each bin. The geometric mean is the square root of the product of the upper and lower bin boundaries. The modified fluence and peak flux values were then calculated using a straight line fit on double logarithmic axes between the two closest points from the raw data energy bins. In most cases it was found that the spectra could be approximated by a power law (a straight line through all the points on double logarithmic axes) but that there was significant deviation probably because the spectrum changed over the course of the event and because the peak fluxes in different energies occur at different times. For this reason a piecewise simple numerical interpolation method was favoured over an analytical method.

Figure 3.21 (top) shows the flux profiles from an SEPE from September 2000 as measured by GOES-8 with gaps filled using GOES-11. Figure 3.21 (bottom left) shows the event fluence spectra with deduced fluences found for the ten standard energy channels. Figure 3.21 (bottom right) shows the event peak flux spectra with deduced fluences found for the ten standard energy channels.

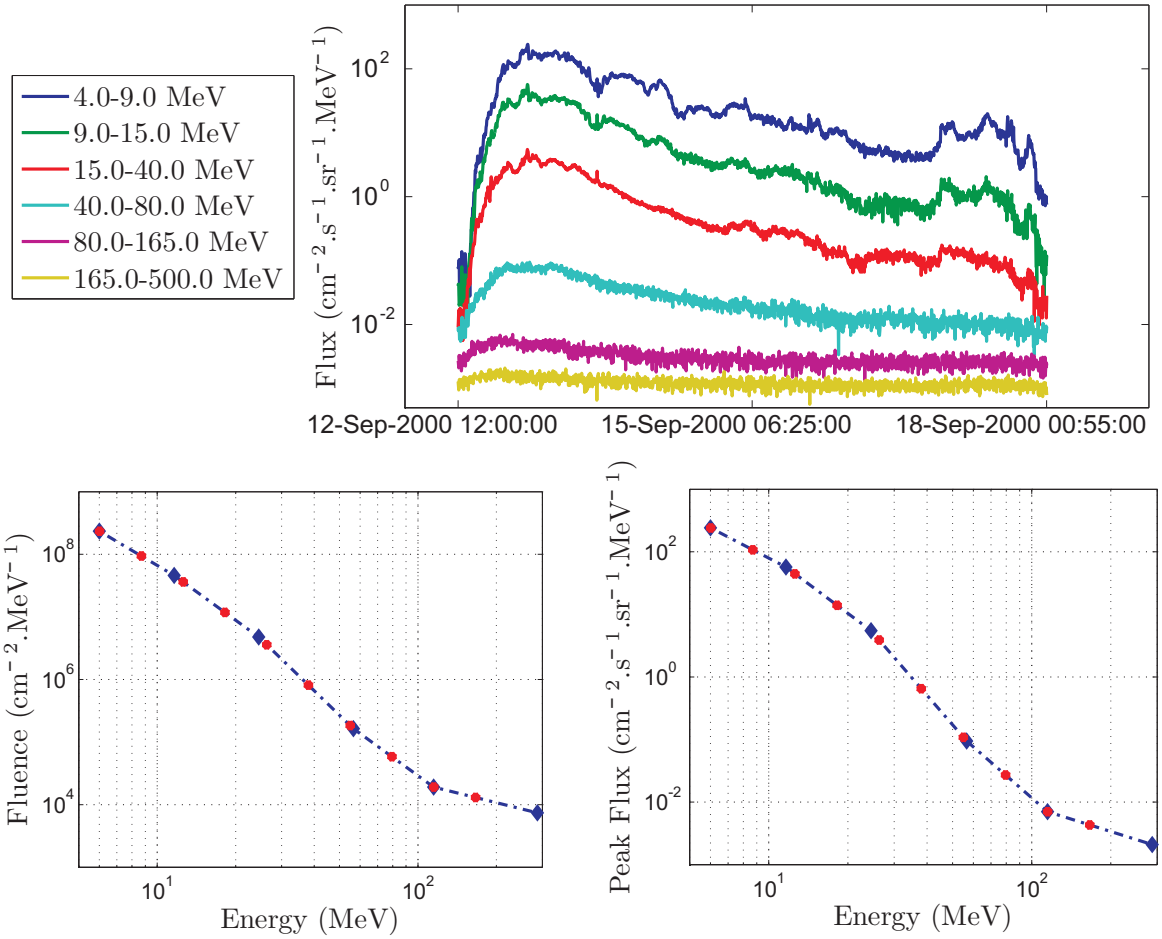

Figure 3.21: Flux profile from event from 12th September 2000 (top), differential fluences for (bottom left), differential peak fluxes (bottom right). Blue diamonds linked by dashed lines show the original values, red circles show the deduced values in standard energy bins.

3.4.6 Minimum Fluence and Peak Flux Exclusions

Some of the events in the list were found to be either insignificant enhancements or some increase in the background not caused by solar sources. It is important to exclude these events as they would skew the waiting time and duration fits. Having

inspected the data the fluence and peak flux thresholds shown in Table 3.14 were found, if an event did not achieve at least one of the 20 parameters it was removed from the list as a 'non-event'. The fluence thresholds displayed here are also to be used for the modelling in the respective energy channels so that only events with a significant enhancement in the energy channel being studied would be included to avoid skewing the distributions. The units for both the fluences and peak fluxes include MeV^{-1} due to the data being from differential channels rather than integral.

Table 3.14: Minimum event fluences and peak fluxes.

	Bin 1	Bin 2	Bin 3	Bin 4	Bin 5
Min. Fluence ($cm^{-2}MeV^{-1}$)	2.5×10^6	10^6	3.5×10^5	1.5×10^5	5×10^4
Min. Peak Flux (pfu/MeV)	12	2.5	1	0.4	0.2
	Bin 6	Bin 7	Bin 8	Bin 9	Bin 10
Min. Fluence ($cm^{-2}MeV^{-1}$)	2.5×10^4	10^4	10^4	10^4	10^4
Min. Peak Flux (pfu/MeV)	0.075	0.05	0.025	0.01	0.005

3.4.7 Final List

The complete SARG Proton Model event list is included in Appendix Section A.3. This event list includes 176 events in a time period of 23 years (1986-2009) at a rate of 7.65 per year. During the 14 years of solar maximum data 158 events were recorded at a rate of 11.29 per year.

It would be desirable to extend this list further and to include data from the 1960s to 1985 which would double the size of the data set. However, due to data caveats such as saturation confidence in the intensity (fluence and peak flux) values is poor in older data. An example of this is the August 1972 event. This event is the most important SEPE from the start of space-based particle observations to the beginning of the GOES data set used for the SARG event list. Mewaldt et al. (2005) show a > 10 MeV fluence of approximately 2×10^{10} cm^{-2} which is approximately equal to the fluence of the October 1989 event which is the largest in the GOES data. However, this fluence is quoted as 1.1×10^{10} cm^{-2} in the JPL-85 list (Feynman et al., 1990) which, upon visual inspection of plots, is the same value used for the JPL-91 model (Feynman et al., 1993). The King model (King, 1974) used a value of 2.25×10^{10}

cm^{-2} for the fluence of the August 1972 event in the > 10 MeV integral channel.

The JPL list included in Appendix Section A.1 shows that for the complete time period 1965-present there are 6 events with a fluence $> 10^{10}$ cm^{-2} in the > 10 MeV energy channel. These events are listed in Table 3.15. Only the August 1972 event is prior to 1986 and the quoted fluence is the 2^{nd} lowest from the six listed. Were the King value of 2.25×10^{10} cm^{-2} used it would be the largest, however, it would lie within the distribution of the highest event fluences.

Table 3.15: Largest events in JPL event list.

Start Date		Duration	Fluence
Year	DoY	(days)	> 10 MeV
1972	217	23	1.10E+10
1989	292	22	1.93E+10
2000	195	11	1.65E+10
2000	314	11	1.08E+10
2003	299	17	1.58E+10
2001	308	9	1.52E+10

There are two possibilities from the consideration of the timings of the largest events in the JPL list. The first is that the majority of the largest SEPEs occurred in cycles 22 and 23 while the GOES satellites were operational. The second is that there were a greater number of large events which occurred prior to 1986 but that the instruments failed to correctly record the fluences. Therefore inclusion of data prior to 1986 without some processing (to account for instrument saturation especially) would not significantly increase the number of large large events in the data set. However, it must be accepted that if cycle 22 and 23 were more active, using only the SARG list will affect model results predicting a harsher environment than if other, less active cycles were included.

Chapter 4

Statistical Modelling of SEPEs

4.1 Introduction to SEPE Modelling

Prior to this work there were two distinct methodologies for modelling with SEPE environment. The first follows the King method (King, 1974) and is followed by all the variants of the JPL solar proton models (Feynman et al., 1990, 1993, 2002; Rosenqvist et al., 2005). All these models are mission cumulative fluence models designed to predict the total fluence of particles that will arrive at 1 AU over an area of one square centimetre for a given time period against confidence level (the confidence with which it can be said that the value will not be exceeded). Here a Monte-Carlo method is applied to combine distributions of SEPE frequency and SEPE fluence. The event frequency distribution gives the likelihood of any integer number of events from zero upwards. A percentage of the Monte-Carlo runs equal to this likelihood for each number of events are carried out. So, for example, if there was a 10% chance of seeing 7 events in any given year and 100,000 Monte-Carlo runs were being performed then 10,000 of these would be done with 7 SEPEs. The fluences for the number of SEPEs in each Monte-Carlo iteration are generated using the fluence distribution (see Section 2.2.5). These are then summed to generate the cumulative fluence for that run. Once all the fluences for all the iterations have been calculated these are then sorted in ascending order and plotted against a uniform vector of the same length with range [0,1] sorted in descending order which represents the likelihood that the corresponding fluence will be exceeded. If a user wished to calculate the fluence for the 90% confidence level (10% likelihood of being exceeded)

this would be the value which 90% of the Monte-Carlo runs' fluences were lower and only 10% were greater. These fluences vary depending on the mission length with a longer mission length having a different event frequency probability density function (pdf) to reflect this. These fluences would also vary with energy with lower fluences for higher energy particles. The MSU model extrapolates the energy dependence using an analytical formula (see section 2.3.3) while the King and JPL models use measured data for different energies. This method could easily be extended to consider the worst-case scenario by taking the maximum fluence (or peak flux value) generated for an event for each Monte-Carlo iteration. Xapsos et al. (1998a) gives an analytical way of combining two distribution functions (see section 2.3.4) which avoids the necessity of performing a large number of iterations but this can only be used for the worst-case SEPE fluences (Xapsos et al., 1999) and peak fluxes (Xapsos et al., 1998b) rather than the cumulative fluence model.

Another method for modelling the SEPE environment is to consider the time series in blocks of equal duration rather than to find the SEPEs in the time series. By considering the distribution of fluences of each of these blocks a likelihood that a specified fluence might be exceeded can be generated in a mission of duration equal to the length of the blocks. Xapsos et al. (2000) used the yearly fluences to predict the future SEPE environment and extrapolated this prediction to include predictions of mission lengths other than one year (see section 2.3.4). Feynman et al. (2000) used time blocks of 60 days combined with assumptions of radial dependence of fluences (see section 2.1.6) to estimate the fluence that might be seen by the Solar Probe mission which is intended to travel to 3 solar radii of the solar surface and is to be launched in approximately 2015.

4.2 The SARG Modelling Methodology

The modelling methodology for this work differs slightly from previous methodologies. Through the creation of 'virtual timelines' this methodology allows the inclusion of SEPE waiting times, durations, fluences and peak fluxes. Simply each timeline begins with a waiting time, this is then followed by an event which has an associate fluence and based on this fluence using relationships established a duration (by numerical

regression) and peak flux (by analytical regression) are derived. Another waiting time is then generated and so on until the timeline covers the mission length or period of interest. The inclusion of the SEPE durations means that the waiting times used will be the time from the end of one event to the start of the next. A visualisation of the start of a virtual timeline is shown in Figure 4.1.

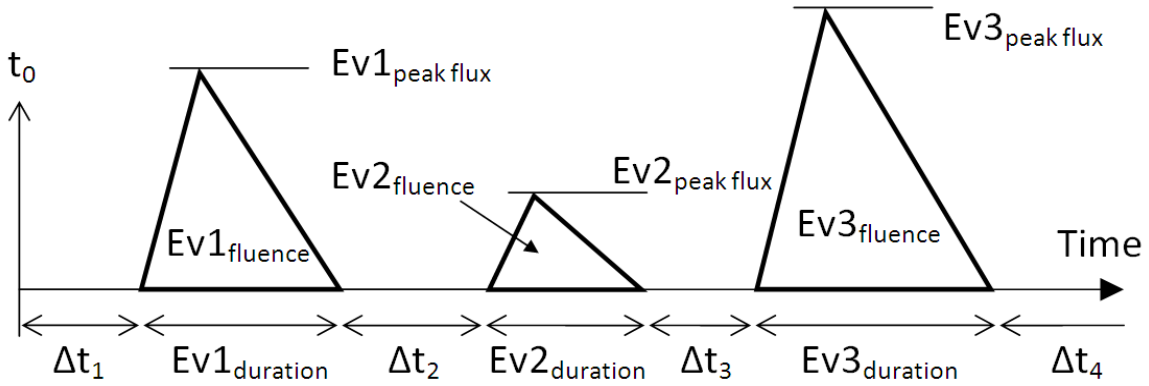

Figure 4.1: Visualisation of SARG virtual timeline methodology.

Using a distribution of event frequency as done in all previous models inherently ignores the differences in SEPE durations as the position of these events in time and their fluences are not considered by the event frequency. An equivalent of this is to take the waiting time to be from the start of one event to the start of the next. By ignoring the effect of durations the likelihood of a high fluence event (which generally have longer durations) being closely followed by another event is over-predicted and the likelihood of a short duration event being closely followed by another event is under-predicted. There is likely an averaging effect of these two possibilities seen in a model with many iterations but if the highest confidences are dominated by iterations with a large number of large fluence (and therefore large duration) events which are being over-predicted the impact could be significant. It is therefore hoped that the SARG method of virtual timelines creates iterations which are more realistic than previous models.

Each virtual timeline considers only a single energy channel. The difficulties of combining all the ten energy channels (from the SARG event list, see section 3.4.5) for both fluence and peak flux along with the SEPE duration are significant. Applying the method to different energies separately avoids possible negative consequences of

assumptions regarding energy spectra which might be flawed. The statistical distributions which form the components of this method are covered in the following sections. The way in which the distributions of waiting times, durations, fluences and peak fluxes are connected and the modelling method outputs are shown in Figure 4.2. The figure shows the regressions of peak flux and duration using event fluences which are crucial to creating realistic timelines and the fits of waiting times and durations which result in the use of new distributions with inter-dependence of SEPEs found which constitute a novel aspect of this work.

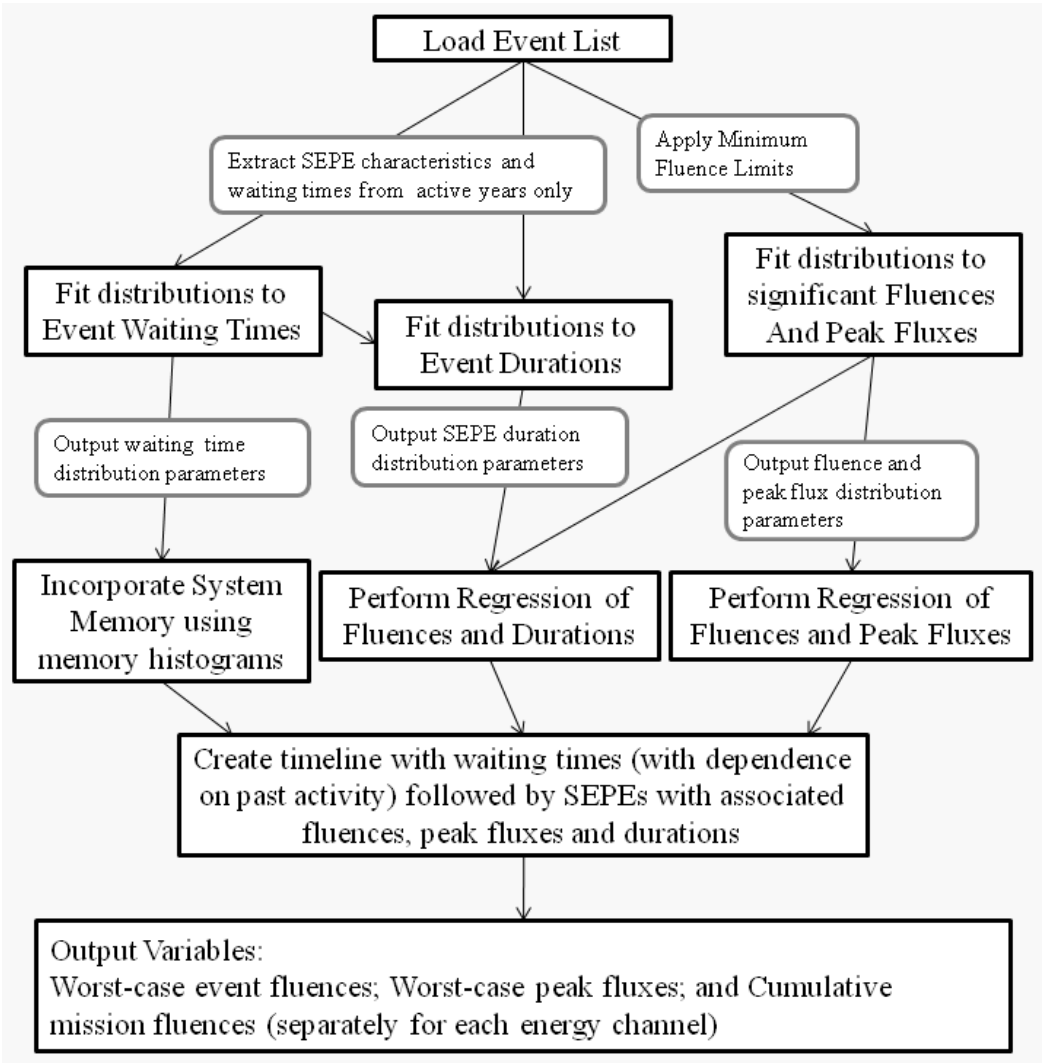

Figure 4.2: Flow chart of SARG modelling methodology.

4.2.1 Number of Iterations

Despite combining the durations, peak fluxes and fluences into a single timeline, there remain a total of 10 channels and 6 time periods for which the model needed to be run. The 10 channels are the aforementioned standard energy channels while the 6 time periods include the 1, 2, 3, 5 and 7 years which are calculated for the JPL model and, additionally, a period of 0.5 years which could be of interest to those planning short missions or wanting a prediction for a small part of the mission length. This is a total of 60 variants each of which was run through 300,000 iterations to produce reliable results. This 300,000 limit is a combination of the time is takes to run the complete model ($\sim$ 34 hours) and the memory capacity to hold all the data. This is still a very high number of iterations compared to the 100,000 or fewer normally seen as sufficient for such calculations.

4.2.2 Irrelevant Events

One additional consideration was the proportion of events for which there was no significant increase in the different energy channels. Inclusion of 'irrelevant events' will skew the distribution fits of SEPE fluence and peak flux. While there are a total of 158 active year events in the SARG event list these are not all important at all energies and a smaller portion of these are important as the energy is increased. Table 4.1 shows the number and percentage of the 158 events which were found to be relevant at each energy using the fluence thresholds given in Table 3.14 in Section 3.4.6. The values for all event energies are still included in the complete list in Appendix Section A.3 from which event spectra may be deduced.

Table 4.1: Number of active year events relevant in each energy channel.

Channel	1	2	3	4	5
No. of Events	132	133	132	131	136
Portion of Total	0.835	0.842	0.835	0.829	0.861
Channel	6	7	8	9	10
No. of Events	129	131	95	59	36
Portion of Total	0.817	0.829	0.601	0.373	0.228

There are two possibilities for accounting for this. The first is to calculate the

waiting time and duration fittings for each of the energy channels separately and following the above method for creating events in each case. The problem with using this method is that by excluding a large number or events is it difficult to perform and validate the fittings for waiting times and durations especially at higher energies.

The method chosen to account for irrelevant events was to generate a random number (between zero and one) and if this was below the value shown in Table 4.1 for that energy channel the fluence was found and the duration was then generated using the regression depending on this value. However, if the random number was above the value shown then only an event duration was calculated from the SEPE duration distribution which was adjusted to account for the likely exclusion of larger events using the maximum duration from the irrelevant events in the SARG event list.

Table **??** shows the numbers of event used for the JPL-91 model for various energies. These are comparable to the numbers shown in Table 4.1. King (1974) had only 25 events on which to perform his analysis. The more events and the longer the time period the more reliable it would be expected that the results would be (see Section 2.2.2), however, compared to the JPL-91 model this data set compares well in terms of size.

Table 4.2: JPL events used (taken from Feynman et al. (1993)).

Parameter	>1 MeV	>4 MeV	>10 MeV	>30 MeV	>60 MeV
No. of Events	89	122	114	122	80
Number of Years	10.6	10.6	16.9	16.9	16.9
Average per year	8.40	11.5	6.75	7.22	4.73

4.2.3 One-Year Start-Up

To randomise the start point a one-year start-up period was used for each iteration. This was necessary because the event occurrence is not random in time as will be shown in the following section. The waiting times, fluences, peak fluxes and durations for this year were calculated as per normal but were not included in the final results the iteration. Where an event began in this start-up year but finished in the period of interest its fluence and peak flux were not included but if they began in the period of interest but finished after the period of interest had ended the fluence and peak flux

were included. This is because in general the higher fluxes occur near the beginning of an SEPE so to assume it was evenly distributed over the course of the event would be inaccurate and there should be an averaging effect over the course of the 300,000 iterations performed for each channel and time period.

4.3 Time Distributions of Solar Energetic Particle Events: Are SEPEs Really Random?

Three separate event lists (JPL, PSYCHIC and NOAA) used in this section, each have different event definitions and therefore on occasion treat a series of enhancements differently as one or more events. By taking these independently created event lists the robustness and sensitivity to different treatment of episodes (or compound events) of the distributions fitted to the SEPE waiting times and durations is tested.

Enhancements can appear very differently at different helioradial distances, a good example of this using electron data from Helios-1 and IMP-8 is given by Cane (2005) (reproduced here in Figure 4.3). However, using all these definitions of an event, which combine such sequences (applied to the electron fluxes) both would be classified as only 1 event as the flux does not return to the background level in between enhancements. It is only shown here that the distributions are applicable at 1 AU, they may or may not be applicable at other helioradial distances but this cannot be determined without further data and they are certainly not applicable for physical process (i.e. flares and CMEs that give rise to SEPEs) on the surface of the Sun.

By identifying these enhancements in the flux time series a list of events is produced and a statistical distribution found to model the frequency of these events. This distribution, in conjunction with the event characteristics (fluence, peak flux and duration), can then be used to predict the SEP environment for the future. It was shown by Feynman et al. (1990) that the 11-year solar cycle can be split into an approximately 4-year quiet period and a 7-year active period and that the fluence contribution from the quiet periods was negligible in comparison to the active years. However, recently there has been interest in models for solar minimum (Xapsos et al., 2004) which does include some events such as those in December 2006 (Myagkova et al., 2009). For this reason in this study both the complete time period and the time period including

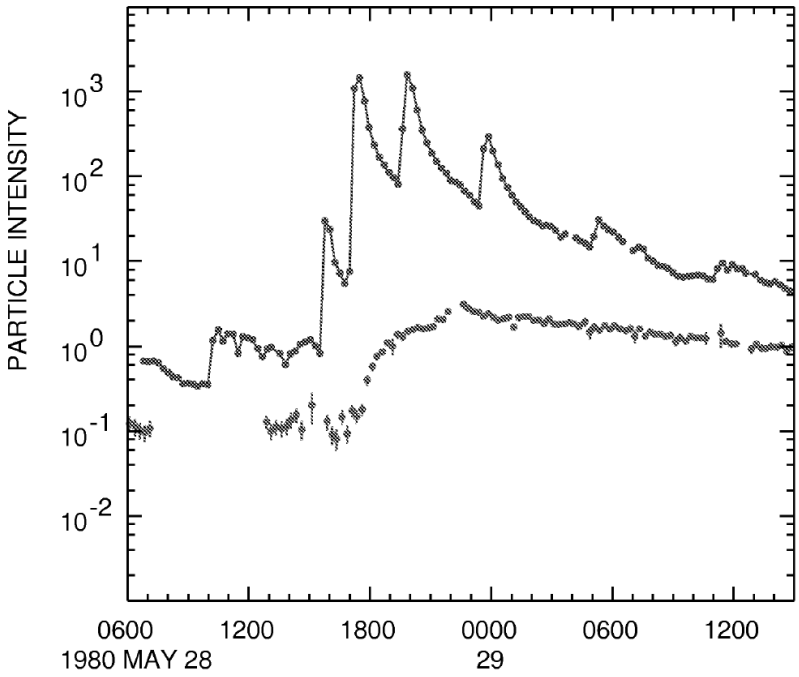

Figure 4.3: Electron fluxes for Helios-1 at 0.3 AU and IMP-8 at 1 AU (lower intensity) for an event in May 1980. Intensities in units of $cm^{-2}ster^{-1}s^{-1}MeV^{-1}$/nuc. Taken from Cane (2005).

only solar maximum years are investigated. The active year periods are assumed to begin 2.5 years before and end 4.5 years after the date of peak sunspot number for that solar cycle. These maxima are taken to be 1968.9, 1979.9, 1989.9 and 2000.2 for cycles 20-23 (Xapsos et al., 2004).

Currently all established models for the SEP environment (King, 1974; Feynman et al., 1993; Nymmik, 1999; Xapsos et al., 1998b, 1999, 2000, 2004) assume a Poisson distribution to model the frequency of SEPEs. The JPL-91 model for cumulative mission fluence (Feynman et al., 1993) employs such a Poisson distribution combined with a Monte-Carlo method and a lognormal distribution to generate event fluences. Nymmik (1999), in the creation of the MSU model, suggested that the event frequency is related to the sunspot number proxy for solar activity. This proxy gives an average event rate which is then input into the Poisson distribution and combined with a modified power law to calculate event fluences. The link between event frequency and sunspot number has been questioned by Feynman et al. (2002) due to a low correlation coefficient of 0.6 between the two. Combined with the difficulty in reliably predicting the future sunspot number this technique is very difficult to justify. The ESP (Emis-

sion of Solar Protons) cumulative fluence model (Xapsos et al., 2000) is based purely on the yearly fluence fitted with a lognormal distribution assuming that events are Poisson distributed and therefore the result for 1-year fluence can be extrapolated to different mission lengths using simple formulae. Related models for worst case event flux (Xapsos et al., 1998b) and worst case event fluence (Xapsos et al., 1999) also use a Poisson assumption to obtain their results.

The Poisson distribution has two major requirements to be applicable: the rate of events must be invariant with time (i.e. the process should be stationary) and the activity of the past should have no impact on the likelihood of a future event (i.e. the system should have no 'memory' or each event is independent of the previous one). In this section the focus on the waiting times between events which are related to the event frequency (being the transform from the frequency domain into the time domain) and the event durations which are one characteristic of events. The assumptions of stationarity of the process and independence of consecutive events are examined and two possible alternatives to the Poisson distribution for modelling event frequency and durations namely a time-dependent Poisson distribution and the Lévy distribution are proposed. It is found that there is memory existing in the process despite efforts to define events in a way that ensures consecutive events are independent and that the process, rather than being stationary, has a long-term time dependence which is not linked to solar cycle variation. In effect, SEPE occurrences are not random in time but are dependent on recent activity and longer-term changes in the Sun even within solar active periods. It is shown that the Poisson process is inadequate to describe the behaviour of SEPEs and that this will impact assumptions and outputs of existing statistical models used for engineering design purposes.

Figure 4.4 shows the event frequency (top) and mean waiting time (bottom) for each of the event lists, this was calculated every 6 months to clearly show the variations in time. The greater sensitivity of the PSYCHIC event definition results in a higher number of events while the JPL and NOAA definitions return similar results. Also shown are the bounds of the 7-year solar active periods when there is greatly increased activity as noted by Feynman et al. (1990).

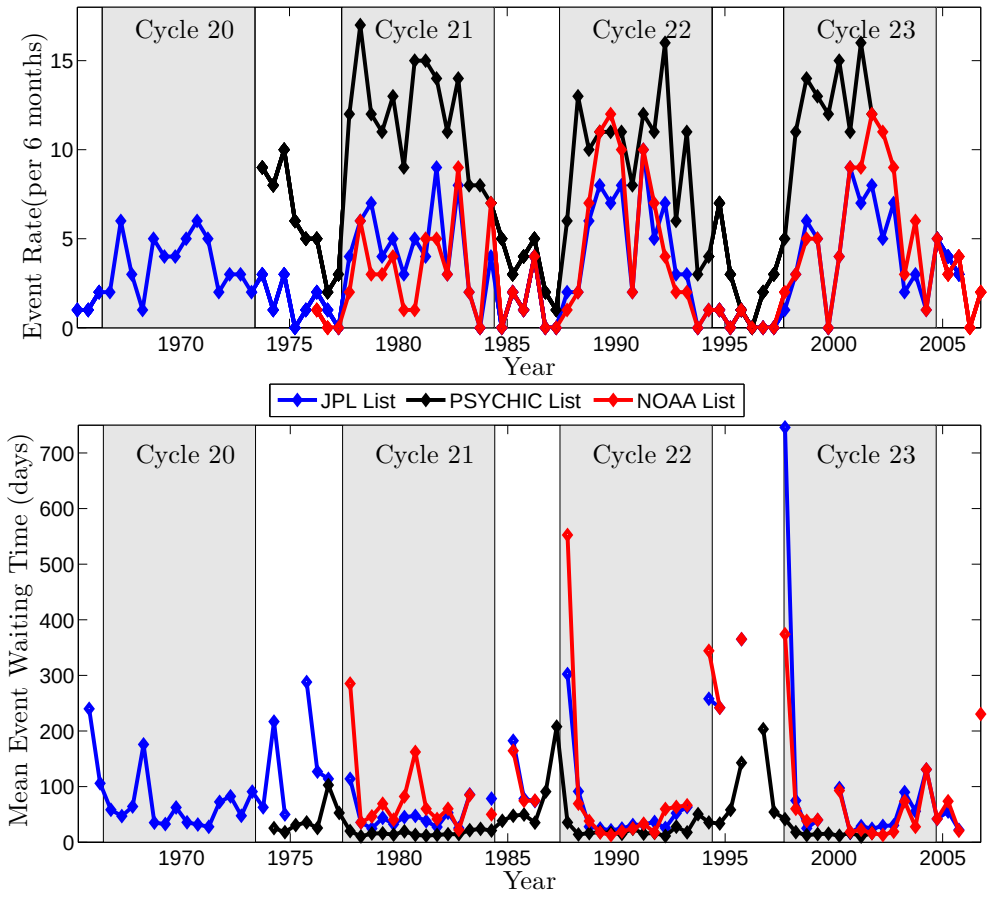

Figure 4.4: Plots of event rates and mean waiting times binned in 6 month periods for each event list, gaps appear in the waiting time plot where there are no events in the 6 month time period. The 7-year active period for solar cycles 20-23 are also shown.

4.3.1 Distributions

The three functions described relate to three processes: a Poisson process, a time-dependent Poisson process and a Lévy process. The functions described here are for application in the time domain (be that event waiting time or duration) and therefore the Fourier transform of any of these functions applied to waiting time will return the probability density function (pdf) of event frequency for that process.

4.3.1.1 Poisson Process

A Poisson process has been assumed in all SEPE engineering environment models up to now. On the basis of basic Poisson assumptions, the likelihood of at least one event occurring in a given time period, Δt, is given by the cumulative density function (cdf)

of the exponential distribution;

$$P(>0;\Delta t) = 1 - e^{-\lambda \Delta t} \tag{4.1}$$

and therefore the expression of a Poisson process in the time domain, or waiting time distribution (wtd), is equal to the pdf of the exponential distribution;

$$P(\Delta t) = \lambda e^{-\lambda \Delta t} \tag{4.2}$$

When plotted with a logarithmic axis of ordinates, Equation 4.2 will be a straight line with intercept $\ln(\lambda)$. Feynman et al. (2002) produced a plot of binned waiting times against the relative number with a straight line fit in support of the events following a Poisson process (Figure 5 in that paper). In the frequency domain the likelihood of seeing k events in a fixed time period, T, is given by:

$$P(k,T) = \frac{e^{-\lambda T}(\lambda T)^k}{k!} \tag{4.3}$$

where λ is the mean number of events per day.

Crucial features of a Poisson process are that the likelihood of an event occurring in a coming time period is not affected by recent activity (i.e. the process has no 'memory') and the mean rate of event occurrence, λ, does not vary with time, i.e. the process is stationary. The first of these factors can be seen as the absence of a short-term time dependence while the second can be seen as the absence of a longer-term time dependence.

4.3.1.2 Stationarity

For the process to be stationary the mean waiting time should be independent of time. To test stationarity the events' waiting times were grouped into 20 segments each of which had the same number of events (and therefore varied in real time covered). The mean waiting time is then calculated for each segment. If the events in the active year periods can be considered to be governed by a Poisson process then there should be some random variability and certainly no trend. The greater the scatter is, the less stable the mean value will be. If the waiting time segments have high scatter this indicates periods of high waiting times (low activity) and periods of low waiting times (high activity) within the selected time period.

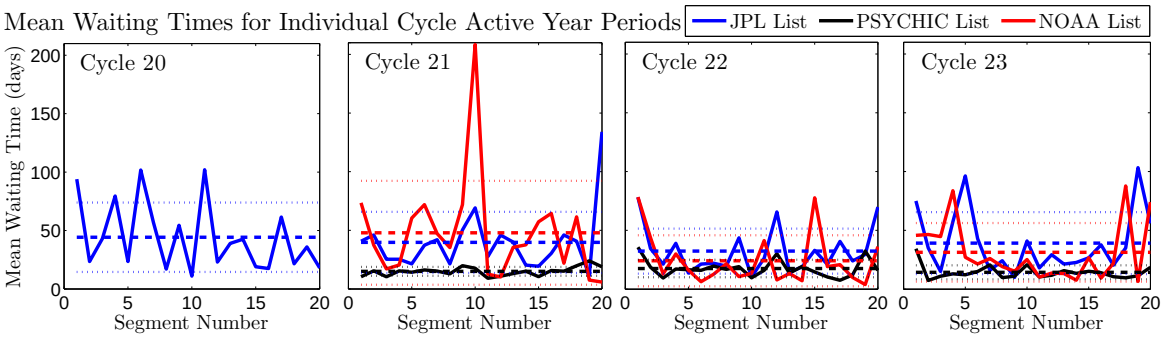

Figure 4.5: Binned waiting times for each cycle's active year periods with mean (dashed lines) and ± 1 standard deviation (dotted lines).

The mean waiting times per 6 months shown in Figure 4.4 (bottom) indicate a lower variation in waiting times for the PSYCHIC list compared to the JPL and NOAA lists due to a lower absolute value for the mean waiting time and hence lower absolute variation. The grouped waiting time for active years for the individual cycles (20-23) with the mean and ± 1 standard deviation are plotted in Figure 4.5, the characteristics are shown in Table 4.3. It is clear that the waiting times for the PSYCHIC list are consistently lower which is to be expected as the list includes far more events. It is also apparent that the JPL and NOAA lists have a greater degree of scatter characterised by a far higher standard deviation. It is possible that some of this scatter is as a result of a low number of events in each bin (notably for the NOAA list in cycle 21 where each bin had only 2 events). Using the mean and standard deviation for 20 segments for the joined active year periods so that each segment includes far more events (Figure 4.6 (bottom)), a very similar trend is uncovered. The plot of the complete time period (Figure 4.6 (top)) shows higher mean values and higher standard deviations as the process is not stationary when the quiet years are included as noted by Feynman et al. (1990).

To test the theory that the mean value is not stationary within reasonable parameters a bootstrap method was used. By randomising the order of the real waiting times a virtual time line is created with 20 new time segments. The mean of the segments is necessarily the same but the standard deviation will vary. To thoroughly test the stationarity of the process 10,000 iterations were carried out and the real time line standard deviations were compared to the virtual ones where it is known that the waiting times are randomised. With this comparison the null hypothesis that

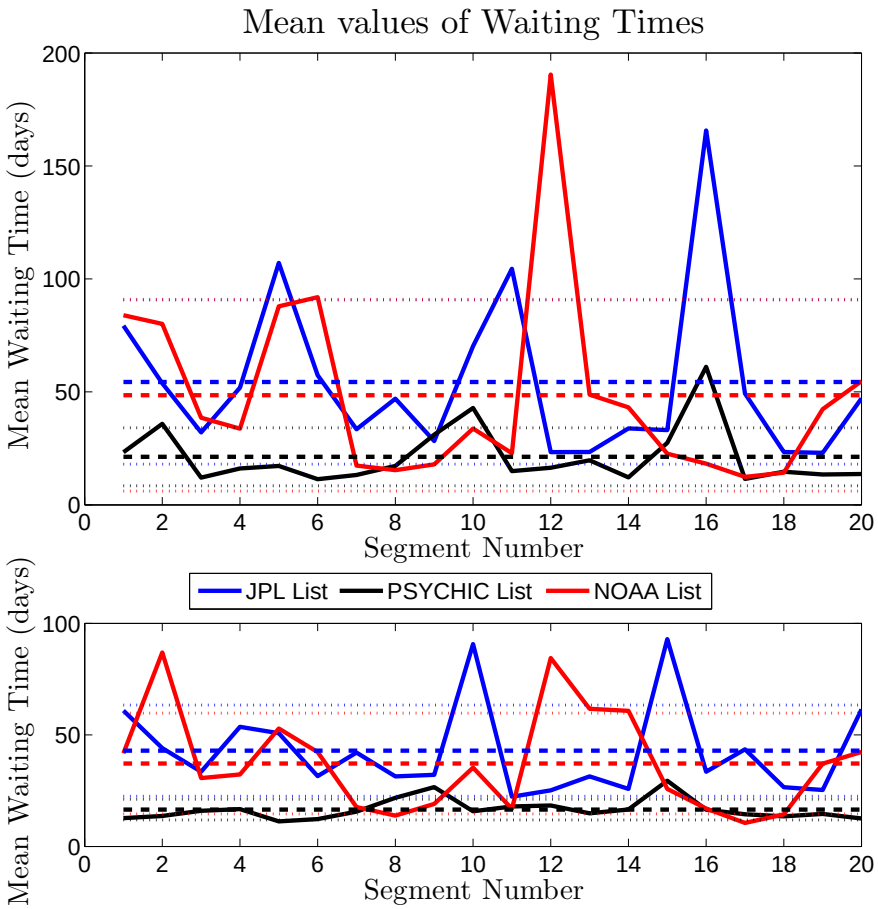

Figure 4.6: Binned waiting times for the total time period (top) and the joined active year periods (bottom) with mean (dashed lines) and ± 1 standard deviation (dotted lines).

Table 4.3: Analysis of mean waiting times in 20 equal segments for cycles 20-23 active years, all active years and the complete event lists.

Event List	Parameter	Cycle 20	Cycle 21	Cycle 22	Cycle 23	Active Years	All Years
JPL	Mean	44.22	39.72	32.35	39.15	42.93	54.35
	St. Dev.	29.68	26.07	19.13	26.33	20.42	36.31
PSYCHIC	Mean	-	15.00	17.55	14.30	16.55	21.26
	St. Dev.	-	3.80	7.46	5.94	4.64	12.81
NOAA	Mean	-	47.91	24.16	31.30	37.17	48.51
	St. Dev.	-	44.27	21.66	24.92	22.59	42.43

the process is stationary can be tested. Table 4.4 shows the mean waiting time, the standard deviation between the 20 time segments in the real time line, the percentage of virtual time lines with a higher standard deviation and the number of events in each segment for both the complete time period and the joined active year waiting times.

Table 4.4: Table assessing stationarity of event waiting times in the complete time period and solar active years only.

	Mean Waiting Time (days)	Standard Deviation (days)	% of Virtual Time Lines Higher	Events per Segment
Complete Time Period				
JPL	54.3538	36.3146	0.02	13
PSYCHIC	21.2604	12.8108	0.00	24
NOAA	48. 5109	42.4299	0.03	11
Active Years Only				
JPL	42.9266	20.4230	0.12	12
PSYCHIC	16.5475	4.6360	0.05	20
NOAA	37.1717	22.5887	1.05	10

The complete time period here operates as a test for the procedure as it is known that there is a difference between the solar active and quiet years which is reflected in the rejection of the null hypothesis at the 99% confidence level in all cases. For the active years it can be seen that in all cases the null hypothesis that the process is stationary can be rejected at the 95% level and in all but the NOAA case it can be rejected at the 99% level. These results are a clear indication that the process is not stationary or completely random and encourage the search for a distribution which does not require the process to be stationary and instead allows the mean event rate to vary.

4.3.1.3 Time-Dependent Poisson Process

It was found that a time-dependent Poisson process can be fit to the waiting times of solar flares (Wheatland, 2000) and CMEs (Wheatland, 2003). Here it is assumed that locally the process will be Poissonian but that over time the mean rate of event

occurrence is allowed to change. For a piecewise solution the wtd is given by:

$$P(\Delta t) = \frac{1}{\varrho}\int_0^\infty P(k)k^2 e^{-k\Delta t}\mathrm{d}k \tag{4.4}$$

where $P(k)$dk is the fraction of time at a specific mean event rate (and therefore the probability of seeing that event rate) in the range of $(k, k + \mathrm{d}k)$ and ϱ is the mean event rate for the complete event list. It was found by Wheatland that the mean rate (of flares, CMEs or in this case SEPEs) can be approximated by an exponential distribution;

$$P(k) = \varrho^{-1}\exp(-k/\varrho) \tag{4.5}$$

Together with a local Poisson assumption this results in a combination of two exponential distributions. When equation 4.5 is substituted into equation 4.4 and the integral evaluated it is found that the waiting time of events is given by:

$$P(\Delta t) = \frac{2\varrho}{(1+\varrho\Delta t)^3} \tag{4.6}$$

This function follows power law behaviour at high waiting times but deviates from it at lower waiting times predicting fewer low waiting time events than a simple power law.

Using the 6-month binned event frequencies (shown in Figure 4.4) and the mean values of event frequency from the sample we can compare the data to the idealised pdfs for the Poisson and time-dependent Poisson processes (Figure 4.7). Again there is significant scatter on the plots as a result of limited data but it can be seen that for active years the PSYCHIC event list is well fit by the Poisson distribution while the NOAA event list is better fit by the exponential distribution.

The complete time period in each case is poorly fit by the Poisson distribution and there is an improvement in all cases when only the active years are considered which follows from the distinct separation of quiet and active years noted by Feynman et al. (1990). The JPL list for the active years is better fit by the Poisson distribution which is surprising given the apparent lack of stationarity shown in Section 4.3.1.2. It should be noted that if the process is not stationary it does not mean that the rates will be exponentially distributed, however, the final form of a truncated power law may still fit the waiting time data well.

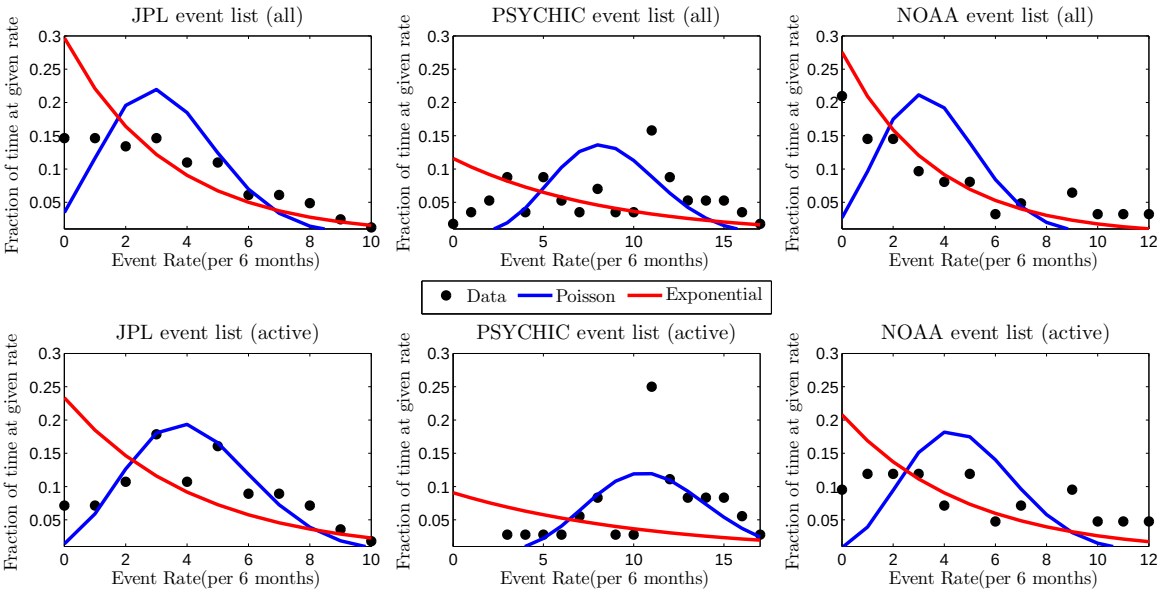

Figure 4.7: Event rates compared with Poisson and exponential (from time-dependent Poisson process) distribution predictions.

4.3.1.4 Test for Local Poisson Distribution

Both the Poisson distribution and the time-dependent Poisson distribution assume that consecutive events are independent of each other, i.e. it is has no 'memory'. To test this assumption the formalism of Bi et al. (1989) applied to the absorption lines of a quasar which has since been applied to solar flares by Lepreti et al. (2001) was followed.

Firstly, the lower of the two waiting times either side of each event is found (δt). If δt is the waiting time before the event $\delta\tau$ becomes the waiting time between the two events before the original event, if it is the event waiting time after the event $\delta\tau$ becomes the waiting time between the two events after the original event:

$$\delta t_i = \min\{t_{i+1} - t_i, t_i - t_{i-1}\}$$

$$\delta\tau_i = t_{i+2} - t_{i+1} \text{ if } \delta t_i = t_{i+1} - t_i \text{ or}$$

$$\delta\tau_i = t_{i-1} - t_{i-2} \text{ if } \delta t_i = t_i - t_{i-1}$$

The resulting distributions (if the wtd is locally Poissonian) should be independently distributed with probability densities:

$$P(\delta t_i) = 2\lambda_i \exp(-2\lambda_i \delta t_i)$$

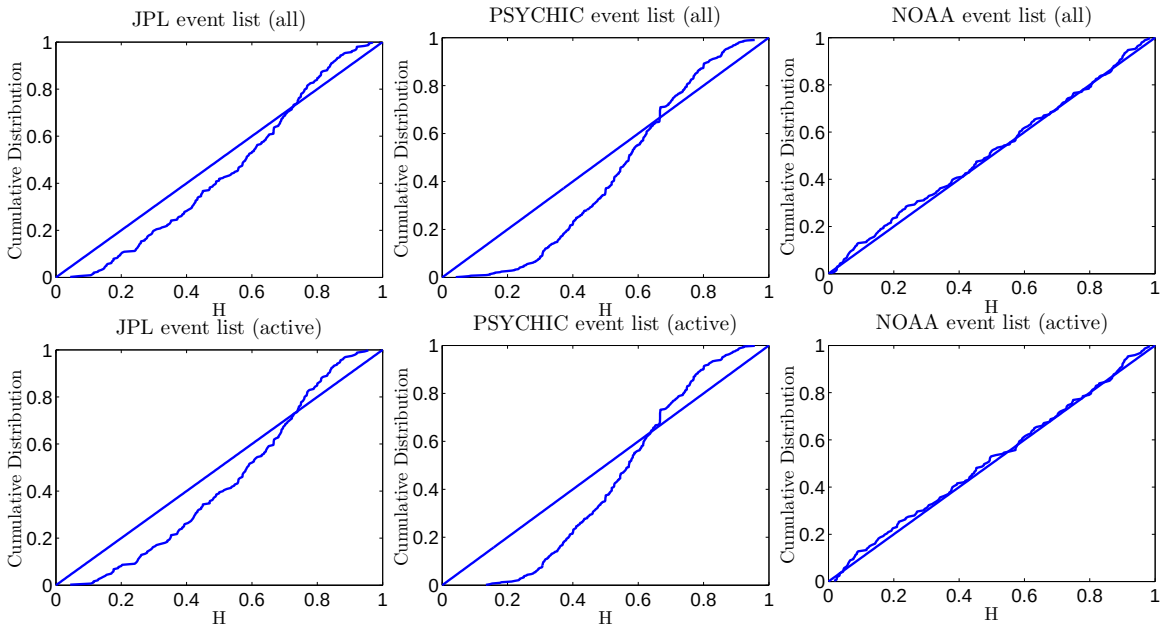

Figure 4.8: The cumulative distribution function of H for the local Poisson distribution (straight line) and the empirical (observed) cumulative distribution function for H.

$$P(\delta\tau_i) = \lambda_i \exp(-\lambda_i \delta\tau_i)$$

Now a stochastic variable, H, is introduced:

$$H = \frac{\delta t_i}{\delta t_i + \frac{1}{2}\delta\tau_i} \tag{4.7}$$

such that if the process is locally Poissonian then the cumulative distribution of H will be a uniform distribution between 0 and 1:

$$F(H) = \int_0^\infty 2\lambda e^{-2\lambda x} \int_0^{2x[(1/H)-1]} \lambda e^{-\lambda y} \mathrm{d}y\mathrm{d}x = 1 - H \tag{4.8}$$

Figure 4.8 shows the plots of observed H (sorted) against the theoretical uniform distribution following from a Poisson assumption for SEPEs for the complete time period and active years for the each event list.

Values of H above 0.5 indicate a clustering of events as the $\delta\tau_i$ values are typically lower than twice the δt_i values while voids are indicated by values of H below 0.5. It is expected for a process which is locally Poissonian that there will be some clustering and some voids. However, deviation below (above) the straight line indicates a higher than expected number of clusters (voids) meaning that the waiting times are not locally Poissonian.

It is clear from visual inspection that there is a high level of clustering of events with some voids for both the JPL and PSYCHIC events while consecutive NOAA

Table 4.5: Significance level for rejection of the independence (Poissonian) nature of consecutive events.

Significance Level (%)	Complete Time Period	Active Years
JPL	99.975	99.994
PSYCHIC	> 99.999	> 99.999
NOAA	28.620	4.143

events appear to have approximately the level of voids and clusters expected for a local Poisson distribution. This conclusion is reinforced by the D-statistics in a two side Kolmogorov-Smirnov test which are shown in Table 4.5 which shows that the null hypothesis of a local Poisson can be rejected at the 99% level in all cases other than the NOAA list. There is no significant change to the results with the inclusion or exclusion of the solar quiet years.

The deviation from a local Poisson distribution in the cases of the JPL and PSYCHIC event lists indicates that consecutive events are not independent, that there is a level of 'memory' at work in the system and therefore that the events are not truly random. The test for local Poisson distribution shows no indication of a short-term time dependence (from event to event) for waiting times for the NOAA event list (required for the Poisson process and time-dependent Poisson process) but this does not take into account a longer-term time dependence. When using the NOAA event list it was shown in Section 4.3.1.2 that the process was not stationary and in Section 4.3.1.3 that the event rate does not follow a Poisson distribution.

4.3.1.5 Lévy Process

It has been found that the process cannot be considered stationary and in both the JPL and the PSYCHIC cases there is strong evidence of local event inter-dependence. Now a distribution that allows for these factors is investigated - the Lévy distribution.

The Lévy skew alpha-stable distribution has four free parameters, for parsimony the skewness and shift parameters are excluded which leaves the symmetric, centred Lévy process. This distribution is related to the Gaussian but it has a fatter tail determined by a characteristic exponent, μ, and was first suggested to model SEP

event waiting times by Gabriel and Patrick (2003). The transform of the symmetric Lévy distribution into the time domain has two free parameters and is given by:

$$P(\Delta t) = \exp(-|c\Delta t|^{\mu}) \tag{4.9}$$

This is sometimes called the characteristic function of the symmetric Lévy distribution. The exponent, μ, must lie in the range $[0, 2]$, for a value of $\mu = 2$ the Gaussian distribution is recovered and if the $\mu = 1$ the Cauchy distribution is recovered (Nolan, 2009). The c parameter is the scaling parameter.

The pdf of the Lévy distribution is given by:

$$P(k) = \frac{1}{\pi} \int_0^{\infty} \exp(-|c\Delta t|^{\mu}) \cos(k\Delta t) \mathrm{d}\Delta t \tag{4.10}$$

which is the inverse Fourier transform of equation 4.9 where $P(k)$ is probability of seeing k events in 1 day. This cannot be evaluated analytically but there are methods for numerically evaluating the integral (see Weron (1996) and references therein).

It has been suggested that the integral distributions of both SEP event fluence and waiting times can be fit by power functions and exhibit 'fractal' or 'scale invariant' behaviour leading to parallels between the size of SEPEs and earthquakes modelled by the Gutenberg-Richter distribution and the possibility that SEPEs are a self-organised critical (SOC) phenomenon (Xapsos et al., 2006; Gabriel and Patrick, 2003). The presence of a characteristic scale in, for example, the exponential distribution destroys the continuous scale invariance property (Laherrére and Sornette, 1998).

The stretched exponential function similar in form to equation 4.9 was introduced by Laherrére and Sornette (1998) as an alternative to the power law for 'fat tail' distributions seen in nature and economics where there appeared to be natural curvature on double logarithmic axis plots deviating from the straight line predicted by power laws. This deviation was additional to the existing limitation resulting from a finite critical system (such as a limited Earth for the production of earthquakes) where a power law must give way to another regime with exponential decay.

This scale invariant property combined with an indication of 'memory' in the system led Lepreti et al. (2001) to fit the waiting times of solar flares numerically with a Lévy pdf (equation 4.10). The pdf results in a power law at high waiting times given by:

$$P(\Delta t) \sim \Delta t^{-(1+\mu)} \tag{4.11}$$

However, the data indicates a deviation from a power law at both extremes and therefore here the characteristic function is fitted.

4.3.2 Results

4.3.2.1 Event Waiting Times

With three possible functions for the waiting time distributions now established (Equations 4.2, 4.6 & 4.9 for Poisson, time-dependent Poisson and Lévy distributions respectively), each of the distribution parameters, λ, ϱ, c and μ can be interpreted as free parameters and fit to the waiting time data from each event list (JPL, PSYCHIC and NOAA). The waiting time is considered to be from the onset of one event to the onset of the next which covers the complete time line and the Fourier transform of the function would therefore yield the event frequency.

To fit the waiting times the probability densities for each bin (Y_i) were calculated by first dividing the number of waiting times in each bin by the total number of waiting times considered and then normalised by dividing by the bin width. As a result the area of the histogram of the Y vector will be equal to 1 which is a necessity for any pdf. The bins were chosen to be uniformly distributed on a logarithmic axis and therefore the higher waiting time bins are far larger than the lower waiting times which is favourable due to the sparsity of higher waiting times.

The functions applicable in the time domain for each of the distributions introduced in Section 4.3.1 were fitted to the binned data for each of the event lists introduced in Section 3.1. These fits were performed by first minimising the sum of the squared residuals of the natural logarithms of Y_i, $S^2 = \sum_{i=1}^{n}(\ln(Y_i) - \ln(P(\Delta t)_i))^2$, by applying a iterative non-linear least squared method using Gaussian elimination and then minimising the χ^2 values in the natural domain ($\chi^2 = \sum_{i=1}^{n} \frac{(Y_i - P(\Delta t)_i)^2}{P(\Delta t)_i}$). The square root of the product of the two fitting parameters, $\sqrt{S^2\chi^2}$, was then minimised using an iterative procedure. The reason for this choice of a combination of fitting parameters was that it was found that the χ^2 fit was heavily weighted to the low waiting times (durations), to the extent that the contribution of the majority of points was negligible, while the S^2 values were more evenly weighted. However, as there is greater uncertainty at high waiting time (duration) points due to the smaller number of events in each bin, fitting to these values is less important so to reflect this it was decided to

Table 4.6: Quality of SPE waiting time fits as measured by $\sqrt{S^2\chi^2}$.

Event List	Years	Poisson	T-D Poisson	Lévy
JPL	1976-2006	0.7704	0.0812	0.1089
	Active Years	0.1764	0.0832	0.0997
PSYCHIC	1976-2006	0.9014	0.3399	0.1378
	Active Years	0.2099	0.6623	0.2711
NOAA	1976-2006	2.1183	0.1460	0.0562
	Active Years	0.8224	0.0963	0.0591

combine the two fitting methods. This is a non-standard method, however, there is good reason behind the choice and the S^2 values (of the natural logarithms) and the χ^2 values (in the natural domain) are both included in Appendix Section B.1.2.

To clarify the decision in choosing the $\sqrt{S^2\chi^2}$ goodness-of-fit criterion the two instances where the results in Table 4.6 differ for one or other of the individual fitting parameters, S^2 and χ^2 was investigated:

1. PSYCHIC event list (active years): The χ^2 goodness-of-fit parameter indicates the Lévy distribution is a better fit than the Poisson distribution. This difference in the χ^2 values is $\sim$ 2%. Studying the data it is found that the Poisson distribution is a better fit to 5 out of the 9 data points than the Lévy distribution. In this case the Lévy distribution is a better fit to 3 binned data points with 1 data point approximately equidistant. However, as the 3 data points the Lévy distribution is a better fit to are at the lower end of the distribution the χ^2 value is lower overall (see Table B.11 in the Appendix). This shows the excessive bias given to the lower waiting time points by a χ^2 fit and justifies combining it with the S^2 goodness-of-fit parameter. [There is a general trend that the Poisson distribution is poorly fit to data at the lowest waiting times, this is likely to result from a failure to allow for the clustering of SEPEs highlighted in Sections 4.3.1.2 and 4.3.1.4.]

2. NOAA event list (active years): The S^2 goodness-of-fit parameter indicates the Lévy distribution is worse than the time-dependent Poisson distribution (see Table B.9 in the Appendix). In this case both distributions are very well fitted to the data but with the Lévy a better fit over the first 10 points (see Figure 4.11

(bottom)). However, the majority of contribution for the S^2 comes from the last data point (the longest waiting time) so the total S^2 goodness-of-fit indicates that the time-dependent Poisson distribution is the best fit to the data. The final bin contained only 2 events, so the confidence in it is low but it was able to significantly alter the result; this example justifies not using the S^2 parameter alone.

3. The product of the goodness-of-fit parameters was taken rather than the sum as in some cases one parameter was significantly larger than the other making the smaller contribution negligible. The square root was taken to counter any exaggeration of differences between distributions caused by multiplying the two goodness-of-fit parameters.

Using a goodness-of-fit criterion of simply $S^2 \times \chi^2$ served to exaggerate any differences while the $\sqrt{S^2\chi^2}$ criterion gave a more balanced measure of the goodness-of-fit. At all stages it was attempted to ensure there was no bias and that the results were not dependent upon the binning. To do this, the bins were varied and the quality of fit values displayed are the mean values across the 5 bins used for each event list.

The distribution parameters for each of the fits are given in Table 4.7. The fits for the stated parameters for the JPL, PSYCHIC and NOAA event waiting times for both the complete time periods and the active years only are shown in Figures 4.9, 4.10 and 4.11 respectively. This table and figures are just one of 5 binnings that were tested, that with the median bin width. It can be seen that in all but one instance the time-dependent Poisson process and the Lévy process provide superior fits to the Poisson process.

Table 4.6 shows the quality of fits using the combined fitting parameter, $\sqrt{S^2\chi^2}$, averaged over all 5 binnings used to remove any possible bias. These results show that the time-dependent Poisson process is the best fit for the JPL event list, the Poisson is best for the PSYCHIC (active years only) and the Lévy is best for the PSYCHIC (complete time period) and the NOAA event list. Furthermore, where the Lévy process is not the best it is always a close second whereas in the other two distributions are never both well fit.

The Poisson distribution is clearly the worst fit in 5 out of 6 cases with the exception being the PSYCHIC active year fit (Figure 4.10 (bottom)). Differences in the selection

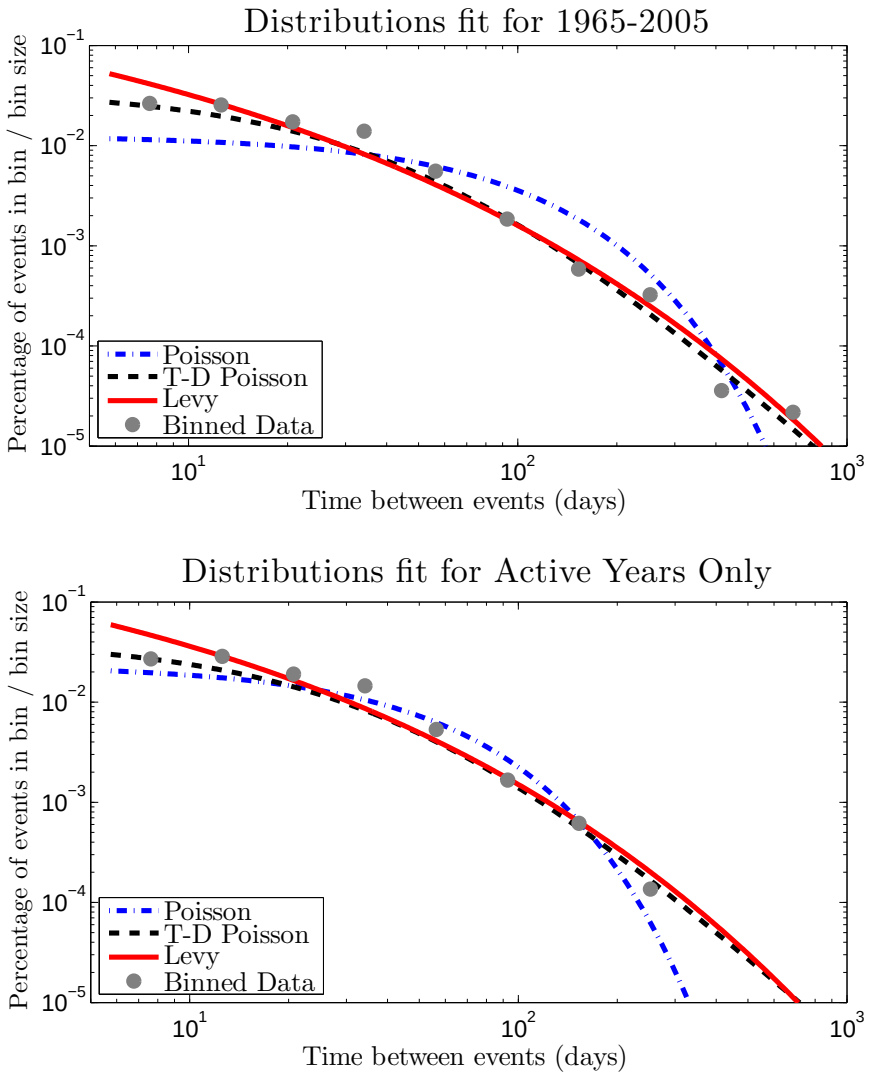

Figure 4.9: Waiting times and distributions for JPL events for complete time period (top) and active years only (bottom).

Table 4.7: Constants for waiting time distributions using median binning width.

	JPL	PSYCHIC	NOAA	Years
λ	0.0126	0.0355	0.0113	1976-2006
	0.0235	0.0745	0.0181	Active Years
ϱ	0.0183	0.0489	0.0259	1976-2006
	0.0212	0.0558	0.0273	Active Years
c	9.0910	1.9230	24.7907	1976-2006
	6.1098	0.9258	19.7865	Active Years
μ	0.2734	0.3835	0.2412	1976-2006
	0.2917	0.4860	0.2489	Active Years

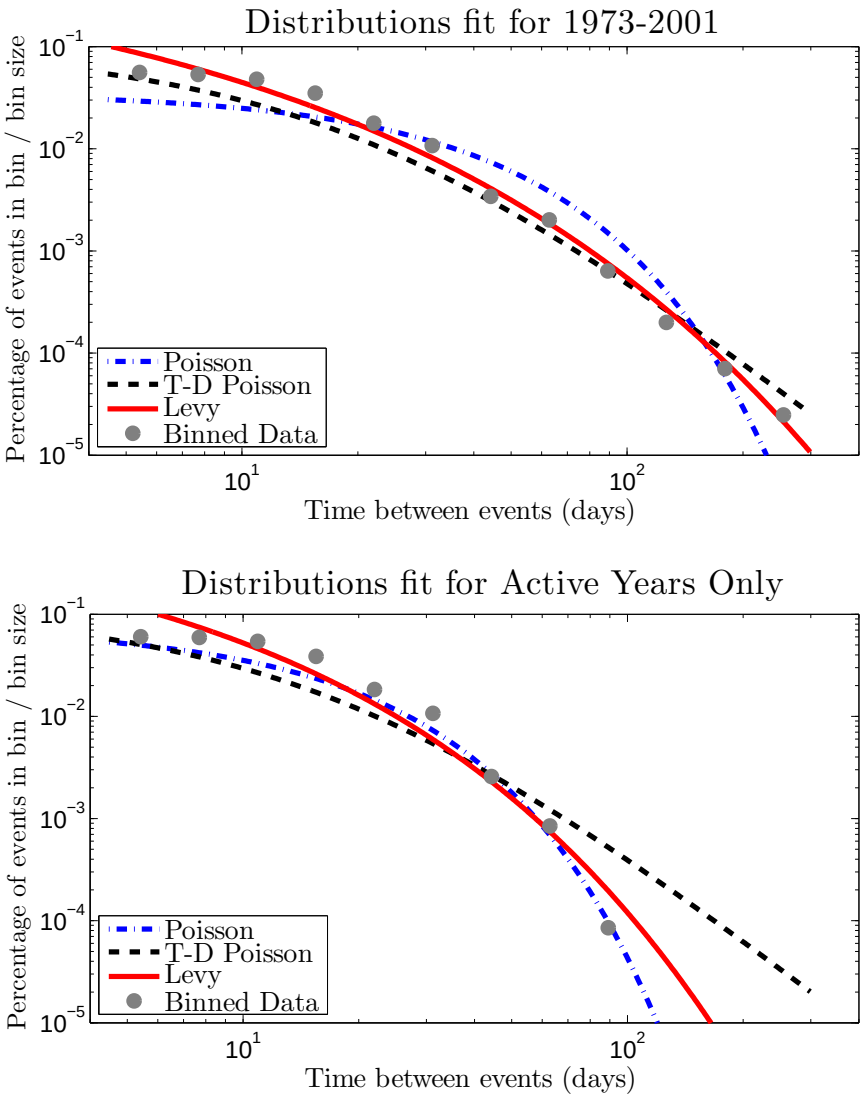

Figure 4.10: Waiting times and distributions for PSYCHIC events for complete time period (top) and active years only (bottom).

of the best fitted distribution could be a result of inherent differences in the event lists or limited data resulting in noise in the system (a possible example of significant noise can be seen in the JPL fit Figure 4.9 (top)). What is clear is that of the 3 distributions the Lévy is the most robust and does not require that the process is stationary or that events are independent in time. However, the analysis cannot always unambiguously determine the best fit distribution.

The individual values for constants using each binning used including those for the figures are listed in the Appendix Section B.1.1 along with the bin boundaries (Appendix Section B.1.3). Also included (in Appendix Section B.1.2) are the S^2, χ^2 and $\sqrt{S^2\chi^2}$ values for all of the fits.

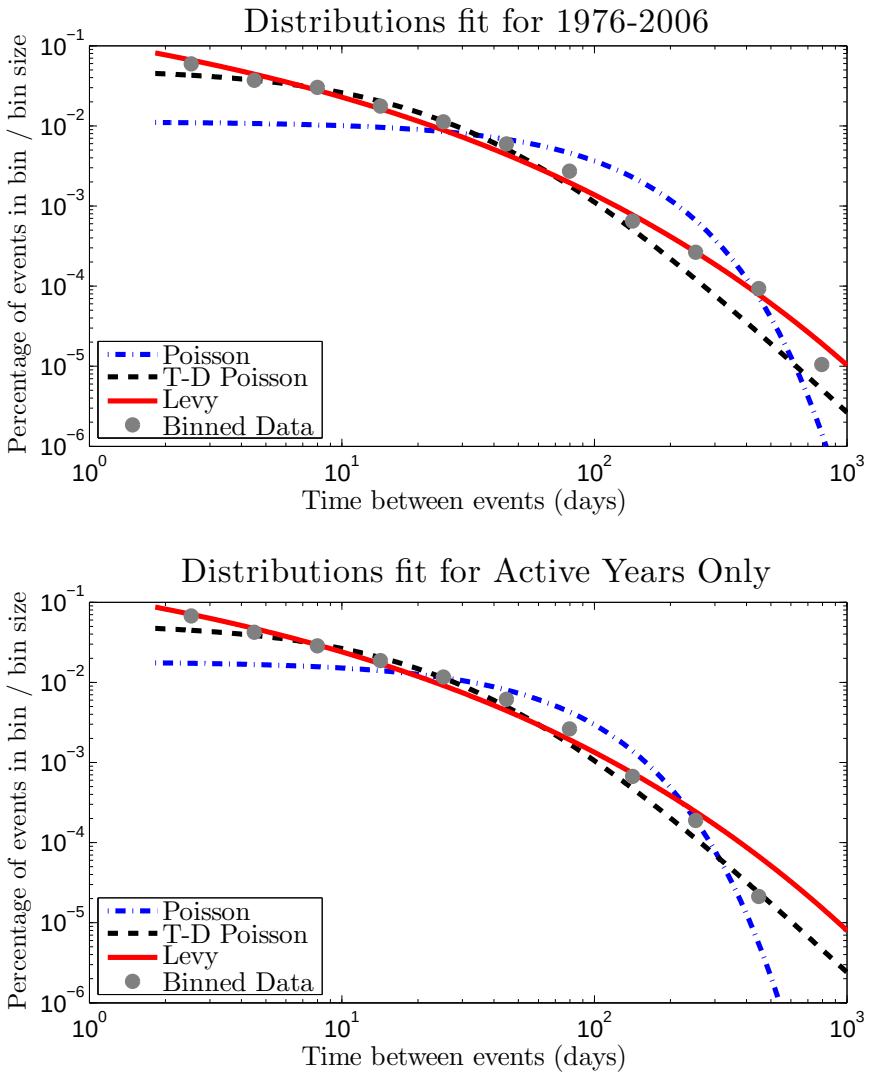

Figure 4.11: Waiting times and distributions for NOAA events for complete time period (top) and active years only (bottom).

In addition to mitigating for bias the various binnings can be used to find the variability in the constants. For each event list the lower boundary of the first bin remained constant and the natural logarithm of the bin width was varied which necessarily changed the final bin boundary.

Table 4.8 shows the variability of the constants using 5 different binnings by taking the range of values divided by the mean value. These constants are displayed for each of the data sets for both the complete time periods and active years only. The table shows that there is some significant variability. The constant which changes the least with the changing binning is the Lévy exponent, μ (mean of 5.10%), while the Lévy scale constant, c (26.87%), shows the most variability. The time-dependent Poisson

Table 4.8: Range of Constants Expressed as a Percentage of the Mean.

	JPL	PSYCHIC	NOAA	Years
λ	13.31	11.49	35.90	1976-2006
	13.00	7.85	24.22	Active Years
ϱ	9.80	6.77	19.01	1976-2006
	13.36	9.97	18.67	Active Years
c	10.28	8.18	27.20	1976-2006
	52.75	16.21	46.57	Active Years
μ	1.97	2.08	4.06	1976-2006
	8.80	5.93	7.78	Active Years

constant, ϱ (12.93%), appears less variable than the Poisson constant, λ (17.63%). A main cause of variation is a lack of knowledge as to where the final bin boundary should lie and as there are relatively few bins (to maximise the confidence in each point) this can change the results markedly. The bin limits can be found in Appendix Section B.1.3.

4.3.2.2 Event Durations

Having considered the distribution of the waiting times of events it seems natural to consider the distribution of the durations of the events and see if similar functions may be fit to the data. Jun et al. (2007) made a fit of the event durations in their data set to an exponential distribution (the function fit to represent the Poisson process for waiting times), this can be extended to the time domain functions derived from the time-dependent Poisson process and the Lévy process. In the case of duration analysis the Δt that previously represented the event waiting times in the equations in Section 4.3.1 will represent the event durations.

The Y_i values for the PSYCHIC events were again determined using exponential bins, on this occasion all 482 event durations were included. As the JPL event list includes only durations of integer days the bin boundaries were set to 0.5 days to avoid bias between bins. Once again larger bins are needed for higher durations where there are fewer events and therefore all the bin limits for the JPL events were set 'manually'.

Figure 4.12 shows the distributions fits for the JPL event list. Figure 4.13 shows

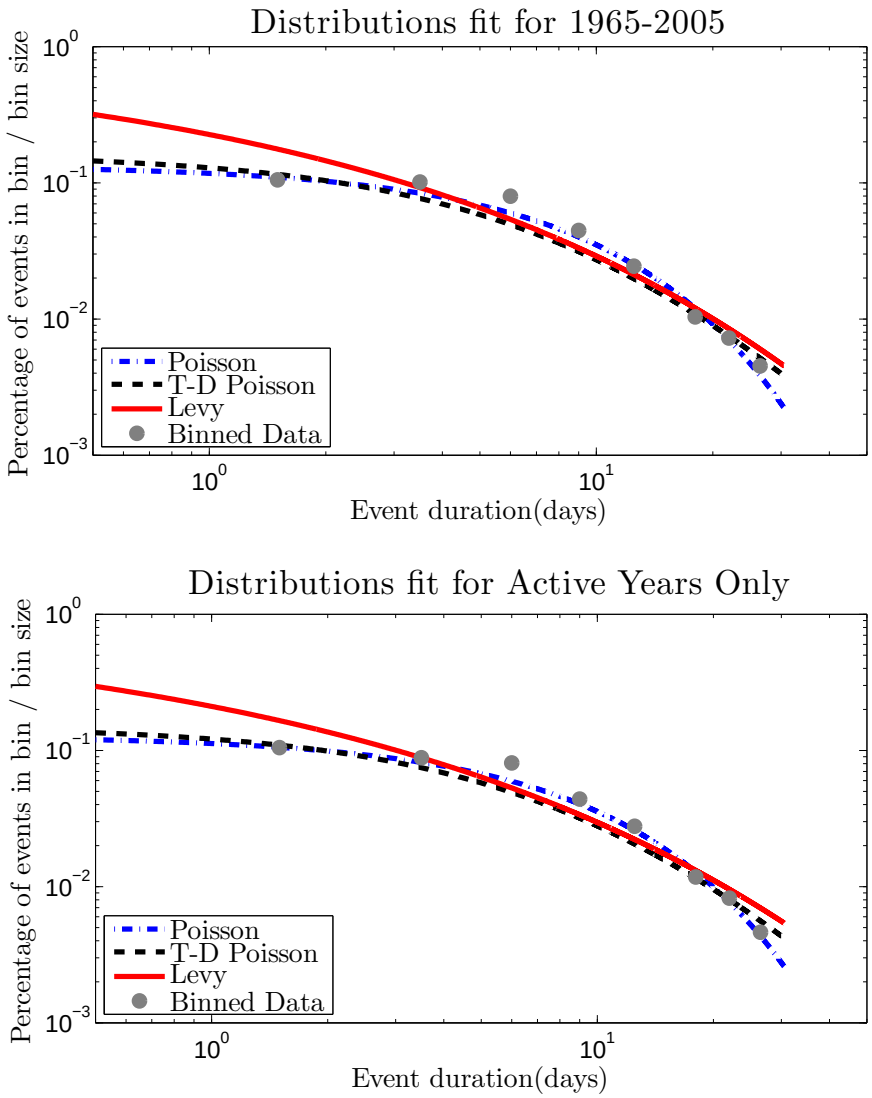

Figure 4.12: Durations and distributions for JPL events for complete time period (top) and active years only (bottom).

the distributions for the PSYCHIC events and here a lognormal distribution has also been included,

$$P(\Delta t) = \frac{1}{\Delta t \sigma \sqrt{2\pi}} \exp\left(-\frac{(\ln(\Delta t) - \mu)^2}{2\sigma^2}\right) \tag{4.12}$$

as it seemed appropriate given the low number of short duration events. Table 4.9 shows the fitted constants for each distribution for event durations for both lists. Presently data is not available for the durations on the NOAA event list.

The fits for the JPL event list are all reasonably good with the Poisson process giving the best results. This supports the result of Jun et al. (2007) regarding this distribution while also indicating the possibility of using either of the other two functions for fitting event durations. The main difference between the three fits is at low

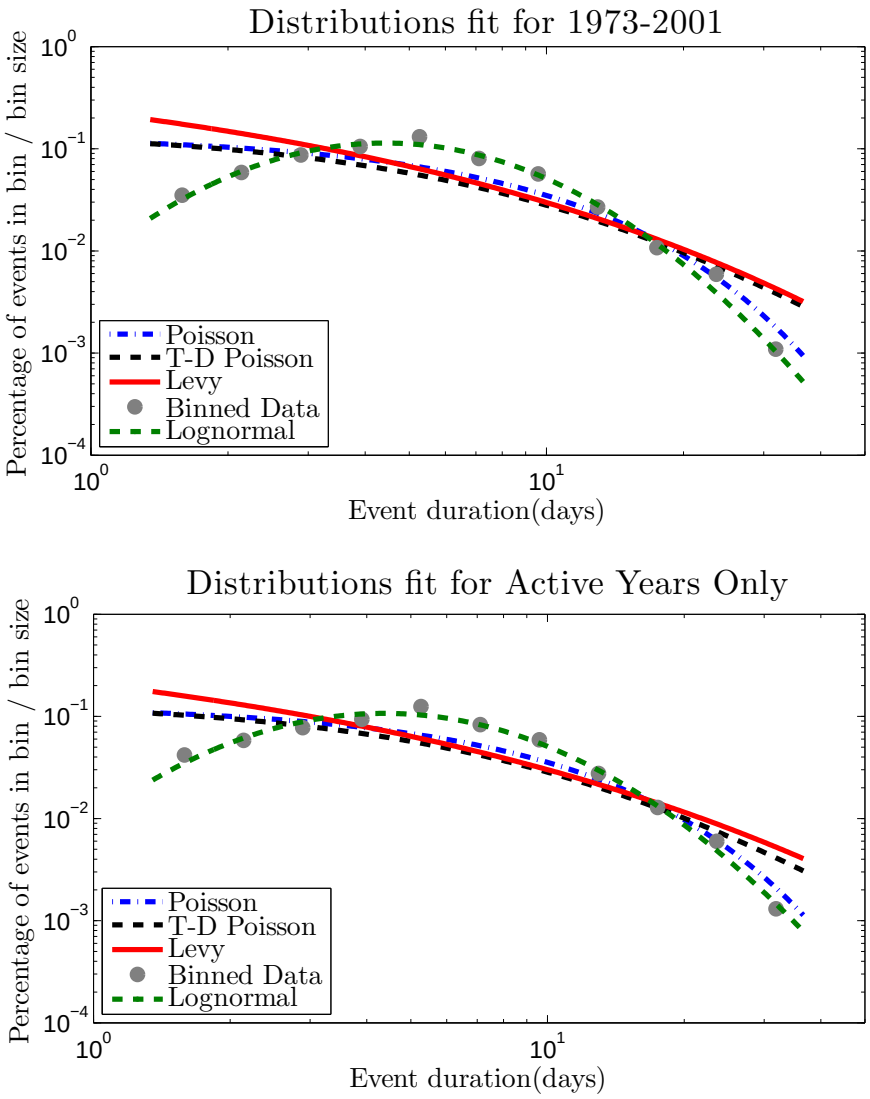

Figure 4.13: Durations and distributions for PSYCHIC events for complete time period (top) and active years only (bottom).

durations.

When investigating the PSYCHIC results a severe drop-off at low durations is found. Noting that the lognormal distribution has been used previously to approximate the event fluence (King, 1974; Feynman et al., 1990, 1993) it was found that the lognormal distribution offered greatly improved results. These two event lists seem to offer very different conclusions for how the event durations are distributed. The $\sqrt{S^2\chi^2}$ for both event lists can be found in Table 4.10.

As a result of the reduced number of low duration events seen the portion of PSYCHIC events with duration above 4.48 days were fit alone - the lower boundary of the exponential bin which had the highest Y_i previously. Figure 4.14 includes the

Table 4.9: Constants for duration distributions using median binning width.

	JPL	PSYCHIC(1)	PSYCHIC(2)	Years
λ	0.1342	0.1358	0.1743	1976-2006
	0.1277	0.1295	0.1683	Active Years
ϱ	0.0816	0.0749	-	1976-2006
	0.0754	0.0705	-	Active Years
c	2.8609	2.7480	0.5213	1976-2006
	3.5023	3.6388	0.5309	Active Years
μ	0.3770	0.3793	0.6742	1976-2006
	0.3537	0.3488	0.6614	Active Years
M	-	1.9023	1.9023	1976-2006
	-	1.9347	1.9347	Active Years
σ	-	0.6440	0.6440	1976-2006
	-	0.6777	0.6777	Active Years

Table 4.10: Quality of SPE duration fits as measured by $\sqrt{S^2\chi^2}$.

Event List	Years	Poisson	T-D Poisson	Lévy	Lognormal
JPL	1976-2006	0.0452	0.1322	0.1788	-
	Active Years	0.0343	0.1241	0.1734	-
PSYCHIC	1976-2006	0.6854	1.1210	1.3960	0.0405
	Active Years	0.5733	0.9664	1.2514	0.0408

original lognormal distribution as well as the Lévy and a version of the Poisson fit to the values above 4.48 days. For the Poisson fit the λ outside the exponential was allowed to vary from the value of that inside the exponential (see equation 4.2). This increases the number of fitting parameters by 1 so the number of degrees of freedom is now the same as the Lévy functional fit. The reason for this is that in the exponential domain (or on semi-logarithmic axes) the function is a straight line with a fixed intercept but as all low duration events have been artificially removed the values of the higher durations would not fit to the correct exponential fit. If there were the expected number of low duration events then the values for the other bins would be reduced allowing a correct fit. It also follows that the Lévy function in this

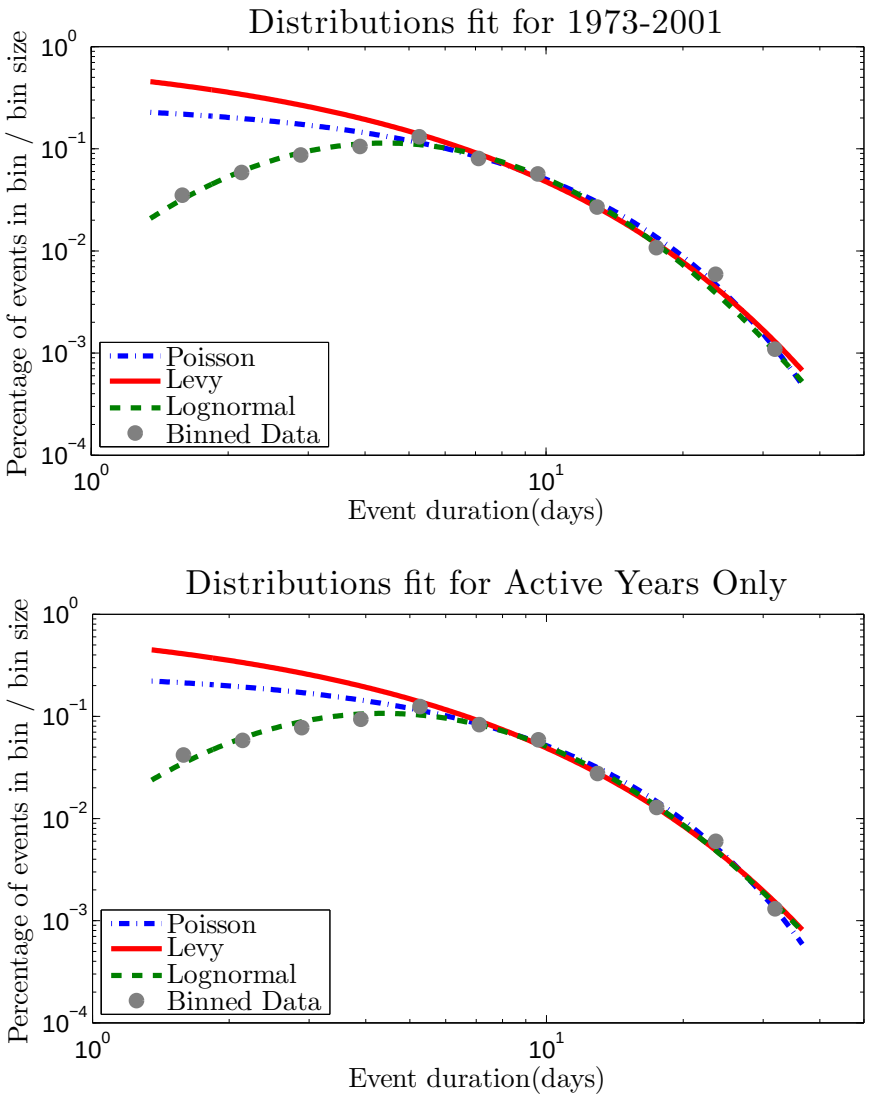

Figure 4.14: Adjusted durations and distributions for PSYCHIC events for complete time period (top) and active years only (bottom).

case is also not a real pdf. This is apparent when the area under the Poisson and Lévy fits is compared to that under the lognormal distribution.

In spite of inherent limitations of excluding the lower bins these plots do show that the functions fit to the waiting times and JPL event durations can be fit to the higher durations for the PSYCHIC event list although the exclusion of the lower bins which contained 121 events results in the use of only 74.9% of the available data.

4.3.3 Discussion

The discussion follows the results for both waiting times and event durations for each data set separately with reasons for any similarities and differences discussed in the

conclusion.

4.3.3.1 JPL Event List

The waiting time results for the JPL list indicate that the time-dependent Poisson process is the best fit, closely followed by a Lévy process and then a Poisson process. This conclusion is supported by the test for stationarity which concluded that even excluding the solar quiet years the process could not be considered stationary. It was also found that despite attempts to ensure that events were independent (particularly the requirement of a 2 day lagtime between events) the likelihood of a future event was affected by the occurrence of a preceding event.

Table 4.11: Percentage of events used for each event list.

Event List	Total Events	Events Used	% of Events Used	Time Period
JPL	275	274	99.64	1976-2006
	243	242	99.59	Active Years
PSYCHIC	481	457	95.01	1976-2006
	404	383	94.80	Active Years
NOAA	224	214	95.54	1976-2006
	201	191	95.02	Active Years

Due to the variable duration of events, as lower waiting times are studied so the number of events for which the waiting time is possible is reduced. This 'non-point-like nature' of SEPEs gives a possible reason for the time-dependent Poisson process being better fit to the waiting time data than the Lévy process. The effect of this lower limit resulting from the previous event duration is reflected in the data set as there is only 1 event with a waiting time below the the lowest bin limit of 5.8 days (see Table 4.11). This reduction is an unavoidable artifact of the data set using this event definition.

To allow for comparison with the waiting times plot produced by Feynman et al. (2002) a plot is produced with axes with a logarithmic ordinate but a linear abscissa (Figure 4.15). It can be seen that although there is significant scatter, the Lévy and time-dependent Poisson fits are better than the straight line Poisson fit.

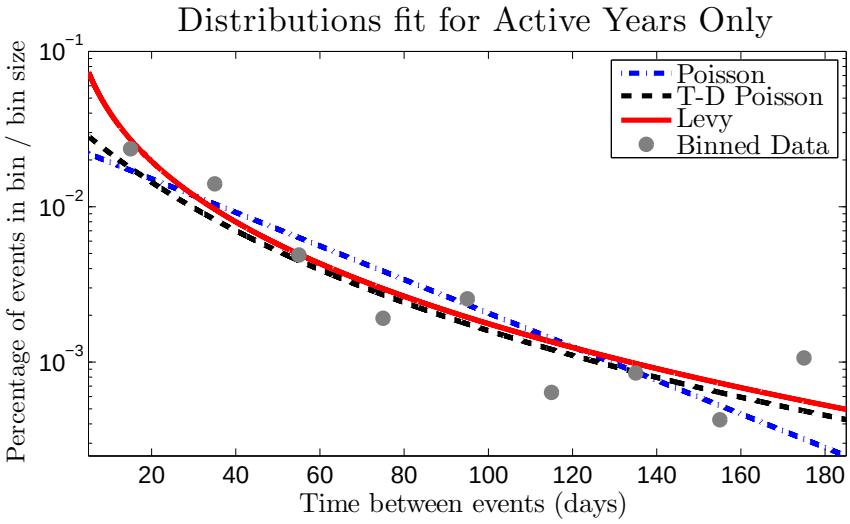

Figure 4.15: JPL waiting time plot with axes with a logarithmic ordinate but a linear abscissa.

The durations of the SEPEs from the JPL list are best fit by a Poisson process (exponential distribution). It is possible that there are a reduced number of short duration events due to the 10^6 cm^{-2} lower fluence limit. A breakdown of the lowest event durations shows that out of 276 events there are 29 occurrences of both 1 and 2 day event durations and 33 occurrences of 3 day event durations before a steady decline. The detection of smaller events is often difficult and may be dependent on other activity at the time so it is likely that this is unavoidable. To test the results of event duration on this event definition it would be desirable to reduce the sampling time so that fractions of days were possible.

4.3.3.2 PSYCHIC Event List

The PSYCHIC list was best fit by the Lévy process for the complete time period but better fit by the Poisson process when considering only the active years. This is surprising as it was found that during active years that process was not stationary and it showed the greatest deviation from a local Poisson assumption. To be better fit by the Lévy process it would expected that there would be a greater number of shorter waiting time events and fewer waiting times of between $\sim 15 - 40$ days. The effect of the non-point-like nature of events could be more strongly felt here than for the JPL list. The ratio between the mean waiting time and mean duration (shown by Table 4.12) is only 1.89 for the PSYCHIC list active years. If events are sparse then

the effect of the duration will be less strongly felt whereas if they are many the effect will be stronger. The longer the event durations in comparison to the waiting times the greater the drop-off at low waiting times.

Table 4.12: Mean values of waiting times and durations and ratios between them.

Event List	Time Period	Waiting Time (days)	Duration (days)	Ratio
JPL	1965-2005	53.84	7.08	7.60
	Active Years	35.50	6.48	5.48
PSYCHIC	1973-2007	21.24	8.22	2.58
	Active Years	13.47	7.13	1.89
NOAA	1976-2006	49.93	-	-
	Active Years	32.10	-	-

The duration fits for the PSYCHIC list show a reducing number of the lowest event durations not predicted by any of the fitted distributions resulting in a better fit for the complete data set by a lognormal distribution. The peak of event duration is between 5 and 6 days with 56 out of the 482 durations (11.6%) falling between these limits. It should be noted that while inspiration for using the lognormal distribution fit was taken from the JPL model (Feynman et al., 1993), even in the case of event fluences considered by that model there was an ever increasing number of lower fluence events not predicted by the distribution.

It is possible that as longer duration events are caused by wider, more energetic CMEs (Wang and Wang, 2005) they have an increased chance of being observed at Earth and that this could contribute to a reduction in the number of low duration events seen. However, it is likely that the biggest contributing factors to this reduction are: an inability to detect the smaller events (which are typically shorter in duration) above the background level and the requirement of minimum peak flux values for events to remain in the PSYCHIC list which would exclude many more shorter duration events than longer ones similar to the fluence cut-off used in the JPL list.

4.3.3.3 NOAA Event List

The NOAA event list was the only one of the three where events were not found to be locally dependent upon one another. However, there were still longer term dependencies as a hypothesis for stationarity could be rejected at the 95% confidence level in both the complete time period and when considering the active years only. The result of the waiting time fits was more comprehensively opposed to a conclusion that the process was Poissonian while the Lévy process was the best fit. The lowest bin limit of only 1.8 days indicates that the effect of the events being non-point-like was less prominent here. It is therefore possible to hypothesise that the reason for this are the higher thresholds used in the event definition resulting in events being shorter while being comparable in number to the JPL list. Unfortunately data on the event durations to quantitatively validate this conclusion were not available.

4.3.4 Summary and Conclusions

It is known that there was variation between the rate of SEPEs during solar maximum and solar minimum (Feynman et al., 1990). It had been assumed that, by using event definitions which linked all related events, during solar maximum the process could be considered Poissonian as the mean SEP event rate was steady. The time distribution of SEPEs have been re-examined, the Poissonian requirements tested and two new possible distributions have been proposed: a time-dependent Poisson process and a Lévy process.

The tests for stationarity show that regardless of event definition the process cannot be considered stationary even considering only active periods of the solar cycle as it was possible to reject the null hypothesis of stationarity at the 95% confidence level in all cases. The tests for local independence of events (at the 99% confidence level) show 'memory' in the system for both the JPL and PSYCHIC event lists but that by setting thresholds to exclude smaller events a list can be created where consecutive events are not locally dependent upon one another (e.g. the NOAA list). However, even in this case there remains a longer-term time dependence of event frequency as shown by the test for stationarity. It was found that in 2 out of the 3 cases (JPL and NOAA) the Poisson function is poorly fit to the waiting time data in comparison with the Lévy fit confirming the earlier results of stationarity. In the 1 case where

the Poisson function was better fit (PSYCHIC) the process was neither stationary nor were events locally independent. Therefore it must be concluded that the waiting time distribution has been skewed by another factor and the most likely candidate appears to be the significance of the event durations which results in a reduced number of the lowest waiting times and an increase in the number of longer waiting times. This makes the distribution of waiting times appear more Poissonian when in fact all other evidence points to a non-Poissonian distribution of events in time.

The time-dependent Poisson process was previously applied to solar flares and CMEs by Wheatland (2000, 2003). The time-dependent Poisson was best fit to the waiting times of the JPL event list. With regards to solar flares Lepreti et al. (2001) noted that since this distribution reduces to a power law for high waiting times the result was at least qualitatively correct despite being based upon incorrect assumptions. One might draw a similar conclusion from these results as, despite event inter-dependence, the distribution gives good results with only one free parameter in all but 1 instance. However, in the case of the active years for the PSYCHIC event list the time-dependent Poisson process did not fit the data well which was to be expected given the poor fit of the exponential distribution to the event rate (see Figure 4.7).

The Lévy process was the best fit in the case of the NOAA event list and well fit in all other cases with a comparable goodness-of-fit parameter to the best fitting function (see Table 4.6). This process allows for an inter-dependence of events suggested by the results of tests for local independence and stationarity. Initially suggested to fit to SEPE waiting times by Gabriel and Patrick (2003) the Lévy process offers the most robust solution to the problem of waiting time fits. The trade-off is that the Lévy process has two free parameters rather than one; this is statistically undesirable as parsimony (preference for the smallest number of free parameters) is desirable due to increased degrees of freedom. The resulting Lévy distribution which would apply to event frequency is a heavy tailed distribution meaning that it is skewed predicting a less stable SEP environment characterised by periods of high activity and periods of lower activity as well as the likelihood of future events being influenced by the occurrence of recent events. This agrees with previous analysis by (Xapsos et al., 2006; Gabriel and Patrick, 2003) where it was concluded that SEPEs might be a self-organised critical (SOC) phenomenon and although it is likely that it is impossible

to predict the occurrence of events there is a long-term correlation between SEPEs similar to other natural phenomena such as earthquakes. It appears that deviation from the Lévy waiting time fit can be attributed to the non-point-like nature of SEPEs.

It has been shown using the JPL and PSYCHIC event lists that it is possible that the waiting time between SEPEs and the durations of these events may be fitted with functions from the same family of distributions. However, as with the event waiting times the number of events with the shortest durations is lower than that predicted by the Poisson, time-dependent Poisson and Lévy distributions. This reduction is possibly contributed to by the increased likelihood of a larger event being observed compared to a smaller one due to the width of the CME. However, more significant factors are the exclusion of and inability to detect the smallest events resulting in a reduced number of low duration events in the lists. As a result it was found that for the PSYCHIC list a lognormal distribution was the best fit to the data; this distribution has been previously applied to SEP event fluences (Feynman et al., 1993).

There is evidence that if an event (of whatever size) has just occurred that there is increased likelihood of another occurring. The difference in result for the NOAA event list (where we have higher flux thresholds) for event independence might indicate that we get clustering of smaller, lower peak flux, events (excluded in the NOAA list) around the larger, higher peak flux, events much like might be expected to see pre-shocks and after-shocks either side of a large earthquake. This is consistent with the idea that SEPEs, like earthquakes, are an SOC phenomenon.

4.3.5 SARG Time Distribution Fits

Using the newly created SARG event list the waiting time and duration distributions could be calculated in the same way as done for the JPL, PSYCHIC and NOAA lists. In this case the fittings are done using the waiting times the end of one event to the start of the next (whose boundaries are now accurately calculated) as the model will incorporate the event durations to complete a whole timeline. Lower event durations should now be possible but due to the exclusion or inability to detect the smallest events there will still be an issue with the lowest durations.

Rather than test the fittings for multiple bin sets a single bin set was used in each case. So as to avoid any bias these bins were selected by an automated process. The

number of bins was set to be equal to the number of waiting times (or durations) divided by 25 rounded to the nearest integer. The lowest bin limit was taken to be the lowest waiting time (or duration) and the highest bins limit was taken to be 1.2 times the highest waiting time (or duration). The bins were then distributed evenly on a logarithmic scale as before.

Again three distributions were fit to the data: the Poisson distribution, the time-dependent Poisson distribution and the Lévy distribution.

4.3.5.1 SARG SEPE Waiting Time Fits

Figure 4.16 shows the fittings of the waiting times for the complete time period (top) and the residuals for each of the fittings (bottom). This appears to show that the Lévy is the best fit to the data, that the Poisson is the worst fit to the data and that the time-dependent Poisson lies between the two.

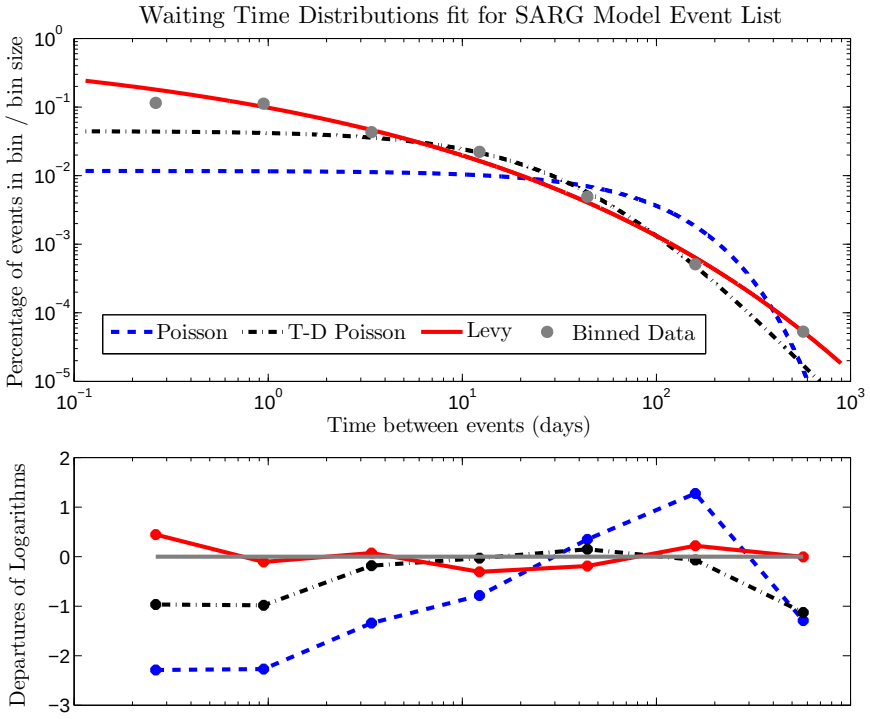

Figure 4.16: Waiting time distributions for SARG events (complete time period).

Table 4.13 shows the parameters for each of the fits in Figure 4.16. Table 4.14 shows the quality of fit parameters for each of the fits in Figure 4.16. Both the sum of squared residuals and the χ^2 quality of fit parameters show that the Lévy distribution

Table 4.13: Waiting time fitting parameters for complete time period.

λ	ρ	c	μ
0.0117	0.0223	40.826	0.2274

Table 4.14: Waiting time quality of fit parameters for complete time period.

	Poisson	T-D Poisson	Lévy
S^2	16.225	3.2333	0.3933
χ^2	1.8955	0.2353	0.0270

is the best fit to the data in this case. It is not surprising that the Poisson distribution is poorly fit to this data as this agrees with the results from Section 4.3.2.

Figure 4.17 shows the fittings of the waiting times for the active years only (top) and the residuals for each of the fittings (bottom). Again, the Lévy appears comfortably the best fit to the data, with the Poisson being the worst fit and that the time-dependent Poisson lying between the two.

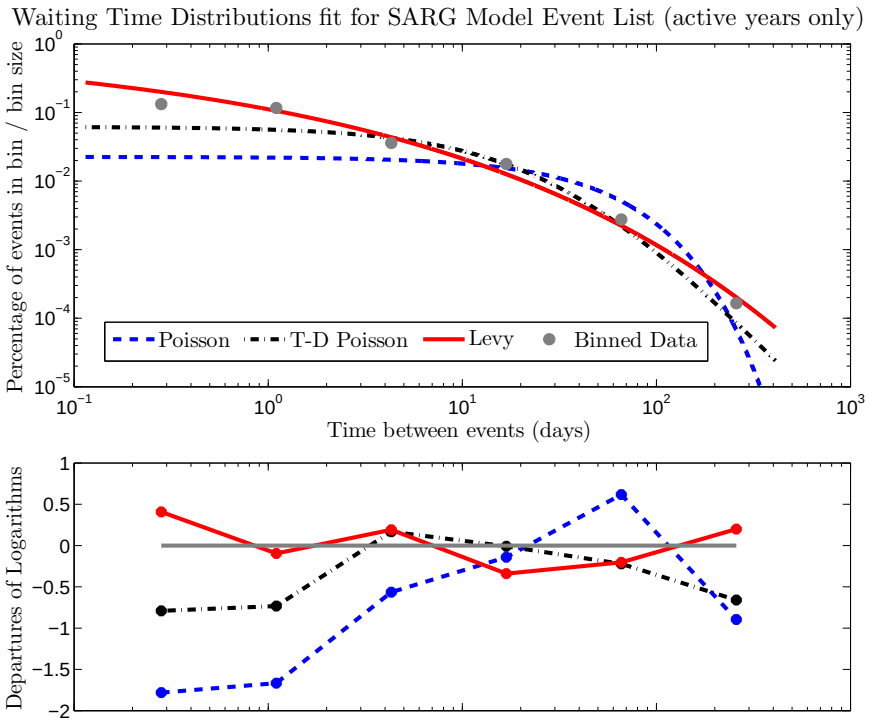

Figure 4.17: Waiting time distributions for SARG events (active years only).

Table 4.15 shows the parameters for each of the fits in Figure 4.17. Table 4.16 shows the quality of fit parameters for each of the fits in Figure 4.17. As before, both

Table 4.15: Waiting time fitting parameters for active years only.

λ	ρ	c	μ
0.0230	0.0321	22.4920	0.2485

Table 4.16: Waiting time quality of fit parameters for active years only.

	Poisson	T-D Poisson	Lévy
S^2	7.3866	1.5487	0.4471
χ^2	0.9656	0.1462	0.0292

the sum of squared residuals and the χ^2 quality of fit parameters show that the Lévy distribution is the best fit to the data. There is a large difference between the quality of fit parameters indicating an obvious choice of the Lévy distribution for modelling using this event list taking waiting times from the end of one event to the start of the next. The effect of excluding the event durations appears to have had the effect of increasing the number of events in the lowest bins as predicted in Section 4.3.4.

4.3.5.2 SARG SEPE Duration Fits

Figure 4.18 shows the fittings of the SEPE durations for the complete time period (top) and the residuals for each of the fittings (bottom). It is unclear from the figure which of the three distributions is best fit to the data.

Table 4.17 shows the parameters for the fittings shown in Figure 4.18 while Table 4.18 shows the quality of fit parameters for the fittings. Using both of the goodness-of-fit parameters (S^2 and χ^2) the Poisson distribution is the best fit to the data while the Lévy is better than the time-dependent Poisson fit using the S^2 parameter but the time-dependent Poisson is better than the Lévy according to the χ^2 parameter. There is overall little difference between the fitting parameters. It should also be noted that there is a reduction in the probability density at the lowest waiting times most likely due to the exclusion of (or inability to detect) the very short duration events.

Table 4.17: Duration fitting parameters for complete time period.

λ	ρ	c	μ
0.2678	0.2194	1.4306	0.5408

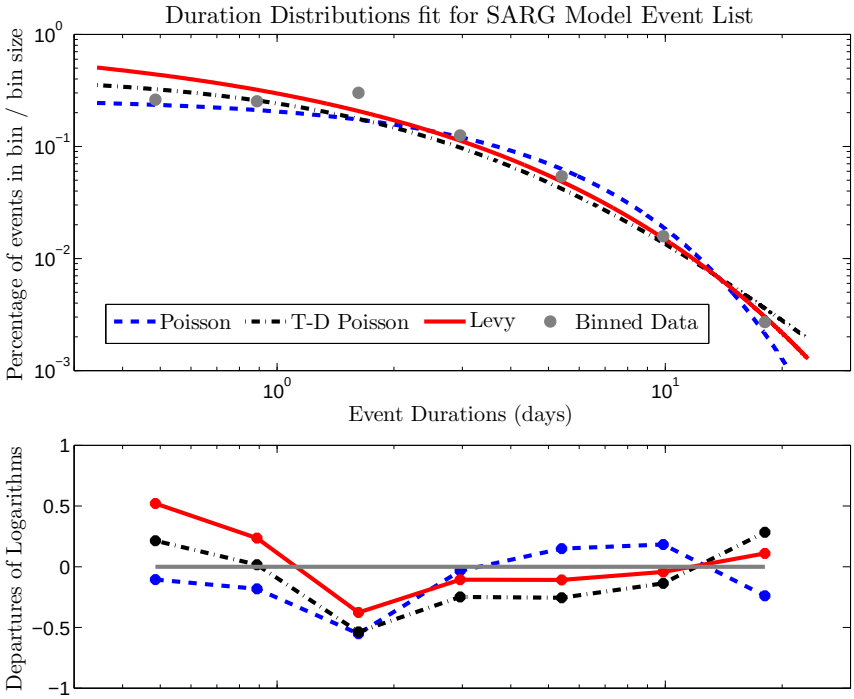

Figure 4.18: Duration distributions for SARG events (complete time period).

Table 4.18: Duration quality of fit parameters for complete time period.

	Poisson	T-D Poisson	Lévy
S^2	0.4631	0.5611	0.5050
χ^2	0.1075	0.1130	0.1318

Figure 4.19 shows the fittings of the SEPE durations for the active years only (top) and the residuals for each of the fittings (bottom). Here it appears that the Lévy distribution is the best fit to that data from the plots.

The fitting parameters for the distribution fits shown in Figure 4.19 are given in Table 4.19 while the quality of fit parameters are given in Table 4.20. Both the quality of fit parameters show that the Lévy distribution is the best fit to the data with the time-dependent Poisson fit next and the Poisson last. This clearly differs to the complete time period fits and the reason for this is not known, it might be that due to a short time period from which the event list is generated there is significant scatter. It does however justify the use of the Lévy distribution for the SEPE duration fit as well as the waiting time fit for a model of SEPE in solar active years.

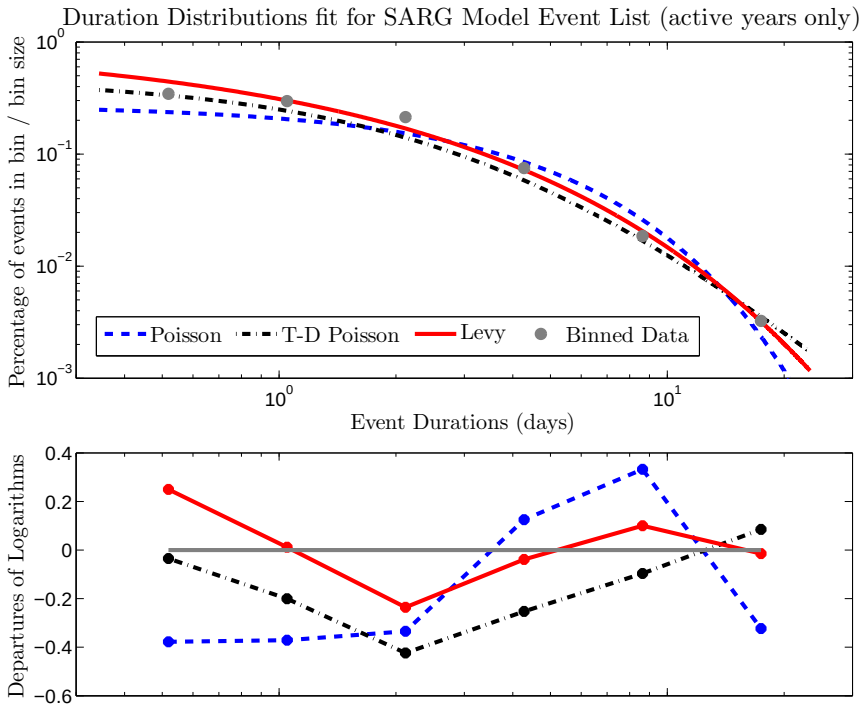

Figure 4.19: Duration distributions for SARG events (active years only).

Table 4.19: Duration fitting parameters for active years only.

λ	ρ	c	μ
0.2726	0.2356	1.3298	0.5561

Table 4.20: Duration quality of fit parameters for active years only.

	Poisson	T-D Poisson	Lévy
S^2	0.6232	0.3013	0.1298
χ^2	0.1190	0.0564	0.0339

4.4 Incorporating System Memory

4.4.1 Introduction

As was shown in the previous section there is 'memory' in the distribution in time of SEPEs rather than them being randomly distributed as previously thought. It was found that overall the better fitting to the event waiting times of SEPEs was that relating to a Lévy distribution of event frequencies rather than a Poisson distribution which has assumptions of a steady mean rate of event occurrence and no system memory. This is true even when only the active years of the solar cycle are considered which is the case for the most widely used models of the SEPE environment.

The choice of the Lévy distribution describes how there are higher number of short and long waiting times and fewer waiting times close to the mean value than would be the case if the SEPEs were randomly distributed. This is reflective of a scenario with periods of higher and lower activity within the time period being investigated. However, the waiting time distributions do not consider the order in which the waiting times occur and therefore any short-term dependency of one waiting time on the previous waiting time that may be present in the system. In this section using one of the three event lists used in the last chapter, that produced by NOAA (the National Oceanic and Atmospheric Administration), a method of incorporating short-term memory into SEPE modelling is presented. The waiting time here is taken to be from the start of one event to the start of the next and the NOAA example shows that with this definition of waiting time memory should be considered. The SARG modelling methodology (see Section 4.2) considers the waiting times from the end of one event to the start of the next and using the SARG event list (introduced in section 3.4) it is shown that the system memory becomes even more pronounced.

4.4.2 Burstiness and Memory

Prior to explaining the method and results first it is necessary to introduce the definitions of two fundamental parameters: Burstiness and Memory. The definitions used here of these parameters are those given by Goh and Barabási (2008). In that paper the authors refer to waiting times as the time between one event and the next event produced by a single source in a system of multiple sources. Whereas the authors refer

to the interevent time as the time between two events regardless of the source. An example is emails being sent where the waiting time is the time between an individual sending emails whereas the interevent time is the time between one email and the next regardless of who they were sent by. In the case of SEPEs, events are caused by various phenomena on the solar surface, so the waiting times (as defined as the time between one event and the next regardless of source) are the same as the interevent times of Goh and Barabási (2008).

Firstly, the burstiness parameter, B, is given by:

$$B \equiv \frac{\sigma_\tau/m_\tau - 1}{\sigma_\tau/m_\tau + 1} = \frac{\sigma_\tau - m_\tau}{\sigma_\tau + m_\tau} \tag{4.13}$$

where m_τ is the mean waiting time and σ_τ is the standard deviation of waiting times. A value of $B = -1$ corresponds to a completely regular (periodic) signal, $B = 0$ corresponds to a random (Poissonian) signal and $B = 1$ corresponds to the most bursty signal. Next the memory, M, is defined as the correlation coefficient of waiting times before and after each event:

$$M \equiv \frac{1}{n_\tau - 1} \sum_{i=1}^{n_\tau - 1} \frac{(\tau_i - m_1)(\tau_{i+1} - m_2)}{\sigma_1 \sigma_2} \tag{4.14}$$

where τ_i is the before event waiting time, τ_{i+1} is the after event waiting time with means m_1 and m_2 and standard deviations σ_1 and σ_2 respectively and n_τ is the total number of waiting times. Again this has a range of [-1,1] where $M = 0$ would be a system with no memory, a negative value of M represents a system where if the previous waiting time was short (long) then the following one is likely to be long (short) and a positive value of M represents a system where if the previous waiting time was short (long) then the following one is likely to be short (long).

Figure 4.20 shows the occurrence of SEPEs using various event definitions over the past 45 years. The blue lines give only the starting time of events and are not reflective in any way of the SEPE flux. It can be very difficult to discern from these plots where a system has burstiness as opposed to memory but immediately two things can be recognised: first that the active year periods have a far higher frequency of events and secondly that the system is not regular or periodic (i.e. does not have heavily negative burstiness).

The calculated burstiness and memory parameters for each of the three event lists used in Section 4.3 are given in Table 4.21. In addition to calculating the burstiness

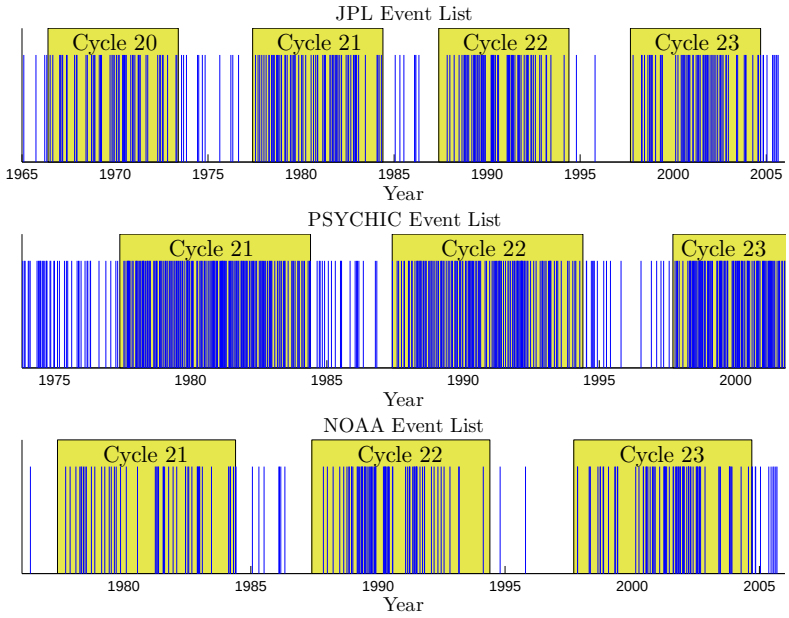

Figure 4.20: Time signals of JPL (top), PSYHIC (middle) and NOAA (bottom) event lists.

and memory for each event list with the usual definition of event waiting time (columns 2 and 3) the parameters have also been calculated for the waiting times taken from the end of one event to the start of the next (columns 4 and 5). This was not possible for the NOAA event list as the event durations were not available.

Table 4.21: Table of data set burstiness and memory.

JPL	all events	active years	end-to-start (all)	end-to-start (active)
Burstiness	0.1841	0.0269	0.2545	0.1227
Memory	0.3098	0.0785	0.3181	0.0854
PSYCHIC	all events	active years	end-to-start (all)	end-to-start (active)
Burstiness	0.0776	-0.1474	0.3174	0.2068
Memory	0.4148	0.1153	0.4684	0.1887
NOAA	all events	active years		
Burstiness	0.2944	0.1651		
Memory	0.2227	0.1048		

The burstiness parameter is nearly always positive except in the PSYCHIC event list for the active years where the negative value indicates that the events are more regular than a random sample would be. As discussed in Section 4.3.4 this is likely due

to the non-point-like nature of SEPEs. To illustrate the effect of the event durations the waiting times from the end of one event to the start of the next show a large positive jump in burstiness over the original waiting time definition. The burstiness parameters are all higher for the complete time period than for the active years only. This is due to the known variation between active and quiet year event frequencies. The positive burstiness found when considering only active year periods shows that there are a greater number of clusters of events and voids than would expected in a random process.

The memory parameters are always significantly positive indicating that it should be considered in an SEPE model. Again columns 4 and 5 show an increase in memory over columns 2 and 3. The measure of memory taken here differs from that used in Section 4.3 (taken from Bi et al. (1989)). However, both are valid and each shows that generally memory is present in the SEPE system. However, the definition of memory given by Goh and Barabási (2008) considers the correlation between all consecutive events giving a quantitative measure of the memory rather than a method of proving the existence of system memory at a given confidence level.

The burstiness gives a measure of the variation of the waiting times which for the NOAA active year example is reflected in the fittings shown in Figure 4.21 (reproduced from the bottom panel of Figure 4.11 in Section 4.3.2.1). However, the short-term memory is not considered by these distribution fits as no notice is paid to the order in which the events occur.

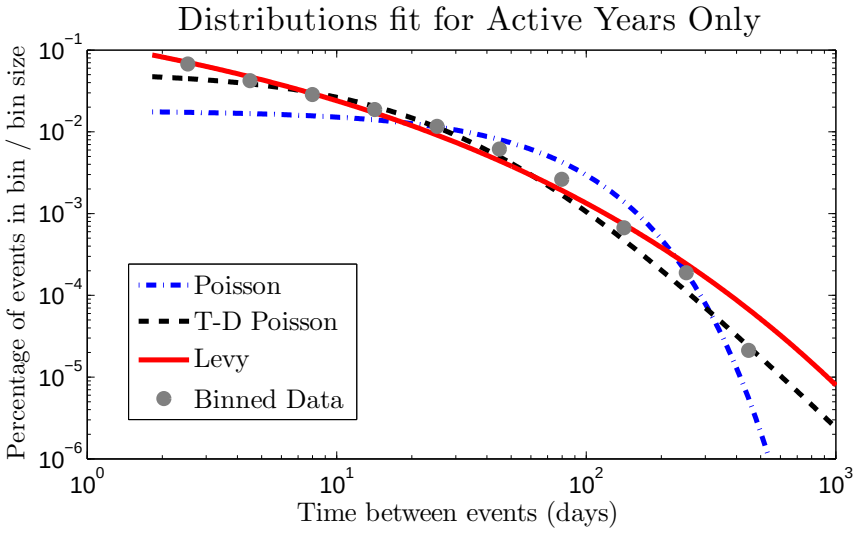

Figure 4.21: Waiting time fits to NOAA active year events.

4.4.3 Theory and Methodology

The preliminary step in this procedure is to normalise the NOAA SEPE waiting times (active years only) using the fitted waiting time distribution function (the integral of the probability density function). In the case of the Lévy distribution this distribution function is given by:

$$P(>0;\Delta t) = 1 - \frac{\Delta t E_{\frac{\mu-1}{\mu}}((c\Delta t)^{\mu})}{\mu} \tag{4.15}$$

here E is the exponential integral whose definition and series expansion are:

$$E_n(x) \equiv \int_1^{\infty} \frac{e^{-xt}}{t^n} \mathrm{d}t = x^{n-1}\Gamma(1-n) + \sum_{m=1}^{\infty} \frac{(-1)^m x^{m-1}}{(m-1)!(m-n)} \tag{4.16}$$

$P(>0;\Delta t)$ gives the cumulative probability for each event; the likelihood that a waiting time would be less than the waiting time Δt. The computation of $P(>0;\Delta t)$ must be done numerically rather than analytically and all values lie between 0 and 1. The distribution function for the time-dependent Poisson process is given by:

$$P(>0;\Delta t) = 1 - \frac{1}{(1+\varrho\Delta t)^2} \tag{4.17}$$

while the distribution function for the Poisson process is given by:

$$P(>0;\Delta t) = 1 - e^{-\lambda\Delta t} \tag{4.18}$$

Using the cumulative probabilities rather than the event waiting times removes the burstiness from the signal so that the memory can be focused upon. Figure 4.22 shows the integration of these functions to find the distribution functions for the SEPE waiting times for the NOAA active year events. It can be seen from both of these graphs that the better fitting Lévy and Time-dependent Poisson distributions differ markedly from the Poisson distribution.

Next a scatter plot is produced of the cumulative probabilities for the waiting times before each event against the cumulative probabilities for waiting times after each event. The scatter plot for the NOAA active years data normalised using the Lévy fitting is shown in Figure 4.23. If there was zero memory in this system the points would be randomly distributed across this grid with no correlation between the pre-event and post-event cumulative probabilities. A negative memory would show increased densities along the $x = -y$ diagonal while for a positive memory we would expect a higher concentration of points along the $x = y$ diagonal.

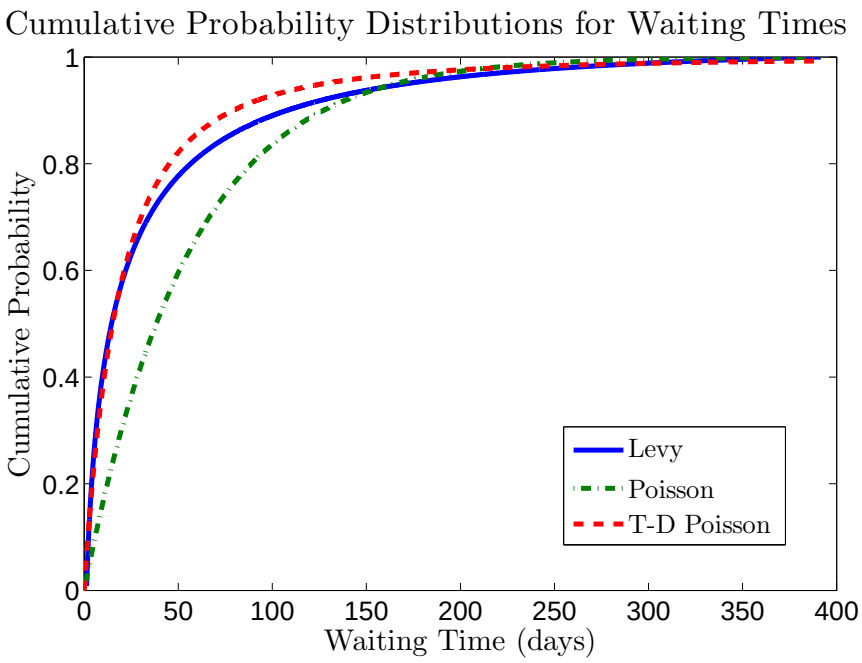

Figure 4.22: Cumulative waiting time fits to NOAA active year events.

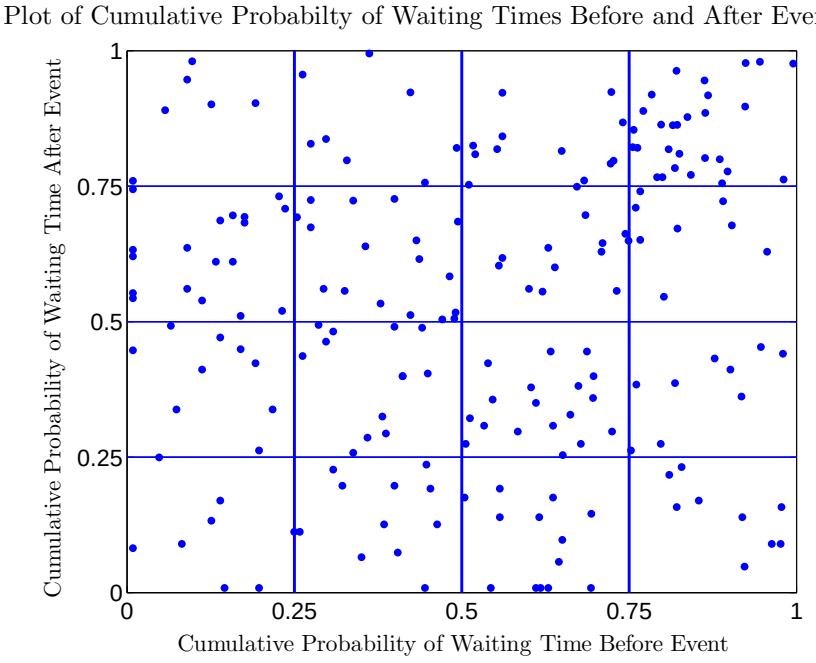

Figure 4.23: Plot of the pre-event waiting times against the post-event waiting times for the NOAA SEPE list.

Here it can be seen that there appears to be some positive correlation between the normalised waiting times but that this correlation is not very strong (reflected in the value of $M = 0.1048$ in Table 4.21). However, the small level of memory apparent in the system does need to be considered. The aim is to incorporate this memory

without impacting the burstiness which has already been accounted for by the fitted distribution. By altering the cumulative probability for a single event waiting time based on the previous cumulative probability the waiting time distribution over a long time period should remain unaffected.

The grid was divided by 4 for both the input (before event) and output (after event) waiting time cumulative probabilities and to plot these as histograms. It is expected that with a positive system memory that there will be a higher number of low cumulative probabilities after events where there was a low cumulative probability before the event and a higher number of high cumulative probabilities after events where there was a high cumulative probability beforehand.

The four points on each histogram were then with fit with quadratic functions (see Figure 4.24). For the highest pre-event cumulative probabilities (> 0.75 & < 1.00 - bottom right) there are a greatly increased number of high post-event cumulative probabilities. The pre-event cumulative probabilities from > 0.25 & < 0.50 (top right) and > 0.50 & < 0.75 (bottom left) also show encouraging results with an increased number of post-event cumulative probabilities between 0.25 and 0.75 compared to the number of high or low post-event cumulative probabilities. Unfortunately, the lowest previous waiting time cumulative probabilities (> 0.00 & < 0.25 - top left) do not show an increased number of the lowest cumulative probabilities for the following events. This could be due to a combination of natural scatter (from a list of 201 events the average number for each bar on each histogram is 12.56) or the impact of the duration of events reducing the possibility of the lowest waiting times.

Taking the top three fits as a starting point 15 'memory histograms' were then produced with varying levels of bias (increasing from histogram 1 to histogram 15). A histogram with a low level of bias has only a small change in the likelihood of the post-event cumulative probabilities depending on the pre-event cumulative probability whereas a histogram with high level of bias greatly increases the likelihood of a low (high) cumulative probability following a low (high) cumulative probability. The 15 memory histograms tested are shown in Tables B.17, B.18 and B.19 in Appendix Section B.2.

The two lowest two memory bands (memband 1 => 0.00 & < 0.25 and memband 2 => 0.25 & < 0.50) must follow the inverse of the top two memory bands (memband

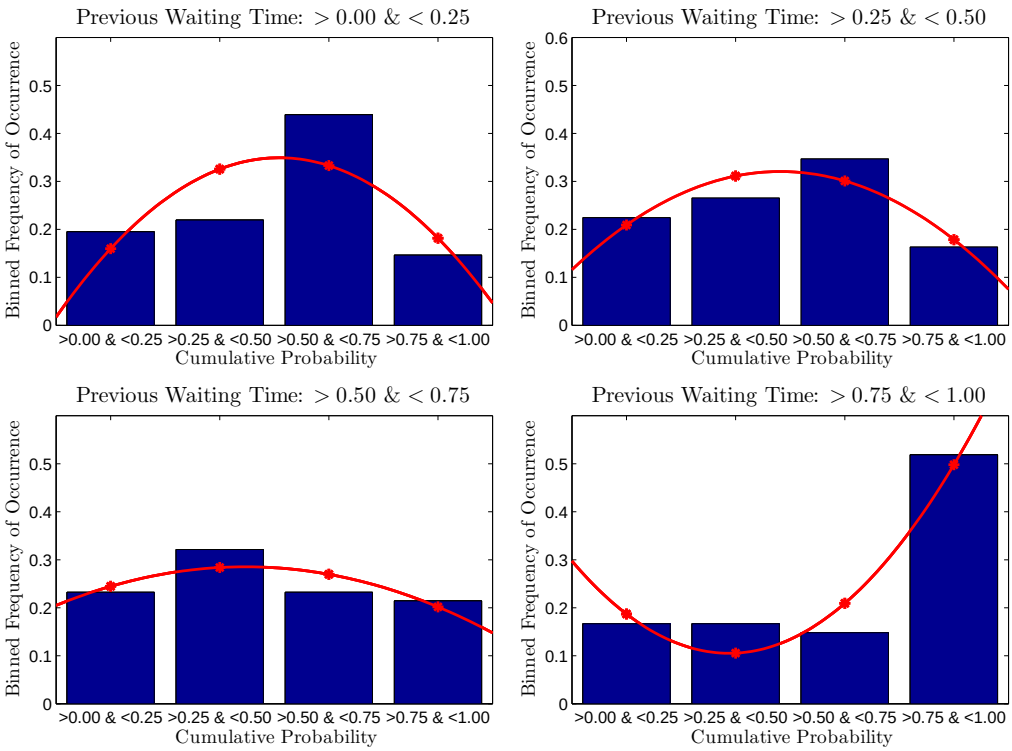

Figure 4.24: Histograms of post-event waiting times grouped by the pre-event waiting times for the NOAA SEPE list.

3 => 0.50 & < 0.75 and memband 4 => 0.75 & < 1.00) in order not to affect the burstiness. It was then necessary to ensure that each of the two columns (containing one value from each memory band) summed to 1 and that the sum of the two memband 1 values and the memband 4 values summed to 1 and then the resulting sum of the two memband 2 and memband 3 values would also sum to 1. This should result in an induced memory with no impact on the burstiness of the cumulative distribution being sampled over a long enough time period. The greater the bias the greater the degree of memory introduced to the system.

4.4.4 Memory Results

For each of the 15 memory histograms and for all three of the distribution functions (Poisson, Time-dependent Poisson and Lévy) a series of 100,000 waiting times were generated each based on the cumulative probability of the previous waiting time (except the first in each series which was randomly sampled from the distribution). In each case the burstiness and memory of the resulting series of waiting times was calculated, these are shown in Tables 4.22 and 4.23 respectively.

Table 4.22: Table of calculated burstiness.

	Histogram				
	1	2	3	4	5
Poisson	0.0024	-0.0002	-0.0006	0.0020	0.0007
T-D Poisson	0.5008	0.5403	0.4559	0.6487	0.6112
Lévy	0.2200	0.2181	0.2175	0.2179	0.2177
	Histogram				
	6	7	8	9	10
Poisson	0.0018	0.0022	-0.0011	-0.0041	0.0001
T-D Poisson	0.4736	0.4844	0.4508	0.4410	0.4649
Lévy	0.2186	0.2191	0.2173	0.2159	0.2172
	Histogram				
	11	12	13	14	15
Poisson	-0.0012	0.0002	-0.0005	0.0014	-0.0006
T-D Poisson	0.5855	0.4735	0.4385	0.5418	0.8496
Lévy	0.2157	0.2174	0.2175	0.2212	0.2169

It can be seen that for the Poisson distribution the burstiness remains at approximately 0 and that for the Lévy distribution it remains at approximately 0.22. However the Time-dependent Poisson distribution shows more significant variance from the $B = 0.5$ starting point. This is possibly as a result of the significant probability this distribution allows for very high waiting times but it is uncertain exactly why there is this high degree of variance.

The Time-dependent Poisson distribution also returns unexpected results for the memory with a very limited and unsteady increase in values despite the increasing bias of the underlying memory histograms. The results for the Poisson distribution and the Lévy distribution are far closer to what had been anticipated with unchanged burstiness and increasing memory as the bias of the memory histogram increases.

Focussing again on the Lévy distribution it can be seen that histogram set 7 has a level of memory close to that found in the NOAA active year sample (this is shown in Figure 4.25). The value of burstiness for the Lévy distribution using the fitting parameters is higher than the 0.1651 from the raw data. This is still the closest of the

Table 4.23: Table of calculated memory.

	Histogram				
	1	2	3	4	5
Poisson	-0.0036	0.0204	0.0415	0.0644	0.0981
T-D Poisson	0.0007	0.0042	0.0086	0.0041	0.0085
Lévy	-0.0017	0.0131	0.0317	0.0419	0.0647
	Histogram				
	6	7	8	9	10
Poisson	0.1210	0.1386	0.1616	0.1866	0.2038
T-D Poisson	0.0230	0.0257	0.0366	0.0465	0.0450
Lévy	0.0814	0.1010	0.1154	0.1316	0.1478
	Histogram				
	11	12	13	14	15
Poisson	0.2432	0.2624	0.2614	0.3051	0.3131
T-D Poisson	0.0244	0.0593	0.0696	0.0422	0.0033
Lévy	0.1734	0.1871	0.1848	0.2138	0.2261

three fitting distributions and the difference is likely a result of the event durations reducing the possibilities for event clustering. The waiting times (using the definition from the start of one event to the start of the next) are limited at the lower end by the duration of the preceding event.

When this histogram is used to adjust the Lévy waiting time distribution function for the prediction of the next waiting time based on each of the 4 memory bands for preceding waiting time cumulative probability the plots shown in Figure 4.26 are arrived at. Also shown is the original Lévy cumulative distribution curve which lies in the middle of the other 4 curves. This is to be expected as there is no bias in the original distribution while the two lower memory bands have a bias towards lower cumulative probabilities (longer waiting times) and the two higher memory bands have a bias towards higher cumulative probabilities (shorter waiting times).

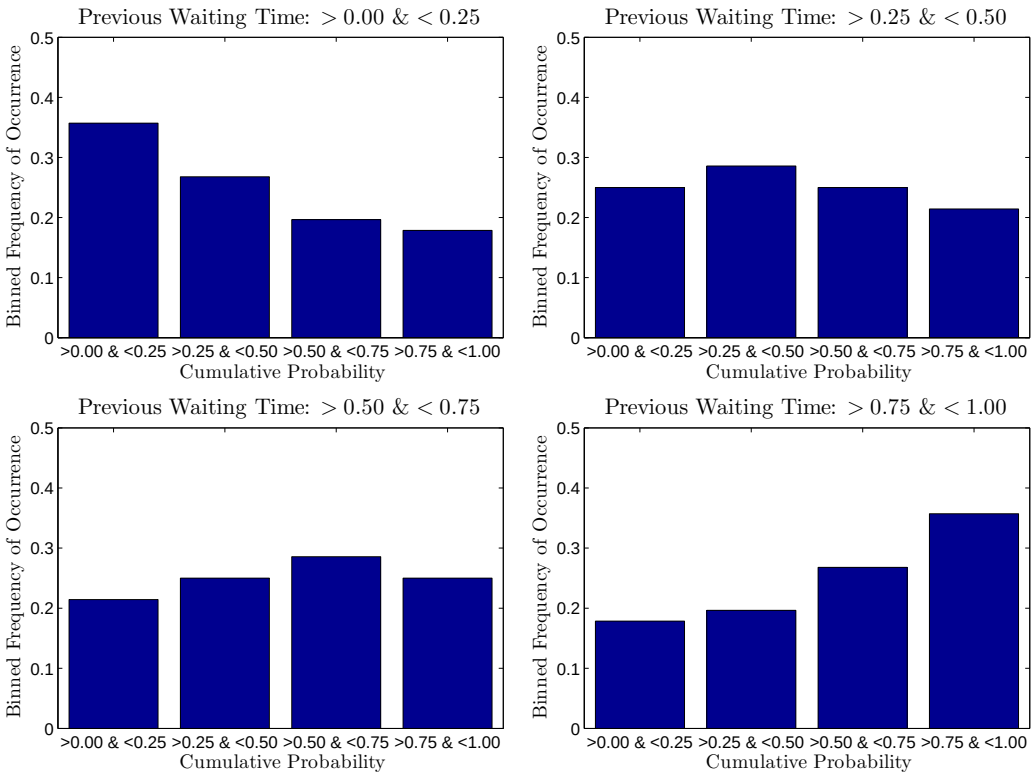

Figure 4.25: Memory histograms used to adjust waiting times based on the NOAA SEPE list.

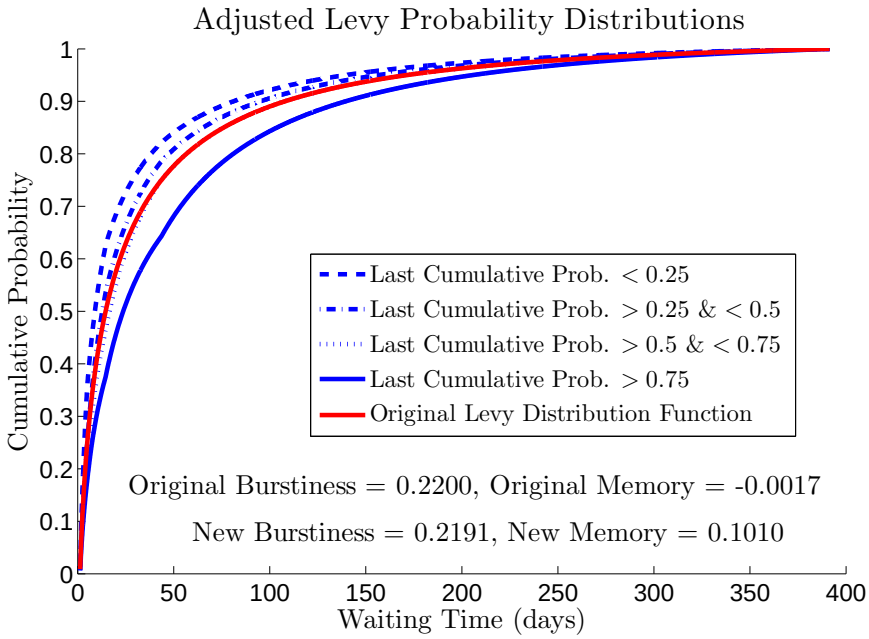

Figure 4.26: Adjusted waiting time distributions using memory histograms.

4.4.5 Effect on Frequency Distributions

The three waiting time distributions introduced in section 4.4.3 were randomly to produce a series of virtual timelines in the same way as introduced in section 4.2 but without any event characteristics (durations, fluences or peak fluxes). The resulting frequency of events for a 2 year time period is given by Figure 4.27. It can be seen that each of the distributions of event frequency are approximately evenly symmetric about a mean value although the variance is different in each case. As the Time-dependent Poisson distribution has the greatest burstiness it is wider and flatter where the Poisson distribution has zero burstiness and therefore is quite narrow and the Lévy lies between the two.

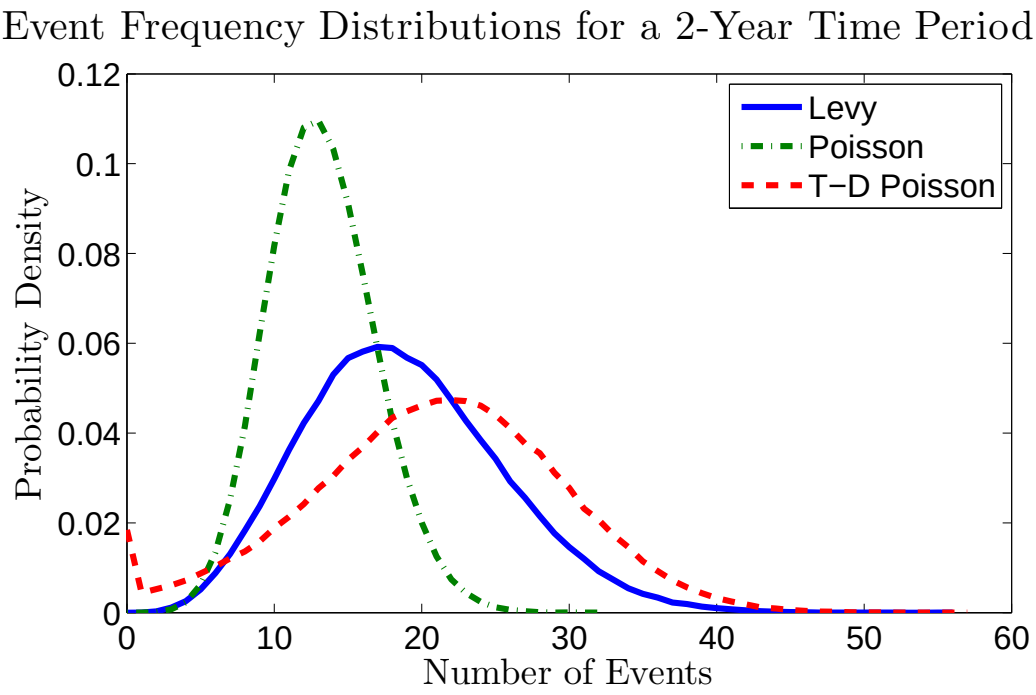

Figure 4.27: Event frequency distributions without memory.

Table 4.24 shows the $10^{th} - 90^{th}$ percentiles for the distributions which show a slight positive skew for the Poisson and Lévy distributions with a slightly larger gap between the 10^{th} and 50^{th} percentiles than between the 50^{th} and 90^{th}. The time-dependent Poisson distribution shows a slight negative skew due to the far higher possibility of zero events occurring using this distribution.

When memory is introduced into the system using memory histogram set 7 (Figure 4.25) more skew is introduced and the tail in the direction of high numbers of events is extended (Figure 4.28). By adjusting the sampling of the waiting times based

Table 4.24: Event numbers of distribution percentiles without adjusted memory.

Percentile	10^{th}	20^{th}	30^{th}	40^{th}	50^{th}	60^{th}	70^{th}	80^{th}	90^{th}
Lévy	10	13	15	17	18	20	22	24	28
Poisson	9	10	11	12	13	14	15	16	18
T-D Poisson	9	14	17	19	21	23	25	28	32

on the previous waiting times the value of M has been increased to account for the memory in the system. The event frequency distribution has been affected while the overall waiting time distribution for the Poisson and Lévy distributions has remained unaffected as shown by the steady values for burstiness (see section 4.4.4). The Time-dependent Poisson distribution failed to work with this method as shown by the fluctuating burstiness and failure to introduce system memory shown in section 4.4.4. Each of these runs was done for 300,000 iterations to produce smooth curves and reliable results.

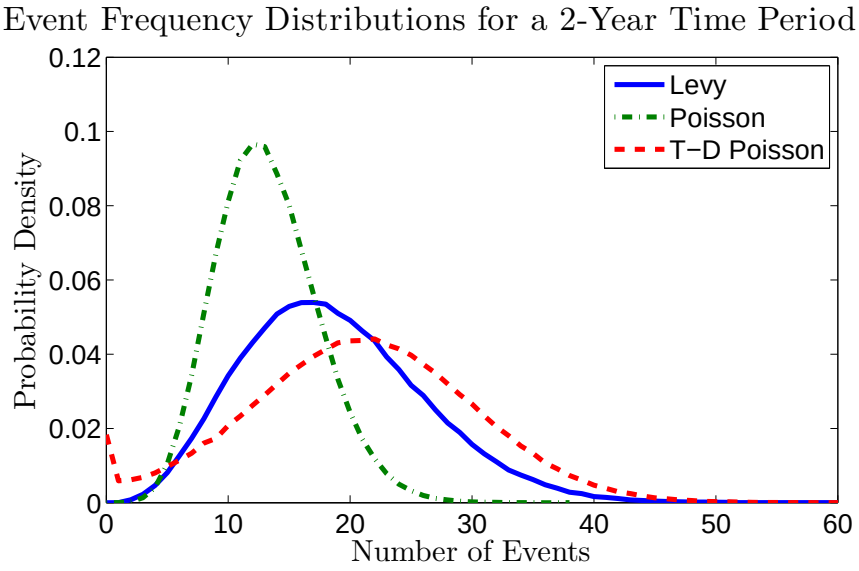

Figure 4.28: Event frequency distributions with memory.

The differences in the event frequency distributions are small as the level of memory in the system was only 0.1010. However, the peaks in Figure 4.28 are lower than those in Figure 4.27, the Lévy distribution shifts from 0.05921 at 17 events to 0.05395 at 17 events, the Poisson distribution from 0.1096 at 13 events to 0.09661 at 12 events and the time-dependent Poisson distribution from 0.04733 at 22 events to 0.04412 at 22 events. The percentiles shown in 4.25 show little change for the time-dependent

Poisson distribution (perhaps unsurprising given the difficulties incorporating system memory as shown in Table 4.23). The Lévy distribution has slightly more skewed distributions shown by the reduction in the event numbers for the 20^{th}, 30^{th} and 40^{th} percentiles and the increase in event numbers in the 80^{th} and 90^{th} percentiles. Likewise the Poisson distribution shows increased skew with a reduction in the 10^{th} percentile and a increase in the 80^{th} and 90^{th} percentiles.

Table 4.25: Event numbers of distribution percentiles using adjusted memory.

Percentile	10^{th}	20^{th}	30^{th}	40^{th}	50^{th}	60^{th}	70^{th}	80^{th}	90^{th}
Lévy	10	12	14	16	18	20	22	25	29
Poisson	8	10	11	12	13	14	15	17	19
T-D Poisson	9	13	16	19	21	23	26	28	32

4.4.6 Application to SARG Event List

The same method using the Lévy distribution was also applied to the SARG event list but taking the waiting times to be the time from the end of one event to the start of the next. The memory histogram used for this list is given in Table 4.26 and plotted in Figure 4.29.

The burstiness and memory for the list of waiting times and the fitted Lévy distribution with incorporated memory are given in Table 4.27. It is clear that there is very good agreement between the sample data and the fitted distribution with memory incorporated.

The effect of building in the memory to the system for each of the 4 memory bands compared to the Lévy distribution fitted to all the binned waiting times can be seen in Figure 4.30. The large deviation from the original distribution function shows how

Table 4.26: Table of memory histograms used for SARG Model.

memband	$> 0 \& < 0.25$	$> 0.25 \& < 0.50$	$> 0.50 \& < 0.75$	$> 0.75 \& < 1.00$
1	0.5357	0.2679	0.1607	0.0357
2	0.2857	0.3571	0.2143	0.1429
3	0.1429	0.2143	0.3571	0.2857
4	0.0357	0.1607	0.2679	0.5357

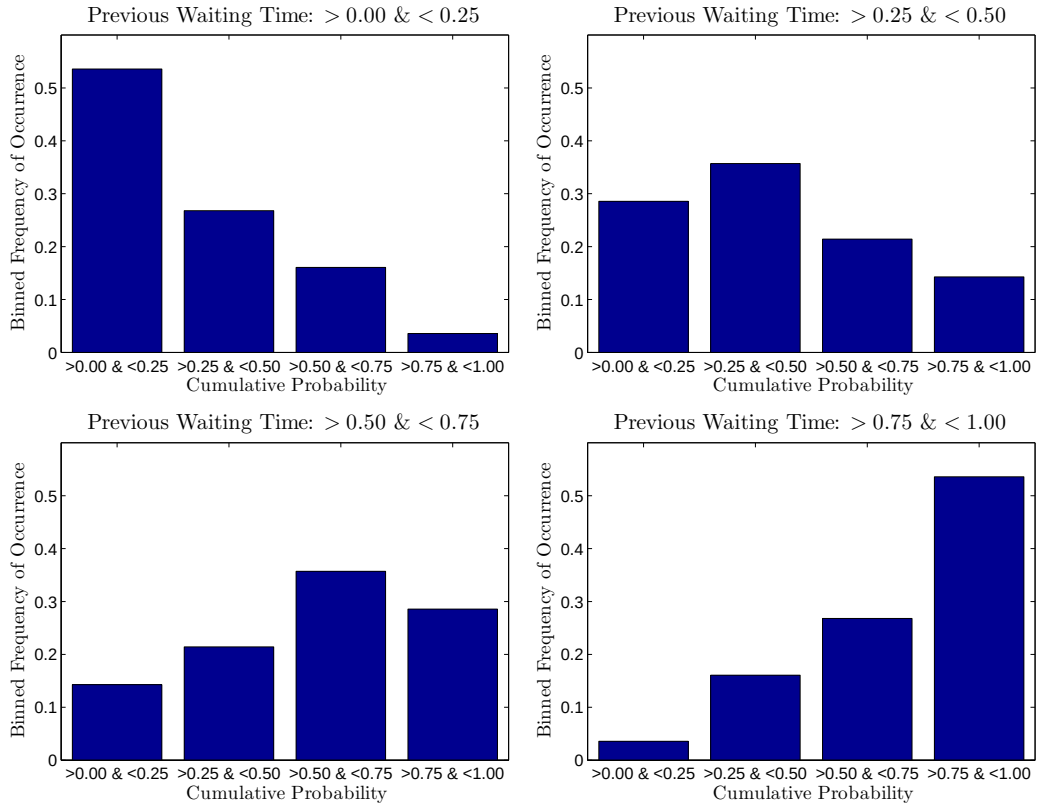

Figure 4.29: Histograms used to model memory for the SARG model.

Table 4.27: Table of memory histograms used for SARG Model.

	Burstiness	Memory
SARG Event List	0.2620	0.2518
Fitted Lévy	0.2588	0.2490

significant the impact of memory is with a value of $M =\sim 0.25$.

The very small difference in the measured burstiness from the SARG event list and burstiness of the generated fitted Lévy distribution using this definition of waiting time indicate that the duration of SEPEs was having an impact on this parameter. This low error gives good reason to use this definition of waiting time as set out in the SARG modelling methodology in Section 4.2.

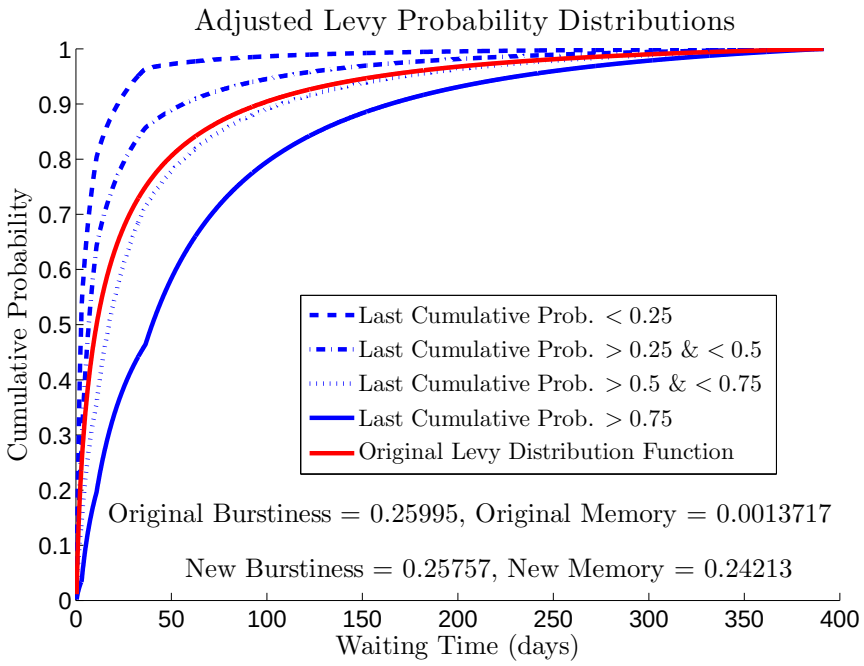

Figure 4.30: Adjusted Lévy distribution depending on previous event waiting time.

4.4.7 Conclusions on System Memory

It has been found that short-term memory (as defined by equation 4.14) in the occurrence of SEPEs is always present in event lists regardless of the definitions of events and waiting times used. To account for this memory a piece-wise method of weighting the random sampling of SEPE waiting times using 'memory histograms' has been created. This deviation from a random distribution of events is separate from the deviation from the Poisson distribution found in section 4.3. This short-term memory is dependent on the order in which the events occur where the burstiness reflected in the waiting time distribution of events reflects higher than expected numbers of low and high waiting times overall. The method allows the inclusion of the dependency of the post-event waiting time on the waiting time prior to the event.

A key aspect of this method is that the underlying weighting time distribution of SEPEs is not affected and in two out of the three cases this has been shown to be true. Crucially this includes the Lévy distribution which was found to be the best most robust fitted distribution to SEPE waiting times in section 4.3 and which will therefore be used in the new solar proton modelling methodology. The reasons for the failure of the method to work with the time-dependent Poisson distribution are unknown.

Over a two-year time period using the NOAA event list there is a small but noticeable effect on the event frequency distribution by including this memory. The fact that there are always a whole number of events is a limit on finding differences using the distribution percentiles. The effect of memory is likely to be greater over short time periods and average out over long time periods. The impact of system memory on the event frequency distribution is likely to even out over longer time periods (mission lengths) as there will be periods of successive short waiting times as well as periods of successive long waiting times.

It was found that the impact of system memory is greater when the waiting times are defined as the time from the end of one event to the start of the next. This was shown firstly with the JPL and PSYCHIC distributions with different waiting time definitions in Table 4.21 and then with the study of the SARG event list in section 4.4.6. Table 4.21 also shows that memory is present in the system when considering only active years or the complete time period. Only a single pre-event waiting time has been considered for this short-term memory, it is possible that there is a dependency on waiting times further in the past.

4.5 Fluence and Peak Flux Distributions

As part of the SARG modelling methodology a distribution must be chosen to be fit to SEPE fluences and peak fluxes. As discussed in Section 2.2.5 previous models have used either the lognormal distribution fit only to the top half of the events fluences (Feynman et al., 1990, 1993) or a type of power law (Nymmik, 1999; Xapsos et al., 1998b, 1999) which is often adjusted to account for deviations at one end of the distribution. In this section a comparison of the goodness-of-fits of the lognormal distribution and truncated power law (Xapsos et al., 1998a) is done using the fluences of the events from the > 10 MeV data in the extended JPL event list (see Appendix Section A.1). The > 10 MeV integral GOES data used in this section includes much of the data spread across the standard energy channels introduced in Section 3.4.5 making it a good data set on which to perform this comparison.

4.5.1 Comparison of Fluence Distributions

The fittings of the lognormal distribution and truncated power law were performed for the complete JPL event list. The confidence level was plotted against the SEPE fluence data was with a normally distributed abscissa and a logarithmic ordinate, an analytical straight line fit applied to the top half of the data as done by Feynman et al. (1993); Rosenqvist et al. (2005). This fitting is shown in Figure 4.31. The distribution function is given in section 2.2.5.1.

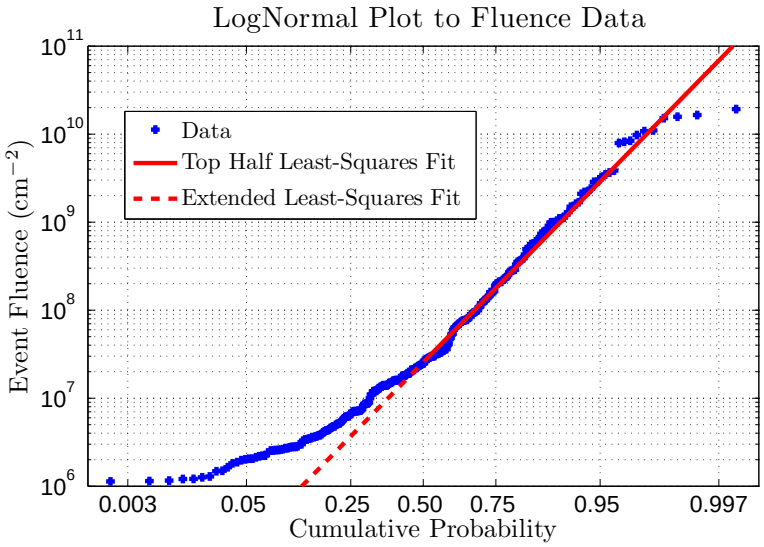

Figure 4.31: Lognormal fit to all JPL event list SEPEs.

The SEPE fluence data was also plotted against the likelihood of exceeding and fit with a truncated power law as done by Xapsos et al. (1999). This fit was done numerically to minimise the sum of squared residuals for fluences above the median value in the data set to be consistent with the method applied for the lognormal distribution. The distribution function for the truncated power law is given in section 2.2.5.3. This fitting is shown in Figure 4.32.

Table 4.28 shows the goodness-of-fit parameters for the lognormal distribution and truncated power law for the top half of the complete JPL event list. The two parameters used to determine the goodness-of-fit were the sum of squared residuals, S^2, given by:

$$S^2 = \sum_{i=1}^{n} (O_i - E_i) \tag{4.19}$$

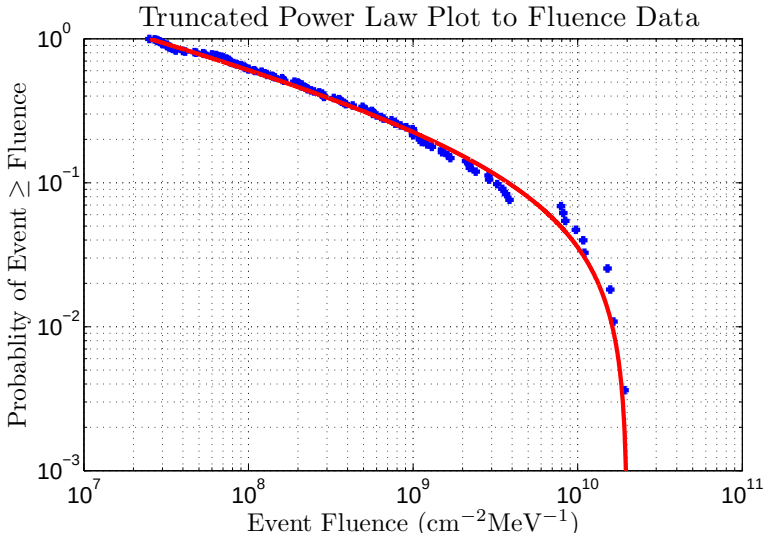

Figure 4.32: Truncated power law fit to all JPL event list SEPEs.

Table 4.28: Goodness-of-fit parameters for complete JPL event list.

Distribution	S^2 (top half)	χ^2 (top half)
Lognormal Distribution ($> 10^6$)	5.97	0.260
Truncated Power Law ($> 10^6$)	2.00	0.100

and a second well known quality of fit parameter, the χ^2 parameter, given by:

$$\chi^2 = \sum_{i=1}^{n} \frac{(O_i - E_i)}{E_i} \tag{4.20}$$

where in both cases O_i is the logarithm of the observed fluence, E_i is the logarithm of the fitted value and n is the total number of observations. Both goodness-of-fit parameters show that the truncated power law is the better fitting distribution although the two are comparable.

However, the JPL-91 model did not apply the lognormal fit to the top half of the distribution of all the SEPE events recorded but only those with fluence $> 10^7$ cm^{-2} for the > 10 MeV channel. This threshold parameter has been applied to the JPL event list and a lognormal fit done for the top half of the 190 remaining larger events (see Figure 4.33).

The events with fluence greater than the median of the $> 10^7$ cm^{-2} SEPEs was also fit with a truncated power law and this is shown in Figure 4.34.

Table 4.29 shows the goodness-of-fit parameters for SEPEs above the median using the lognormal distribution and truncated power law with the $> 10^7$ cm^{-2} threshold

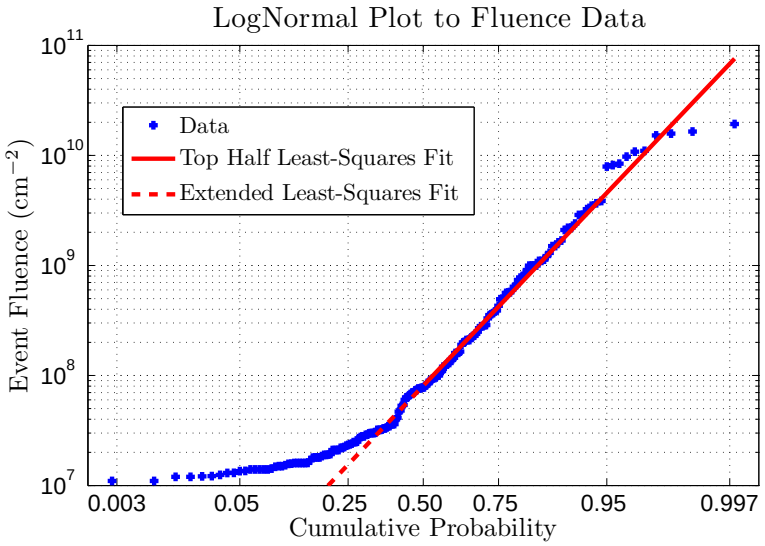

Figure 4.33: Lognormal fit to JPL event list SEPEs ($> 10^7$ cm^{-2}).

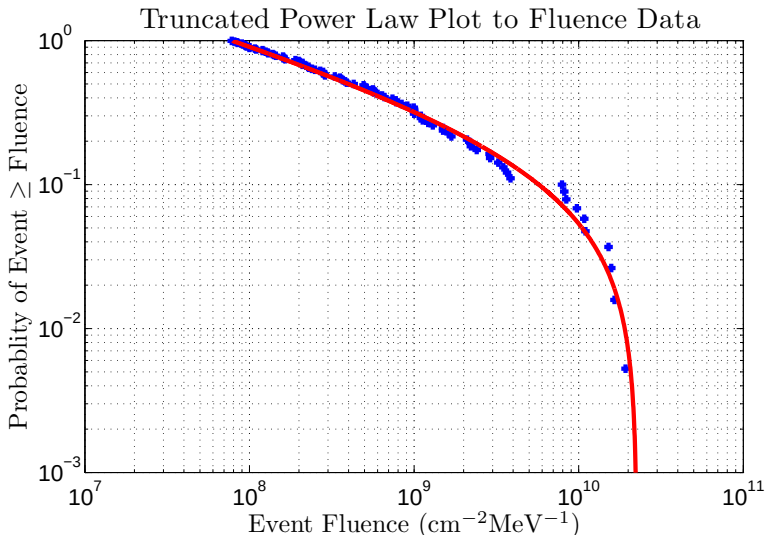

Figure 4.34: Truncated power law fit to JPL event list SEPEs ($> 10^7$ cm^{-2}).

applied. Again the truncated power law is the better fit by a comparable margin (in terms of percentage) to the results from Table 4.29.

One concern with the lognormal distribution is the poor fit to the highest fluence events. The distribution gives a greater likelihood than the data implies in both

Table 4.29: Goodness-of-fit parameters for JPL events $> 10^7$ cm^{-2}.

Distribution	S^2	χ^2
Lognormal Distribution ($> 10^7$)	3.55	0.151
Truncated Power Law ($> 10^7$)	1.03	0.0485

Table 4.30: Goodness-of-fit parameters for JPL events measured by GOES/SEM.

Distribution	S^2	χ^2
Lognormal Distribution (GOES)	8.25	0.357
Truncated Power Law (GOES)	1.42	0.0708

Figures 4.31 and 4.33. This problem was reported for the lognormal distribution fits to the daily fluences by Feynman et al. (1990). Tylka et al. (1997) suggested that the count rate being suppressed during peak rates as a result of the anti-coincidence shield on IMP-8/CPME resulting in dead-time could be the cause of this. No such problem occurs for the GOES/SEM instrument and therefore the fittings can be done again using only the 143 SEPEs detected using the GOES/SEM data (the data in the list from 1986 onwards). Figure 4.35 shows the lognormal fit to the top-half of these event fluences.

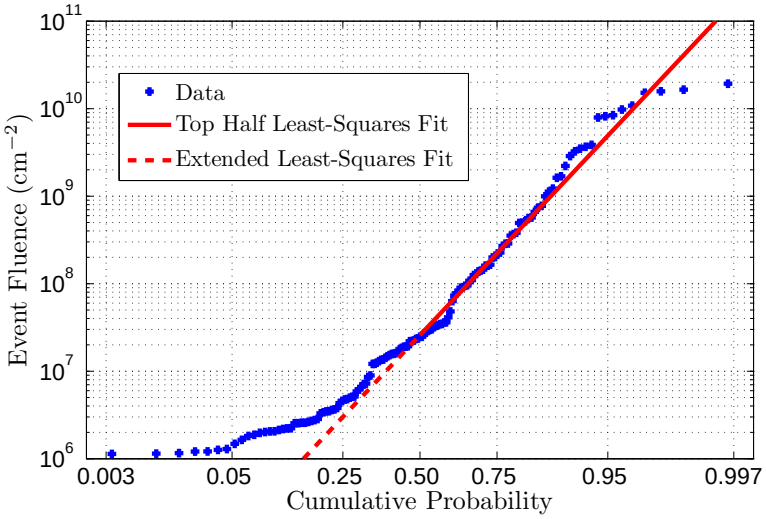

Figure 4.35: Lognormal fit to JPL event list SEPEs (GOES only).

4.36 shows the same fitting applied for the truncated power law for fluences above the median value. Figure 4.35 does not show that the departure of the fit from the data has been resolved. Table 4.30 reflects this again finding the truncated power law to be the better fitting distribution with both the S^2 and χ^2 goodness-of-fit parameters.

In each of the cases for the > 10 MeV SEPE fluences the truncated power law is a better fit to the data. Despite attempts to resolve the poor fit of the lognormal distribution at the highest fluence values first by introducing a fluence threshold of $> 10^7$ cm^{-2} and then by excluding the data prior to 1986 which it is believed suffer

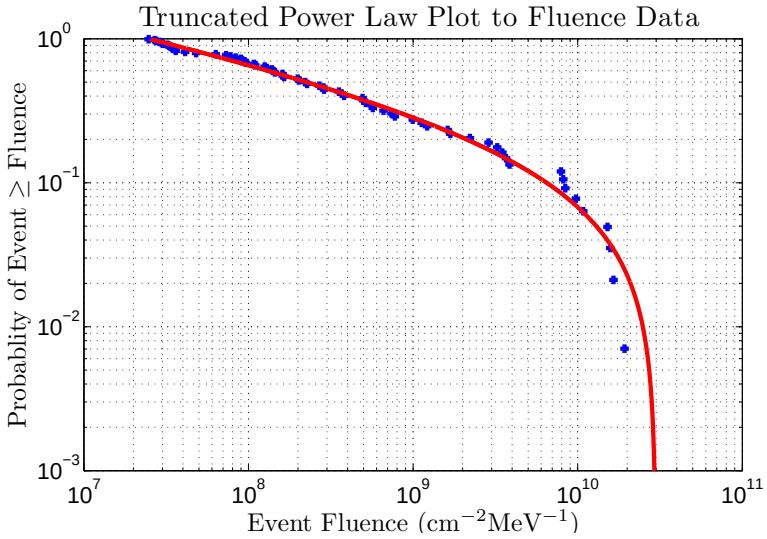

Figure 4.36: Truncated power law fit to JPL event list SEPEs (GOES only).

severe dead-time problems the result was not altered. It should therefore be concluded that the truncated power law, with distribution function given by:

$$F(\phi) = 1 - \frac{\phi_{\min}^{-b} - \phi^{-b}}{\phi_{\min}^{-b} - \phi_{\max}^{-b}} \tag{4.21}$$

where b is the power law exponent, ϕ is the event fluence, $\phi_{\min}$ is the minimum fluence and $\phi_{\max}$ is the maximum fluence, is the more appropriate distribution to use in the creation of an SEPE model.

4.5.2 Peak Flux Distribution

It was shown by (Xapsos et al., 1998b) that the truncated power law can be applied also to the peak flux distribution of SEPEs. Here the fluence parameters, ϕ, are replaced by the peak fluxes of the events. A simple linear fit can be made between the natural logarithms of SEPE fluences and peak fluxes as shown in Figure 4.37 using the GOES/SEM data from the JPL event list. This shows that once a fluence for an SEPE has been generated that this regression may be used to generate a peak flux for the SEPE as per the methodology laid out in Section 4.2.

The statistical variation between the peak flux and fluence can be attributed to the differences in the shape of SEPE flux profiles caused by factors such as the position of the solar origin which were explained in Section 2.1.

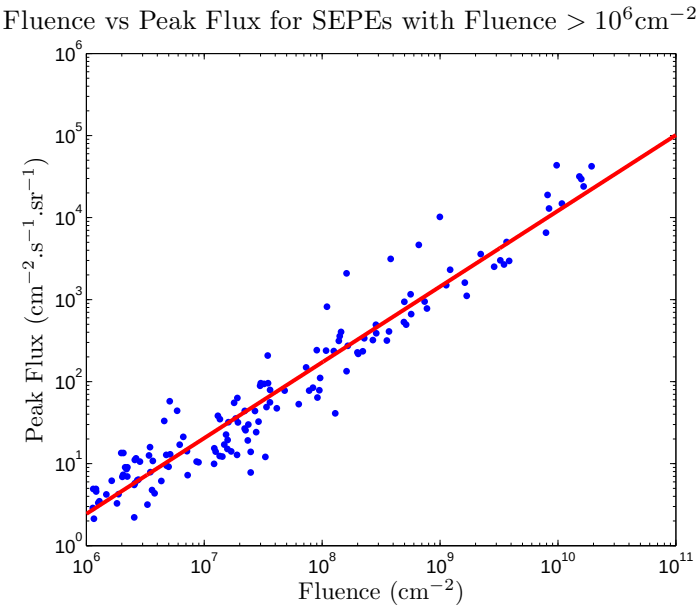

Figure 4.37: Linear regression of event fluence and peak flux using > 10 MeV GOES data.

4.5.3 SARG Model Fits

Having found in Section 4.5.1 that the truncated power law provides a superior fit to the lognormal distribution for the SEPE fluences and knowing that the same distribution may be applied to the SEPE peak fluxes fits can now be performed using the SARG event list (from Section 3.4).

The fittings were performed by taking a grid of 10,000 combinations of possible values for b ranging from 0.01 to 0.85 and $\phi_{\max}$ values from 1 to 50 times the maximum fluence (or peak flux) seen in the sample. Once the sum of squared residuals, S^2 (given by Equation 4.19), had been calculated another grid of 10,000 combinations of parameters was created about the minimum S^2 found for the new grid was found to provide enhanced resolution for finding the values of b and $\phi_{\max}$ which were best fit to the data.

Events were excluded based on the minimum event fluence characteristics given in Table 3.14 in Section 3.4.6. Note that the minimum peak flux values were not used as it is necessary to perform a regression between the two. Figure 4.38 shows the fits for the 3$^{\text{rd}}$ standard energy channel (as defined in Table 3.13).

All ten channel fits along with the distribution parameters and goodness-of-fit parameters are shown in Appendix Section C.

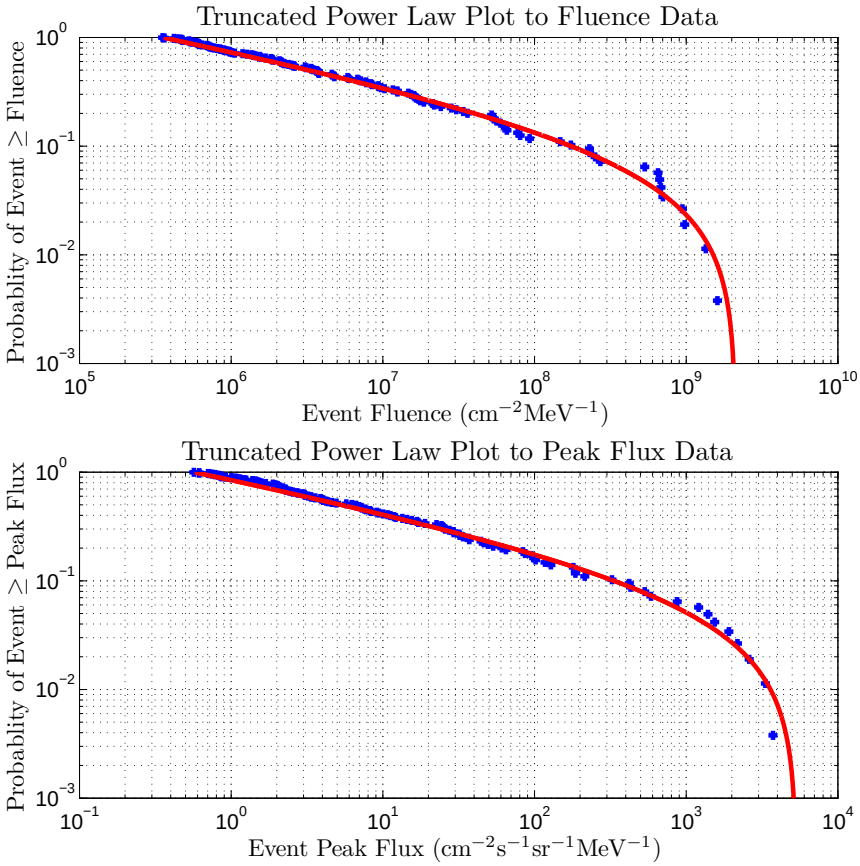

Figure 4.38: Fits of truncated power law to fluence (top) and peak flux (bottom) data in the 10.46 - 15.12 MeV energy channel.

4.5.4 Regression of Peak Flux with Fluence

Using same 3rd standard differential energy channel data from the SARG event list as fitted with the truncated power law in Figure 4.38 a straight line regression is applied to the SEPE peak flux data with the fluence data as was done with the $>$ 10 MeV GOES/SEM integral data in Figure 4.37. This straight line best fit is shown in Figure 4.39 (top) while the plot of the departures from the fit (residuals) are shown below fitted with a normal distribution to quantify the statistical variation from the straight line fit. The departures can be fit by the normal distribution which supports the use of the straight line regression used.

Table 4.31 shows the gradient and intercept parameters of the straight line fit and the standard deviation of the residuals. These three parameters can be used to generate a peak flux for an SEPE for which the fluence has been previously determined using the truncated power law plotted in Figure 4.38 (top).

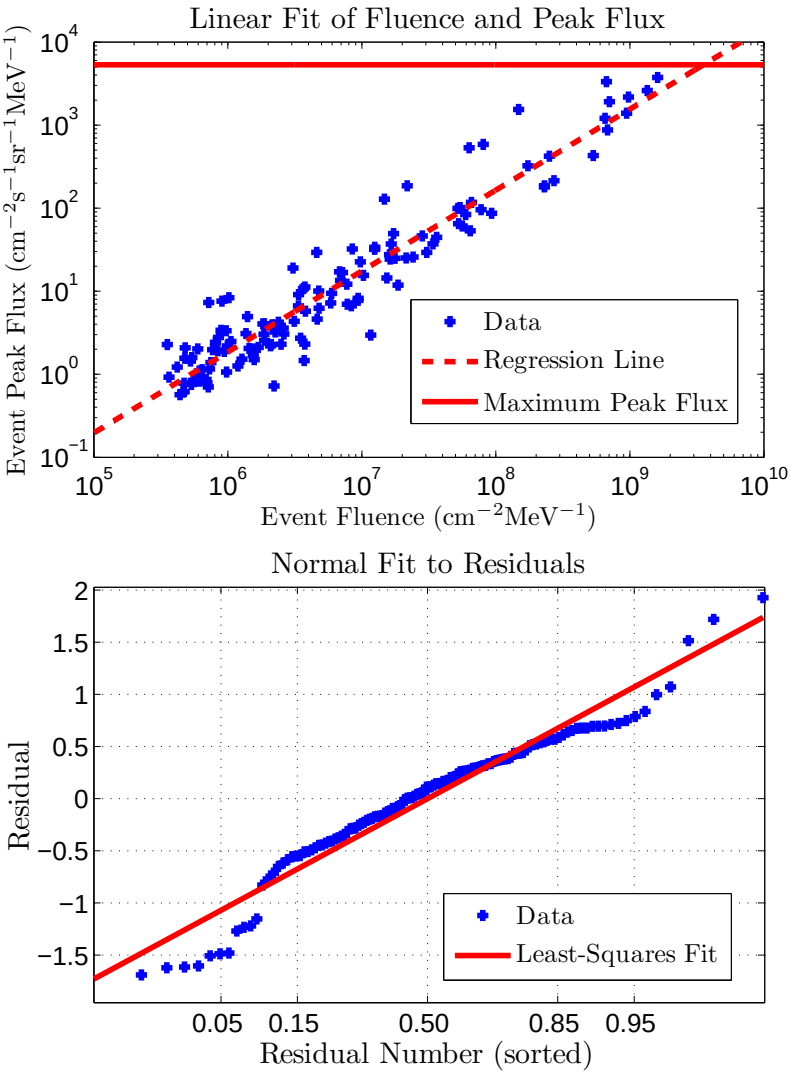

Figure 4.39: Regression of peak flux with fluence (top) and residual plot (bottom) $10.46 - 15.12$ MeV.

Table 4.31: Peak flux regression parameters for Channel 3.

Gradient	Intercept	Residual σ
0.9745	-12.8453	0.6508

One further restriction applied to the peak flux of each SEPE is the maximum value deduced from the truncated power law fit in Figure 4.38 (bottom). This maximum value is shown by the solid red line 4.39. If a peak flux generated using this regression with statistical variation exceeds this maximum value the random variation using σ must be re-calculated until this value is not exceeded.

4.5.5 Regression of Duration with Fluence

The fittings to the SARG event list SEPE durations are shown in Figure 4.19 in Section 4.3.5.2. Performing a regression of the event durations with event fluences was more complex as the functional forms that fit these parameters are not the same and it was not possible to deduce a analytical functional dependence between the two. Therefore a numerical regression method was deduced by first taking each fluence value and finding its fitted cumulative fluence value using Equation 4.21 and then finding the idealised duration using the Lévy cumulative distribution function (Equation 4.15 from Section 4.4.3). The inherent assumption here is that the higher the fluence of an SEPE the longer the SEPE duration is in general (there will always be some scatter reflected in the departures). This assumption holds true from plotting the data.

Again the departures from this fit were fitted with a normal distribution to deduce the standard deviation. Figure 4.40 shows the regression of duration with fluence for the 3^{rd} standard energy channel ($10.46 - 15.12$ MeV).

There is one clear difference in the fit of the departures from that of the peak fluxes which is that the mean value found is not zero. The reason for this is that the fit to event durations was done on all the event durations whereas the durations plotted here are only those from the events with significant fluence in that energy as determined by the threshold values given in Table 3.14. The mean value was therefore always negative and was used to adjust the regression line, the line shown in Figure 4.40 (top) is the adjusted line which now has normal deviation about it with zero mean. The maximum duration shown by the solid red line in Figure 4.40 was taken to be the maximum duration in the event list ($\sim$ 20 days). Table 4.32 shows the adjustment parameter for the SEPE duration natural logarithms and the residual to be applied for random statistical variation.

Table 4.32: Duration regression parameters for Channel 3.

Adjust	Residual σ
-0.1712	0.4935

Using the regression techniques of SEPE peak flux and duration with fluence shown in Figures 4.40 and 4.39 the three parameters can be determined for each SEPE generated in the virtual timeline methodology introduced in Section 4.2.

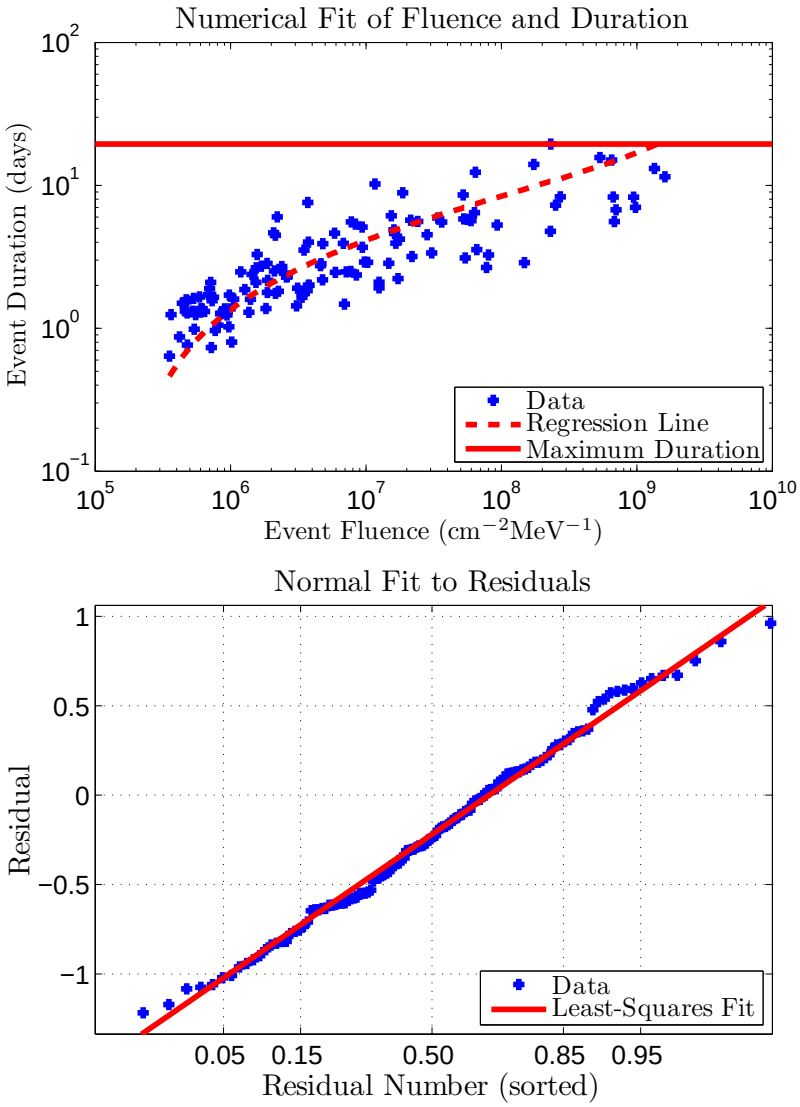

Figure 4.40: Regression of duration with fluence (top) and residual plot (bottom) $10.46 - 15.12$ MeV.

4.5.6 Model Duration Outputs

During the iterations run the code records three primary model outputs: the cumulative mission fluence, the worst-case event fluence and the worst-case peak flux. Additionally the time spent during SEPEs and the worst-case SEPE duration were recorded. These two additional parameters might be of interest to users but in the case of the SARG event list the result will always be the time spent above the threshold value (0.3 cm^{-2}s^{-1}sr^{-1}MeV^{-1}) in the channel used (either $8.7 - 14.5$ MeV or $9 - 15$ MeV). The events were also manually extended (as explained in Section 3.4.3) so the values have little direct meaning.

There are an infinite number of possible combinations of energy ranges and thresh-

old values that a user might be interested in, given one of each it is straight forward to re-run the model using that event definition. The event list would be recreated in using the stipulated energy range and with the stated flux threshold. This is best done by not incorporating the SEPE fluence and peak fluxes into the model. An example of a time spent above a threshold using GOES > 10 MeV data from 1986 to the present day (as stated in the JPL list in Appendix Section A.1) for 5 time periods (1, 2, 3, 5 and 7 years) is shown in Figure 4.41 for the time spent above a threshold of 1 pfu. Table 4.33 gives the values at 5 confidence levels.

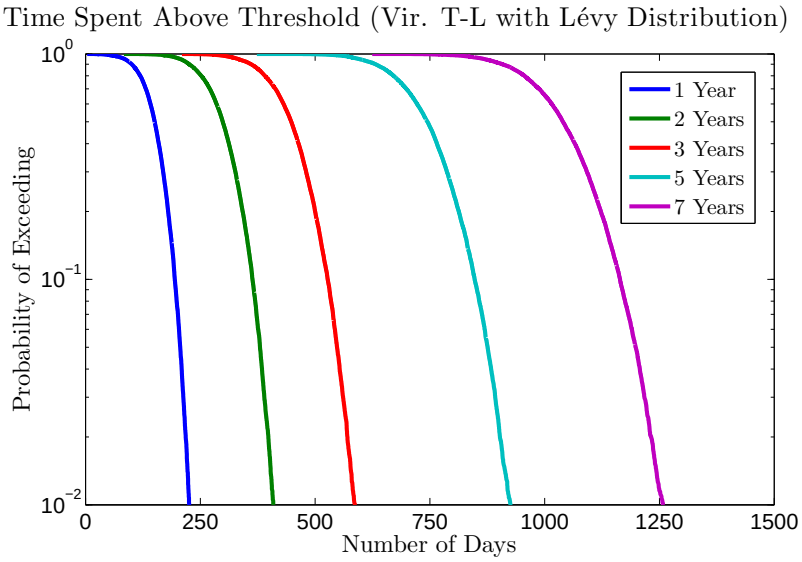

Figure 4.41: Time above stated threshold not to be exceeded for various mission lengths using a Lévy distribution.

Mission	Confidence Level				
Duration	0.7	0.8	0.9	0.95	0.99
1 yr	184.7	196.0	212.2	226.6	260.9
2 yr	343.3	359.1	381.2	399.0	437.9
3 yr	498.2	518.3	544.7	566.9	609.2
5 yr	806.7	832.4	867.1	895.0	951.9
7 yr	1,1117	1,1424	1,1844	1,2177	1,281.1

Table 4.33: Table of predictions for time spent above a threshold (days)

Figure 4.42 gives the worst case event duration using the same event definition parameters while Table 4.34 gives the values at the same 5 confidence level.

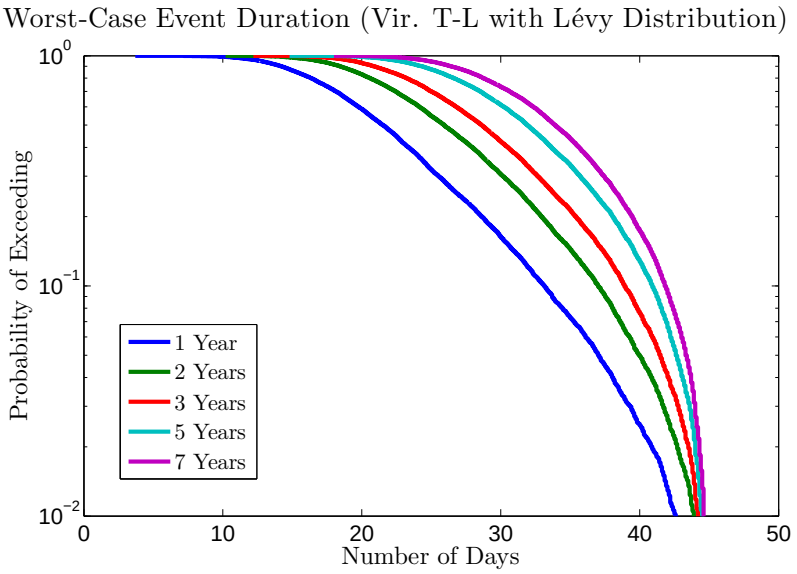

Figure 4.42: Worst-Case event duration for various mission lengths using a Lévy distribution.

Mission	Confidence Level				
Duration	0.7	0.8	0.9	0.95	0.99
1 yr	25.5	28.6	33.1	37.0	42.6
2 yr	30.2	32.9	37.0	40.0	43.9
3 yr	32.7	35.4	38.9	41.5	44.2
5 yr	35.7	38.1	40.9	42.6	44.5
7 yr	37.4	39.5	41.8	43.3	44.6

Table 4.34: Table of predictions for worst-case event duration (days)

It should be noted that as a 1 pfu threshold in the $>$ 10 MeV integral channel is lower relatively than the 0.3 $\mathrm{cm^{-2}s^{-1}sr^{-1}MeV^{-1}}$ threshold in either the $8.7 - 14.5$ MeV or the $9 - 15$ MeV differential channels that the event durations here are longer than those in the SARG event list. This could be due to the extension of events or the joining together of events close in time as discussed in Section 2.2.4.

Chapter 5

Results of The SARG Modelling Methodology

The modelling outputs are first discussed in this section and then spectra are displayed using the results from all of the ten channels. To produce these results 300,000 virtual timelines were created (as described in Section 4.2) for a combination of six mission lengths (0.5, 1, 2, 3, 5 and 7 years) and ten standard energy channels (as described in Section 3.4.5). As well as the three major model outputs of worst-case peak flux, worst-case event fluence and mission cumulative fluence, the frequency of events at the specified energy is given. The frequency was calculated primarily as a check that the algorithm was running correctly.

Xapsos et al. (2004) noted that during solar minimum, the event frequencies are lower, the event magnitudes are smaller, and the energy spectra are softer than during solar active years. As a consequence of this the waiting time, fluence, peak flux and duration distributions will vary from those during solar maximum. To avoid the inherent complications of these variances the methodology is applied to active year periods only. As the well known JPL (Feynman et al., 1990) and ESP (Xapsos et al., 2000) models were also created for active year periods only, results can be easily compared.

In this work a new methodology, 'The SARG Modelling Methodology', has been introduced. The algorithms from Chapter 4 run on an extensive and cleaned data set would constitute a new solar proton model. However, the data used here although cleaned is limited to only solar cycles 22 and 23 (for reasons discussed in Section

3.4) and therefore this is not now officially titled 'The SARG Solar Proton Model'. It is hoped that in the future the data set (and therefore event list) on which the methodology has been tested can be expanded and this will then form a new solar proton model.

5.1 Initial Model Outputs

The model outputs introduced in this section are those which are directly output by the methodology introduced in Chapter 4. These are separate for each of the ten standard energy channels and may then be combined to produce spectra results.

5.1.1 Event Frequency

The plots of event frequency include only those events which were relevant for the specified energy channel. A portion of events in each timeline were classified as 'not significant' using the ratio of significant events in the event list as set-out in Section 4.2.2 (Table 4.1 in that section shows the ratio used for each energy channel). This means that there are fewer events at the higher energies due to there being fewer events with noticeable enhancement above the background level. It is necessary to exclude the smallest events for a good fit of the truncated power law to the peak fluxes and fluences (see Section 4.5). The thresholds for significant events were calculated separately for the different energy channels so the list of remaining events were different for different energies while every event in the final SARG list is significant for at least one energy channel. In each timeline only events starting during the period of interest (stated mission duration) were included so those starting in the start-up year (see Section 4.2.3) but finishing in the period interest were excluded and the flux of those events which continued past the end of the period of interest were included in their entirety.

SEPE frequency is sensitive to the event definition, the inclusion of smaller events may have no effect on the major model outputs despite an increase in the number of events due to a compensating change in the fluence/peak flux distribution. Event definition is covered in Section 2.2.4. The event frequency plot for the 3rd standard differential energy channel is shown in Figure 5.1.

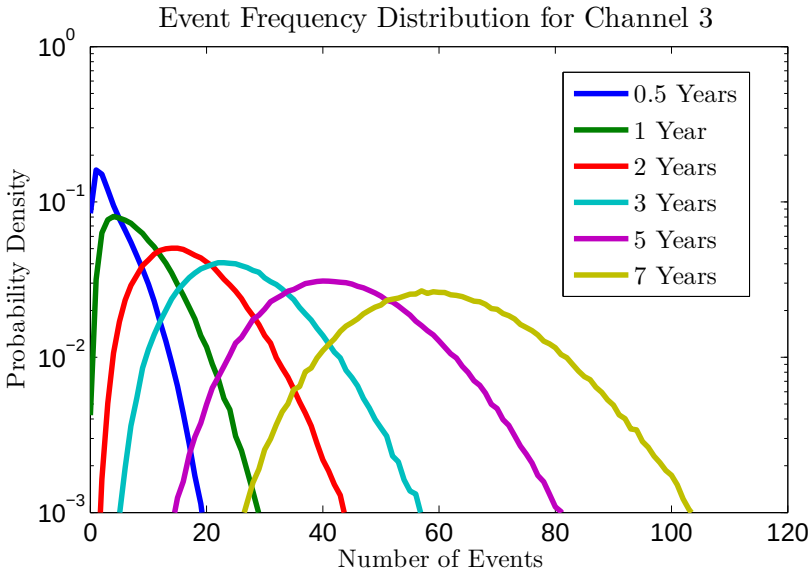

Figure 5.1: Event Frequency Plot for Channel 3: 10.46 - 15.12 MeV (active years only).

It can be seen that there is greater skew in the event frequency distribution for the shorter mission lengths. This skew was expected due to the more pronounced effect of memory over the shorter time periods. Over a longer time period groupings of events and periods without events will average out so that the distribution shows very little skew. This limited skew is seen for the 7-year mission duration in comparison with the other mission lengths. Table 5.1 shows the mean modelled event frequencies for the 3rd standard differential energy channel and the number of significant events in the SARG event list (132) divided by the total number of active years (14) multiplied by the mission length (in years). Each of the modelled frequencies are lower but comparable to the data set values.

Table 5.1: Average event frequency for Channel 3.

	0.5 Years	1 Year	2 Years	3 Years	5 Years	7 Years
Modelled	4.40	8.79	17.6	26.3	43.9	61.5
Measured	4.71	9.43	18.9	28.3	47.1	66.0

5.1.1.1 Event Duration Results

The durations of the events are calculated primarily to create a realistic timeline. As mentioned in Section 4.5.6, if a user were interested in the time spent above a threshold

or the worst-case event duration then the event list should be formed based upon a user-specified energy range and flux threshold. However, the times spent during an event and the worst-case event durations were recorded including both the significant events and 'non-events' in each energy channel. These outputs can be used as a check that the methodology is sound as there should be little difference between the values for the different channels. Table 5.2 shows the yearly time spent during an event for each channel averaged over the 300,000 iterations and the six time periods.

Table 5.2: Average time spent during events in each energy channel per year (days).

Channel 1	Channel 2	Channel 3	Channel 4	Channel 5
40.24	41.99	41.28	42.94	41.30
Channel 6	Channel 7	Channel 8	Channel 9	Channel 10
41.70	42.18	45.38	43.20	38.34

The average year time spent during an event in active years from the SARG event list is 36.27 days. Each of the channels show a slightly higher time spent above the threshold than the sample. There are two possible reasons for this, the first is that there are a greater number of events being generated in each timeline, the second is that each event is, on average, longer than those seen in the sample. A greater number of events would indicate an over-prediction of the fluences and peak fluxes while a longer average event duration would result in an under-prediction of these parameters due to more time being used up which could have allowed for the occurrence of another event. However, the difference is not great ranging from 2.07 days to 9.11 out of the 365 days in a year. Generally, these numbers compare very well to the data set average and can stand as a verification that the methodology is sound and that the model is performing as expected.

Table 5.3 shows the average worst-case event duration for Channels 3 and 9 for each of the six mission lengths. As expected, there is an increase in the worst-case event duration seen with increasing mission duration. The worst-case duration is in each case greater for Channel 9 than for Channel 3. This difference is similar to that seen in Table 5.2 where Channel 3 has the 2nd lowest average time spent during an event while Channel 9 has the 2nd highest.

Comparing these to the worse-case event duration seen in data the set of 19.44

Table 5.3: Average worst-case event durations for Channels 3 and 9 (days).

	0.5 years	1 year	2 years	3 years	5 years	7 years
Channel 3	8.01	11.03	13.79	15.12	16.49	17.19
Channel 9	8.40	11.54	14.35	15.69	17.01	17.65

(which the algorithm specified could not be exceeded) they are all lower but appear to be asymptotically heading towards this value (see Figure 5.2). As the SARG event list includes 14 active years of data these results indicate that, in the worst case, the event duration is not being over-predicted which would result in an under-prediction of the fluence and peak flux.

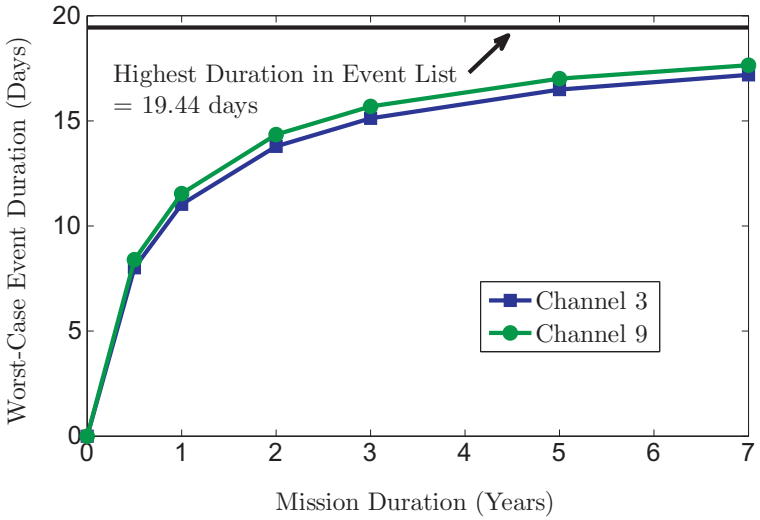

Figure 5.2: Worst-case event durations for Channels 3 and 9.

It should be remembered that these durations are not a SARG final output. However, the good agreement between the different channels and the sample of the data indicates that the method of incorporating event duration to create realistic timelines is operating well.

5.1.2 Worst-Case Peak Flux

The worst-case peak flux is the highest predicted peak flux that will be seen by a spacecraft at 1 AU as a result of SEPs. Figure 5.3 shows the worst-case peak flux outputs for the 3rd standard differential energy channel. The peak flux for each event is based upon a regression of the SEPE peak flux with the SEPE fluence with a check that the maximum peak flux as fit by the distribution is never exceeded (see

Section 4.5.4). The worst-case peak flux is the highest SEPE peak flux seen in each timeline. Worst-case here is defined as the highest flux likely to be seen given a specified confidence level as opposed to the "design limit" which is the worst possible case as defined by the truncated power law. The sorted worst-case peak flux vector (from largest to smallest) is then plotted against a uniform vector between 0 and 1 given by:

$$prop = \frac{[1 : noit] - 0.5}{noit} \tag{5.1}$$

where *noit* is the total number of iterations (or timelines), i.e. 300,000. $[1 : noit]$ is a vector of integers with a step of 1 between them from 1 to 300,000. *prop* is the proportion of instances which exceed the reciprocal peak flux value and $1 - prop$ is the confidence at which a stated value will not be exceeded.

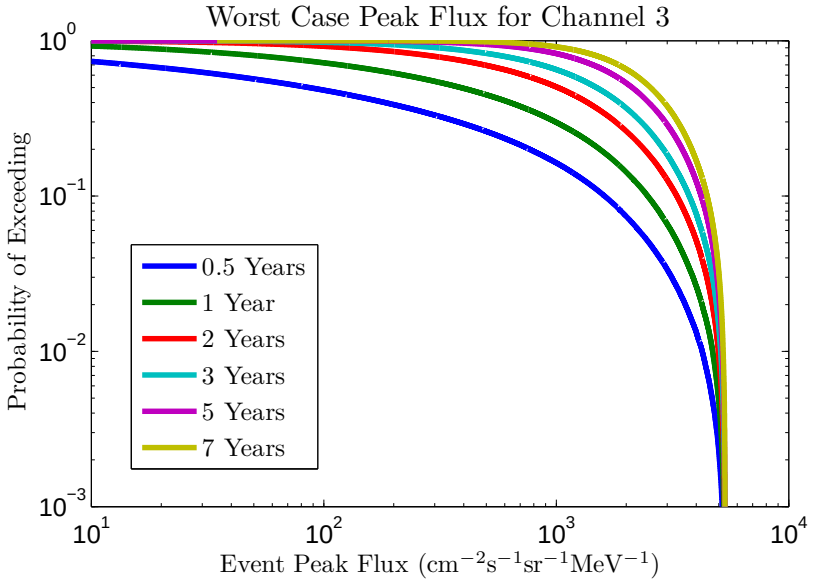

Figure 5.3: Worst-case peak flux plot for Channel 3: 10.46 - 15.12 MeV (active years only).

In the case of the 3rd energy channel the maximum value found was 5.33×10^3 cm^{-2}sr^{-1}s^{-1}MeV^{-1} (see Figure 4.38 (bottom)), it can be seen that this value called the 'design limit' (Xapsos et al., 1998b) is never exceeded. The longer time periods give, as expected, harsher predictions and each of the curves are smooth which is another good indication that the method is operating correctly.

5.1.3 Worst-Case Event Fluence

The worst-case event fluence is the highest fluence produced by any single SEPE over the stated mission length seen by a spacecraft at 1 AU as a result of SEPs. Figure 5.4 shows the worst-case event fluence outputs for the 3rd standard differential energy channel. The fluence parameter for each virtual SEPE is randomly selected from the truncated power law distribution after it has been determined whether the event is significant for the energy channel (if not the fluence and peak flux are zero). The worst-case event fluence is the largest event fluence occurring in each timeline not the "design limit" which is the worst possible case as defined by the truncated power law. The sorted worst-case fluence vector is then plotted against the uniform vector *prop* from Equation 5.1.

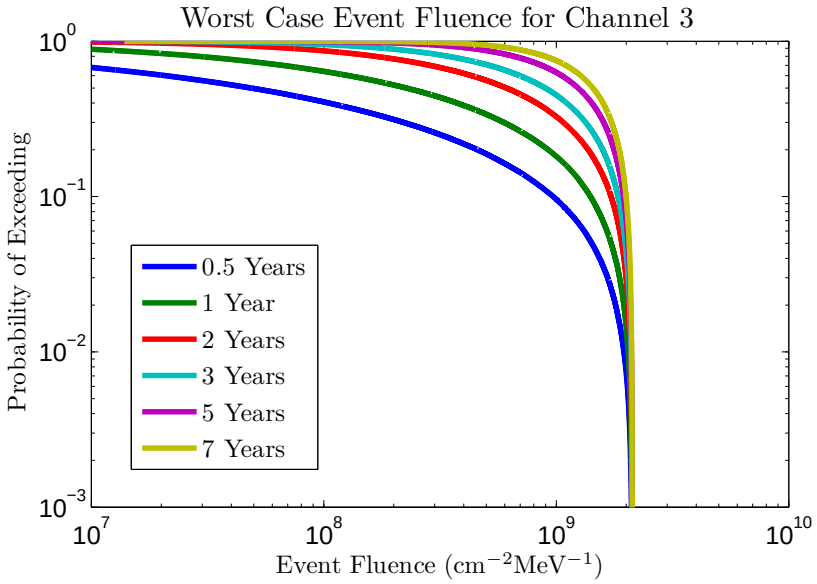

Figure 5.4: Worst-case event fluence plot for Channel 3: 10.46 - 15.12 MeV (active years only).

The maximum value given by the fitting for the truncated power law for the 3rd energy channel was 2.12×10^9 cm^{-2}MeV^{-1} (see Figure 4.38 (top)) and it can be seen from the figure that this 'design limit' is never exceeded.

5.1.4 Cumulative Mission Fluence

The cumulative mission fluence is the fluence summed over all the SEPEs for the complete mission length. Only the fluence from those events which began in the time

period were included (not those beginning in the 1-year start-up period). Clearly it is possible that some fluence from an event beginning before the time period might arrive during the time period of interest. However, it is assumed that this fluence would average out with any fluence included from those events which extended beyond the end of the time period which were included. Additionally, the majority of fluence often arrives during the first part of an SEPE and therefore assuming that the fluence was spread evenly over the event would likely give a less reliable result. Figure 5.5 shows the mission cumulative fluence outputs for the 3rd standard differential energy channel. The sorted cumulative fluence vector is again plotted against the uniform vector *prop* from Equation 5.1.

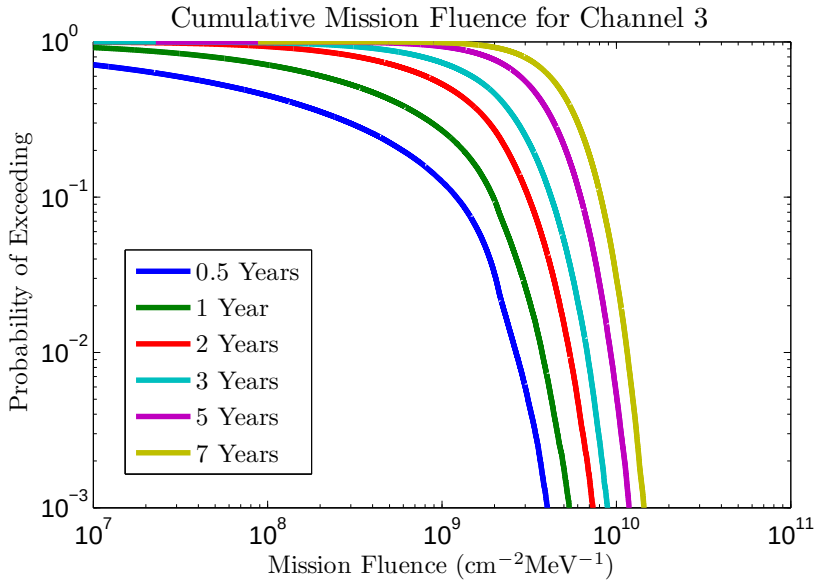

Figure 5.5: Cumulative mission fluence plot for Channel 3: 10.46 - 15.12 MeV (active years only).

In Figure 5.5 there is no asymptotic limit and the values are up to an order of magnitude greater than the outputs for the worst-case event fluence for the 7-year time period. This plot is of the same form as those output from the JPL-91 model (see Figure 2.6 in Section 2.3.2) although the energy range is differential as opposed to integral and therefore the units are also different.

5.1.5 Graphs and Tables of Initial Model Outputs

The graphs for each of the standard differential energy channels and tables showing the 70%, 80%, 90%, 95% and 99% confidence levels for all six mission lengths for the three parameters of worst-case peak flux, worst-case event fluence and mission cumulative fluence are given in Appendix Section C. There are 4 pages for each channel, the first two display the truncated power law distribution fits and parameters and regression fits and parameters while the model outputs are on the 3rd and 4th pages.

5.2 Differential Energy Spectra

For each of the three main model parameters differential spectra across the ten differential energy bins were produced for each of the mission lengths. Including all the energies and six mission lengths in the plots means that it is only possible to include a single confidence level in each plot. In all cases here the 90% confidence level is displayed, however, the spectra for the 70%, 80%, 95% and 99% confidence levels are included in Appendix Section D.1.

5.2.1 Worst-Case Peak Flux

Figure 5.6 shows the worst-case peak flux at the 90% confidence level on double logarithmic axes for all ten standard energy channels and all six mission lengths.

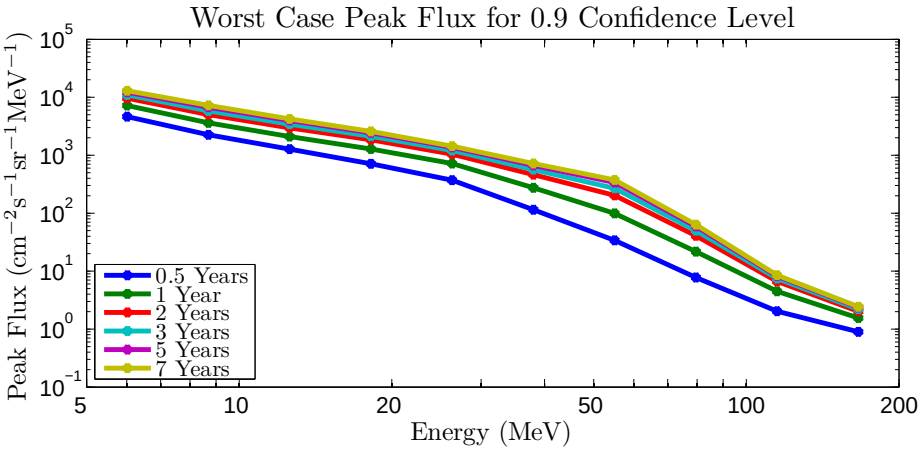

Figure 5.6: Differential energy plots for worst-case peak flux at 90% confidence level.

It can be seen that the spectra in each case at lower energies have a low gradient

approaching straight lines but that they deviate at the higher energies. A straight line on double logarithmic axes indicates a power law in energy. It appears that the longer mission lengths maintain a lower gradient over a greater energy range than the short mission lengths but that the gradient at the highest energies is steeper.

5.2.2 Worst-Case Event Fluence

Figure 5.7 shows the worst-case event fluence at the 90% confidence level on double logarithmic axes for all ten standard energy channels and all six mission lengths.

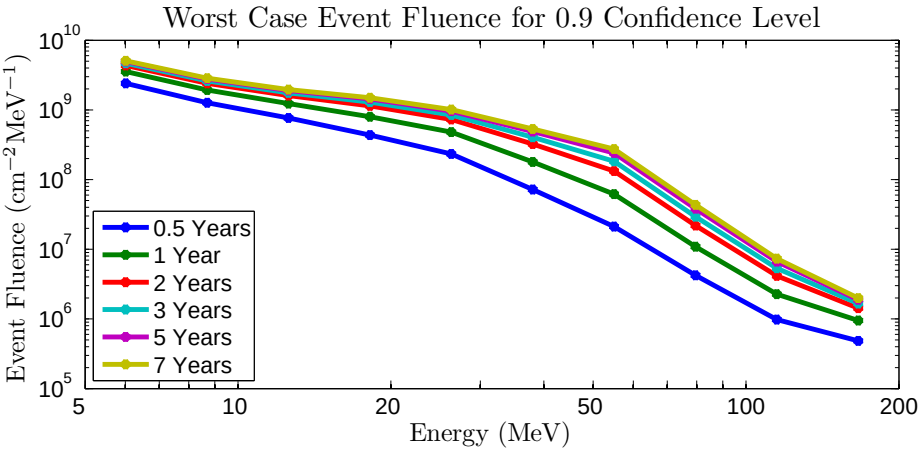

Figure 5.7: Differential energy plots for worst-case event fluence at 90% confidence level.

These results show a similar result to the wort-case peak fluxes with an increasing rate of reduction in worst-case event fluence at the highest energies. Additionally, there appears to be a subtle upturn in the lowest energy bin.

5.2.3 Mission Cumulative Fluence

Figure 5.8 shows the mission cumulative fluence at the 90% confidence level on double logarithmic axes for all ten standard energy channels and all six mission lengths.

Again, similarly to the past two fittings, the lower energies for mission cumulative fluence appear to deviate little from a power law in energy but that there is an increased rate of reduction in fluence predictions at the higher energies. There is greater separation for the different mission lengths as to be expected with no asymptotic limit for cumulative fluence (unlike in the cases of the two worst-case model outputs).

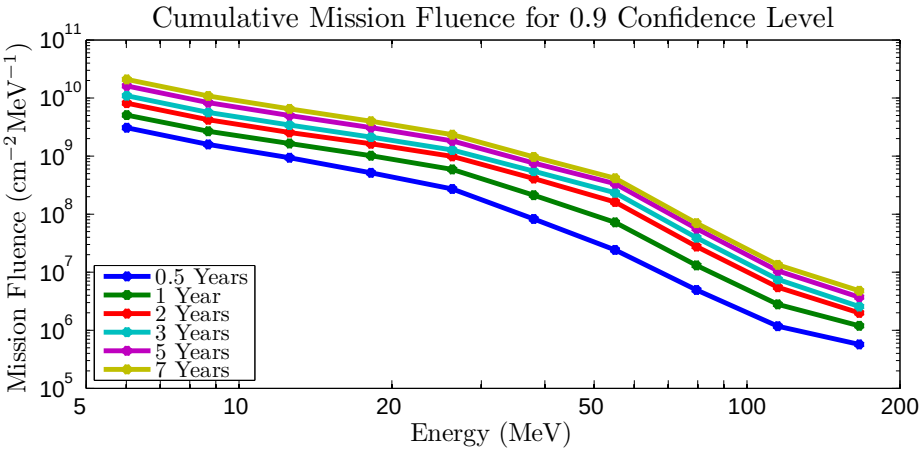

Figure 5.8: Differential energy plots for cumulative mission fluence at 90% confidence level.

5.3 Integral Energy Spectra

For each of the three main model parameters integral spectra across the energy bins were also produced for each of the mission lengths. To do this each value in the differential binnings was multiplied by the bin width and was then summed with each of the values for higher bins. Therefore, the value for protons > 10 MeV can be found by finding where the plot crosses the 10 MeV threshold energy. An assumption here is that the number of particles above 200 MeV are negligible in comparison to those included in the model. In reality the quoted values for > 10 MeV is the total flux of particles in the $10 - 200$ MeV energy range. This assumption is less valid the higher the threshold energy being considered but for most integral energy ranges this will make little difference. In the same way as for the differential energy spectra the 90% confidence level is displayed, however, the spectra for the 70%, 80%, 95% and 99% confidence levels are included in Appendix Section D.2.

5.3.1 Worst-Case Peak Flux

The plots in Figure 5.9 show the integral worst-case peak flux. Here, a slight curvature at the lowest energies can be seen increasing at the higher energies (albeit at different points depending on the mission length). It is possible that the lack of events at the high energies is responsible for the deviation from a smooth curve although more data would be required to confirm this.

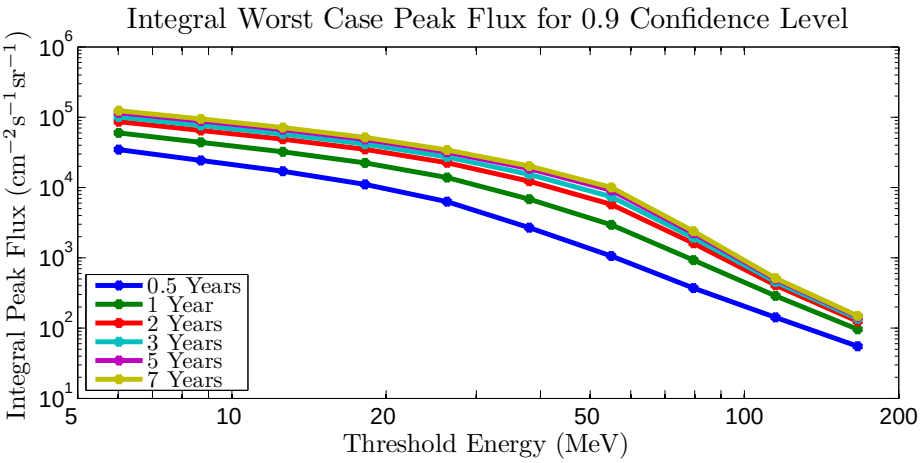

Figure 5.9: Integral energy plots for worst-case peak flux at 90% confidence level.

5.3.2 Worst-Case Event Fluence

Figure 5.10 shows the integral worst-case event fluence for the six mission lengths. The curves here appear to show a similar trend across the threshold energies to the worst-case peak flux integral energy plot from Figure 5.9. Once more there is an indication that with a larger number of events especially in the highest energy channels that these fluence values may produce smoother curves.

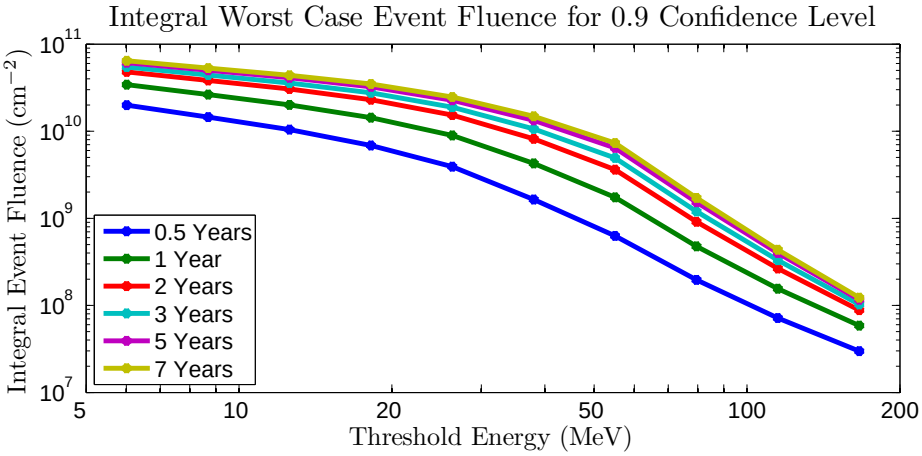

Figure 5.10: Integral energy plots for worst-case event fluence at 90% confidence level.

5.3.3 Mission Cumulative Fluence

Figure 5.11 shows the same plots for the integral cumulative mission fluence. The lines here are smoother than for both the worst-case peak flux and worst-case event fluence integral plots and the differential cumulative fluence plot (Figure 5.5).

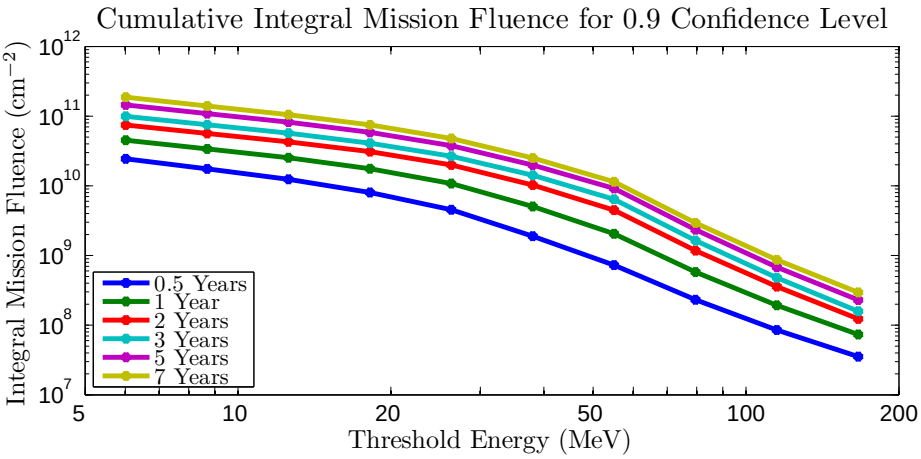

Figure 5.11: Integral energy plots for cumulative mission fluence at 90% confidence level.

As the lines in the differential energy plots appear less smooth than those in the integral plots indicating that if there is a spectral inconsistency in the modelling that it would be easier to spot it there. However, any such problems are likely linked to a lack of SEPEs especially at the highest energies. Deviation from a smooth curve is again seen above the 60 MeV energy threshold.

5.4 Comparison of Cumulative Fluence Models

Figure 5.12 shows the ESP (Xapsos et al., 2000), JPL-91 (Feynman et al., 1990), King (King, 1974) and PSYCHIC (Xapsos et al., 2004) cumulative fluence models along with the output using the new SARG modelling methodology using the SARG event list for a 2-year time period at the 90% confidence level.

The SARG output predicts a harsher environment at the lower and middling energies (with the King model predicting a harsher environment above 60 MeV). There is good agreement with the JPL-91, ESP and PSYCHIC models above 80 MeV. If the SARG spectra was extended to lower energies it appear it would be comparable to these models below 5 MeV. There are a variety of differences between the methods and from this plot it is unclear whether the cause is the data, the statistical distributions of fluence, the waiting time distributions or the incorporation of system memory.

To investigate these differences the JPL, ESP and SARG modelling methodologies were all run on the SARG event list for a 1-year mission length and compared to the

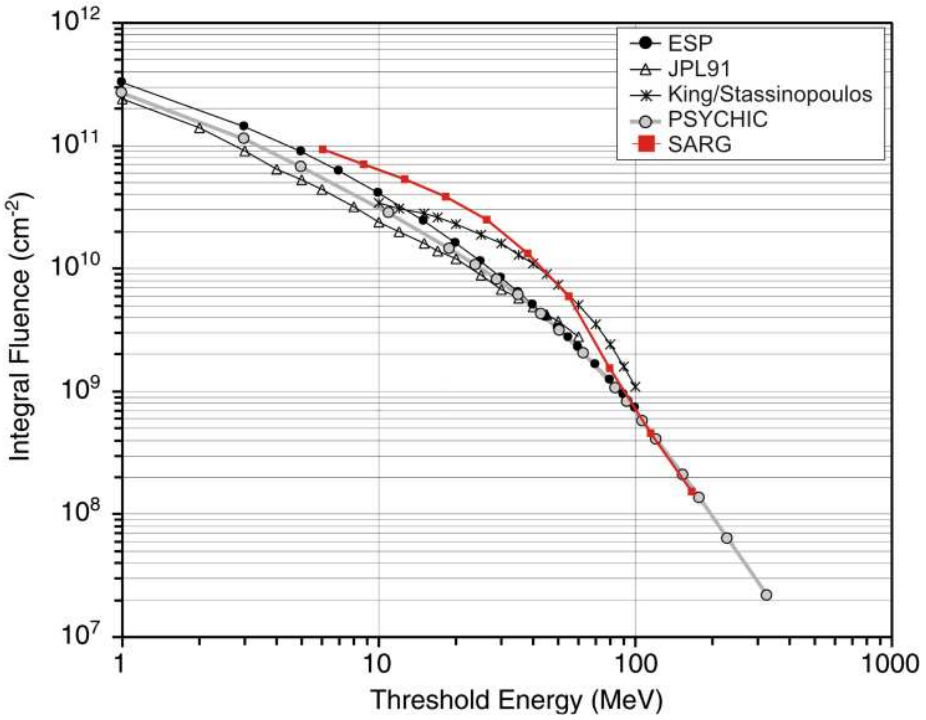

Figure 5.12: Comparison of SARG Solar Proton cumulative fluence model with other well-known models for a 2-year mission during solar maximum at the 90% confidence level (original plot taken from Xapsos et al. (2007)).

raw 1-year fluence data (taken to be the sum of all the fluences of SEPEs starting in each year). The data used was differential.

The JPL method assumes events are Poissonian in nature of with a mean yearly frequency in each energy channel taken from the total number of significant active year events in the channel (using the SARG fluence cut-offs from Table 3.14 in Section 3.4.6) divided by 14 (the number of solar active years of data in the data set). This is combined with a lognormal fit for SEPE fluences using a Monte-Carlo method where the number of iterations with a set number of events is proportional to the value given by the Poisson probability density function. For more details on the JPL method see Section 2.3.2. Figure 5.13 shows the JPL method output plotted against the uniform vector *prop* given in Equation 5.1. The yearly fluences are plotted against a uniform vector but with a value of *noit* of 14 (the number of years of active year data).

The JPL method appears reasonably well fit to the data at low confidence levels (high chance of exceeding) but appears to over-predict the fluences at high confidence levels (low chance of exceeding). As there are only 14 data points it is dangerous

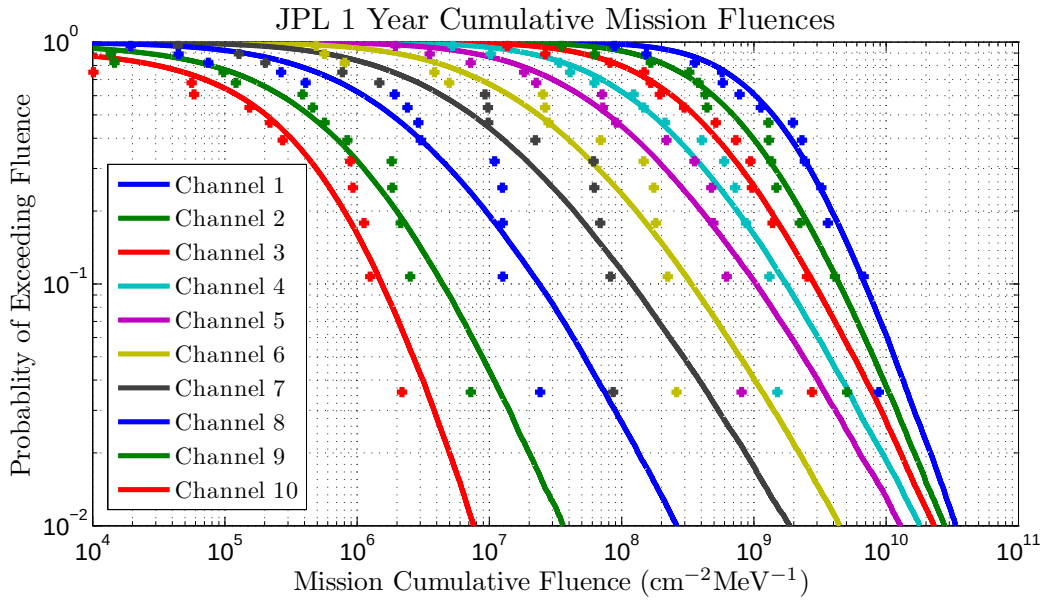

Figure 5.13: JPL Model for 1-year mission using SARG event list and measured fluence data.

to draw concrete conclusions from this plot but the trend does follow through all ten energy channels. A possible reason for this deviation over-predicting fluence at the highest confidences was given in Section 4.5.1 where the lognormal distribution appears to over-predict the likelihood of very large SEPE fluences with no maximum event size. As there are multiple events in a single year this can have an impact at lower confidence levels and this problem would likely be greater for longer time periods where the probability of generating an enormous event using the lognormal distribution is increased. As an example, if there is a 97.5% chance for a single event that a fluence will not be exceeded then in an iteration containing five events there is only an 88.12% chance that no one of the events will exceed that fluence value.

The ESP method for 1-year cumulative mission fluences is to fit of the yearly fluences with a lognormal distribution. Details of this method are included in Section 2.3.4. Using the SARG event list there are only 14 points to perform this fit unlike the ESP model (Xapsos et al., 2000) where there were 21 data points. This lack of data can cause uncertainty in the results. With little data the likely deviation from the true distribution is increased and therefore confidence is reduced. Conversely as it is fit directly to the yearly fluences it would be expected that if the lognormal distribution were a suitable fit that the deviation would be small. It was assumed

that the fluence from the SEPEs is all that is relevant and therefore the contribution from the remainder of the time series can be ignored.

Figure 5.14 shows the ESP method applied to the SARG data along with the measured fluence data. The resulting plots look similar to the JPL plots from Figure 5.13 with a tendency to over-predict the fluence at high confidence level (low chance of exceeding). It is stated by Xapsos et al. (2000) that the lognormal distribution for yearly fluence is consistent with a truncated power law for SEPE fluences used for the worst-case fluence model (Xapsos et al., 1999). However, it is unclear how the lognormal distribution accounts for the truncation of the power law.

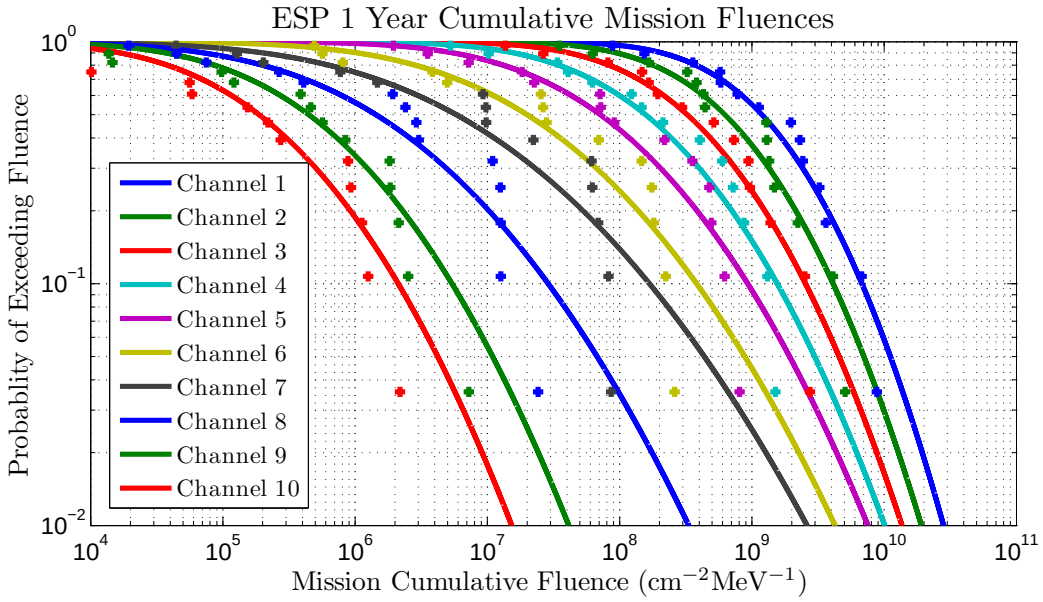

Figure 5.14: ESP Model for 1-year mission using SARG event list and measured fluence data.

Finally the SARG method cumulative proton fluence output for 1 year missions is plotted with the yearly fluence data (see Figure 5.14). It is clear that the fluence values are lower at the highest confidences than for the JPL and ESP methods. On visual inspection the SARG method does not appear to over-predict these fluences unlike the JPL and ESP methods.

To quantitatively compare these results the sum of the squares of the departures of the logarithms of the fluences was measured. The results are shown in Table 5.4. This shows that for the 4 lowest energy channels that the SARG method is inferior to the JPL and ESP methods, that the ESP method is the best fit for the first 5 energy

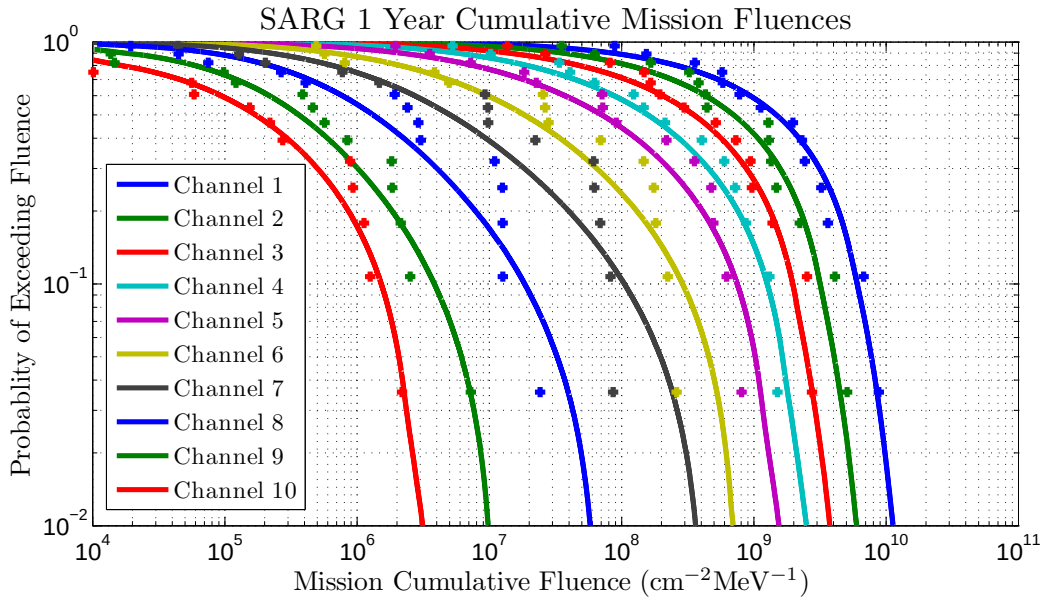

Figure 5.15: SARG Model for 1-year mission and measured fluence data.

channels but that the SARG method is the best fit for the top 5 energy channels.

Table 5.4: Sum of squared residuals of logarithms for model predictions compared with measured yearly fluence.

Channel	JPL	ESP	SARG
1	1.2574	0.6736	2.8955
2	1.6961	1.2784	3.4812
3	2.0138	1.3750	3.7097
4	2.8379	1.9325	3.4235
5	4.7862	3.4449	3.7087
6	9.3556	7.3416	5.5382
7	14.3812	9.9184	8.5569
8	8.0961	6.3696	5.6162
9	4.0534	5.4796	3.0959
10	4.1040	4.9178	1.9621

The results in Table 5.4 seem somewhat surprising upon visual inspection of the plots but it can be shown that it is at the lower confidence levels that the SARG method outputs are in worse agreement with the data due to the use of logarithms of fluence values used to calculate the residuals. These low confidence points will

inevitably be those years with the fewest events and therefore it can be argued that the confidence in these points is lower (as there would be greater variability). Furthermore, users of models are more interested in the higher confidence levels (lower probability of exceeding). Therefore measures of the sum of squared residuals for the 5 highest fluence points were also taken for all of the ten standard energy channels (this is all the points above 65% confidence) and displayed in Table 5.5. This table shows the superiority of the SARG method over the JPL and ESP methods at high confidence levels in every channel when compared to the actual fluence data.

Table 5.5: Table of sum of squared residuals of logarithms for modelling methodologies compared with measured yearly fluence for confidence levels above 65%.

Channel	JPL	ESP	SARG
1	0.2808	0.2372	0.1383
2	0.5795	0.3461	0.1683
3	1.1862	0.6846	0.1181
4	1.8821	1.3073	0.2285
5	2.9260	2.2742	0.6485
6	3.6286	3.9654	1.8951
7	4.6945	6.1854	3.7782
8	2.7848	3.7289	2.3723
9	0.9037	1.3102	0.7279
10	0.8968	1.6765	0.6280

It is perhaps surprising that the SARG method out-performs the ESP method which uses a fit to the yearly fluences directly. It is likely that the ESP method's output has been skewed by scatter from the lower fluence years. However, this highlights a very real drawback of the method: a lack of data points.

Finally, the three methods using the SARG event list were extended to 2-years by the analytical method given by Xapsos et al. (2000) in the case of the ESP method, by doubling of the Poisson mean event frequency in the case of the JPL method and by extending the virtual timeline in the case of the SARG method. The results are displayed in Figure 5.16. This shows that the SARG method gives lower predictions at the 90% confidence level. The over-prediction of fluences by the JPL and ESP models

shown in Figures 5.13 and 5.14 is exaggerated due to the Poissonian assumption of the random occurrence of SEPEs which fails to account for event clustering (memory) which should reduce in impact for longer mission lengths.

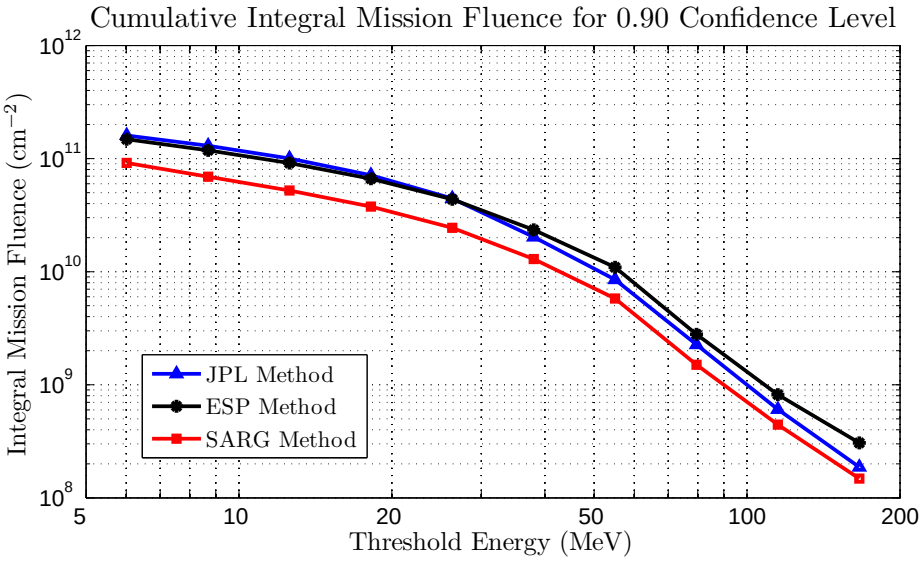

Figure 5.16: Comparison of SARG Solar Proton cumulative fluence model with JPL and ESP Models for a 2-year mission during solar maximum at the 90% confidence level using the SARG event list.

Figure 5.16 shows that the comparison in Figure 5.12 which shows a harsher environment predicted by the SARG method must be largely on account of the data used. This might be due to cycles 22 and 23 being harsher than earlier cycles (data from which was included in the JPL and ESP models) or that the instruments used during those cycles failed to detect the highest fluxes due to saturation effects (see Section 3.4.7). When the same data is used for all the models the SARG method predicts an environment which is less harsh than would be predicted using previous methods.

Chapter 6

Conclusions

This PhD thesis has investigated various facets of the modelling of solar protons arriving at the Earth in bursts known as Solar Energetic Particle Events (SEPEs). The distribution of SEPEs has been found not to be random in time (or Poissonian). A methodology considering the distributions of SEPE fluences, peak fluxes and durations (as they are not a point-like process) combined with a new waiting time distribution and incorporating system memory has been introduced to obtain predictions of the Solar Energetic Particle (SEP) environment at 1 AU. Ultimately a new modelling methodology for solar protons at 1 AU has been created: The SARG (Southampton Astronautic Research Group) Modelling Methodology.

The proton fluxes measured by instruments can be erroneous in some cases with the occurrence of spikes, data gaps or gain errors. To correct the first two of these problems two data processing algorithms were introduced in Sections 3.2 and 3.3; these were tested showing good results when compared with raw data. In the creation of the SARG event list covered in Section 3.4 these algorithms were applied as well as a cross-calibration of data sets where they overlapped (similar to that done by Rosenqvist et al. (2005)). Manual inspection of all the event fluxes was carried out after processing but only 2 spikes in 201 initial events needed to be removed manually. The new list comprises accurately calculated start and end times of the SEPEs, the SEPE fluences and peak fluxes re-binned into ten standard standard energy bins including events that are relevant in any of the channels. This new list shows very good fits for SEPE waiting times (from the end of one event to the start of the next) and durations using a Lévy distribution, showing that the precautions taken creating

the list were successful and the conclusions of earlier chapters correct.

By including event durations in the modelling for the first time the failure of waiting time distributions or event frequency distributions to account for the durations of SEPEs was overcome making the method more realistic than those used in previous models. The method was applied separately for the different energy channels using the same time distributions (for waiting times and SEPE durations) by excluding those events which did not have flux sufficiently higher than the background level for the specified energy.

The assumption that SEPEs follow a Poisson distribution in time, which is used in some way for all existing statistical models, was tested. This assumption requires a random occurrence of SEPEs which means the process must be stationary (with a lack of long-term memory). It is also necessary that events are unaffected by recent activity (or that there is no short-term memory). It was found in that even when considering only the solar active years that the process was not stationary as the occurrence of SEPEs is bursty in nature (with more clusters of events than would be found in a random distribution) and that for the most part there was also short-term system memory present (based on consecutive event waiting times). It was found that a Lévy distribution was a better fit to the SEPE waiting times than the Poisson distribution or the time-dependent Poisson distribution which allowed for a lack of stationarity but not a presence of short-term memory. This work on the time distributions of SEPEs and event inter-dependence is currently in print (Jiggens and Gabriel, 2009). One issue which became apparent at this juncture was the possible impact of the SEPE durations which had not previously been accounted for in the fits for SEPE waiting times or in the probability density functions of event frequency used for solar proton models. The non-point-like nature of these events could skew the waiting time distributions and failure to account for these durations (which can vary from days to weeks) could result in unrealistic scenarios for model iterations. The distribution fits for SEPE durations in two established event lists (JPL and PSYCHIC) showed that there was a reduced number of short duration events (something not predicted by any of the distributions), this lack of short duration events was most likely due to the exclusion of the smallest SEPEs. This problem was mitigated for the SARG Event List through accurate measurement of the event start and end times and careful choice

of flux thresholds such that low duration events were detected and the distributions were well fit.

A piecewise method to account for the short-term memory present in the system of SEPEs has been introduced. Tests of this method of adjusting one waiting time distribution based upon the previous waiting time showed that the system memory could be incorporated without affecting the burstiness (or overall waiting time distribution).

The fluences and peak flux values for the SEPEs in each of the ten energy channels were fitted with a truncated power law as done by Xapsos et al. (1998b, 1999). Although this distribution has been used for models of worst-case event fluence and peak flux by those authors, it has never been used in the creation of a cumulative fluence model. Minimum fluence values were introduced for each of the ten energy channels below which events were certainly insignificant, hard to detect and adversely affected the fitting of the distribution. The use of a truncated power law as opposed to a lognormal distribution prevents over-predicting the likelihood of very large events which can dominate SEPE models.

The event frequencies plus the three main SARG modelling outputs; worst-case peak flux, worst-case event fluence and cumulative mission fluence were found and expressed in individual channels, differential energy spectra and integral energy spectra. A comparison of the new SARG method with the previous JPL (Feynman et al., 1993) and ESP (Xapsos et al., 2000) models indicates that it predicts a harsher environment for the most part than the previous models. However, it was found that this result was primarily due to the data and the processing. Comparison of the 3 methods applied to the measured 1-year fluences from the SARG event list shows a significant improvement with the SARG method at high confidences ($> 65\%$) which are widely used. Comparison of the 2-year JPL, ESP and SARG methodologies using the same data showed a less harsh environment predicted using the SARG method.

Accounting for burstiness and memory in the system using the SARG method results in the prediction of a harsher environment at higher confidence levels due to greater variability than previously thought. The inclusion in the SARG method of event durations based on the fluence of events results in reduced mission cumulative fluences at the highest confidence levels as the fact that large fluence events cover larger portions of the available time is accounted for. The distribution used by the

JPL model fails to properly account for reduced probability of SEPEs with very high fluences which also results in higher mission cumulative fluences. As the SARG method predictions are lower than previous models it must be concluded that the inclusion of event durations and the truncation of the power law distribution fit to the event fluences are the differences in modelling methodologies which have the greater impact resulting in lower fluence predictions overall than previous models.

Uncertainty on measured waiting times and durations are small due to the nature of SEPEs and their shape on the flux profile making them very distinct. The departures from the fitting distributions can be considered as normal statistical variation and the effect of this has been accounted for by varying the bins used for the analysis to confirm to results. However, it is possible that with the inclusion of more data that the best fitting distribution might change from Lévy to another distribution. A more probable outcome are changes to the distribution parameters especially if data was included from solar cycles which were less (or more) active than 22 and 23. It would be expected that the biggest changes could be to the bins with the fewest events (which are the higher waiting times) although the combined goodness-of-fit parameter used to find the fitting parameters gives reduced weighting to these bins for precisely this reason therefore minimising this effect.

The measurements of flux and fluence may include instrument errors but it is difficult to quantify these errors. It is often unclear which instruments are the most reliable, any degradation of the instruments with time and how great any errors might be. To minimise the possible effects of such errors the GOES/SEM data was used as it is possible to compare data from multiple GOES satellites, there is a long heritage of particle detectors and these instruments do no saturate unlike others. This leaves the problem of data set size, the effect of which was investigated for the JPL method by Rosenqvist and Hilgers (2003). The validation of earlier data and subsequent inclusion in the model is the only feasible way to mitigate against the problems of data set size.

This work has shown that SEPEs are not random time (i.e. not independent of one another) and there is an element of memory in their occurrence. Both the non-Poissonian nature of SEPEs and system memory have been incorporated into a new statistical modelling methodology. These scientific findings and method used for modelling the SEPE environment are new to this work.

6.1 Further Work

There are a few areas of SEPE environment modelling which might be further improved upon.

The SARG modelling methodology of virtual timelines is powerful and could be adapted to allow for a change in the nature of the environment being modelled. The work here could be extended to include some solar minimum modelling. It was shown that the Lévy distribution could be applied to the complete time period and could most likely be applied to solar quiet times as long as there were sufficient events to perform the analysis. It would also be necessary to quantify any differences over the solar cycle in SEPE spectra of the fluence and peak flux distributions which have been reported by Xapsos et al. (2004). With a method of estimating the characteristics of an SEPE at different helioradial distances the SARG methodology could be adapted to account for change to the orbit of the spacecraft (such as seen by interplanetary missions).

The SARG timeline model produced could be run over a short time period using real data rather than the start-up period to see if this improves the accuracy of predictions. This might give a way of improving predictions of the SEPE environment by using the system memory reported here. Another improvement could be the extension of the memory to include more than one previous waiting time. With an extension of the findings on event waiting times, inter-dependence of events and system memory and using the virtual timeline method it may be possible to create an engineering tool which could help predict when a big event is going to occur based on what happened previously.

Further work could also be done on the regression methods of SEPE fluence, peak flux and duration so that the timelines created are more realistic. At present regression is done for SEPE peak fluxes and durations based on fluences individually. A multiple regression to find event durations based on fluences and peak fluxes could provide an improvement to the method.

The SARG data set has been thoroughly processed but an extension of this data set further backwards in time to include cycles 20 and 21 would improve the reliability of a model based upon it. The quality of available IMP-8 data has been questioned but an ability to correct for any data errors (especially saturation) would allow an

easy extension of the data set. Shea et al. (2006) provided a list of 19 SEPEs from between 1570 and 1950 along with fluences in the > 30 MeV energy range derived from the nitrate levels in the Greenland ice sheet in all but one case (where the ice was taken from the Antarctic). This data could be used to give increased resolution for the distribution of large SEPEs for so long as it was certain that all events above a specified fluence were detected and that the fluences were accurate. There is also the possibility of using radionuclides in rocks returned from the Moon by Apollo astronauts as reported by Reedy (1996). Finally, to deduce SEP fluxes authors including Belov et al. (2005) have used data from neutron monitors which is results could be verified would provide a significant extension in time to the available data set.

Appendix A

Data Processing and Event Lists

A.1 JPL Event List

The following five pages display the JPL event list introduced in Section 3.1 and used for analysis in Chapter 4. This list comprises of the list published by Feynman (1989) which used IMP-8/CPME data and the extension to the list using the same event definition using GOES/SEM data.

Event	Start Date		Duration	Fluence	Event	Start Date		Duration	Fluence
No.	Year	DoY	(days)	> 10 MeV	No.	Year	DoY	(days)	> 10 MeV
1	1965	37	3	1.60E+07	19	1968	304	10	2.10E+08
2	1965	277	4	2.60E+06	20	1968	324	8	1.00E+09
3	1966	83	4	1.10E+07	21	1968	338	11	2.30E+08
4	1966	124	6	1.50E+06	22	1969	57	6	7.60E+07
5	1966	189	5	6.40E+07	23	1969	81	3	7.10E+06
6	1966	241	27	1.00E+09	24	1969	90	13	7.80E+07
7	1967	12	2	3.60E+06	25	1969	103	16	2.20E+09
8	1967	29	20	1.10E+09	26	1969	269	6	1.80E+07
9	1967	59	9	7.10E+06	27	1969	307	9	6.40E+08
10	1967	71	4	1.60E+07	28	1969	329	10	7.10E+06
11	1967	145	11	7.80E+08	29	1969	353	5	5.20E+06
12	1967	158	13	2.40E+07	30	1970	29	7	2.80E+07
13	1967	304	22	3.00E+07	31	1970	66	6	6.80E+07
14	1967	338	5	2.50E+07	32	1970	83	18	9.40E+07
15	1967	351	7	1.50E+07	33	1970	151	5	1.40E+07
16	1968	162	5	1.90E+08	34	1970	167	5	2.80E+06
17	1968	190	10	4.70E+07	35	1970	189	3	4.10E+06
18	1968	271	12	7.40E+07	36	1970	203	6	3.60E+07

Event No.	Start Date Year	DoY	Duration (days)	Fluence > 10 MeV	Event No.	Start Date Year	DoY	Duration (days)	Fluence > 10 MeV
37	1970	224	15	9.10E+08	67	1977	204	9	6.10E+06
38	1970	310	9	6.60E+07	68	1977	252	24	4.30E+08
39	1970	347	4	4.20E+06	69	1977	286	3	3.90E+06
40	1970	359	8	1.60E+07	70	1977	326	7	2.80E+08
41	1971	25	16	1.50E+09	71	1978	3	11	1.20E+07
42	1971	92	4	3.00E+06	72	1978	45	10	1.50E+09
43	1971	97	5	3.20E+07	73	1978	99	8	7.00E+07
44	1971	111	5	4.30E+06	74	1978	108	28	2.40E+09
45	1971	133	11	1.40E+07	75	1978	152	5	1.80E+07
46	1971	245	17	3.90E+08	76	1978	175	7	5.30E+07
47	1971	278	5	7.00E+06	77	1978	194	7	3.20E+07
48	1972	109	6	3.00E+07	78	1978	206	5	2.70E+06
49	1972	150	9	7.60E+07	79	1978	251	3	2.80E+06
50	1972	161	15	4.00E+07	80	1978	267	15	2.90E+09
51	1972	202	15	5.40E+07	81	1978	283	7	8.60E+06
52	1972	217	23	1.10E+10	82	1978	315	5	1.80E+07
53	1972	304	5	6.00E+07	83	1978	347	5	6.20E+06
54	1973	103	7	8.20E+06	84	1979	49	6	1.60E+07
55	1973	120	11	1.60E+07	85	1979	62	16	2.10E+07
56	1973	211	6	7.20E+06	86	1979	94	4	2.10E+07
57	1973	251	5	1.90E+07	87	1979	158	9	2.10E+08
58	1973	308	3	4.70E+06	88	1979	188	6	2.10E+07
59	1974	160	4	4.40E+06	89	1979	214	15	1.20E+07
60	1974	185	8	2.40E+08	90	1979	232	12	6.00E+08
61	1974	255	25	3.30E+08	91	1979	252	25	3.60E+08
62	1974	310	4	1.30E+07	92	1979	321	3	3.20E+07
63	1975	233	4	6.60E+06	93	1980	12	3	2.80E+06
64	1976	84	9	5.40E+06	94	1980	38	4	3.00E+06
65	1976	122	5	1.00E+08	95	1980	92	8	8.70E+06
66	1976	236	3	1.00E+07	96	1980	199	12	1.20E+08

Event	Start Date		Duration	Fluence	Event	Start Date		Duration	Fluence
No.	Year	DoY	(days)	> 10 MeV	No.	Year	DoY	(days)	> 10 MeV
97	1980	246	6	3.70E+06	127	1984	32	2	2.40E+06
98	1980	290	9	3.00E+07	128	1984	47	13	1.60E+08
99	1980	321	6	6.30E+06	129	1984	72	9	2.90E+07
100	1980	329	11	1.40E+07	130	1984	116	13	1.30E+09
101	1981	63	6	3.40E+06	131	1985	22	4	8.70E+06
102	1981	90	8	2.80E+07	132	1985	115	7	2.80E+08
103	1981	101	12	8.50E+07	133	1985	193	8	2.30E+07
104	1981	115	30	1.00E+09	134	1986	37	3	7.80E+07
105	1981	202	7	8.10E+07	135	1986	45	4	9.60E+07
106	1981	221	5	1.40E+07	136	1986	65	1	2.00E+06
107	1981	251	4	7.30E+06	137	1986	124	1	3.00E+06
108	1981	263	9	1.50E+07	138	1987	312	2	3.00E+07
109	1981	282	18	2.10E+09	139	1987	364	8	9.50E+07
110	1981	315	6	5.60E+06	140	1988	85	2	5.00E+06
111	1981	327	4	3.80E+06	141	1988	182	1	3.00E+06
112	1981	340	9	7.70E+07	142	1988	238	6	1.40E+07
113	1981	362	4	7.50E+06	143	1988	279	1	1.00E+06
114	1982	31	13	1.10E+09	144	1988	286	1	2.00E+06
115	1982	66	4	1.10E+07	145	1988	313	3	7.00E+06
116	1982	156	17	7.00E+07	146	1988	319	1	2.00E+06
117	1982	191	12	8.40E+08	147	1988	350	5	1.90E+07
118	1982	204	5	1.20E+08	148	1989	5	1	3.00E+06
119	1982	248	5	1.40E+07	149	1989	67	17	1.13E+09
120	1982	298	3	3.30E+07	150	1989	101	6	2.02E+08
121	1982	326	13	2.50E+08	151	1989	113	1	3.00E+06
122	1982	339	10	5.70E+08	152	1989	121	8	4.10E+07
123	1982	349	9	1.30E+08	153	1989	142	7	2.20E+07
124	1982	360	7	2.10E+08	154	1989	169	2	4.00E+06
125	1983	35	5	1.00E+08	155	1989	181	2	4.00E+06
126	1983	167	13	2.10E+07	156	1989	206	2	1.60E+07

Event No.	Start Date Year	DoY	Duration (days)	Fluence > 10 MeV	Event No.	Start Date Year	DoY	Duration (days)	Fluence > 10 MeV
157	1989	224	25	7.92E+09	187	1991	363	1	1.00E+06
158	1989	255	5	2.90E+07	188	1992	38	2	4.80E+07
159	1989	272	14	3.86E+09	189	1992	58	1	2.00E+06
160	1989	292	22	1.93E+10	190	1992	68	1	3.00E+06
161	1989	319	2	1.30E+07	191	1992	75	3	9.00E+06
162	1989	331	8	2.21E+09	192	1992	130	5	6.61E+08
163	1990	78	3	7.39E+08	193	1992	145	1	1.00E+06
164	1990	88	1	3.00E+06	194	1992	177	7	2.88E+08
165	1990	97	6	2.30E+07	195	1992	219	2	7.00E+06
166	1990	106	7	3.30E+07	196	1992	304	9	3.49E+09
167	1990	118	2	7.30E+07	197	1992	334	1	2.00E+06
168	1990	128	2	3.00E+06	198	1993	63	5	1.50E+07
169	1990	136	16	3.69E+08	199	1993	71	3	2.20E+07
170	1990	163	2	3.60E+07	200	1993	158	1	2.00E+06
171	1990	207	11	1.99E+08	201	1994	51	3	9.95E+08
172	1990	225	2	4.00E+06	202	1994	293	1	1.40E+07
173	1991	28	5	9.00E+07	203	1995	293	2	1.80E+07
174	1991	39	2	5.00E+06	204	1997	308	7	4.93E+08
175	1991	56	2	5.00E+06	205	1998	110	6	1.62E+09
176	1991	72	3	1.20E+07	206	1998	120	11	1.08E+08
177	1991	82	17	9.75E+09	207	1998	168	2	3.00E+06
178	1991	113	1	3.00E+06	208	1998	235	9	5.69E+08
179	1991	130	5	1.41E+08	209	1998	267	2	6.00E+06
180	1991	139	9	2.50E+07	210	1998	273	4	5.63E+08
181	1991	151	21	3.25E+09	211	1998	292	1	2.00E+06
182	1991	181	13	1.22E+09	212	1998	310	3	9.00E+06
183	1991	238	5	1.25E+08	213	1998	318	4	1.38E+08
184	1991	250	1	1.00E+06	214	1999	21	4	1.70E+07
185	1991	273	3	1.40E+07	215	1999	114	3	1.90E+07
186	1991	301	4	3.20E+07	216	1999	125	3	1.20E+07

Event No.	Start Date Year	DoY	Duration (days)	Fluence > 10 MeV	Event No.	Start Date Year	DoY	Duration (days)	Fluence > 10 MeV
217	1999	147	1	2.00E+06	247	2002	27	1	2.00E+06
218	1999	153	6	9.10E+07	248	2002	51	1	2.00E+06
219	2000	49	2	5.00E+06	249	2002	75	8	6.30E+07
220	2000	95	3	3.60E+07	250	2002	107	15	2.88E+09
221	2000	159	6	8.40E+07	251	2002	142	3	1.10E+08
222	2000	178	1	1.00E+06	252	2002	188	4	1.50E+07
223	2000	195	11	1.65E+10	253	2002	197	14	2.21E+08
224	2000	210	2	7.00E+06	254	2002	226	14	3.54E+08
225	2000	226	1	1.00E+06	255	2002	249	3	3.50E+07
226	2000	256	6	2.69E+08	256	2002	306	1	1.00E+06
227	2000	290	3	1.60E+07	257	2002	313	3	1.45E+08
228	2000	299	3	1.20E+07	258	2002	354	1	1.00E+06
229	2000	305	2	4.00E+06	259	2003	148	4	3.50E+07
230	2000	314	11	1.08E+10	260	2003	169	3	1.60E+07
231	2000	329	10	4.98E+08	261	2003	299	17	1.58E+10
232	2001	22	2	3.00E+06	262	2003	324	5	2.50E+07
233	2001	28	3	3.40E+07	263	2003	336	4	3.00E+07
234	2001	86	26	1.68E+09	264	2004	102	2	1.80E+07
235	2001	117	2	5.00E+06	265	2004	205	6	1.61E+08
236	2001	127	3	2.40E+07	266	2004	214	2	3.00E+06
237	2001	140	2	5.00E+06	267	2004	257	9	1.65E+08
238	2001	166	3	2.20E+07	268	2004	306	2	1.90E+07
239	2001	222	1	6.00E+06	269	2004	312	10	5.16E+08
240	2001	228	10	2.86E+08	270	2005	15	9	3.67E+09
241	2001	258	1	3.00E+06	271	2005	127	1	2.00E+06
242	2001	267	18	8.41E+09	272	2005	134	3	3.81E+08
243	2001	292	7	2.80E+07	273	2005	167	3	2.70E+07
244	2001	308	9	1.52E+10	274	2005	195	6	1.61E+08
245	2001	322	13	8.17E+09	275	2005	208	7	1.29E+08
246	2001	360	24	7.75E+08	276	2005	234	2	2.27E+08

A.2 De-Spiking Algorithm

Each point in the flux time series is compared to the mean of a vector made up of 6 out of the 10 surrounding points (5 either side of the point being assessed). Firstly a vector of the 10 nearest points is taken:

$$surpts = sort(Flux([i-5:i-1, i+1:i+5])) \tag{A.1}$$

where i is the position of the point being assessed in the flux time series $Flux$ and $[a:b]$ is a uniform integer vector from a to b of step 1 used here to establish the position of the points to form the comparison vector $surpts$. $sort$ is a function to arrange the vector in ascending order, using MATLAB the null or drop-out values labelled NaN (Not a Number) are positioned at the top end of the vector. As a result a $shift$ parameter needs to be calculated to account for these NaN values:

$$shift = ceil\left(\frac{\sum surpts == NaN}{2}\right) \tag{A.2}$$

where $ceil$ is a function which rounds any value up in cases where the sum of NaN points is an odd number. Recalling that the NaN values have been positioned at the top end of the sorted $surpts$ vector, now, the middle 6 values not including the NaN values are extracted:

$$cvect(i) = surpts([3-shift:8-shift]) \tag{A.3}$$

applied at each position on the $Flux$ vector, this gives the comparison vector $cvect$. Next the ratio between each flux value and the associated comparison vector point is found:

$$ratiovect = \frac{Flux}{cvect} \tag{A.4}$$

As there is proportionally more noise at the lower fluxes, a logical vector, $lowpts$, is introduced:

$$lowpts = Flux < background \tag{A.5}$$

which is 1 where the flux is less than (and 0 where the flux is greater than) a value $background$ which is defined as anything below the 10^{th} percentile of the sorted flux vector for each SEPE. Applied to the complete data set, given the relative sparsity of enhancements, it might be more appropriate to use the 90^{th} or even 95^{th} percentile

instead. Now a logical *spikes* vector can be deduced:

$$spikes = ratiovect > spikeratio \text{ AND NOT } (lowpts) \tag{A.6}$$

which is 1 only if the $Flux$ value at a specific point in time is above the stated parameter *background* and the *spikeratio* which is a limit of how much higher than the surrounding points the value can be before it is considered a spike. Finally the spikes are removed from the $Flux$ vector and replaced with NaN values:

$$Flux(spikes) = NaN \tag{A.7}$$

The *spikeratio* value must be chosen carefully as if it is too low it will eliminate non-spikes and, importantly, event peaks while if it is too high it will fail to eliminate all the spikes in the time series. Values for *spikeratio* of 1.5 and 3 have been used in this analysis to show the effect of altering this value.

A.3 SARG Model Event List

The following 32 pages show the complete event list produced for the creation of the SARG (Southampton Astronautic Research Group) Solar Proton Model. This includes the start and end times of the events, the fluences and peak fluxes across the ten standard energy bins shown in Section 3.4, Table 3.13 and the primary spacecraft from which the data was taken and the secondary spacecraft which was used to fill data gaps (where applicable). There are 22 events per page with 4 page listings for each block of 22 events:

- Event fluences for channels 1-5 (1^{st} page)
- Event fluences for channels 6-10 (2^{nd} page)
- Event peak fluxes for channels 1-5 (3^{rd} page)
- Event peak fluxes for channels 6-10 (4^{th} page)

There are a total of 176 events in this event list.

Table A.1: SARG Event List - Fluences ($cm^{-2}MeV^{-1}$) Channels 1-5 [1].

Start Date and Time	End Date and Time	Channel 1	Channel 2	Channel 3	Channel 4	Channel 5	Primary S/C	Secondary S/C
05/02/1986 15:35	09/02/1986 03:45	8.75E+07	3.27E+07	1.37E+07	7.45E+06	3.88E+06	GOES-6	GOES-5
14/02/1986 06:00	18/02/1986 06:45	6.66E+07	3.48E+07	1.85E+07	1.01E+07	5.19E+06	GOES-6	GOES-5
06/03/1986 15:20	07/03/1986 06:30	2.24E+06	9.55E+05	4.52E+05	2.69E+05	1.52E+05	GOES-6	GOES-5
04/05/1986 09:50	04/05/1986 22:55	6.70E+05	4.28E+05	3.08E+05	2.89E+05	2.48E+05	GOES-6	GOES-5
07/11/1987 20:20	09/11/1987 16:20	2.51E+07	9.86E+06	3.67E+06	1.22E+06	3.97E+05	GOES-7	GOES-6
30/12/1987 06:55	31/12/1987 15:45	3.80E+06	1.57E+06	6.16E+05	2.17E+05	7.69E+04	GOES-7	GOES-6
02/01/1988 20:15	06/01/1988 12:50	5.97E+07	2.37E+07	9.38E+06	3.68E+06	1.39E+06	GOES-7	GOES-6
25/03/1988 19:35	26/03/1988 08:45	1.30E+06	6.47E+05	3.25E+05	1.65E+05	8.26E+04	GOES-7	GOES-6
30/06/1988 07:55	30/06/1988 23:45	1.36E+06	6.31E+05	2.98E+05	1.46E+05	7.04E+04	GOES-7	None
25/08/1988 19:35	30/08/1988 11:20	3.80E+07	8.77E+06	2.08E+06	5.24E+05	1.39E+05	GOES-7	GOES-6
04/10/1988 21:15	06/10/1988 14:30	5.36E+06	1.12E+06	2.68E+05	8.94E+04	3.12E+04	GOES-7	GOES-6
08/11/1988 11:10	10/11/1988 00:05	1.26E+06	8.01E+05	4.73E+05	2.36E+05	1.18E+05	GOES-7	GOES-6
16/12/1988 09:25	19/12/1988 16:10	1.38E+07	4.62E+06	1.57E+06	5.61E+05	2.07E+05	GOES-7	GOES-6
04/01/1989 19:45	06/01/1989 02:30	6.07E+06	1.71E+06	4.78E+05	1.31E+05	3.70E+04	GOES-7	GOES-6
08/03/1989 10:45	14/03/1989 21:30	5.25E+08	1.81E+08	6.32E+07	2.23E+07	7.53E+06	GOES-7	GOES-6
17/03/1989 15:55	21/03/1989 05:05	3.12E+08	1.45E+08	6.58E+07	2.79E+07	1.10E+07	GOES-7	GOES-6
23/03/1989 17:45	24/03/1989 18:20	4.92E+06	2.19E+06	9.71E+05	4.24E+05	1.81E+05	GOES-7	GOES-6
11/04/1989 11:05	17/04/1989 01:20	1.57E+08	6.29E+07	2.41E+07	8.26E+06	2.69E+06	GOES-7	GOES-6
04/05/1989 19:25	08/05/1989 17:20	4.55E+07	1.51E+07	4.80E+06	1.38E+06	3.93E+05	GOES-7	GOES-6
23/05/1989 04:15	27/05/1989 15:50	2.17E+07	6.67E+06	2.14E+06	7.56E+05	2.69E+05	GOES-7	GOES-6
18/06/1989 14:15	19/06/1989 02:05	2.27E+05	2.02E+05	1.62E+05	1.03E+05	6.44E+04	GOES-7	GOES-6
29/06/1989 21:15	30/06/1989 17:10	3.07E+06	8.54E+05	2.52E+05	8.46E+04	2.89E+04	GOES-7	GOES-6

Table A.2: SARG Event List - Fluences ($cm^{-2}MeV^{-1}$) Channels 6-10 [1].

Start Date and Time	End Date and Time	Channel 6	Channel 7	Channel 8	Channel 9	Channel 10	Primary S/C	Secondary S/C
05/02/1986 15:35	09/02/1986 03:45	1.09E+06	3.07E+05	1.01E+05	3.37E+04	1.14E+04	GOES-6	GOES-5
14/02/1986 06:00	18/02/1986 06:45	1.03E+06	2.04E+05	6.78E+04	2.35E+04	8.76E+03	GOES-6	GOES-5
06/03/1986 15:20	07/03/1986 06:30	3.71E+04	9.06E+03	4.50E+03	2.37E+03	1.11E+03	GOES-6	GOES-5
04/05/1986 09:50	04/05/1986 22:55	5.81E+04	1.36E+04	6.00E+03	2.79E+03	1.20E+03	GOES-6	GOES-5
07/11/1987 20:20	09/11/1987 16:20	1.00E+05	2.54E+04	1.31E+04	7.20E+03	3.26E+03	GOES-7	GOES-6
30/12/1987 06:55	31/12/1987 15:45	3.09E+04	1.24E+04	7.57E+03	4.77E+03	2.27E+03	GOES-7	GOES-6
02/01/1988 20:15	06/01/1988 12:50	3.26E+05	7.63E+04	3.16E+04	1.37E+04	5.76E+03	GOES-7	GOES-6
25/03/1988 19:35	26/03/1988 08:45	3.38E+04	1.38E+04	6.18E+03	2.79E+03	1.13E+03	GOES-7	GOES-6
30/06/1988 07:55	30/06/1988 23:45	2.76E+04	1.08E+04	5.30E+03	2.65E+03	1.13E+03	GOES-7	None
25/08/1988 19:35	30/08/1988 11:20	7.60E+04	4.16E+04	2.50E+04	1.52E+04	7.07E+03	GOES-7	GOES-6
04/10/1988 21:15	06/10/1988 14:30	2.21E+04	1.56E+04	9.51E+03	5.73E+03	2.63E+03	GOES-7	GOES-6
08/11/1988 11:10	10/11/1988 00:05	6.28E+04	3.33E+04	1.58E+04	7.43E+03	3.00E+03	GOES-7	GOES-6
16/12/1988 09:25	19/12/1988 16:10	1.20E+05	6.99E+04	3.70E+04	1.95E+04	8.46E+03	GOES-7	GOES-6
04/01/1989 19:45	06/01/1989 02:30	1.73E+04	8.12E+03	4.93E+03	3.05E+03	1.44E+03	GOES-7	GOES-6
08/03/1989 10:45	14/03/1989 21:30	1.33E+06	2.34E+05	7.50E+04	2.53E+04	9.18E+03	GOES-7	GOES-6
17/03/1989 15:55	21/03/1989 05:05	1.55E+06	2.18E+05	4.78E+04	1.08E+04	3.56E+03	GOES-7	GOES-6
23/03/1989 17:45	24/03/1989 18:20	5.79E+04	1.85E+04	7.79E+03	3.36E+03	1.34E+03	GOES-7	GOES-6
11/04/1989 11:05	17/04/1989 01:20	4.10E+05	6.25E+04	2.84E+04	1.41E+04	6.06E+03	GOES-7	GOES-6
04/05/1989 19:25	08/05/1989 17:20	9.79E+04	2.43E+04	1.37E+04	8.29E+03	3.81E+03	GOES-7	GOES-6
23/05/1989 04:15	27/05/1989 15:50	1.09E+05	4.38E+04	2.35E+04	1.29E+04	5.61E+03	GOES-7	GOES-6
18/06/1989 14:15	19/06/1989 02:05	3.31E+04	1.70E+04	7.11E+03	2.92E+03	1.06E+03	GOES-7	GOES-6
29/06/1989 21:15	30/06/1989 17:10	1.30E+04	5.81E+03	3.34E+03	1.97E+03	8.99E+02	GOES-7	GOES-6

Table A.3: SARG Event List - Peak Fluxes ($cm^{-2}ster^{-1}s^{-1}MeV^{-1}$) Channels 1-5 [1].

Start Date and Time	End Date and Time	Channel 1	Channel 2	Channel 3	Channel 4	Channel 5	Primary S/C	Secondary S/C
05/02/1986 15:35	09/02/1986 03:45	1.08E+02	3.35E+01	1.28E+01	7.86E+00	4.61E+00	GOES-6	GOES-5
14/02/1986 06:00	18/02/1986 06:45	8.39E+01	4.38E+01	2.29E+01	1.20E+01	5.92E+00	GOES-6	GOES-5
06/03/1986 15:20	07/03/1986 06:30	7.45E+00	4.18E+00	2.49E+00	1.69E+00	1.06E+00	GOES-6	GOES-5
04/05/1986 09:50	04/05/1986 22:55	3.44E+00	2.06E+00	1.39E+00	1.24E+00	1.02E+00	GOES-6	GOES-5
07/11/1987 20:20	09/11/1987 16:20	4.65E+01	2.35E+01	1.08E+01	3.89E+00	1.35E+00	GOES-7	GOES-6
30/12/1987 06:55	31/12/1987 15:45	6.32E+00	2.60E+00	1.00E+00	3.36E-01	1.13E-01	GOES-7	GOES-6
02/01/1988 20:15	06/01/1988 12:50	9.33E+01	2.63E+01	8.22E+00	3.27E+00	1.26E+00	GOES-7	GOES-6
25/03/1988 19:35	26/03/1988 08:45	1.13E+01	6.18E+00	3.28E+00	1.62E+00	7.86E-01	GOES-7	GOES-6
30/06/1988 07:55	30/06/1988 23:45	4.08E+00	1.94E+00	9.66E-01	5.33E-01	2.88E-01	GOES-7	None
25/08/1988 19:35	30/08/1988 11:20	5.06E+01	1.09E+01	2.20E+00	3.74E-01	6.78E-02	GOES-7	GOES-6
04/10/1988 21:15	06/10/1988 14:30	1.03E+01	2.17E+00	4.93E-01	1.35E-01	3.90E-02	GOES-7	GOES-6
08/11/1988 11:10	10/11/1988 00:05	1.66E+00	1.06E+00	6.17E-01	2.95E-01	1.42E-01	GOES-7	GOES-6
16/12/1988 09:25	19/12/1988 16:10	1.69E+01	5.04E+00	1.50E+00	4.44E-01	1.36E-01	GOES-7	GOES-6
04/01/1989 19:45	06/01/1989 02:30	1.81E+01	5.48E+00	1.56E+00	3.87E-01	9.77E-02	GOES-7	GOES-6
08/03/1989 10:45	14/03/1989 21:30	5.80E+03	1.75E+03	5.34E+02	1.64E+02	4.74E+01	GOES-7	GOES-6
17/03/1989 15:55	21/03/1989 05:05	5.52E+02	2.51E+02	1.17E+02	5.90E+01	2.76E+01	GOES-7	GOES-6
23/03/1989 17:45	24/03/1989 18:20	1.98E+01	7.87E+00	3.34E+00	1.64E+00	7.80E-01	GOES-7	GOES-6
11/04/1989 11:05	17/04/1989 01:20	1.68E+02	6.70E+01	2.58E+01	9.20E+00	3.08E+00	GOES-7	GOES-6
04/05/1989 19:25	08/05/1989 17:20	4.73E+01	1.78E+01	6.24E+00	1.87E+00	5.37E-01	GOES-7	GOES-6
23/05/1989 04:15	27/05/1989 15:50	9.76E+01	1.95E+01	3.88E+00	7.60E-01	1.54E-01	GOES-7	GOES-6
18/06/1989 14:15	19/06/1989 02:05	1.19E+00	9.83E-01	7.29E-01	4.27E-01	2.49E-01	GOES-7	GOES-6
29/06/1989 21:15	30/06/1989 17:10	9.44E+00	3.17E+00	1.02E+00	2.96E-01	8.74E-02	GOES-7	GOES-6

Table A.4: SARG Event List - Peak Fluxes ($cm^{-2}ster^{-1}s^{-1}MeV^{-1}$) Channels 6-10 [1].

Start Date and Time	End Date and Time	Channel 6	Channel 7	Channel 8	Channel 9	Channel 10	Primary S/C	Secondary S/C
05/02/1986 15:35	09/02/1986 03:45	1.38E+00	4.14E-01	1.15E-01	3.20E-02	8.82E-03	GOES-6	GOES-5
14/02/1986 06:00	18/02/1986 06:45	1.22E+00	2.52E-01	7.39E-02	2.23E-02	6.63E-03	GOES-6	GOES-5
06/03/1986 15:20	07/03/1986 06:30	1.91E-01	3.45E-02	1.29E-02	5.15E-03	2.13E-03	GOES-6	GOES-5
04/05/1986 09:50	04/05/1986 22:55	2.17E-01	4.62E-02	1.79E-02	7.27E-03	2.86E-03	GOES-6	GOES-5
07/11/1987 20:20	09/11/1987 16:20	2.61E-01	5.03E-02	1.68E-02	5.84E-03	2.24E-03	GOES-7	GOES-6
30/12/1987 06:55	31/12/1987 15:45	4.02E-02	1.43E-02	7.91E-03	4.55E-03	2.06E-03	GOES-7	GOES-6
02/01/1988 20:15	06/01/1988 12:50	3.03E-01	7.26E-02	2.04E-02	5.79E-03	2.13E-03	GOES-7	GOES-6
25/03/1988 19:35	26/03/1988 08:45	2.83E-01	1.02E-01	3.52E-02	1.21E-02	4.10E-03	GOES-7	GOES-6
30/06/1988 07:55	30/06/1988 23:45	1.13E-01	4.45E-02	1.64E-02	5.97E-03	2.22E-03	GOES-7	None
25/08/1988 19:35	30/08/1988 11:20	3.17E-02	1.48E-02	8.15E-03	4.53E-03	2.01E-03	GOES-7	GOES-6
04/10/1988 21:15	06/10/1988 14:30	2.39E-02	1.46E-02	8.63E-03	5.07E-03	2.14E-03	GOES-7	GOES-6
08/11/1988 11:10	10/11/1988 00:05	7.61E-02	4.07E-02	1.86E-02	8.43E-03	3.24E-03	GOES-7	GOES-6
16/12/1988 09:25	19/12/1988 16:10	7.21E-02	3.81E-02	1.96E-02	1.01E-02	4.49E-03	GOES-7	GOES-6
04/01/1989 19:45	06/01/1989 02:30	3.13E-02	1.00E-02	5.74E-03	3.45E-03	1.53E-03	GOES-7	GOES-6
08/03/1989 10:45	14/03/1989 21:30	5.47E+00	6.32E-01	8.08E-02	1.04E-02	2.60E-03	GOES-7	GOES-6
17/03/1989 15:55	21/03/1989 05:05	4.39E+00	6.99E-01	6.85E-02	6.45E-03	1.53E-03	GOES-7	GOES-6
23/03/1989 17:45	24/03/1989 18:20	2.51E-01	8.06E-02	2.38E-02	7.01E-03	2.21E-03	GOES-7	GOES-6
11/04/1989 11:05	17/04/1989 01:20	4.08E-01	5.40E-02	1.52E-02	4.55E-03	1.58E-03	GOES-7	GOES-6
04/05/1989 19:25	08/05/1989 17:20	8.11E-02	1.22E-02	6.31E-03	3.60E-03	1.50E-03	GOES-7	GOES-6
23/05/1989 04:15	27/05/1989 15:50	5.06E-02	1.66E-02	8.58E-03	4.59E-03	1.96E-03	GOES-7	GOES-6
18/06/1989 14:15	19/06/1989 02:05	1.36E-01	7.43E-02	2.96E-02	1.15E-02	4.10E-03	GOES-7	GOES-6
29/06/1989 21:15	30/06/1989 17:10	3.30E-02	1.25E-02	7.41E-03	4.56E-03	1.74E-03	GOES-7	GOES-6

Table A.5: SARG Event List - Fluences ($cm^{-2}MeV^{-1}$) Channels 1-5 [2].

Start Date and Time	End Date and Time	Channel 1	Channel 2	Channel 3	Channel 4	Channel 5	Primary S/C	Secondary S/C
30/06/1989 19:55	02/07/1989 01:50	4.32E+06	1.24E+06	3.64E+05	1.12E+05	3.53E+04	GOES-7	GOES-6
25/07/1989 06:15	26/07/1989 12:00	1.82E+06	1.36E+06	9.39E+05	5.31E+05	3.00E+05	GOES-7	GOES-6
12/08/1989 13:05	28/08/1989 04:45	1.35E+09	8.60E+08	5.33E+08	3.08E+08	1.72E+08	GOES-7	GOES-6
28/08/1989 14:20	30/08/1989 16:40	3.10E+06	1.51E+06	7.14E+05	3.19E+05	1.41E+05	GOES-7	GOES-6
03/09/1989 09:00	05/09/1989 12:55	3.69E+07	8.17E+06	1.88E+06	4.73E+05	1.21E+05	GOES-7	GOES-6
12/09/1989 11:45	14/09/1989 19:10	1.37E+07	6.05E+06	2.62E+06	1.09E+06	4.35E+05	GOES-7	GOES-6
29/09/1989 09:20	04/10/1989 03:50	4.92E+08	3.46E+08	2.30E+08	1.35E+08	7.82E+07	GOES-7	GOES-6
05/10/1989 20:25	07/10/1989 09:50	4.76E+06	1.82E+06	7.30E+05	3.23E+05	1.44E+05	GOES-7	GOES-6
19/10/1989 10:15	30/10/1989 21:55	5.40E+09	3.05E+09	1.61E+09	7.23E+08	3.21E+08	GOES-7	GOES-6
02/11/1989 03:25	08/11/1989 04:00	7.59E+06	4.30E+06	2.21E+06	9.19E+05	3.80E+05	GOES-7	GOES-6
08/11/1989 18:45	09/11/1989 20:00	9.50E+06	2.85E+06	8.09E+05	2.03E+05	5.14E+04	GOES-7	GOES-6
15/11/1989 04:30	16/11/1989 11:55	1.93E+06	1.40E+06	8.90E+05	4.10E+05	1.92E+05	GOES-7	GOES-6
27/11/1989 06:25	04/12/1989 13:10	9.86E+08	5.31E+08	2.51E+08	8.79E+07	2.98E+07	GOES-7	GOES-6
19/03/1990 04:55	21/03/1990 20:55	3.25E+08	1.64E+08	7.76E+07	3.20E+07	1.22E+07	GOES-7	GOES-6
28/03/1990 18:05	30/03/1990 01:15	1.01E+07	2.39E+06	5.96E+05	1.67E+05	4.78E+04	GOES-7	GOES-6
07/04/1990 10:20	09/04/1990 20:40	1.74E+07	6.78E+06	2.50E+06	8.05E+05	2.55E+05	GOES-7	GOES-6
11/04/1990 17:40	12/04/1990 09:00	8.20E+06	1.74E+06	3.54E+05	6.47E+04	1.26E+04	GOES-7	GOES-6
16/04/1990 00:45	23/04/1990 14:55	2.30E+07	9.31E+06	3.71E+06	1.43E+06	5.45E+05	GOES-7	GOES-6
28/04/1990 04:10	29/04/1990 15:35	2.53E+07	1.36E+07	6.94E+06	3.10E+06	1.31E+06	GOES-7	GOES-6
18/05/1990 16:05	20/05/1990 13:30	5.51E+06	1.99E+06	6.99E+05	2.30E+05	7.61E+04	GOES-7	GOES-6
21/05/1990 20:55	24/05/1990 05:35	2.70E+07	1.52E+07	8.48E+06	4.54E+06	2.40E+06	GOES-7	GOES-6
24/05/1990 18:25	30/05/1990 21:35	5.96E+07	3.02E+07	1.54E+07	7.91E+06	4.05E+06	GOES-7	GOES-6

Table A.6: SARG Event List - Fluences ($cm^{-2}MeV^{-1}$) Channels 6-10 [2].

Start Date and Time	End Date and Time	Channel 6	Channel 7	Channel 8	Channel 9	Channel 10	Primary S/C	Secondary S/C
30/06/1989 19:55	02/07/1989 01:50	1.67E+04	7.92E+03	4.70E+03	2.84E+03	1.31E+03	GOES-7	GOES-6
25/07/1989 06:15	26/07/1989 12:00	1.63E+05	8.85E+04	3.94E+04	1.72E+04	6.46E+03	GOES-7	GOES-6
12/08/1989 13:05	28/08/1989 04:45	5.53E+07	1.78E+07	3.47E+06	6.50E+05	1.52E+05	GOES-7	GOES-6
28/08/1989 14:20	30/08/1989 16:40	5.20E+04	1.92E+04	9.49E+03	4.81E+03	2.06E+03	GOES-7	GOES-6
03/09/1989 09:00	05/09/1989 12:55	4.20E+04	1.45E+04	8.02E+03	4.60E+03	2.07E+03	GOES-7	GOES-6
12/09/1989 11:45	14/09/1989 19:10	1.03E+05	2.45E+04	1.08E+04	5.04E+03	2.10E+03	GOES-7	GOES-6
29/09/1989 09:20	04/10/1989 03:50	3.59E+07	1.64E+07	5.61E+06	1.87E+06	5.66E+05	GOES-7	GOES-6
05/10/1989 20:25	07/10/1989 09:50	6.81E+04	3.23E+04	1.38E+04	5.87E+03	2.28E+03	GOES-7	GOES-6
19/10/1989 10:15	30/10/1989 21:55	1.20E+08	4.48E+07	1.41E+07	4.39E+06	1.37E+06	GOES-7	GOES-6
02/11/1989 03:25	08/11/1989 04:00	1.50E+05	5.94E+04	2.66E+04	1.20E+04	5.01E+03	GOES-7	GOES-6
08/11/1989 18:45	09/11/1989 20:00	1.57E+04	4.78E+03	2.61E+03	1.50E+03	6.87E+02	GOES-7	GOES-6
15/11/1989 04:30	16/11/1989 11:55	1.09E+05	6.15E+04	2.71E+04	1.17E+04	4.45E+03	GOES-7	GOES-6
27/11/1989 06:25	04/12/1989 13:10	6.13E+06	1.26E+06	1.86E+05	2.67E+04	6.90E+03	GOES-7	GOES-6
19/03/1990 04:55	21/03/1990 20:55	1.44E+06	1.70E+05	3.66E+04	8.31E+03	2.68E+03	GOES-7	GOES-6
28/03/1990 18:05	30/03/1990 01:15	1.82E+04	6.96E+03	4.09E+03	2.49E+03	1.15E+03	GOES-7	GOES-6
07/04/1990 10:20	09/04/1990 20:40	6.20E+04	1.50E+04	8.33E+03	4.94E+03	2.24E+03	GOES-7	GOES-6
11/04/1990 17:40	12/04/1990 09:00	6.01E+03	2.87E+03	1.76E+03	1.10E+03	5.12E+02	GOES-7	GOES-6
16/04/1990 00:45	23/04/1990 14:55	1.70E+05	5.33E+04	2.73E+04	1.46E+04	6.36E+03	GOES-7	GOES-6
28/04/1990 04:10	29/04/1990 15:35	2.46E+05	4.62E+04	1.26E+04	3.57E+03	1.25E+03	GOES-7	GOES-6
18/05/1990 16:05	20/05/1990 13:30	2.77E+04	1.01E+04	5.87E+03	3.57E+03	1.61E+03	GOES-7	GOES-6
21/05/1990 20:55	24/05/1990 05:35	1.06E+06	4.71E+05	1.82E+05	6.96E+04	2.34E+04	GOES-7	GOES-6
24/05/1990 18:25	30/05/1990 21:35	1.96E+06	9.43E+05	4.17E+05	1.83E+05	6.75E+04	GOES-7	GOES-6

Table A.7: SARG Event List - Peak Fluxes ($cm^{-2}ster^{-1}s^{-1}MeV^{-1}$) Channels 1-5 [2].

Start Date and Time	End Date and Time	Channel 1	Channel 2	Channel 3	Channel 4	Channel 5	Primary S/C	Secondary S/C
30/06/1989 19:55	02/07/1989 01:50	1.39E+01	3.55E+00	9.23E-01	2.49E-01	6.86E-02	GOES-7	GOES-6
25/07/1989 06:15	26/07/1989 12:00	3.31E+00	2.63E+00	1.89E+00	1.08E+00	6.19E-01	GOES-7	GOES-6
12/08/1989 13:05	28/08/1989 04:45	1.34E+03	7.48E+02	4.30E+02	2.64E+02	1.57E+02	GOES-7	GOES-6
28/08/1989 14:20	30/08/1989 16:40	2.60E+00	1.43E+00	7.05E-01	2.71E-01	1.05E-01	GOES-7	GOES-6
03/09/1989 09:00	05/09/1989 12:55	4.99E+01	1.11E+01	2.56E+00	6.33E-01	1.58E-01	GOES-7	GOES-6
12/09/1989 11:45	14/09/1989 19:10	1.35E+01	6.44E+00	3.05E+00	1.42E+00	6.31E-01	GOES-7	GOES-6
29/09/1989 09:20	04/10/1989 03:50	4.42E+02	2.85E+02	1.81E+02	1.10E+02	6.64E+01	GOES-7	GOES-6
05/10/1989 20:25	07/10/1989 09:50	9.74E+00	3.31E+00	1.16E+00	4.27E-01	1.59E-01	GOES-7	GOES-6
19/10/1989 10:15	30/10/1989 21:55	1.53E+04	7.71E+03	3.74E+03	1.64E+03	7.08E+02	GOES-7	GOES-6
02/11/1989 03:25	08/11/1989 04:00	2.75E+00	1.50E+00	7.21E-01	2.61E-01	9.56E-02	GOES-7	GOES-6
08/11/1989 18:45	09/11/1989 20:00	3.22E+01	9.11E+00	2.42E+00	5.51E-01	1.27E-01	GOES-7	GOES-6
15/11/1989 04:30	16/11/1989 11:55	4.04E+00	4.22E+00	3.38E+00	1.47E+00	6.49E-01	GOES-7	GOES-6
27/11/1989 06:25	04/12/1989 13:10	1.44E+03	8.44E+02	4.22E+02	1.47E+02	4.92E+01	GOES-7	GOES-6
19/03/1990 04:55	21/03/1990 20:55	4.08E+02	1.99E+02	9.57E+01	4.45E+01	1.90E+01	GOES-7	GOES-6
28/03/1990 18:05	30/03/1990 01:15	2.52E+01	6.94E+00	2.02E+00	6.59E-01	2.10E-01	GOES-7	GOES-6
07/04/1990 10:20	09/04/1990 20:40	1.50E+01	6.06E+00	2.30E+00	7.58E-01	2.44E-01	GOES-7	GOES-6
11/04/1990 17:40	12/04/1990 09:00	4.18E+01	1.03E+01	2.28E+00	3.94E-01	7.09E-02	GOES-7	GOES-6
16/04/1990 00:45	23/04/1990 14:55	1.06E+01	3.92E+00	1.46E+00	5.55E-01	2.07E-01	GOES-7	GOES-6
28/04/1990 04:10	29/04/1990 15:35	5.03E+01	2.62E+01	1.35E+01	6.64E+00	3.12E+00	GOES-7	GOES-6
18/05/1990 16:05	20/05/1990 13:30	5.93E+00	2.20E+00	7.88E-01	2.58E-01	8.46E-02	GOES-7	GOES-6
21/05/1990 20:55	24/05/1990 05:35	1.46E+02	6.82E+01	3.22E+01	1.55E+01	7.37E+00	GOES-7	GOES-6
24/05/1990 18:25	30/05/1990 21:35	6.04E+01	2.99E+01	1.44E+01	6.53E+00	2.96E+00	GOES-7	GOES-6

Table A.8: SARG Event List - Peak Fluxes ($cm^{-2}ster^{-1}s^{-1}MeV^{-1}$) Channels 6-10 [2].

Start Date and Time	End Date and Time	Channel 6	Channel 7	Channel 8	Channel 9	Channel 10	Primary S/C	Secondary S/C
30/06/1989 19:55	02/07/1989 01:50	2.65E-02	1.02E-02	5.80E-03	3.39E-03	1.45E-03	GOES-7	GOES-6
25/07/1989 06:15	26/07/1989 12:00	3.83E-01	2.37E-01	1.11E-01	5.03E-02	1.95E-02	GOES-7	GOES-6
12/08/1989 13:05	28/08/1989 04:45	6.01E+01	2.30E+01	4.02E+00	6.58E-01	1.66E-01	GOES-7	GOES-6
28/08/1989 14:20	30/08/1989 16:40	4.15E-02	1.64E-02	7.70E-03	3.66E-03	1.44E-03	GOES-7	GOES-6
03/09/1989 09:00	05/09/1989 12:55	4.37E-02	1.21E-02	6.03E-03	3.15E-03	1.35E-03	GOES-7	GOES-6
12/09/1989 11:45	14/09/1989 19:10	1.35E-01	2.91E-02	9.66E-03	3.32E-03	1.25E-03	GOES-7	GOES-6
29/09/1989 09:20	04/10/1989 03:50	3.22E+01	1.56E+01	6.27E+00	2.47E+00	8.26E-01	GOES-7	GOES-6
05/10/1989 20:25	07/10/1989 09:50	6.97E-02	3.05E-02	1.27E-02	5.30E-03	2.15E-03	GOES-7	GOES-6
19/10/1989 10:15	30/10/1989 21:55	2.44E+02	8.39E+01	2.23E+01	5.83E+00	1.55E+00	GOES-7	GOES-6
02/11/1989 03:25	08/11/1989 04:00	4.04E-02	1.71E-02	7.40E-03	3.21E-03	1.32E-03	GOES-7	GOES-6
08/11/1989 18:45	09/11/1989 20:00	3.39E-02	9.03E-03	4.34E-03	2.19E-03	9.65E-04	GOES-7	GOES-6
15/11/1989 04:30	16/11/1989 11:55	3.47E-01	1.86E-01	7.64E-02	3.08E-02	1.16E-02	GOES-7	GOES-6
27/11/1989 06:25	04/12/1989 13:10	9.31E+00	1.76E+00	2.17E-01	2.59E-02	4.69E-03	GOES-7	GOES-6
19/03/1990 04:55	21/03/1990 20:55	2.40E+00	3.03E-01	4.47E-02	6.67E-03	1.76E-03	GOES-7	GOES-6
28/03/1990 18:05	30/03/1990 01:15	4.82E-02	1.10E-02	5.52E-03	2.94E-03	1.28E-03	GOES-7	GOES-6
07/04/1990 10:20	09/04/1990 20:40	5.53E-02	1.25E-02	6.29E-03	3.37E-03	1.42E-03	GOES-7	GOES-6
11/04/1990 17:40	12/04/1990 09:00	2.35E-02	7.76E-03	4.23E-03	2.40E-03	1.08E-03	GOES-7	GOES-6
16/04/1990 00:45	23/04/1990 14:55	6.16E-02	1.83E-02	7.59E-03	3.23E-03	1.24E-03	GOES-7	GOES-6
28/04/1990 04:10	29/04/1990 15:35	7.07E-01	1.60E-01	2.73E-02	4.56E-03	1.23E-03	GOES-7	GOES-6
18/05/1990 16:05	20/05/1990 13:30	2.85E-02	9.61E-03	5.13E-03	2.84E-03	1.23E-03	GOES-7	GOES-6
21/05/1990 20:55	24/05/1990 05:35	3.01E+00	1.23E+00	4.71E-01	1.79E-01	5.80E-02	GOES-7	GOES-6
24/05/1990 18:25	30/05/1990 21:35	1.35E+00	6.15E-01	3.09E-01	1.57E-01	6.17E-02	GOES-7	GOES-6

Table A.9: SARG Event List - Fluences ($cm^{-2}MeV^{-1}$) Channels 1-5 [3].

Start Date and Time	End Date and Time	Channel 1	Channel 2	Channel 3	Channel 4	Channel 5	Primary S/C	Secondary S/C
12/06/1990 05:05	14/06/1990 09:25	5.85E+07	1.65E+07	4.77E+06	1.47E+06	4.44E+05	GOES-7	GOES-6
13/07/1990 17:45	14/07/1990 09:55	4.56E+06	9.62E+05	1.97E+05	3.74E+04	7.72E+03	GOES-7	GOES-6
26/07/1990 00:20	29/07/1990 13:00	2.81E+07	9.75E+06	3.49E+06	1.33E+06	5.03E+05	GOES-7	GOES-6
31/07/1990 12:40	04/08/1990 17:35	9.88E+07	4.25E+07	1.77E+07	6.84E+06	2.51E+06	GOES-7	GOES-6
13/08/1990 00:45	14/08/1990 14:45	4.64E+06	1.50E+06	4.71E+05	1.39E+05	4.23E+04	GOES-7	GOES-6
28/01/1991 00:55	29/01/1991 16:40	3.66E+06	1.56E+06	5.90E+05	1.72E+05	5.14E+04	GOES-7	GOES-6
31/01/1991 03:05	02/02/1991 05:30	9.34E+07	3.72E+07	1.25E+07	2.84E+06	6.32E+05	GOES-7	GOES-6
08/02/1991 07:25	09/02/1991 14:50	3.95E+06	1.69E+06	6.42E+05	1.86E+05	5.45E+04	GOES-7	GOES-6
25/02/1991 08:15	26/02/1991 15:50	2.35E+06	1.18E+06	5.26E+05	1.81E+05	6.26E+04	GOES-7	GOES-6
13/03/1991 00:15	14/03/1991 17:15	3.38E+06	1.88E+06	9.79E+05	4.36E+05	1.88E+05	GOES-7	GOES-6
23/03/1991 04:55	31/03/1991 12:00	1.88E+09	1.13E+09	6.69E+08	3.81E+08	2.10E+08	GOES-7	GOES-6
02/04/1991 17:35	08/04/1991 02:05	6.61E+07	2.36E+07	8.36E+06	2.92E+06	9.90E+05	GOES-7	GOES-6
12/05/1991 23:50	14/05/1991 21:55	5.09E+07	2.56E+07	1.25E+07	5.59E+06	2.44E+06	GOES-7	GOES-6
18/05/1991 23:15	20/05/1991 16:30	1.57E+06	1.08E+06	6.88E+05	3.72E+05	1.94E+05	GOES-7	GOES-6
21/05/1991 01:10	22/05/1991 08:50	4.06E+06	1.35E+06	4.63E+05	1.74E+05	6.53E+04	GOES-7	GOES-6
23/05/1991 12:15	24/05/1991 18:10	7.01E+06	1.94E+06	5.52E+05	1.68E+05	5.25E+04	GOES-7	GOES-6
31/05/1991 00:10	19/06/1991 10:50	1.00E+09	4.73E+08	2.31E+08	1.23E+08	6.40E+07	GOES-7	GOES-6
29/06/1991 13:20	13/07/1991 13:55	1.29E+09	4.84E+08	1.74E+08	5.60E+07	1.71E+07	GOES-7	GOES-6
25/08/1991 18:40	30/08/1991 15:45	1.49E+08	4.95E+07	1.61E+07	4.96E+06	1.48E+06	GOES-7	GOES-6
06/09/1991 15:20	07/09/1991 13:45	3.57E+06	9.51E+05	2.60E+05	7.56E+04	2.27E+04	GOES-7	GOES-6
30/09/1991 07:55	02/10/1991 23:35	1.37E+07	4.56E+06	1.55E+06	5.49E+05	1.95E+05	GOES-7	GOES-6
28/10/1991 05:25	28/10/1991 23:00	1.50E+06	1.24E+06	7.20E+05	1.88E+05	4.89E+04	GOES-7	GOES-6

Table A.10: SARG Event List - Fluences ($cm^{-2}MeV^{-1}$) Channels 6-10 [3].

Start Date and Time	End Date and Time	Channel 6	Channel 7	Channel 8	Channel 9	Channel 10	Primary S/C	Secondary S/C
12/06/1990 05:05	14/06/1990 09:25	9.68E+04	2.11E+04	9.45E+03	4.49E+03	1.83E+03	GOES-7	GOES-6
13/07/1990 17:45	14/07/1990 09:55	5.21E+03	3.51E+03	2.17E+03	1.33E+03	6.11E+02	GOES-7	GOES-6
26/07/1990 00:20	29/07/1990 13:00	1.55E+05	4.79E+04	2.08E+04	9.26E+03	3.62E+03	GOES-7	GOES-6
31/07/1990 12:40	04/08/1990 17:35	4.29E+05	7.33E+04	2.52E+04	9.17E+03	3.50E+03	GOES-7	GOES-6
13/08/1990 00:45	14/08/1990 14:45	1.87E+04	8.26E+03	4.89E+03	2.97E+03	1.35E+03	GOES-7	GOES-6
28/01/1991 00:55	29/01/1991 16:40	2.26E+04	9.93E+03	5.77E+03	3.44E+03	1.57E+03	GOES-7	GOES-6
31/01/1991 03:05	02/02/1991 05:30	1.00E+05	1.59E+04	7.49E+03	3.87E+03	1.72E+03	GOES-7	GOES-6
08/02/1991 07:25	09/02/1991 14:50	1.89E+04	6.57E+03	3.90E+03	2.42E+03	1.13E+03	GOES-7	GOES-6
25/02/1991 08:15	26/02/1991 15:50	2.24E+04	8.02E+03	4.60E+03	2.74E+03	1.25E+03	GOES-7	GOES-6
13/03/1991 00:15	14/03/1991 17:15	4.99E+04	1.32E+04	6.69E+03	3.57E+03	1.55E+03	GOES-7	GOES-6
23/03/1991 04:55	31/03/1991 12:00	6.76E+07	2.18E+07	2.90E+06	3.59E+05	5.85E+04	GOES-7	GOES-6
02/04/1991 17:35	08/04/1991 02:05	2.15E+05	4.64E+04	2.22E+04	1.13E+04	4.83E+03	GOES-7	GOES-6
12/05/1991 23:50	14/05/1991 21:55	6.87E+05	1.94E+05	5.72E+04	1.70E+04	5.08E+03	GOES-7	GOES-6
18/05/1991 23:15	20/05/1991 16:30	5.79E+04	1.73E+04	8.34E+03	4.19E+03	1.79E+03	GOES-7	GOES-6
21/05/1991 01:10	22/05/1991 08:50	2.56E+04	1.00E+04	5.44E+03	3.04E+03	1.33E+03	GOES-7	GOES-6
23/05/1991 12:15	24/05/1991 18:10	2.25E+04	9.66E+03	5.35E+03	3.02E+03	1.34E+03	GOES-7	GOES-6
31/05/1991 00:10	19/06/1991 10:50	2.41E+07	9.11E+06	2.69E+06	7.81E+05	2.06E+05	GOES-7	GOES-6
29/06/1991 13:20	13/07/1991 13:55	2.32E+06	3.16E+05	1.02E+05	3.56E+04	1.30E+04	GOES-7	GOES-6
25/08/1991 18:40	30/08/1991 15:45	2.55E+05	4.42E+04	2.01E+04	9.88E+03	4.18E+03	GOES-7	GOES-6
06/09/1991 15:20	07/09/1991 13:45	1.08E+04	5.13E+03	3.06E+03	1.86E+03	8.47E+02	GOES-7	GOES-6
30/09/1991 07:55	02/10/1991 23:35	6.94E+04	2.47E+04	1.23E+04	6.28E+03	2.67E+03	GOES-7	GOES-6
28/10/1991 05:25	28/10/1991 23:00	1.29E+04	3.40E+03	1.91E+03	1.15E+03	5.36E+02	GOES-7	GOES-6

Table A.11: SARG Event List - Peak Fluxes ($cm^{-2}ster^{-1}s^{-1}MeV^{-1}$) Channels 1-5 [3].

Start Date and Time	End Date and Time	Channel 1	Channel 2	Channel 3	Channel 4	Channel 5	Primary S/C	Secondary S/C
12/06/1990 05:05	14/06/1990 09:25	1.04E+02	3.25E+01	1.01E+01	3.06E+00	9.00E-01	GOES-7	GOES-6
13/07/1990 17:45	14/07/1990 09:55	1.10E+01	2.59E+00	5.76E-01	1.14E-01	2.39E-02	GOES-7	GOES-6
26/07/1990 00:20	29/07/1990 13:00	2.75E+01	8.47E+00	2.72E+00	9.47E-01	3.30E-01	GOES-7	GOES-6
31/07/1990 12:40	04/08/1990 17:35	1.44E+02	6.07E+01	2.49E+01	9.49E+00	3.41E+00	GOES-7	GOES-6
13/08/1990 00:45	14/08/1990 14:45	6.54E+00	2.34E+00	7.82E-01	2.22E-01	6.41E-02	GOES-7	GOES-6
28/01/1991 00:55	29/01/1991 16:40	5.17E+00	2.29E+00	8.50E-01	2.13E-01	5.51E-02	GOES-7	GOES-6
31/01/1991 03:05	02/02/1991 05:30	1.65E+02	8.25E+01	3.38E+01	8.80E+00	2.19E+00	GOES-7	GOES-6
08/02/1991 07:25	09/02/1991 14:50	5.94E+00	2.71E+00	1.14E+00	3.95E-01	1.36E-01	GOES-7	GOES-6
25/02/1991 08:15	26/02/1991 15:50	4.88E+00	2.82E+00	1.44E+00	5.58E-01	2.11E-01	GOES-7	GOES-6
13/03/1991 00:15	14/03/1991 17:15	3.85E+00	2.08E+00	1.06E+00	4.76E-01	2.07E-01	GOES-7	GOES-6
23/03/1991 04:55	31/03/1991 12:00	1.17E+04	6.24E+03	3.33E+03	1.78E+03	9.28E+02	GOES-7	GOES-6
02/04/1991 17:35	08/04/1991 02:05	7.97E+01	2.26E+01	6.69E+00	2.16E+00	6.71E-01	GOES-7	GOES-6
12/05/1991 23:50	14/05/1991 21:55	1.21E+02	6.29E+01	3.19E+01	1.55E+01	7.26E+00	GOES-7	GOES-6
18/05/1991 23:15	20/05/1991 16:30	3.14E+00	1.68E+00	8.66E-01	4.10E-01	1.88E-01	GOES-7	GOES-6
21/05/1991 01:10	22/05/1991 08:50	5.54E+00	1.84E+00	6.14E-01	2.06E-01	6.96E-02	GOES-7	GOES-6
23/05/1991 12:15	24/05/1991 18:10	1.23E+01	3.21E+00	8.42E-01	2.26E-01	6.27E-02	GOES-7	GOES-6
31/05/1991 00:10	19/06/1991 10:50	5.69E+02	3.22E+02	1.86E+02	1.13E+02	6.61E+01	GOES-7	GOES-6
29/06/1991 13:20	13/07/1991 13:55	3.36E+03	1.07E+03	3.24E+02	8.65E+01	2.12E+01	GOES-7	GOES-6
25/08/1991 18:40	30/08/1991 15:45	1.91E+02	7.35E+01	2.75E+01	9.54E+00	3.12E+00	GOES-7	GOES-6
06/09/1991 15:20	07/09/1991 13:45	7.80E+00	2.21E+00	6.33E-01	1.84E-01	5.50E-02	GOES-7	GOES-6
30/09/1991 07:55	02/10/1991 23:35	1.56E+01	5.18E+00	1.69E+00	5.30E-01	1.67E-01	GOES-7	GOES-6
28/10/1991 05:25	28/10/1991 23:00	1.38E+01	1.29E+01	7.30E+00	1.33E+00	2.42E-01	GOES-7	GOES-6

Table A.12: SARG Event List - Peak Fluxes ($cm^{-2}ster^{-1}s^{-1}MeV^{-1}$) Channels 6-10 [3].

Start Date and Time	End Date and Time	Channel 6	Channel 7	Channel 8	Channel 9	Channel 10	Primary S/C	Secondary S/C
12/06/1990 05:05	14/06/1990 09:25	1.70E-01	3.21E-02	1.04E-02	3.49E-03	1.24E-03	GOES-7	GOES-6
13/07/1990 17:45	14/07/1990 09:55	1.37E-02	7.80E-03	4.84E-03	3.03E-03	1.27E-03	GOES-7	GOES-6
26/07/1990 00:20	29/07/1990 13:00	1.13E-01	3.84E-02	1.50E-02	5.90E-03	2.03E-03	GOES-7	GOES-6
31/07/1990 12:40	04/08/1990 17:35	5.05E-01	7.48E-02	1.68E-02	3.93E-03	1.27E-03	GOES-7	GOES-6
13/08/1990 00:45	14/08/1990 14:45	2.47E-02	9.51E-03	5.13E-03	2.84E-03	1.19E-03	GOES-7	GOES-6
28/01/1991 00:55	29/01/1991 16:40	2.37E-02	1.02E-02	5.45E-03	2.98E-03	1.31E-03	GOES-7	GOES-6
31/01/1991 03:05	02/02/1991 05:30	2.90E-01	3.85E-02	1.11E-02	3.44E-03	1.22E-03	GOES-7	GOES-6
08/02/1991 07:25	09/02/1991 14:50	4.21E-02	1.30E-02	5.90E-03	2.76E-03	1.16E-03	GOES-7	GOES-6
25/02/1991 08:15	26/02/1991 15:50	5.63E-02	1.50E-02	6.72E-03	3.14E-03	1.28E-03	GOES-7	GOES-6
13/03/1991 00:15	14/03/1991 17:15	5.80E-02	1.63E-02	7.01E-03	3.12E-03	1.22E-03	GOES-7	GOES-6
23/03/1991 04:55	31/03/1991 12:00	3.19E+02	1.10E+02	1.49E+01	1.88E+00	2.87E-01	GOES-7	GOES-6
02/04/1991 17:35	08/04/1991 02:05	1.22E-01	2.21E-02	8.36E-03	3.36E-03	1.30E-03	GOES-7	GOES-6
12/05/1991 23:50	14/05/1991 21:55	2.21E+00	6.70E-01	2.08E-01	6.46E-02	1.84E-02	GOES-7	GOES-6
18/05/1991 23:15	20/05/1991 16:30	5.56E-02	1.65E-02	7.41E-03	3.46E-03	1.41E-03	GOES-7	GOES-6
21/05/1991 01:10	22/05/1991 08:50	2.76E-02	1.09E-02	5.86E-03	3.22E-03	1.70E-03	GOES-7	GOES-6
23/05/1991 12:15	24/05/1991 18:10	2.74E-02	1.19E-02	6.23E-03	3.30E-03	1.40E-03	GOES-7	GOES-6
31/05/1991 00:10	19/06/1991 10:50	2.38E+01	8.57E+00	2.43E+00	6.74E-01	2.17E-01	GOES-7	GOES-6
29/06/1991 13:20	13/07/1991 13:55	1.50E+00	1.06E-01	2.41E-02	6.03E-03	1.86E-03	GOES-7	GOES-6
25/08/1991 18:40	30/08/1991 15:45	4.26E-01	5.80E-02	1.47E-02	3.94E-03	1.34E-03	GOES-7	GOES-6
06/09/1991 15:20	07/09/1991 13:45	2.32E-02	9.80E-03	5.29E-03	2.91E-03	1.26E-03	GOES-7	GOES-6
30/09/1991 07:55	02/10/1991 23:35	5.39E-02	1.74E-02	7.91E-03	3.69E-03	1.44E-03	GOES-7	GOES-6
28/10/1991 05:25	28/10/1991 23:00	4.43E-02	8.12E-03	4.41E-03	2.62E-03	1.16E-03	GOES-7	GOES-6

Table A.13: SARG Event List - Fluences ($cm^{-2}MeV^{-1}$) Channels 1-5 [4].

Start Date and Time	End Date and Time	Channel 1	Channel 2	Channel 3	Channel 4	Channel 5	Primary S/C	Secondary S/C
30/10/1991 04:35	31/10/1991 22:10	3.79E+07	1.09E+07	3.38E+06	1.23E+06	4.59E+05	GOES-7	GOES-6
06/02/1992 20:30	09/02/1992 08:30	9.35E+07	2.91E+07	7.73E+06	1.44E+06	2.71E+05	GOES-7	GOES-6
27/02/1992 11:05	28/02/1992 07:00	2.92E+06	1.01E+06	3.31E+05	9.66E+04	2.87E+04	GOES-7	GOES-6
16/03/1992 02:55	17/03/1992 11:10	3.90E+06	1.52E+06	6.13E+05	2.70E+05	1.18E+05	GOES-7	GOES-6
09/05/1992 03:20	12/05/1992 09:30	6.38E+08	2.32E+08	8.04E+07	2.51E+07	7.36E+06	GOES-7	GOES-6
25/06/1992 17:45	01/07/1992 10:40	6.56E+07	3.78E+07	2.14E+07	1.15E+07	5.97E+06	GOES-7	GOES-6
06/08/1992 04:45	07/08/1992 11:05	7.40E+06	2.52E+06	8.43E+05	2.69E+05	8.65E+04	GOES-7	GOES-6
30/10/1992 16:20	07/11/1992 23:45	5.01E+08	3.97E+08	2.72E+08	1.33E+08	6.45E+07	GOES-7	GOES-6
29/11/1992 09:05	29/11/1992 23:45	8.78E+05	4.97E+05	2.46E+05	9.01E+04	3.32E+04	GOES-7	GOES-6
04/03/1993 11:30	05/03/1993 11:10	1.87E+06	1.02E+06	5.38E+05	2.60E+05	1.25E+05	GOES-7	GOES-6
06/03/1993 21:20	07/03/1993 18:15	2.19E+06	9.57E+05	4.20E+05	1.86E+05	8.14E+04	GOES-7	GOES-6
12/03/1993 16:30	14/03/1993 11:15	7.66E+06	3.83E+06	1.87E+06	8.71E+05	4.00E+05	GOES-7	GOES-6
19/02/1994 23:40	22/02/1994 20:50	7.80E+08	3.81E+08	1.48E+08	3.38E+07	7.23E+06	GOES-7	GOES-6
19/10/1994 20:25	21/10/1994 01:15	1.14E+07	4.84E+06	1.81E+06	5.16E+05	1.49E+05	GOES-7	GOES-6
20/10/1995 05:00	21/10/1995 14:15	1.42E+07	5.99E+06	2.56E+06	1.13E+06	4.67E+05	GOES-8	GOES-7
04/11/1997 05:25	10/11/1997 03:20	9.43E+07	5.63E+07	3.39E+07	2.10E+07	1.23E+07	GOES-8	None
20/04/1998 09:30	25/04/1998 16:10	1.52E+08	1.19E+08	9.29E+07	7.09E+07	4.63E+07	GOES-8	None
02/05/1998 11:10	04/05/1998 11:05	1.02E+07	6.14E+06	3.76E+06	2.45E+06	1.49E+06	GOES-8	None
06/05/1998 05:30	07/05/1998 15:55	9.34E+06	5.34E+06	3.07E+06	1.80E+06	9.68E+05	GOES-8	None
09/05/1998 04:00	10/05/1998 19:35	2.48E+06	1.36E+06	7.47E+05	4.15E+05	2.20E+05	GOES-8	None
22/08/1998 18:15	24/08/1998 06:10	3.04E+06	1.15E+06	4.40E+05	1.80E+05	7.83E+04	GOES-8	GOES-10
24/08/1998 20:10	30/08/1998 12:10	3.06E+08	1.35E+08	5.96E+07	2.64E+07	1.05E+07	GOES-8	GOES-10

Table A.14: SARG Event List - Fluences ($cm^{-2}MeV^{-1}$) Channels 6-10 [4].

Start Date and Time	End Date and Time	Channel 6	Channel 7	Channel 8	Channel 9	Channel 10	Primary S/C	Secondary S/C
30/10/1991 04:35	31/10/1991 22:10	2.13E+05	9.89E+04	4.10E+04	1.69E+04	6.37E+03	GOES-7	GOES-6
06/02/1992 20:30	09/02/1992 08:30	5.91E+04	1.29E+04	7.35E+03	4.54E+03	2.15E+03	GOES-7	GOES-6
27/02/1992 11:05	28/02/1992 07:00	1.14E+04	4.56E+03	2.64E+03	1.58E+03	7.22E+02	GOES-7	GOES-6
16/03/1992 02:55	17/03/1992 11:10	4.64E+04	1.83E+04	8.63E+03	4.13E+03	1.71E+03	GOES-7	GOES-6
09/05/1992 03:20	12/05/1992 09:30	9.02E+05	1.11E+05	3.42E+04	1.14E+04	4.21E+03	GOES-7	GOES-6
25/06/1992 17:45	01/07/1992 10:40	1.77E+06	5.26E+05	1.62E+05	5.01E+04	1.63E+04	GOES-7	GOES-6
06/08/1992 04:45	07/08/1992 11:05	3.12E+04	1.12E+04	6.48E+03	3.88E+03	1.77E+03	GOES-7	GOES-6
30/10/1992 16:20	07/11/1992 23:45	2.43E+07	9.17E+06	2.22E+06	5.17E+05	1.37E+05	GOES-7	GOES-6
29/11/1992 09:05	29/11/1992 23:45	1.34E+04	5.38E+03	2.95E+03	1.66E+03	7.60E+02	GOES-7	GOES-6
04/03/1993 11:30	05/03/1993 11:10	5.20E+04	2.17E+04	9.63E+03	4.29E+03	1.72E+03	GOES-7	GOES-6
06/03/1993 21:20	07/03/1993 18:15	3.23E+04	1.28E+04	6.25E+03	3.11E+03	1.33E+03	GOES-7	GOES-6
12/03/1993 16:30	14/03/1993 11:15	1.51E+05	5.66E+04	2.31E+04	9.47E+03	3.57E+03	GOES-7	GOES-6
19/02/1994 23:40	22/02/1994 20:50	5.66E+05	4.43E+04	1.94E+04	9.78E+03	4.30E+03	GOES-7	GOES-6
19/10/1994 20:25	21/10/1994 01:15	5.55E+04	2.07E+04	9.94E+03	4.88E+03	2.11E+03	GOES-7	GOES-6
20/10/1995 05:00	21/10/1995 14:15	1.40E+05	4.21E+04	1.77E+04	7.67E+03	5.59E+03	GOES-8	GOES-7
04/11/1997 05:25	10/11/1997 03:20	5.77E+06	2.70E+06	8.98E+05	2.91E+05	1.78E+05	GOES-8	None
20/04/1998 09:30	25/04/1998 16:10	1.58E+07	5.38E+06	6.66E+05	7.60E+04	4.24E+04	GOES-8	None
02/05/1998 11:10	04/05/1998 11:05	6.94E+05	3.23E+05	1.10E+05	3.68E+04	2.35E+04	GOES-8	None
06/05/1998 05:30	07/05/1998 15:55	3.62E+05	1.36E+05	4.51E+04	1.49E+04	9.79E+03	GOES-8	None
09/05/1998 04:00	10/05/1998 19:35	9.58E+04	4.17E+04	1.88E+04	8.48E+03	6.16E+03	GOES-8	None
22/08/1998 18:15	24/08/1998 06:10	4.39E+04	2.46E+04	1.33E+04	7.11E+03	5.19E+03	GOES-8	GOES-10
24/08/1998 20:10	30/08/1998 12:10	2.64E+06	6.67E+05	1.71E+05	4.39E+04	3.00E+04	GOES-8	GOES-10

Table A.15: SARG Event List - Peak Fluxes ($cm^{-2}ster^{-1}s^{-1}MeV^{-1}$) Channels 1-5 [4].

Start Date and Time	End Date and Time	Channel 1	Channel 2	Channel 3	Channel 4	Channel 5	Primary S/C	Secondary S/C
30/10/1991 04:35	31/10/1991 22:10	2.29E+02	3.97E+01	9.11E+00	3.92E+00	1.66E+00	GOES-7	GOES-6
06/02/1992 20:30	09/02/1992 08:30	1.21E+02	4.14E+01	1.22E+01	2.52E+00	5.11E-01	GOES-7	GOES-6
27/02/1992 11:05	28/02/1992 07:00	1.19E+01	3.85E+00	1.16E+00	2.97E-01	7.78E-02	GOES-7	GOES-6
16/03/1992 02:55	17/03/1992 11:10	6.64E+00	2.67E+00	1.10E+00	4.72E-01	2.00E-01	GOES-7	GOES-6
09/05/1992 03:20	12/05/1992 09:30	4.03E+03	1.60E+03	5.86E+02	1.82E+02	5.24E+01	GOES-7	GOES-6
25/06/1992 17:45	01/07/1992 10:40	6.36E+01	4.02E+01	2.51E+01	1.53E+01	8.86E+00	GOES-7	GOES-6
06/08/1992 04:45	07/08/1992 11:05	1.45E+01	5.43E+00	1.91E+00	5.87E-01	1.80E-01	GOES-7	GOES-6
30/10/1992 16:20	07/11/1992 23:45	3.28E+02	2.88E+02	2.15E+02	1.10E+02	5.58E+01	GOES-7	GOES-6
29/11/1992 09:05	29/11/1992 23:45	4.45E+00	2.27E+00	1.02E+00	3.48E-01	1.19E-01	GOES-7	GOES-6
04/03/1993 11:30	05/03/1993 11:10	5.46E+00	3.03E+00	1.59E+00	7.38E-01	3.41E-01	GOES-7	GOES-6
06/03/1993 21:20	07/03/1993 18:15	6.87E+00	2.86E+00	1.22E+00	5.47E-01	2.41E-01	GOES-7	GOES-6
12/03/1993 16:30	14/03/1993 11:15	1.39E+01	7.76E+00	4.05E+00	1.81E+00	8.10E-01	GOES-7	GOES-6
19/02/1994 23:40	22/02/1994 20:50	8.31E+03	4.05E+03	1.54E+03	3.37E+02	6.55E+01	GOES-7	GOES-6
19/10/1994 20:25	21/10/1994 01:15	2.18E+01	1.05E+01	4.30E+00	1.25E+00	3.69E-01	GOES-7	GOES-6
20/10/1995 05:00	21/10/1995 14:15	3.56E+01	1.56E+01	6.86E+00	3.12E+00	1.27E+00	GOES-8	GOES-7
04/11/1997 05:25	10/11/1997 03:20	1.04E+02	6.21E+01	3.72E+01	2.23E+01	1.29E+01	GOES-8	None
20/04/1998 09:30	25/04/1998 16:10	1.30E+02	1.07E+02	8.69E+01	6.94E+01	4.75E+01	GOES-8	None
02/05/1998 11:10	04/05/1998 11:05	2.56E+01	1.70E+01	1.12E+01	7.37E+00	4.43E+00	GOES-8	None
06/05/1998 05:30	07/05/1998 15:55	2.42E+01	2.22E+01	1.90E+01	1.23E+01	7.09E+00	GOES-8	None
09/05/1998 04:00	10/05/1998 19:35	4.45E+00	2.55E+00	1.39E+00	6.13E-01	2.66E-01	GOES-8	None
22/08/1998 18:15	24/08/1998 06:10	3.47E+00	1.42E+00	5.68E-01	2.03E-01	7.83E-02	GOES-8	GOES-10
24/08/1998 20:10	30/08/1998 12:10	6.57E+02	2.31E+02	8.39E+01	3.37E+01	1.20E+01	GOES-8	GOES-10

Table A.16: SARG Event List - Peak Fluxes ($cm^{-2}ster^{-1}s^{-1}MeV^{-1}$) Channels 6-10 [4].

Start Date and Time	End Date and Time	Channel 6	Channel 7	Channel 8	Channel 9	Channel 10	Primary S/C	Secondary S/C
30/10/1991 04:35	31/10/1991 22:10	5.31E-01	1.70E-01	6.96E-02	2.91E-02	1.09E-02	GOES-7	GOES-6
06/02/1992 20:30	09/02/1992 08:30	7.24E-02	1.03E-02	5.13E-03	2.84E-03	1.27E-03	GOES-7	GOES-6
27/02/1992 11:05	28/02/1992 07:00	2.88E-02	1.06E-02	5.33E-03	2.74E-03	1.17E-03	GOES-7	GOES-6
16/03/1992 02:55	17/03/1992 11:10	7.08E-02	2.50E-02	1.15E-02	5.38E-03	2.01E-03	GOES-7	GOES-6
09/05/1992 03:20	12/05/1992 09:30	4.82E+00	4.42E-01	6.09E-02	8.67E-03	2.26E-03	GOES-7	GOES-6
25/06/1992 17:45	01/07/1992 10:40	2.62E+00	7.74E-01	3.13E-01	1.30E-01	4.26E-02	GOES-7	GOES-6
06/08/1992 04:45	07/08/1992 11:05	5.49E-02	1.67E-02	8.49E-03	4.49E-03	1.87E-03	GOES-7	GOES-6
30/10/1992 16:20	07/11/1992 23:45	2.20E+01	8.64E+00	3.07E+00	1.08E+00	3.59E-01	GOES-7	GOES-6
29/11/1992 09:05	29/11/1992 23:45	4.39E-02	1.62E-02	7.51E-03	3.56E-03	1.53E-03	GOES-7	GOES-6
04/03/1993 11:30	05/03/1993 11:10	1.44E-01	6.06E-02	2.37E-02	9.21E-03	3.29E-03	GOES-7	GOES-6
06/03/1993 21:20	07/03/1993 18:15	8.20E-02	2.79E-02	1.18E-02	5.11E-03	1.98E-03	GOES-7	GOES-6
12/03/1993 16:30	14/03/1993 11:15	3.48E-01	1.49E-01	5.84E-02	2.27E-02	7.41E-03	GOES-7	GOES-6
19/02/1994 23:40	22/02/1994 20:50	2.34E+00	8.35E-02	2.35E-02	7.80E-03	2.66E-03	GOES-7	GOES-6
19/10/1994 20:25	21/10/1994 01:15	1.25E-01	4.26E-02	1.73E-02	7.14E-03	2.60E-03	GOES-7	GOES-6
20/10/1995 05:00	21/10/1995 14:15	3.32E-01	8.67E-02	2.53E-02	7.47E-03	5.24E-03	GOES-8	GOES-7
04/11/1997 05:25	10/11/1997 03:20	6.60E+00	3.37E+00	1.28E+00	4.78E-01	3.02E-01	GOES-8	None
20/04/1998 09:30	25/04/1998 16:10	1.71E+01	6.12E+00	7.51E-01	8.45E-02	3.72E-02	GOES-8	None
02/05/1998 11:10	04/05/1998 11:05	1.84E+00	7.68E-01	2.81E-01	1.02E-01	6.47E-02	GOES-8	None
06/05/1998 05:30	07/05/1998 15:55	2.40E+00	8.10E-01	2.13E-01	5.51E-02	3.23E-02	GOES-8	None
09/05/1998 04:00	10/05/1998 19:35	1.08E-01	4.36E-02	1.70E-02	6.58E-03	4.70E-03	GOES-8	None
22/08/1998 18:15	24/08/1998 06:10	4.19E-02	2.24E-02	1.24E-02	6.92E-03	4.75E-03	GOES-8	GOES-10
24/08/1998 20:10	30/08/1998 12:10	2.56E+00	5.49E-01	1.50E-01	4.19E-02	2.65E-02	GOES-8	GOES-10

Table A.17: SARG Event List - Fluences ($cm^{-2}MeV^{-1}$) Channels 1-5 [5].

Start Date and Time	End Date and Time	Channel 1	Channel 2	Channel 3	Channel 4	Channel 5	Primary S/C	Secondary S/C
24/09/1998 15:40	25/09/1998 10:55	2.11E+07	4.66E+06	1.02E+06	2.11E+05	5.18E+04	GOES-8	GOES-10
30/09/1998 11:40	03/10/1998 14:15	2.05E+08	1.05E+08	5.40E+07	2.75E+07	1.19E+07	GOES-8	GOES-10
06/11/1998 05:35	08/11/1998 14:50	2.40E+07	5.75E+06	1.44E+06	4.22E+05	1.40E+05	GOES-8	GOES-10
14/11/1998 04:45	17/11/1998 02:35	2.42E+07	1.54E+07	9.75E+06	6.06E+06	3.44E+06	GOES-8	GOES-10
21/01/1999 19:40	24/01/1999 12:50	1.20E+07	4.44E+06	1.69E+06	6.93E+05	2.89E+05	GOES-8	GOES-10
24/04/1999 13:40	26/04/1999 07:50	9.66E+06	4.60E+06	2.15E+06	9.24E+05	3.75E+05	GOES-8	GOES-10
05/05/1999 03:10	07/05/1999 15:40	2.35E+07	7.17E+06	2.11E+06	5.36E+05	1.55E+05	GOES-8	GOES-10
27/05/1999 09:35	27/05/1999 21:00	4.72E+05	2.91E+05	1.76E+05	9.92E+04	5.37E+04	GOES-8	GOES-10
01/06/1999 17:20	06/06/1999 20:00	3.83E+07	1.90E+07	9.36E+06	4.40E+06	1.90E+06	GOES-8	GOES-10
18/02/2000 07:40	18/02/2000 21:15	7.92E+05	4.99E+05	3.04E+05	1.62E+05	8.27E+04	GOES-8	GOES-10
04/04/2000 14:15	07/04/2000 01:25	5.87E+07	1.93E+07	5.95E+06	1.46E+06	3.70E+05	GOES-8	GOES-10
07/06/2000 01:00	09/06/2000 22:30	1.27E+08	3.71E+07	1.03E+07	2.39E+06	5.68E+05	GOES-8	GOES-10
10/06/2000 14:45	11/06/2000 23:45	7.30E+06	3.62E+06	1.83E+06	9.73E+05	4.80E+05	GOES-8	GOES-10
25/06/2000 18:55	26/06/2000 11:10	2.83E+06	8.15E+05	2.38E+05	7.25E+04	2.45E+04	GOES-8	GOES-10
13/07/2000 06:05	21/07/2000 12:25	1.77E+09	1.29E+09	9.46E+08	7.16E+08	4.75E+08	GOES-8	GOES-11
22/07/2000 10:10	23/07/2000 09:20	4.27E+06	1.80E+06	7.71E+05	3.48E+05	1.50E+05	GOES-8	GOES-11
28/07/2000 00:40	28/07/2000 19:00	1.53E+06	8.76E+05	4.80E+05	2.25E+05	9.72E+04	GOES-8	GOES-11
11/08/2000 12:50	11/08/2000 21:05	1.62E+06	5.49E+05	1.72E+05	4.11E+04	1.14E+04	GOES-8	GOES-11
12/08/2000 23:55	13/08/2000 12:55	4.31E+06	9.25E+05	1.96E+05	3.92E+04	9.94E+03	GOES-8	GOES-11
12/09/2000 12:00	18/09/2000 00:55	2.33E+08	9.39E+07	3.62E+07	1.18E+07	3.58E+06	GOES-8	GOES-11
16/10/2000 06:50	18/10/2000 03:35	4.22E+06	2.32E+06	1.27E+06	6.85E+05	3.43E+05	GOES-8	GOES-11
25/10/2000 11:10	27/10/2000 13:25	9.96E+06	3.94E+06	1.54E+06	5.75E+05	2.12E+05	GOES-8	GOES-10

Table A.18: SARG Event List - Fluences ($cm^{-2}MeV^{-1}$) Channels 6-10 [5].

Start Date and Time	End Date and Time	Channel 6	Channel 7	Channel 8	Channel 9	Channel 10	Primary S/C	Secondary S/C
24/09/1998 15:40	25/09/1998 10:55	2.61E+04	1.32E+04	7.06E+03	3.80E+03	2.76E+03	GOES-8	GOES-10
30/09/1998 11:40	03/10/1998 14:15	2.62E+06	5.78E+05	1.19E+05	2.47E+04	1.65E+04	GOES-8	GOES-10
06/11/1998 05:35	08/11/1998 14:50	7.63E+04	4.17E+04	2.24E+04	1.20E+04	8.88E+03	GOES-8	GOES-10
14/11/1998 04:45	17/11/1998 02:35	1.35E+06	5.27E+05	1.36E+05	3.38E+04	2.08E+04	GOES-8	GOES-10
21/01/1999 19:40	24/01/1999 12:50	1.29E+05	5.71E+04	2.68E+04	1.27E+04	9.19E+03	GOES-8	GOES-10
24/04/1999 13:40	26/04/1999 07:50	1.18E+05	3.74E+04	1.70E+04	7.93E+03	5.80E+03	GOES-8	GOES-10
05/05/1999 03:10	07/05/1999 15:40	7.64E+04	3.77E+04	2.08E+04	1.16E+04	8.47E+03	GOES-8	GOES-10
27/05/1999 09:35	27/05/1999 21:00	2.46E+04	1.13E+04	5.16E+03	2.37E+03	1.69E+03	GOES-8	GOES-10
01/06/1999 17:20	06/06/1999 20:00	5.67E+05	1.69E+05	6.60E+04	2.64E+04	1.88E+04	GOES-8	GOES-10
18/02/2000 07:40	18/02/2000 21:15	3.49E+04	1.47E+04	5.99E+03	2.44E+03	1.69E+03	GOES-8	GOES-10
04/04/2000 14:15	07/04/2000 01:25	1.05E+05	2.99E+04	1.51E+04	8.02E+03	5.81E+03	GOES-8	GOES-10
07/06/2000 01:00	09/06/2000 22:30	1.49E+05	3.93E+04	1.79E+04	8.56E+03	6.11E+03	GOES-8	GOES-10
10/06/2000 14:45	11/06/2000 23:45	1.71E+05	6.12E+04	1.93E+04	6.05E+03	3.98E+03	GOES-8	GOES-10
25/06/2000 18:55	26/06/2000 11:10	1.27E+04	6.59E+03	3.63E+03	2.01E+03	1.45E+03	GOES-8	GOES-10
13/07/2000 06:05	21/07/2000 12:25	1.81E+08	6.87E+07	1.25E+07	2.14E+06	1.13E+06	GOES-8	GOES-11
22/07/2000 10:10	23/07/2000 09:20	5.47E+04	1.99E+04	7.52E+03	2.86E+03	2.00E+03	GOES-8	GOES-11
28/07/2000 00:40	28/07/2000 19:00	3.00E+04	9.26E+03	4.35E+03	2.12E+03	1.52E+03	GOES-8	GOES-11
11/08/2000 12:50	11/08/2000 21:05	5.80E+03	2.96E+03	1.63E+03	9.04E+02	6.49E+02	GOES-8	GOES-11
12/08/2000 23:55	13/08/2000 12:55	6.75E+03	4.59E+03	2.55E+03	1.39E+03	9.97E+02	GOES-8	GOES-11
12/09/2000 12:00	18/09/2000 00:55	8.11E+05	1.83E+05	5.83E+04	1.91E+04	1.30E+04	GOES-8	GOES-11
16/10/2000 06:50	18/10/2000 03:35	1.27E+05	4.72E+04	1.72E+04	6.28E+03	4.37E+03	GOES-8	GOES-11
25/10/2000 11:10	27/10/2000 13:25	7.44E+04	2.61E+04	1.28E+04	6.42E+03	4.61E+03	GOES-8	GOES-10

Table A.19: SARG Event List - Peak Fluxes ($cm^{-2}ster^{-1}s^{-1}MeV^{-1}$) Channels 1-5 [5].

Start Date and Time	End Date and Time	Channel 1	Channel 2	Channel 3	Channel 4	Channel 5	Primary S/C	Secondary S/C
24/09/1998 15:40	25/09/1998 10:55	1.83E+02	4.04E+01	8.35E+00	1.37E+00	2.56E-01	GOES-8	GOES-10
30/09/1998 11:40	03/10/1998 14:15	3.24E+02	1.81E+02	1.02E+02	5.74E+01	2.79E+01	GOES-8	GOES-10
06/11/1998 05:35	08/11/1998 14:50	2.91E+01	7.62E+00	2.05E+00	6.07E-01	1.88E-01	GOES-8	GOES-10
14/11/1998 04:45	17/11/1998 02:35	5.70E+01	3.61E+01	2.26E+01	1.36E+01	7.58E+00	GOES-8	GOES-10
21/01/1999 19:40	24/01/1999 12:50	1.77E+01	6.20E+00	2.11E+00	6.45E-01	2.10E-01	GOES-8	GOES-10
24/04/1999 13:40	26/04/1999 07:50	1.75E+01	8.47E+00	3.94E+00	1.58E+00	5.86E-01	GOES-8	GOES-10
05/05/1999 03:10	07/05/1999 15:40	2.72E+01	7.96E+00	2.27E+00	5.98E-01	1.67E-01	GOES-8	GOES-10
27/05/1999 09:35	27/05/1999 21:00	2.12E+00	1.46E+00	9.58E-01	5.24E-01	2.68E-01	GOES-8	GOES-10
01/06/1999 17:20	06/06/1999 20:00	3.93E+01	1.77E+01	7.76E+00	3.08E+00	1.16E+00	GOES-8	GOES-10
18/02/2000 07:40	18/02/2000 21:15	4.23E+00	2.59E+00	1.50E+00	7.02E-01	3.25E-01	GOES-8	GOES-10
04/04/2000 14:15	07/04/2000 01:25	8.17E+01	2.92E+01	9.43E+00	2.11E+00	4.69E-01	GOES-8	GOES-10
07/06/2000 01:00	09/06/2000 22:30	2.37E+02	6.21E+01	1.55E+01	3.26E+00	6.71E-01	GOES-8	GOES-10
10/06/2000 14:45	11/06/2000 23:45	1.37E+01	7.39E+00	4.03E+00	2.26E+00	1.22E+00	GOES-8	GOES-10
25/06/2000 18:55	26/06/2000 11:10	8.47E+00	2.64E+00	7.86E-01	1.95E-01	5.52E-02	GOES-8	GOES-10
13/07/2000 06:05	21/07/2000 12:25	3.31E+03	2.10E+03	1.39E+03	1.08E+03	7.23E+02	GOES-8	GOES-11
22/07/2000 10:10	23/07/2000 09:20	1.13E+01	4.62E+00	1.97E+00	1.01E+00	4.88E-01	GOES-8	GOES-11
28/07/2000 00:40	28/07/2000 19:00	8.04E+00	4.15E+00	2.08E+00	9.30E-01	3.70E-01	GOES-8	GOES-11
11/08/2000 12:50	11/08/2000 21:05	3.02E+01	1.07E+01	3.26E+00	5.69E-01	1.14E-01	GOES-8	GOES-11
12/08/2000 23:55	13/08/2000 12:55	2.69E+01	5.80E+00	1.15E+00	1.71E-01	3.35E-02	GOES-8	GOES-11
12/09/2000 12:00	18/09/2000 00:55	2.41E+02	1.07E+02	4.45E+01	1.40E+01	3.88E+00	GOES-8	GOES-11
16/10/2000 06:50	18/10/2000 03:35	4.49E+00	2.64E+00	1.52E+00	8.13E-01	4.18E-01	GOES-8	GOES-11
25/10/2000 11:10	27/10/2000 13:25	1.35E+01	5.25E+00	2.02E+00	7.41E-01	2.64E-01	GOES-8	GOES-10

Table A.20: SARG Event List - Peak Fluxes ($cm^{-2}ster^{-1}s^{-1}MeV^{-1}$) Channels 6-10 [5].

Start Date and Time	End Date and Time	Channel 6	Channel 7	Channel 8	Channel 9	Channel 10	Primary S/C	Secondary S/C
24/09/1998 15:40	25/09/1998 10:55	8.02E-02	2.51E-02	1.23E-02	6.29E-03	4.50E-03	GOES-8	GOES-10
30/09/1998 11:40	03/10/1998 14:15	7.17E+00	1.84E+00	2.66E-01	3.66E-02	2.10E-02	GOES-8	GOES-10
06/11/1998 05:35	08/11/1998 14:50	7.09E-02	2.67E-02	1.30E-02	6.43E-03	4.59E-03	GOES-8	GOES-10
14/11/1998 04:45	17/11/1998 02:35	3.05E+00	1.22E+00	2.94E-01	6.77E-02	3.59E-02	GOES-8	GOES-10
21/01/1999 19:40	24/01/1999 12:50	8.82E-02	3.71E-02	1.53E-02	6.29E-03	4.43E-03	GOES-8	GOES-10
24/04/1999 13:40	26/04/1999 07:50	1.55E-01	4.10E-02	1.61E-02	6.51E-03	4.52E-03	GOES-8	GOES-10
05/05/1999 03:10	07/05/1999 15:40	6.12E-02	2.24E-02	1.18E-02	6.43E-03	4.47E-03	GOES-8	GOES-10
27/05/1999 09:35	27/05/1999 21:00	1.04E-01	4.02E-02	1.59E-02	6.29E-03	4.44E-03	GOES-8	GOES-10
01/06/1999 17:20	06/06/1999 20:00	3.56E-01	1.09E-01	3.40E-02	1.07E-02	6.92E-03	GOES-8	GOES-10
18/02/2000 07:40	18/02/2000 21:15	1.43E-01	6.25E-02	2.16E-02	7.32E-03	4.56E-03	GOES-8	GOES-10
04/04/2000 14:15	07/04/2000 01:25	1.01E-01	2.17E-02	9.42E-03	4.34E-03	3.14E-03	GOES-8	GOES-10
07/06/2000 01:00	09/06/2000 22:30	1.28E-01	2.43E-02	1.01E-02	4.49E-03	3.10E-03	GOES-8	GOES-10
10/06/2000 14:45	11/06/2000 23:45	5.55E-01	2.53E-01	7.09E-02	1.92E-02	1.10E-02	GOES-8	GOES-10
25/06/2000 18:55	26/06/2000 11:10	2.76E-02	1.38E-02	7.57E-03	4.19E-03	2.92E-03	GOES-8	GOES-10
13/07/2000 06:05	21/07/2000 12:25	2.60E+02	9.33E+01	2.05E+01	4.34E+00	2.60E+00	GOES-8	GOES-11
22/07/2000 10:10	23/07/2000 09:20	1.95E-01	7.76E-02	2.22E-02	6.20E-03	4.10E-03	GOES-8	GOES-11
28/07/2000 00:40	28/07/2000 19:00	8.92E-02	2.15E-02	9.50E-03	4.42E-03	2.95E-03	GOES-8	GOES-11
11/08/2000 12:50	11/08/2000 21:05	4.02E-02	1.42E-02	7.25E-03	3.83E-03	2.69E-03	GOES-8	GOES-11
12/08/2000 23:55	13/08/2000 12:55	2.13E-02	1.36E-02	6.82E-03	3.37E-03	2.45E-03	GOES-8	GOES-11
12/09/2000 12:00	18/09/2000 00:55	6.49E-01	1.08E-01	2.71E-02	7.02E-03	4.31E-03	GOES-8	GOES-11
16/10/2000 06:50	18/10/2000 03:35	1.82E-01	7.95E-02	2.20E-02	5.85E-03	3.66E-03	GOES-8	GOES-11
25/10/2000 11:10	27/10/2000 13:25	8.25E-02	2.58E-02	1.05E-02	4.42E-03	3.12E-03	GOES-8	GOES-10

Table A.21: SARG Event List - Fluences ($cm^{-2}MeV^{-1}$) Channels 1-5 [6].

Start Date and Time	End Date and Time	Channel 1	Channel 2	Channel 3	Channel 4	Channel 5	Primary S/C	Secondary S/C
31/10/2000 04:35	01/11/2000 19:25	4.23E+06	1.51E+06	5.34E+05	1.78E+05	6.41E+04	GOES-8	GOES-11
08/11/2000 20:50	14/11/2000 10:35	1.29E+09	9.44E+08	6.81E+08	4.69E+08	2.94E+08	GOES-8	GOES-11
24/11/2000 03:10	02/12/2000 16:35	2.07E+08	1.06E+08	5.22E+07	2.31E+07	9.25E+06	GOES-8	GOES-11
28/01/2001 16:10	30/01/2001 16:15	3.71E+07	1.15E+07	3.79E+06	1.55E+06	6.03E+05	GOES-8	GOES-11
27/03/2001 03:15	27/03/2001 21:55	6.47E+06	1.48E+06	3.42E+05	7.99E+04	2.24E+04	GOES-8	GOES-11
29/03/2001 10:15	01/04/2001 06:10	2.72E+07	1.11E+07	4.64E+06	2.08E+06	8.54E+05	GOES-8	GOES-11
02/04/2001 20:15	08/04/2001 16:00	1.76E+08	9.55E+07	5.27E+07	3.05E+07	1.55E+07	GOES-8	GOES-11
10/04/2001 02:00	14/04/2001 14:20	1.79E+08	7.03E+07	2.83E+07	1.25E+07	5.06E+06	GOES-8	GOES-11
15/04/2001 11:10	21/04/2001 05:45	1.63E+08	9.62E+07	5.61E+07	3.11E+07	1.64E+07	GOES-8	GOES-11
27/04/2001 11:15	28/04/2001 20:05	1.88E+07	4.11E+06	9.02E+05	1.97E+05	5.10E+04	GOES-8	GOES-11
07/05/2001 10:35	09/05/2001 08:25	1.62E+07	7.31E+06	3.13E+06	1.10E+06	3.66E+05	GOES-8	GOES-11
20/05/2001 05:20	20/05/2001 20:35	2.87E+05	2.37E+05	1.87E+05	1.24E+05	7.83E+04	GOES-8	GOES-11
15/06/2001 14:20	17/06/2001 21:05	1.21E+07	5.69E+06	2.59E+06	1.05E+06	4.11E+05	GOES-8	GOES-11
09/08/2001 18:35	11/08/2001 09:00	1.20E+07	3.55E+06	1.06E+06	3.19E+05	1.03E+05	GOES-8	GOES-11
15/08/2001 22:20	20/08/2001 12:50	2.96E+07	2.21E+07	1.63E+07	1.15E+07	7.48E+06	GOES-8	GOES-11
21/08/2001 12:45	22/08/2001 01:30	9.43E+05	4.20E+05	1.96E+05	1.09E+05	5.76E+04	GOES-8	GOES-11
15/09/2001 10:20	16/09/2001 03:40	1.63E+06	7.38E+05	3.32E+05	1.47E+05	6.36E+04	GOES-8	GOES-10
24/09/2001 08:15	09/10/2001 08:55	1.88E+09	1.11E+09	6.52E+08	3.84E+08	2.00E+08	GOES-8	GOES-10
09/10/2001 19:05	11/10/2001 04:00	5.13E+06	1.77E+06	6.04E+05	2.03E+05	7.21E+04	GOES-8	GOES-10
18/10/2001 22:10	21/10/2001 09:45	6.12E+06	2.67E+06	1.19E+06	5.78E+05	2.74E+05	GOES-8	GOES-10
22/10/2001 13:30	23/10/2001 20:05	4.52E+06	1.93E+06	8.52E+05	4.26E+05	2.15E+05	GOES-8	GOES-10
04/11/2001 14:05	11/11/2001 14:30	2.01E+09	1.41E+09	9.78E+08	6.55E+08	3.91E+08	GOES-8	GOES-10

Table A.22: SARG Event List - Fluences ($cm^{-2}MeV^{-1}$) Channels 6-10 [6].

Start Date and Time	End Date and Time	Channel 6	Channel 7	Channel 8	Channel 9	Channel 10	Primary S/C	Secondary S/C
31/10/2000 04:35	01/11/2000 19:25	3.14E+04	1.53E+04	8.32E+03	4.56E+03	3.26E+03	GOES-8	GOES-11
08/11/2000 20:50	14/11/2000 10:35	1.26E+08	5.39E+07	1.04E+07	1.89E+06	8.59E+05	GOES-8	GOES-11
24/11/2000 03:10	02/12/2000 16:35	2.48E+06	6.64E+05	1.49E+05	3.28E+04	2.17E+04	GOES-8	GOES-11
28/01/2001 16:10	30/01/2001 16:15	1.96E+05	6.35E+04	2.06E+04	6.71E+03	4.63E+03	GOES-8	GOES-11
27/03/2001 03:15	27/03/2001 21:55	1.34E+04	8.00E+03	4.43E+03	2.44E+03	1.75E+03	GOES-8	GOES-11
29/03/2001 10:15	01/04/2001 06:10	2.46E+05	7.10E+04	2.53E+04	9.16E+03	6.44E+03	GOES-8	GOES-11
02/04/2001 20:15	08/04/2001 16:00	4.64E+06	1.38E+06	2.62E+05	4.79E+04	2.82E+04	GOES-8	GOES-11
10/04/2001 02:00	14/04/2001 14:20	1.39E+06	3.81E+05	9.28E+04	2.25E+04	1.46E+04	GOES-8	GOES-11
15/04/2001 11:10	21/04/2001 05:45	6.94E+06	2.93E+06	1.08E+06	3.95E+05	2.58E+05	GOES-8	GOES-11
27/04/2001 11:15	28/04/2001 20:05	2.65E+04	1.38E+04	7.64E+03	4.25E+03	3.04E+03	GOES-8	GOES-11
07/05/2001 10:35	09/05/2001 08:25	9.84E+04	2.64E+04	1.23E+04	5.97E+03	4.28E+03	GOES-8	GOES-11
20/05/2001 05:20	20/05/2001 20:35	4.17E+04	2.22E+04	9.34E+03	3.86E+03	2.63E+03	GOES-8	GOES-11
15/06/2001 14:20	17/06/2001 21:05	1.36E+05	4.52E+04	1.87E+04	7.84E+03	5.52E+03	GOES-8	GOES-11
09/08/2001 18:35	11/08/2001 09:00	4.29E+04	1.79E+04	9.51E+03	5.17E+03	3.71E+03	GOES-8	GOES-11
15/08/2001 22:20	20/08/2001 12:50	3.53E+06	1.67E+06	4.38E+05	1.10E+05	6.08E+04	GOES-8	GOES-11
21/08/2001 12:45	22/08/2001 01:30	2.51E+04	1.10E+04	4.57E+03	1.90E+03	1.33E+03	GOES-8	GOES-11
15/09/2001 10:20	16/09/2001 03:40	2.52E+04	1.00E+04	4.83E+03	2.37E+03	1.68E+03	GOES-8	GOES-10
24/09/2001 08:15	09/10/2001 08:55	6.16E+07	1.90E+07	2.77E+06	3.80E+05	1.85E+05	GOES-8	GOES-10
09/10/2001 19:05	11/10/2001 04:00	3.29E+04	1.50E+04	7.84E+03	4.14E+03	3.00E+03	GOES-8	GOES-10
18/10/2001 22:10	21/10/2001 09:45	1.16E+05	4.91E+04	2.10E+04	8.97E+03	6.28E+03	GOES-8	GOES-10
22/10/2001 13:30	23/10/2001 20:05	1.12E+05	5.84E+04	2.30E+04	8.90E+03	5.90E+03	GOES-8	GOES-10
04/11/2001 14:05	11/11/2001 14:30	1.44E+08	5.29E+07	7.91E+06	1.10E+06	5.28E+05	GOES-8	GOES-10

Table A.23: SARG Event List - Peak Fluxes ($cm^{-2}ster^{-1}s^{-1}MeV^{-1}$) Channels 1-5 [6].

Start Date and Time	End Date and Time	Channel 1	Channel 2	Channel 3	Channel 4	Channel 5	Primary S/C	Secondary S/C
31/10/2000 04:35	01/11/2000 19:25	6.17E+00	2.21E+00	7.53E-01	2.14E-01	6.70E-02	GOES-8	GOES-11
08/11/2000 20:50	14/11/2000 10:35	1.52E+03	1.15E+03	8.73E+02	6.58E+02	4.45E+02	GOES-8	GOES-11
24/11/2000 03:10	02/12/2000 16:35	3.53E+02	1.90E+02	9.92E+01	4.61E+01	1.91E+01	GOES-8	GOES-11
28/01/2001 16:10	30/01/2001 16:15	6.50E+01	1.87E+01	5.75E+00	2.26E+00	8.68E-01	GOES-8	GOES-11
27/03/2001 03:15	27/03/2001 21:55	3.93E+01	7.41E+00	1.38E+00	2.48E-01	5.51E-02	GOES-8	GOES-11
29/03/2001 10:15	01/04/2001 06:10	4.37E+01	1.38E+01	4.61E+00	1.94E+00	7.63E-01	GOES-8	GOES-11
02/04/2001 20:15	08/04/2001 16:00	1.40E+02	9.34E+01	6.49E+01	5.17E+01	3.40E+01	GOES-8	GOES-11
10/04/2001 02:00	14/04/2001 14:20	3.02E+02	1.20E+02	4.63E+01	1.60E+01	5.04E+00	GOES-8	GOES-11
15/04/2001 11:10	21/04/2001 05:45	1.67E+02	9.92E+01	6.09E+01	4.15E+01	2.66E+01	GOES-8	GOES-11
27/04/2001 11:15	28/04/2001 20:05	1.58E+02	3.76E+01	7.58E+00	8.27E-01	1.15E-01	GOES-8	GOES-11
07/05/2001 10:35	09/05/2001 08:25	1.97E+01	9.53E+00	4.34E+00	1.60E+00	5.39E-01	GOES-8	GOES-11
20/05/2001 05:20	20/05/2001 20:35	1.11E+00	8.71E-01	6.62E-01	4.43E-01	2.77E-01	GOES-8	GOES-11
15/06/2001 14:20	17/06/2001 21:05	1.74E+01	8.01E+00	3.59E+00	1.47E+00	5.94E-01	GOES-8	GOES-11
09/08/2001 18:35	11/08/2001 09:00	2.07E+01	7.24E+00	2.48E+00	7.84E-01	2.42E-01	GOES-8	GOES-11
15/08/2001 22:20	20/08/2001 12:50	2.70E+01	2.63E+01	2.44E+01	1.86E+01	1.38E+01	GOES-8	GOES-11
21/08/2001 12:45	22/08/2001 01:30	3.92E+00	1.47E+00	5.88E-01	2.97E-01	1.45E-01	GOES-8	GOES-11
15/09/2001 10:20	16/09/2001 03:40	4.66E+00	2.49E+00	1.30E+00	6.23E-01	2.73E-01	GOES-8	GOES-10
24/09/2001 08:15	09/10/2001 08:55	3.99E+03	2.22E+03	1.21E+03	6.07E+02	2.68E+02	GOES-8	GOES-10
09/10/2001 19:05	11/10/2001 04:00	7.59E+00	2.60E+00	8.64E-01	2.57E-01	8.29E-02	GOES-8	GOES-10
18/10/2001 22:10	21/10/2001 09:45	9.18E+00	3.30E+00	1.26E+00	5.83E-01	2.68E-01	GOES-8	GOES-10
22/10/2001 13:30	23/10/2001 20:05	1.56E+01	6.63E+00	2.77E+00	1.10E+00	4.43E-01	GOES-8	GOES-10
04/11/2001 14:05	11/11/2001 14:30	5.21E+03	3.38E+03	2.18E+03	1.36E+03	7.73E+02	GOES-8	GOES-10

Table A.24: SARG Event List - Peak Fluxes ($cm^{-2}ster^{-1}s^{-1}MeV^{-1}$) Channels 6-10 [6].

Start Date and Time	End Date and Time	Channel 6	Channel 7	Channel 8	Channel 9	Channel 10	Primary S/C	Secondary S/C
31/10/2000 04:35	01/11/2000 19:25	3.18E-02	1.51E-02	7.65E-03	3.89E-03	2.78E-03	GOES-8	GOES-11
08/11/2000 20:50	14/11/2000 10:35	1.91E+02	8.17E+01	1.81E+01	3.79E+00	1.72E+00	GOES-8	GOES-11
24/11/2000 03:10	02/12/2000 16:35	4.85E+00	1.23E+00	1.54E-01	1.83E-02	1.01E-02	GOES-8	GOES-11
28/01/2001 16:10	30/01/2001 16:15	3.08E-01	1.09E-01	2.48E-02	5.45E-03	3.62E-03	GOES-8	GOES-11
27/03/2001 03:15	27/03/2001 21:55	3.06E-02	1.69E-02	8.73E-03	4.48E-03	3.00E-03	GOES-8	GOES-11
29/03/2001 10:15	01/04/2001 06:10	2.26E-01	6.70E-02	1.91E-02	5.45E-03	3.59E-03	GOES-8	GOES-11
02/04/2001 20:15	08/04/2001 16:00	9.97E+00	2.92E+00	4.28E-01	5.95E-02	3.05E-02	GOES-8	GOES-11
10/04/2001 02:00	14/04/2001 14:20	1.08E+00	2.31E-01	6.38E-02	1.81E-02	1.08E-02	GOES-8	GOES-11
15/04/2001 11:10	21/04/2001 05:45	1.34E+01	6.78E+00	3.16E+00	1.47E+00	1.03E+00	GOES-8	GOES-11
27/04/2001 11:15	28/04/2001 20:05	4.37E-02	1.67E-02	8.48E-03	4.42E-03	3.15E-03	GOES-8	GOES-11
07/05/2001 10:35	09/05/2001 08:25	1.27E-01	3.02E-02	1.12E-02	4.34E-03	3.06E-03	GOES-8	GOES-11
20/05/2001 05:20	20/05/2001 20:35	1.30E-01	6.05E-02	2.42E-02	9.56E-03	6.24E-03	GOES-8	GOES-11
15/06/2001 14:20	17/06/2001 21:05	2.28E-01	8.77E-02	2.32E-02	5.97E-03	3.83E-03	GOES-8	GOES-11
09/08/2001 18:35	11/08/2001 09:00	6.86E-02	1.94E-02	9.13E-03	4.49E-03	3.07E-03	GOES-8	GOES-11
15/08/2001 22:20	20/08/2001 12:50	9.10E+00	5.98E+00	1.44E+00	3.19E-01	1.63E-01	GOES-8	GOES-11
21/08/2001 12:45	22/08/2001 01:30	6.25E-02	2.69E-02	1.10E-02	4.49E-03	3.17E-03	GOES-8	GOES-11
15/09/2001 10:20	16/09/2001 03:40	8.21E-02	2.47E-02	1.07E-02	4.78E-03	3.21E-03	GOES-8	GOES-10
24/09/2001 08:15	09/10/2001 08:55	6.88E+01	1.76E+01	2.52E+00	3.43E-01	1.57E-01	GOES-8	GOES-10
09/10/2001 19:05	11/10/2001 04:00	3.70E-02	1.65E-02	8.40E-03	4.34E-03	2.98E-03	GOES-8	GOES-10
18/10/2001 22:10	21/10/2001 09:45	1.17E-01	5.13E-02	1.75E-02	5.82E-03	3.85E-03	GOES-8	GOES-10
22/10/2001 13:30	23/10/2001 20:05	1.97E-01	8.73E-02	3.22E-02	1.17E-02	7.74E-03	GOES-8	GOES-10
04/11/2001 14:05	11/11/2001 14:30	2.88E+02	1.07E+02	1.76E+01	2.72E+00	1.27E+00	GOES-8	GOES-10

Table A.25: SARG Event List - Fluences ($cm^{-2}MeV^{-1}$) Channels 1-5 [7].

Start Date and Time	End Date and Time	Channel 1	Channel 2	Channel 3	Channel 4	Channel 5	Primary S/C	Secondary S/C
17/11/2001 21:25	22/11/2001 12:25	6.91E+07	2.08E+07	5.85E+06	1.29E+06	3.20E+05	GOES-8	GOES-10
22/11/2001 19:10	29/11/2001 12:55	1.83E+09	1.15E+09	7.03E+08	3.91E+08	1.85E+08	GOES-8	GOES-10
26/12/2001 03:05	07/01/2002 11:30	2.16E+08	1.20E+08	6.43E+07	2.98E+07	1.31E+07	GOES-8	GOES-10
10/01/2002 02:05	18/01/2002 23:10	8.75E+07	4.16E+07	1.86E+07	6.67E+06	2.25E+06	GOES-8	GOES-10
27/01/2002 12:15	28/01/2002 01:20	4.82E+05	3.15E+05	1.98E+05	1.05E+05	5.34E+04	GOES-8	GOES-10
20/02/2002 04:20	20/02/2002 13:10	3.49E+05	2.14E+05	1.28E+05	6.91E+04	3.52E+04	GOES-8	GOES-10
16/03/2002 05:20	21/03/2002 18:35	1.07E+08	2.85E+07	7.79E+06	2.32E+06	7.07E+05	GOES-8	GOES-10
22/03/2002 10:40	24/03/2002 06:15	2.89E+07	8.45E+06	2.25E+06	4.26E+05	9.47E+04	GOES-8	GOES-10
17/04/2002 08:50	20/04/2002 05:05	2.25E+07	6.39E+06	1.86E+06	5.87E+05	1.95E+05	GOES-8	GOES-10
22/05/2002 06:20	25/05/2002 02:45	1.19E+08	4.22E+07	1.47E+07	4.97E+06	1.54E+06	GOES-8	GOES-10
07/07/2002 11:15	08/07/2002 20:05	2.46E+06	1.57E+06	9.92E+05	5.90E+05	3.12E+05	GOES-8	GOES-10
16/07/2002 09:30	20/07/2002 07:55	1.52E+08	5.08E+07	1.66E+07	4.92E+06	1.41E+06	GOES-8	GOES-10
20/07/2002 10:55	30/07/2002 16:10	4.90E+07	2.41E+07	1.17E+07	5.38E+06	2.27E+06	GOES-8	GOES-10
14/08/2002 02:20	15/08/2002 16:35	1.41E+07	4.57E+06	1.40E+06	3.58E+05	1.00E+05	GOES-8	GOES-10
17/08/2002 00:55	18/08/2002 09:45	6.16E+06	1.96E+06	6.15E+05	1.81E+05	5.87E+04	GOES-8	GOES-10
19/08/2002 00:30	19/08/2002 16:00	2.67E+06	7.36E+05	2.19E+05	8.57E+04	3.47E+04	GOES-8	GOES-10
22/08/2002 00:45	23/08/2002 07:50	3.44E+06	2.18E+06	1.36E+06	8.27E+05	4.68E+05	GOES-8	GOES-10
23/08/2002 22:35	27/08/2002 07:30	1.04E+08	5.69E+07	3.05E+07	1.50E+07	6.84E+06	GOES-8	GOES-10
06/09/2002 01:55	08/09/2002 19:50	3.47E+07	1.27E+07	4.61E+06	1.61E+06	5.33E+05	GOES-8	GOES-10
09/11/2002 13:30	11/11/2002 18:55	6.95E+07	3.55E+07	1.72E+07	6.94E+06	2.39E+06	GOES-8	GOES-10
27/11/2002 00:10	27/11/2002 08:35	2.98E+06	5.19E+05	9.43E+04	1.99E+04	5.42E+03	GOES-8	GOES-10
28/05/2003 01:35	31/05/2003 23:55	6.42E+07	2.07E+07	6.81E+06	2.44E+06	8.58E+05	GOES-8	GOES-10

Table A.26: SARG Event List - Fluences ($cm^{-2}MeV^{-1}$) Channels 6-10 [7].

Start Date and Time	End Date and Time	Channel 6	Channel 7	Channel 8	Channel 9	Channel 10	Primary S/C	Secondary S/C
17/11/2001 21:25	22/11/2001 12:25	1.30E+05	5.28E+04	2.76E+04	1.47E+04	1.06E+04	GOES-8	GOES-10
22/11/2001 19:10	29/11/2001 12:55	4.50E+07	1.09E+07	9.19E+05	7.10E+04	3.88E+04	GOES-8	GOES-10
26/12/2001 03:05	07/01/2002 11:30	4.58E+06	1.60E+06	4.39E+05	1.18E+05	7.34E+04	GOES-8	GOES-10
10/01/2002 02:05	18/01/2002 23:10	5.96E+05	1.57E+05	6.37E+04	2.68E+04	1.92E+04	GOES-8	GOES-10
27/01/2002 12:15	28/01/2002 01:20	2.20E+04	9.04E+03	4.02E+03	1.81E+03	1.29E+03	GOES-8	GOES-10
20/02/2002 04:20	20/02/2002 13:10	1.43E+04	5.77E+03	2.66E+03	1.24E+03	8.96E+02	GOES-8	GOES-10
16/03/2002 05:20	21/03/2002 18:35	2.33E+05	7.71E+04	3.66E+04	1.79E+04	1.29E+04	GOES-8	GOES-10
22/03/2002 10:40	24/03/2002 06:15	4.15E+04	1.82E+04	9.85E+03	5.44E+03	3.93E+03	GOES-8	GOES-10
17/04/2002 08:50	20/04/2002 05:05	8.10E+04	3.36E+04	1.70E+04	8.73E+03	6.29E+03	GOES-8	GOES-10
22/05/2002 06:20	25/05/2002 02:45	3.43E+05	7.61E+04	2.56E+04	8.92E+03	6.40E+03	GOES-8	GOES-10
07/07/2002 11:15	08/07/2002 20:05	1.00E+05	3.22E+04	1.21E+04	4.61E+03	3.28E+03	GOES-8	GOES-10
16/07/2002 09:30	20/07/2002 07:55	3.44E+05	8.42E+04	3.33E+04	1.38E+04	9.82E+03	GOES-8	GOES-10
20/07/2002 10:55	30/07/2002 16:10	6.61E+05	1.92E+05	7.75E+04	3.21E+04	2.30E+04	GOES-8	GOES-10
14/08/2002 02:20	15/08/2002 16:35	4.20E+04	1.76E+04	9.38E+03	5.12E+03	3.69E+03	GOES-8	GOES-10
17/08/2002 00:55	18/08/2002 09:45	2.93E+04	1.46E+04	7.97E+03	4.38E+03	3.14E+03	GOES-8	GOES-10
19/08/2002 00:30	19/08/2002 16:00	1.62E+04	7.56E+03	3.86E+03	1.98E+03	1.43E+03	GOES-8	GOES-10
22/08/2002 00:45	23/08/2002 07:50	2.01E+05	8.61E+04	2.78E+04	8.76E+03	5.60E+03	GOES-8	GOES-10
23/08/2002 22:35	27/08/2002 07:30	2.27E+06	7.51E+05	2.21E+05	6.44E+04	3.93E+04	GOES-8	GOES-10
06/09/2002 01:55	08/09/2002 19:50	1.43E+05	3.84E+04	1.78E+04	8.61E+03	6.18E+03	GOES-8	GOES-10
09/11/2002 13:30	11/11/2002 18:55	4.24E+05	7.53E+04	2.25E+04	7.06E+03	5.08E+03	GOES-8	GOES-10
27/11/2002 00:10	27/11/2002 08:35	4.38E+03	3.54E+03	1.97E+03	1.06E+03	7.63E+02	GOES-8	GOES-10
28/05/2003 01:35	31/05/2003 23:55	2.81E+05	9.21E+04	3.64E+04	1.46E+04	1.01E+04	GOES-8	GOES-10

Table A.27: SARG Event List - Peak Fluxes ($cm^{-2}ster^{-1}s^{-1}MeV^{-1}$) Channels 1-5 [7].

Start Date and Time	End Date and Time	Channel 1	Channel 2	Channel 3	Channel 4	Channel 5	Primary S/C	Secondary S/C
17/11/2001 21:25	22/11/2001 12:25	7.42E+01	2.55E+01	7.21E+00	1.01E+00	1.70E-01	GOES-8	GOES-10
22/11/2001 19:10	29/11/2001 12:55	7.77E+03	3.87E+03	1.91E+03	9.12E+02	3.64E+02	GOES-8	GOES-10
26/12/2001 03:05	07/01/2002 11:30	9.64E+01	7.32E+01	5.34E+01	3.39E+01	2.10E+01	GOES-8	GOES-10
10/01/2002 02:05	18/01/2002 23:10	5.64E+01	2.65E+01	1.18E+01	4.33E+00	1.38E+00	GOES-8	GOES-10
27/01/2002 12:15	28/01/2002 01:20	1.74E+00	1.27E+00	8.80E-01	4.84E-01	2.50E-01	GOES-8	GOES-10
20/02/2002 04:20	20/02/2002 13:10	2.57E+00	2.44E+00	2.01E+00	9.96E-01	4.40E-01	GOES-8	GOES-10
16/03/2002 05:20	21/03/2002 18:35	9.35E+01	2.46E+01	6.97E+00	2.55E+00	8.37E-01	GOES-8	GOES-10
22/03/2002 10:40	24/03/2002 06:15	4.60E+01	1.28E+01	3.22E+00	5.80E-01	1.20E-01	GOES-8	GOES-10
17/04/2002 08:50	20/04/2002 05:05	3.22E+01	9.70E+00	3.04E+00	1.11E+00	3.78E-01	GOES-8	GOES-10
22/05/2002 06:20	25/05/2002 02:45	1.55E+03	4.52E+02	1.28E+02	3.28E+01	7.22E+00	GOES-8	GOES-10
07/07/2002 11:15	08/07/2002 20:05	4.90E+00	3.35E+00	2.19E+00	1.20E+00	5.85E-01	GOES-8	GOES-10
16/07/2002 09:30	20/07/2002 07:55	4.37E+02	1.29E+02	3.69E+01	9.26E+00	2.18E+00	GOES-8	GOES-10
20/07/2002 10:55	30/07/2002 16:10	1.17E+01	5.91E+00	2.96E+00	1.40E+00	5.97E-01	GOES-8	GOES-10
14/08/2002 02:20	15/08/2002 16:35	4.63E+01	1.58E+01	4.94E+00	1.14E+00	2.69E-01	GOES-8	GOES-10
17/08/2002 00:55	18/08/2002 09:45	6.89E+00	2.41E+00	8.27E-01	2.60E-01	8.67E-02	GOES-8	GOES-10
19/08/2002 00:30	19/08/2002 16:00	9.60E+00	2.38E+00	6.42E-01	2.38E-01	9.16E-02	GOES-8	GOES-10
22/08/2002 00:45	23/08/2002 07:50	1.03E+01	5.64E+00	3.09E+00	1.69E+00	9.09E-01	GOES-8	GOES-10
23/08/2002 22:35	27/08/2002 07:30	1.23E+02	5.93E+01	2.93E+01	1.63E+01	8.92E+00	GOES-8	GOES-10
06/09/2002 01:55	08/09/2002 19:50	2.50E+02	8.64E+01	2.93E+01	9.13E+00	2.40E+00	GOES-8	GOES-10
09/11/2002 13:30	11/11/2002 18:55	2.04E+02	1.03E+02	4.94E+01	1.94E+01	6.28E+00	GOES-8	GOES-10
27/11/2002 00:10	27/11/2002 08:35	1.68E+01	3.02E+00	5.62E-01	1.20E-01	3.24E-02	GOES-8	GOES-10
28/05/2003 01:35	31/05/2003 23:55	1.55E+02	5.19E+01	1.71E+01	5.35E+00	1.63E+00	GOES-8	GOES-10

Table A.28: SARG Event List - Peak Fluxes ($cm^{-2}ster^{-1}s^{-1}MeV^{-1}$) Channels 6-10 [7].

Start Date and Time	End Date and Time	Channel 6	Channel 7	Channel 8	Channel 9	Channel 10	Primary S/C	Secondary S/C
17/11/2001 21:25	22/11/2001 12:25	6.27E-02	2.31E-02	1.00E-02	4.42E-03	3.10E-03	GOES-8	GOES-10
22/11/2001 19:10	29/11/2001 12:55	6.87E+01	1.30E+01	8.75E-01	5.46E-02	2.59E-02	GOES-8	GOES-10
26/12/2001 03:05	07/01/2002 11:30	1.16E+01	6.40E+00	1.86E+00	5.14E-01	2.96E-01	GOES-8	GOES-10
10/01/2002 02:05	18/01/2002 23:10	2.50E-01	4.51E-02	1.37E-02	4.34E-03	3.10E-03	GOES-8	GOES-10
27/01/2002 12:15	28/01/2002 01:20	9.84E-02	3.88E-02	1.33E-02	4.49E-03	3.09E-03	GOES-8	GOES-10
20/02/2002 04:20	20/02/2002 13:10	1.21E-01	3.33E-02	1.15E-02	4.04E-03	3.02E-03	GOES-8	GOES-10
16/03/2002 05:20	21/03/2002 18:35	1.76E-01	3.70E-02	1.35E-02	5.15E-03	3.47E-03	GOES-8	GOES-10
22/03/2002 10:40	24/03/2002 06:15	4.48E-02	1.67E-02	8.40E-03	4.34E-03	2.98E-03	GOES-8	GOES-10
17/04/2002 08:50	20/04/2002 05:05	1.00E-01	2.65E-02	1.06E-02	4.42E-03	3.12E-03	GOES-8	GOES-10
22/05/2002 06:20	25/05/2002 02:45	8.47E-01	9.93E-02	2.12E-02	4.78E-03	3.30E-03	GOES-8	GOES-10
07/07/2002 11:15	08/07/2002 20:05	1.73E-01	5.11E-02	1.58E-02	4.91E-03	3.29E-03	GOES-8	GOES-10
16/07/2002 09:30	20/07/2002 07:55	3.89E-01	6.94E-02	1.88E-02	5.27E-03	3.62E-03	GOES-8	GOES-10
20/07/2002 10:55	30/07/2002 16:10	1.66E-01	4.62E-02	1.49E-02	4.85E-03	3.39E-03	GOES-8	GOES-10
14/08/2002 02:20	15/08/2002 16:35	7.23E-02	1.95E-02	8.83E-03	4.19E-03	2.99E-03	GOES-8	GOES-10
17/08/2002 00:55	18/08/2002 09:45	3.74E-02	1.61E-02	8.43E-03	4.49E-03	3.17E-03	GOES-8	GOES-10
19/08/2002 00:30	19/08/2002 16:00	4.09E-02	1.83E-02	8.87E-03	4.34E-03	2.94E-03	GOES-8	GOES-10
22/08/2002 00:45	23/08/2002 07:50	4.51E-01	2.24E-01	6.78E-02	1.98E-02	1.17E-02	GOES-8	GOES-10
23/08/2002 22:35	27/08/2002 07:30	4.67E+00	2.45E+00	8.78E-01	3.06E-01	1.89E-01	GOES-8	GOES-10
06/09/2002 01:55	08/09/2002 19:50	3.07E-01	3.93E-02	1.27E-02	4.42E-03	3.09E-03	GOES-8	GOES-10
09/11/2002 13:30	11/11/2002 18:55	8.80E-01	1.23E-01	2.36E-02	4.65E-03	3.31E-03	GOES-8	GOES-10
27/11/2002 00:10	27/11/2002 08:35	2.29E-02	1.62E-02	8.56E-03	4.42E-03	3.00E-03	GOES-8	GOES-10
28/05/2003 01:35	31/05/2003 23:55	4.47E-01	1.23E-01	3.76E-02	1.17E-02	7.11E-03	GOES-8	GOES-10

Table A.29: SARG Event List - Fluences ($cm^{-2}MeV^{-1}$) Channels 1-5 [8].

Start Date and Time	End Date and Time	Channel 1	Channel 2	Channel 3	Channel 4	Channel 5	Primary S/C	Secondary S/C
18/06/2003 07:00	20/06/2003 23:55	1.69E+07	6.41E+06	2.39E+06	8.36E+05	2.92E+05	GOES-10	GOES-11
24/10/2003 03:35	24/10/2003 17:55	1.01E+07	1.19E+06	1.68E+05	4.47E+04	1.42E+04	GOES-11	GOES-10
26/10/2003 15:15	08/11/2003 18:20	3.37E+09	2.13E+09	1.35E+09	8.58E+08	4.89E+08	GOES-11	GOES-10
20/11/2003 07:40	20/11/2003 22:05	2.34E+06	7.40E+05	2.51E+05	1.09E+05	4.69E+04	GOES-11	GOES-10
21/11/2003 03:40	25/11/2003 04:00	2.60E+07	9.86E+06	3.75E+06	1.45E+06	5.24E+05	GOES-11	GOES-10
02/12/2003 10:25	04/12/2003 21:55	4.55E+07	1.82E+07	7.16E+06	2.68E+06	8.78E+05	GOES-11	GOES-10
11/04/2004 03:50	12/04/2004 19:25	3.31E+07	1.06E+07	3.37E+06	1.06E+06	3.27E+05	GOES-11	GOES-10
23/07/2004 21:05	24/07/2004 12:25	1.84E+06	5.90E+05	2.05E+05	9.52E+04	4.46E+04	GOES-11	GOES-10
25/07/2004 14:40	28/07/2004 19:00	1.40E+08	5.51E+07	2.18E+07	8.85E+06	3.07E+06	GOES-11	GOES-10
01/08/2004 14:10	02/08/2004 09:55	1.42E+06	6.98E+05	3.42E+05	1.63E+05	7.51E+04	GOES-11	GOES-10
13/09/2004 17:00	16/09/2004 16:55	2.47E+08	7.95E+07	2.55E+07	8.13E+06	2.25E+06	GOES-11	GOES-10
19/09/2004 16:25	20/09/2004 20:20	6.28E+06	3.69E+06	2.15E+06	1.21E+06	6.03E+05	GOES-11	GOES-10
01/11/2004 03:35	02/11/2004 05:50	2.61E+06	2.07E+06	1.56E+06	9.77E+05	5.60E+05	GOES-11	GOES-10
07/11/2004 11:35	14/11/2004 18:50	3.52E+08	1.55E+08	6.83E+07	3.09E+07	1.22E+07	GOES-11	GOES-10
15/01/2005 06:35	23/01/2005 06:30	8.70E+08	5.10E+08	3.04E+08	1.91E+08	1.10E+08	GOES-11	GOES-10
13/05/2005 23:05	16/05/2005 13:50	4.89E+08	1.89E+08	6.98E+07	2.14E+07	5.43E+06	GOES-11	GOES-10
16/06/2005 18:25	17/06/2005 23:55	3.56E+06	2.77E+06	2.07E+06	1.33E+06	8.05E+05	GOES-11	GOES-10
13/07/2005 12:50	19/07/2005 11:55	6.77E+07	3.71E+07	1.99E+07	9.93E+06	4.31E+06	GOES-11	GOES-10
26/07/2005 13:20	03/08/2005 11:40	9.38E+07	4.10E+07	1.80E+07	8.11E+06	3.27E+06	GOES-11	GOES-10
21/08/2005 23:30	25/08/2005 19:20	2.31E+08	9.87E+07	4.21E+07	1.79E+07	6.47E+06	GOES-11	GOES-10
07/09/2005 18:40	17/09/2005 02:55	1.15E+09	5.30E+08	2.49E+08	1.24E+08	5.55E+07	GOES-11	GOES-10
05/12/2006 22:40	16/12/2006 09:55	9.02E+08	4.93E+08	2.68E+08	1.43E+08	7.05E+07	GOES-11	GOES-10

Table A.30: SARG Event List - Fluences ($cm^{-2}MeV^{-1}$) Channels 6-10 [8].

Start Date and Time	End Date and Time	Channel 6	Channel 7	Channel 8	Channel 9	Channel 10	Primary S/C	Secondary S/C
18/06/2003 07:00	20/06/2003 23:55	1.01E+05	3.51E+04	1.60E+04	7.46E+03	5.49E+03	GOES-10	GOES-11
24/10/2003 03:35	24/10/2003 17:55	9.44E+03	6.27E+03	3.41E+03	1.82E+03	1.35E+03	GOES-11	GOES-10
26/10/2003 15:15	08/11/2003 18:20	1.74E+08	6.19E+07	1.09E+07	1.80E+06	8.84E+05	GOES-11	GOES-10
20/11/2003 07:40	20/11/2003 22:05	1.89E+04	7.64E+03	3.58E+03	1.70E+03	1.21E+03	GOES-11	GOES-10
21/11/2003 03:40	25/11/2003 04:00	1.47E+05	4.11E+04	2.01E+04	1.03E+04	7.53E+03	GOES-11	GOES-10
02/12/2003 10:25	04/12/2003 21:55	1.64E+05	3.08E+04	1.43E+04	7.19E+03	5.27E+03	GOES-11	GOES-10
11/04/2004 03:50	12/04/2004 19:25	9.58E+04	2.80E+04	1.28E+04	6.08E+03	4.46E+03	GOES-11	GOES-10
23/07/2004 21:05	24/07/2004 12:25	2.17E+04	1.05E+04	5.03E+03	2.40E+03	1.74E+03	GOES-11	GOES-10
25/07/2004 14:40	28/07/2004 19:00	5.49E+05	9.83E+04	3.20E+04	1.09E+04	8.11E+03	GOES-11	GOES-10
01/08/2004 14:10	02/08/2004 09:55	3.03E+04	1.22E+04	6.04E+03	3.05E+03	2.26E+03	GOES-11	GOES-10
13/09/2004 17:00	16/09/2004 16:55	3.50E+05	5.44E+04	2.37E+04	1.13E+04	8.36E+03	GOES-11	GOES-10
19/09/2004 16:25	20/09/2004 20:20	1.83E+05	5.54E+04	1.69E+04	5.17E+03	3.68E+03	GOES-11	GOES-10
01/11/2004 03:35	02/11/2004 05:50	2.19E+05	8.57E+04	2.57E+04	7.53E+03	5.01E+03	GOES-11	GOES-10
07/11/2004 11:35	14/11/2004 18:50	2.76E+06	6.25E+05	1.56E+05	3.92E+04	2.70E+04	GOES-11	GOES-10
15/01/2005 06:35	23/01/2005 06:30	4.34E+07	1.72E+07	4.25E+06	1.01E+06	6.17E+05	GOES-11	GOES-10
13/05/2005 23:05	16/05/2005 13:50	6.17E+05	7.00E+04	2.62E+04	1.09E+04	7.78E+03	GOES-11	GOES-10
16/06/2005 18:25	17/06/2005 23:55	3.70E+05	1.70E+05	5.18E+04	1.53E+04	9.48E+03	GOES-11	GOES-10
13/07/2005 12:50	19/07/2005 11:55	1.04E+06	2.50E+05	7.67E+04	2.41E+04	1.76E+04	GOES-11	GOES-10
26/07/2005 13:20	03/08/2005 11:40	8.24E+05	2.08E+05	8.09E+04	3.27E+04	2.41E+04	GOES-11	GOES-10
21/08/2005 23:30	25/08/2005 19:20	1.20E+06	2.22E+05	5.89E+04	1.61E+04	1.17E+04	GOES-11	GOES-10
07/09/2005 18:40	17/09/2005 02:55	1.57E+07	4.46E+06	9.62E+05	2.04E+05	1.17E+05	GOES-11	GOES-10
05/12/2006 22:40	16/12/2006 09:55	2.43E+07	8.41E+06	2.05E+06	4.86E+05	2.84E+05	GOES-11	GOES-10

Table A.31: SARG Event List - Peak Fluxes ($cm^{-2}ster^{-1}s^{-1}MeV^{-1}$) Channels 1-5 [8].

Start Date and Time	End Date and Time	Channel 1	Channel 2	Channel 3	Channel 4	Channel 5	Primary S/C	Secondary S/C
18/06/2003 07:00	20/06/2003 23:55	3.19E+01	1.19E+01	4.23E+00	1.30E+00	3.83E-01	GOES-10	GOES-11
24/10/2003 03:35	24/10/2003 17:55	3.35E+01	4.37E+00	6.51E-01	1.58E-01	4.52E-02	GOES-11	GOES-10
26/10/2003 15:15	08/11/2003 18:20	9.22E+03	4.79E+03	2.60E+03	1.66E+03	9.18E+02	GOES-11	GOES-10
20/11/2003 07:40	20/11/2003 22:05	9.40E+00	3.05E+00	1.02E+00	3.81E-01	1.43E-01	GOES-11	GOES-10
21/11/2003 03:40	25/11/2003 04:00	1.53E+01	5.89E+00	2.31E+00	9.68E-01	3.71E-01	GOES-11	GOES-10
02/12/2003 10:25	04/12/2003 21:55	1.08E+02	4.28E+01	1.68E+01	6.46E+00	2.02E+00	GOES-11	GOES-10
11/04/2004 03:50	12/04/2004 19:25	6.67E+01	2.13E+01	6.65E+00	1.92E+00	5.36E-01	GOES-11	GOES-10
23/07/2004 21:05	24/07/2004 12:25	6.36E+00	1.93E+00	6.23E-01	2.51E-01	1.05E-01	GOES-11	GOES-10
25/07/2004 14:40	28/07/2004 19:00	1.29E+03	4.97E+02	1.86E+02	6.25E+01	1.71E+01	GOES-11	GOES-10
01/08/2004 14:10	02/08/2004 09:55	6.16E+00	2.86E+00	1.31E+00	5.66E-01	2.33E-01	GOES-11	GOES-10
13/09/2004 17:00	16/09/2004 16:55	3.87E+02	1.33E+02	4.57E+01	1.61E+01	4.64E+00	GOES-11	GOES-10
19/09/2004 16:25	20/09/2004 20:20	1.86E+01	1.20E+01	7.31E+00	3.59E+00	1.60E+00	GOES-11	GOES-10
01/11/2004 03:35	02/11/2004 05:50	1.08E+01	8.57E+00	6.37E+00	3.71E+00	2.03E+00	GOES-11	GOES-10
07/11/2004 11:35	14/11/2004 18:50	3.61E+02	1.65E+02	7.39E+01	3.10E+01	1.17E+01	GOES-11	GOES-10
15/01/2005 06:35	23/01/2005 06:30	7.69E+02	5.25E+02	3.62E+02	2.60E+02	1.69E+02	GOES-11	GOES-10
13/05/2005 23:05	16/05/2005 13:50	5.71E+03	1.93E+03	6.22E+02	1.67E+02	3.23E+01	GOES-11	GOES-10
16/06/2005 18:25	17/06/2005 23:55	6.38E+00	5.02E+00	3.77E+00	2.38E+00	1.43E+00	GOES-11	GOES-10
13/07/2005 12:50	19/07/2005 11:55	3.89E+01	2.48E+01	1.53E+01	8.42E+00	3.90E+00	GOES-11	GOES-10
26/07/2005 13:20	03/08/2005 11:40	4.45E+01	1.59E+01	5.92E+00	2.64E+00	1.03E+00	GOES-11	GOES-10
21/08/2005 23:30	25/08/2005 19:20	2.65E+02	1.13E+02	4.86E+01	2.20E+01	8.47E+00	GOES-11	GOES-10
07/09/2005 18:40	17/09/2005 02:55	1.27E+03	5.83E+02	2.63E+02	1.13E+02	4.35E+01	GOES-11	GOES-10
05/12/2006 22:40	16/12/2006 09:55	1.12E+03	5.09E+02	2.39E+02	1.23E+02	5.94E+01	GOES-11	GOES-10

Table A.32: SARG Event List - Peak Fluxes ($cm^{-2}ster^{-1}s^{-1}MeV^{-1}$) Channels 6-10 [8].

Start Date and Time	End Date and Time	Channel 6	Channel 7	Channel 8	Channel 9	Channel 10	Primary S/C	Secondary S/C
18/06/2003 07:00	20/06/2003 23:55	9.31E-02	2.26E-02	9.57E-03	4.25E-03	3.00E-03	GOES-10	GOES-11
24/10/2003 03:35	24/10/2003 17:55	2.52E-02	1.40E-02	7.67E-03	4.20E-03	3.13E-03	GOES-11	GOES-10
26/10/2003 15:15	08/11/2003 18:20	2.84E+02	8.77E+01	1.40E+01	2.11E+00	9.57E-01	GOES-11	GOES-10
20/11/2003 07:40	20/11/2003 22:05	5.40E-02	2.05E-02	8.98E-03	4.00E-03	2.74E-03	GOES-11	GOES-10
21/11/2003 03:40	25/11/2003 04:00	9.68E-02	2.53E-02	9.87E-03	4.00E-03	2.90E-03	GOES-11	GOES-10
02/12/2003 10:25	04/12/2003 21:55	2.62E-01	3.40E-02	1.25E-02	4.98E-03	3.33E-03	GOES-11	GOES-10
11/04/2004 03:50	12/04/2004 19:25	1.32E-01	3.26E-02	1.30E-02	5.43E-03	3.87E-03	GOES-11	GOES-10
23/07/2004 21:05	24/07/2004 12:25	5.25E-02	2.63E-02	1.15E-02	4.97E-03	3.53E-03	GOES-11	GOES-10
25/07/2004 14:40	28/07/2004 19:00	2.01E+00	2.35E-01	3.50E-02	5.36E-03	3.94E-03	GOES-11	GOES-10
01/08/2004 14:10	02/08/2004 09:55	7.94E-02	2.70E-02	1.13E-02	4.80E-03	3.61E-03	GOES-11	GOES-10
13/09/2004 17:00	16/09/2004 16:55	5.71E-01	7.02E-02	1.95E-02	5.82E-03	4.13E-03	GOES-11	GOES-10
19/09/2004 16:25	20/09/2004 20:20	4.70E-01	1.38E-01	3.33E-02	7.89E-03	5.07E-03	GOES-11	GOES-10
01/11/2004 03:35	02/11/2004 05:50	8.39E-01	3.48E-01	8.59E-02	2.04E-02	1.16E-02	GOES-11	GOES-10
07/11/2004 11:35	14/11/2004 18:50	2.75E+00	6.47E-01	1.37E-01	2.89E-02	1.67E-02	GOES-11	GOES-10
15/01/2005 06:35	23/01/2005 06:30	7.34E+01	3.18E+01	1.48E+01	6.96E+00	5.01E+00	GOES-11	GOES-10
13/05/2005 23:05	16/05/2005 13:50	1.56E+00	7.58E-02	2.13E-02	6.92E-03	4.75E-03	GOES-11	GOES-10
16/06/2005 18:25	17/06/2005 23:55	6.91E-01	3.35E-01	1.09E-01	3.42E-02	2.03E-02	GOES-11	GOES-10
13/07/2005 12:50	19/07/2005 11:55	8.78E-01	1.97E-01	3.52E-02	6.17E-03	4.26E-03	GOES-11	GOES-10
26/07/2005 13:20	03/08/2005 11:40	2.37E-01	5.43E-02	1.79E-02	6.10E-03	4.31E-03	GOES-11	GOES-10
21/08/2005 23:30	25/08/2005 19:20	1.66E+00	3.24E-01	4.84E-02	7.11E-03	4.81E-03	GOES-11	GOES-10
07/09/2005 18:40	17/09/2005 02:55	1.07E+01	2.62E+00	4.89E-01	8.97E-02	5.15E-02	GOES-11	GOES-10
05/12/2006 22:40	16/12/2006 09:55	2.16E+01	7.88E+00	2.71E+00	9.31E-01	5.74E-01	GOES-11	GOES-10

Appendix B

Statistical Modelling Tables

B.1 Time Distribution Tables

The following pages contains additional tables which support the work introduced in Section 4.3.

B.1.1 Constants

This section contains the constants found for the best fits to waiting times for the JPL, PSYCHIC and NOAA event lists for the Poisson (λ), Time-dependent Poisson (ϱ) and Lévy distributions (c and μ).

Table B.1: Constants for waiting time distributions for JPL Event List.

	Binning 1	Binning 2	Binning 3	Binning 4	Binning 5	Years
λ	0.0127	0.0111	0.0126	0.0111	0.0126	1976-2006
	0.0227	0.0207	0.0235	0.0210	0.0236	Active Years
ϱ	0.0182	0.0189	0.0183	0.0191	0.0173	1976-2006
	0.0217	0.0218	0.0212	0.0211	0.0190	Active Years
c	9.0597	8.4971	9.0910	8.1884	9.0542	1976-2006
	5.8589	5.7124	6.1098	5.6672	9.0896	Active Years
μ	0.2728	0.2766	0.2734	0.2782	0.2730	1976-2006
	0.2938	0.2965	0.2917	0.2960	0.2710	Active Years

Table B.2: Constants for waiting time distributions for PSYCHIC Event List.

	Binning 1	Binning 2	Binning 3	Binning 4	Binning 5	Years
λ	0.0355	0.0350	0.0355	0.0360	0.0320	1976-2006
	0.0776	0.0718	0.0745	0.0724	0.0731	Active Years
ϱ	0.0494	0.0488	0.0489	0.0467	0.0500	1976-2006
	0.0542	0.0577	0.0558	0.0522	0.0558	Active Years
c	1.9360	2.0139	1.9230	2.0863	2.0212	1976-2006
	1.0288	0.9563	0.9258	1.0855	0.9294	Active Years
μ	0.3832	0.3796	0.3835	0.3756	0.3791	1976-2006
	0.4687	0.4809	0.4860	0.4578	0.4850	Active Years

Table B.3: Constants for waiting time distributions for NOAA Event List.

	Binning 1	Binning 2	Binning 3	Binning 4	Binning 5	Years
λ	0.0114	0.0134	0.0113	0.0093	0.0117	1976-2006
	0.0231	0.0206	0.0181	0.0213	0.0201	Active Years
ϱ	0.0222	0.0271	0.0259	0.0269	0.0268	1976-2006
	0.0251	0.0256	0.0273	0.0258	0.0301	Active Years
c	24.2685	31.4232	24.7907	24.1726	28.6271	1976-2006
	22.9500	20.3264	19.7865	21.2535	30.4789	Active Years
μ	0.2423	0.2326	0.2412	0.2418	0.2359	1976-2006
	0.2424	0.2484	0.2489	0.2455	0.2300	Active Years

B.1.2 Measures of Goodness-of-Fits

This section gives the various goodness-of-fit parameters for the three event lists and three distributions for SEPE waiting times.

Table B.4: $\sqrt{S^2\chi^2}$ values for JPL waiting time fits.

Binning	Years	Poisson	T-D Poisson	Lévy
1	1965-2005	0.7979	0.0796	0.0785
	Active Years	0.1883	0.0830	0.0828
2	1965-2005	0.9427	0.0833	0.1185
	Active Years	0.2232	0.0803	0.1047
3	1965-2005	0.7119	0.0811	0.1143
	Active Years	0.1365	0.0789	0.1030
4	1965-2005	0.8606	0.0923	0.1352
	Active Years	0.1868	0.0835	0.1086
5	1965-2005	0.5390	0.0696	0.0983
	Active Years	0.1471	0.0903	0.0992
Mean	1965-2005	0.7704	0.0812	0.1089
	Active Years	0.1764	0.0832	0.0997

Table B.5: $\sqrt{S^2\chi^2}$ values for PSYCHIC waiting time fits.

Binning	Years	Poisson	T-D Poisson	Lévy
1	1973-2001	1.0069	0.4177	0.1751
	Active Years	0.2874	0.7774	0.3576
2	1973-2001	0.9525	0.3514	0.1435
	Active Years	0.2369	0.7517	0.2899
3	1973-2001	0.7873	0.3156	0.1069
	Active Years	0.1805	0.6744	0.2697
4	1973-2001	0.7749	0.2739	0.1108
	Active Years	0.1707	0.4712	0.1744
5	1973-2001	0.9852	0.3407	0.1528
	Active Years	0.1743	0.6366	0.2641
Mean	1973-2001	0.9014	0.3399	0.1378
	Active Years	0.2099	0.6623	0.2711

Table B.6: $\sqrt{S^2\chi^2}$ values for NOAA waiting time fits.

Binning	Years	Poisson	T-D Poisson	Lévy
1	1976-2006	2.1594	0.1639	0.0703
	Active Years	0.7278	0.1133	0.0483
2	1976-2006	1.8107	0.1322	0.0616
	Active Years	0.8217	0.0788	0.0641
3	1976-2006	2.0426	0.1560	0.0525
	Active Years	1.0788	0.1049	0.0646
4	1976-2006	2.6603	0.1480	0.0413
	Active Years	0.7855	0.0968	0.0382
5	1976-2006	1.9182	0.1299	0.0555
	Active Years	0.6982	0.0879	0.0805
Mean	1976-2006	2.1183	0.1460	0.0562
	Active Years	0.8224	0.0963	0.0591

Table B.7: S^2 values for JPL waiting time fits.

Binning	Years	Poisson	T-D Poisson	Lévy
1	1965-2005	9.2676	0.8955	0.8733
	Active Years	1.6267	0.6892	0.6749
2	1965-2005	12.2399	1.1945	1.4457
	Active Years	2.3514	0.7263	0.8606
3	1965-2005	9.8122	1.0127	1.2653
	Active Years	1.3758	0.6369	0.8128
4	1965-2005	11.6083	1.3638	1.7035
	Active Years	1.7932	0.6678	0.8341
5	1965-2005	6.2464	0.6474	0.8910
	Active Years	1.4818	0.6806	0.7988
Mean	1965-2005	9.8349	1.0228	1.2358
	Active Years	1.7258	0.6801	0.7962

Table B.8: S^2 values for PSYCHIC waiting time fits.

Binning	Years	Poisson	T-D Poisson	Lévy
1	1973-2001	8.9476	2.7709	1.2257
	Active Years	1.7468	6.1199	2.9266
2	1973-2001	9.1074	2.4050	1.1216
	Active Years	1.3928	6.4379	2.0328
3	1973-2001	7.0427	2.0609	0.6385
	Active Years	0.9177	5.6244	1.7953
4	1973-2001	6.9992	1.6164	0.8015
	Active Years	0.8253	3.0209	1.0868
5	1973-2001	10.0424	2.5133	1.3057
	Active Years	0.9023	5.4833	1.8685
Mean	1973-2001	8.4279	2.2733	1.0186
	Active Years	1.1570	5.3373	1.9420

Table B.9: S^2 values for NOAA waiting time fits.

Binning	Years	Poisson	T-D Poisson	Lévy
1	1976-2006	13.9417	1.9097	0.7263
	Active Years	4.2781	0.7454	0.5538
2	1976-2006	14.0845	4.0392	0.9797
	Active Years	4.7728	0.5002	0.9545
3	1976-2006	12.7098	3.1435	0.7411
	Active Years	5.8476	0.8301	1.6854
4	1976-2006	17.7759	4.5374	0.3914
	Active Years	4.8497	0.7587	0.4805
5	1976-2006	14.1721	3.8050	0.8519
	Active Years	3.6673	1.2236	4.7372
Mean	1976-2006	14.5368	3.4870	0.7381
	Active Years	4.6831	0.8116	1.6823

Table B.10: χ^2 values for JPL waiting time fits.

Binning	Years	Poisson	T-D Poisson	Lévy
1	1965-2005	0.0687	0.0071	0.0071
	Active Years	0.0218	0.0100	0.0102
2	1965-2005	0.0726	0.0058	0.0097
	Active Years	0.0212	0.0089	0.0127
3	1965-2005	0.0517	0.0065	0.0103
	Active Years	0.0135	0.0098	0.0131
4	1965-2005	0.0638	0.0062	0.0107
	Active Years	0.0194	0.0104	0.0141
5	1965-2005	0.0465	0.0075	0.0108
	Active Years	0.0146	0.0120	0.0123
Mean	1965-2005	0.0607	0.0066	0.0097
	Active Years	0.0181	0.0102	0.0125

Table B.11: χ^2 values for PSYCHIC waiting time fits.

Binning	Years	Poisson	T-D Poisson	Lévy
1	1973-2001	0.1133	0.0630	0.0250
	Active Years	0.0473	0.0987	0.0437
2	1973-2001	0.0996	0.0514	0.0184
	Active Years	0.0403	0.0878	0.0413
3	1973-2001	0.0880	0.0483	0.0179
	Active Years	0.0355	0.0809	0.0405
4	1973-2001	0.0858	0.0464	0.0153
	Active Years	0.0353	0.0735	0.0280
5	1973-2001	0.0967	0.0462	0.0179
	Active Years	0.0337	0.0739	0.0373
Mean	1973-2001	0.0967	0.0511	0.0189
	Active Years	0.0384	0.0830	0.0382

Table B.12: χ^2 values for NOAA waiting time fits.

Binning	Years	Poisson	T-D Poisson	Lévy
1	1976-2006	0.3345	0.0141	0.0068
	Active Years	0.1238	0.0172	0.0042
2	1976-2006	0.2328	0.0043	0.0039
	Active Years	0.1415	0.0124	0.0043
3	1976-2006	0.3283	0.0077	0.0037
	Active Years	0.1990	0.0133	0.0025
4	1976-2006	0.3981	0.0048	0.0044
	Active Years	0.1272	0.0123	0.0030
5	1976-2006	0.2596	0.0044	0.0036
	Active Years	0.1329	0.0063	0.0014
Mean	1976-2006	0.3107	0.0071	0.0045
	Active Years	0.1449	0.0123	0.0031

B.1.3 Bins used for Analysis

This section gives the bin limits used for the analysis carried out.

Table B.13: Bins end limits used for JPL Event List waiting time analysis (days).

	Binning 1	Binning 2	Binning 3	Binning 4	Binning 5
Start	5.8	5.8	5.8	5.8	5.8
Bin 1	9.0	9.3	9.5	9.7	10.0
Bin 2	14.2	14.9	15.6	16.4	17.3
Bin 3	22.2	23.9	25.8	27.8	30.0
Bin 4	34.8	38.5	42.5	47.0	51.9
Bin 5	54.6	61.9	70.1	79.4	90.0
Bin 6	85.6	99.5	115.6	134.3	156.0
Bin 7	134.3	160.0	190.6	227.0	270.4
Bin 8	210.6	257.2	314.2	383.8	468.7
Bin 9	330.3	413.6	518.0	648.7	812.4
Bin 10	518.0	665.1	854.1	1096.6	
Bin 11	812.4	1069.6			

Table B.14: Bins end limits used for PSYCHIC Event List waiting time analysis (days).

	Binning 1	Binning 2	Binning 3	Binning 4	Binning 5
Start	4.5	4.5	4.5	4.5	4.5
Bin 1	6.0	6.2	6.4	6.5	6.7
Bin 2	8.2	8.6	9.0	9.5	10.0
Bin 3	11.0	11.9	12.8	13.8	14.9
Bin 4	14.9	16.4	18.2	20.1	22.2
Bin 5	20.1	22.8	25.8	29.2	33.1
Bin 6	27.1	31.5	36.6	42.5	49.4
Bin 7	36.6	43.6	51.9	61.9	73.7
Bin 8	49.4	60.3	73.7	90.0	109.9
Bin 9	66.7	83.5	104.6	131.0	164.0
Bin 10	90.0	115.6	148.4	190.6	244.7
Bin 11	121.5	160.0	210.6	277.3	365.0
Bin 12	164.0	221.4	298.9		
Bin 13	221.4	306.4			
Bin 14	298.9				

Table B.15: Bins end limits used for NOAA Event List waiting time analysis (days).

	Binning 1	Binning 2	Binning 3	Binning 4	Binning 5
Start	1.8	1.8	1.8	1.8	1.8
Bin 1	3.1	3.2	3.2	3.3	3.4
Bin 2	5.2	5.5	5.8	6	6.4
Bin 3	8.8	9.5	10.2	11	11.9
Bin 4	14.9	16.4	18.2	20.1	22.2
Bin 5	25.2	28.5	32.3	36.6	41.5
Bin 6	42.5	49.4	57.4	66.7	77.5
Bin 7	71.9	85.6	102	121.5	144.7
Bin 8	121.5	148.4	181.3	221.4	270.4
Bin 9	205.4	257.2	322.1	403.4	505.2
Bin 10	347.2	445.9	572.5	735.1	943.9
Bin 11	587	772.8	1017.4	1339.4	
Bin 12	992.3				

Table B.16: Bins used for duration analysis (days).

	JPL	PSYCHIC
Start	0.5	1.35
Bin 1	2.5	1.82
Bin 2	4.5	2.46
Bin 3	7.5	3.32
Bin 4	10.5	4.48
Bin 5	14.5	6.05
Bin 6	21.5	8.17
Bin 7	22.5	11.02
Bin 8	30.5	14.88
Bin 9		20.09
Bin 10		27.11
Bin 11		36.60

B.2 Memory Histograms

The following 3 pages cover the 15 histograms used to incorporate memory into waiting times based on the previous waiting time in Section 4.4. The memory bands are explained in Section 4.4.3.

Table B.17: Histograms used to introduce memory [1].

		Histogram 1		
memband	$> 0\& < 0.25$	$> 0.25\& < 0.50$	$> 0.50\& < 0.75$	$> 0.75\& < 1.00$
1	0.250	0.250	0.250	0.250
2	0.250	0.250	0.250	0.250
3	0.250	0.250	0.250	0.250
4	0.250	0.250	0.250	0.250
		Histogram 2		
memband	$> 0\& < 0.25$	$> 0.25\& < 0.50$	$> 0.50\& < 0.75$	$> 0.75\& < 1.00$
1	0.268	0.250	0.250	0.232
2	0.250	0.250	0.250	0.250
3	0.250	0.250	0.250	0.250
4	0.232	0.250	0.250	0.268
		Histogram 3		
memband	$> 0\& < 0.25$	$> 0.25\& < 0.50$	$> 0.50\& < 0.75$	$> 0.75\& < 1.00$
1	0.286	0.250	0.232	0.232
2	0.250	0.268	0.250	0.232
3	0.232	0.250	0.268	0.250
4	0.232	0.232	0.250	0.286
		Histogram 4		
memband	$> 0\& < 0.25$	$> 0.25\& < 0.50$	$> 0.50\& < 0.75$	$> 0.75\& < 1.00$
1	0.304	0.268	0.214	0.214
2	0.250	0.286	0.232	0.232
3	0.232	0.232	0.286	0.250
4	0.214	0.214	0.268	0.304
		Histogram 5		
memband	$> 0\& < 0.25$	$> 0.25\& < 0.50$	$> 0.50\& < 0.75$	$> 0.75\& < 1.00$
1	0.321	0.268	0.214	0.196
2	0.268	0.286	0.232	0.214
3	0.214	0.232	0.286	0.268
4	0.196	0.214	0.268	0.321

Table B.18: Histograms used to introduce memory [2].

Histogram 6				
memband	$> 0\& < 0.25$	$> 0.25\& < 0.50$	$> 0.50\& < 0.75$	$> 0.75\& < 1.00$
1	0.339	0.268	0.232	0.161
2	0.268	0.286	0.214	0.232
3	0.232	0.214	0.286	0.268
4	0.161	0.232	0.268	0.339
Histogram 7				
memband	$> 0\& < 0.25$	$> 0.25\& < 0.50$	$> 0.50\& < 0.75$	$> 0.75\& < 1.00$
1	0.357	0.268	0.196	0.179
2	0.250	0.286	0.250	0.214
3	0.214	0.250	0.286	0.250
4	0.179	0.196	0.268	0.357
Histogram 8				
memband	$> 0\& < 0.25$	$> 0.25\& < 0.50$	$> 0.50\& < 0.75$	$> 0.75\& < 1.00$
1	0.375	0.250	0.214	0.161
2	0.268	0.304	0.232	0.196
3	0.196	0.232	0.304	0.268
4	0.161	0.214	0.250	0.375
Histogram 9				
memband	$> 0\& < 0.25$	$> 0.25\& < 0.50$	$> 0.50\& < 0.75$	$> 0.75\& < 1.00$
1	0.393	0.268	0.196	0.143
2	0.268	0.286	0.250	0.196
3	0.196	0.250	0.286	0.268
4	0.143	0.196	0.268	0.393
Histogram 10				
memband	$> 0\& < 0.25$	$> 0.25\& < 0.50$	$> 0.50\& < 0.75$	$> 0.75\& < 1.00$
1	0.411	0.268	0.179	0.143
2	0.268	0.304	0.250	0.179
3	0.179	0.250	0.304	0.268
4	0.143	0.179	0.268	0.411

Table B.19: Histograms used to introduce memory [3].

Histogram 11				
memband	$> 0\& < 0.25$	$> 0.25\& < 0.50$	$> 0.50\& < 0.75$	$> 0.75\& < 1.00$
1	0.429	0.286	0.179	0.107
2	0.286	0.286	0.250	0.179
3	0.179	0.250	0.286	0.286
4	0.107	0.179	0.286	0.429
Histogram 12				
memband	$> 0\& < 0.25$	$> 0.25\& < 0.50$	$> 0.50\& < 0.75$	$> 0.75\& < 1.00$
1	0.446	0.268	0.179	0.107
2	0.304	0.304	0.250	0.143
3	0.143	0.250	0.304	0.304
4	0.107	0.179	0.268	0.446
Histogram 13				
memband	$> 0\& < 0.25$	$> 0.25\& < 0.50$	$> 0.50\& < 0.75$	$> 0.75\& < 1.00$
1	0.464	0.286	0.125	0.125
2	0.250	0.321	0.268	0.161
3	0.161	0.268	0.321	0.250
4	0.125	0.125	0.286	0.464
Histogram 14				
memband	$> 0\& < 0.25$	$> 0.25\& < 0.50$	$> 0.50\& < 0.75$	$> 0.75\& < 1.00$
1	0.482	0.268	0.161	0.089
2	0.304	0.357	0.214	0.125
3	0.125	0.214	0.357	0.304
4	0.089	0.161	0.268	0.482
Histogram 15				
memband	$> 0\& < 0.25$	$> 0.25\& < 0.50$	$> 0.50\& < 0.75$	$> 0.75\& < 1.00$
1	0.500	0.250	0.179	0.071
2	0.286	0.339	0.232	0.143
3	0.143	0.232	0.339	0.286
4	0.071	0.179	0.250	0.500

Appendix C

Results by Channel

This Appendix Chapter provides all the results separated by channel for the following:

- Truncated power law fittings of SEPE fluence and peak flux (1st page top)
- Truncated power law parameters and quality of fits (1st page middle)
- Regression parameters and residuals for SEPE peak flux and duration with fluence (1st page bottom)
- Plots of Regression fits and normal residual fits for SEPE peak flux with fluence (2nd page left)
- Plots of Regression fits and normal residual fits for SEPE duration with fluence (2nd page right)
- Plot of frequency of significant SEPEs at stated energy (3rd page top left)
- Plot of worst-case peak flux at stated energy (3rd page top right)
- Plot of worst-case event fluence at stated energy (3rd page bottom left)
- Plot of cumulative mission fluence at stated energy (3rd page bottom right)
- Tabulated results for worst-case peak flux (4th page top)
- Tabulated results for worst-case event fluence (4th page middle)
- Tabulated results for mission cumulative fluence (4th page bottom)

C.1 Channel 1 Figures and Tables

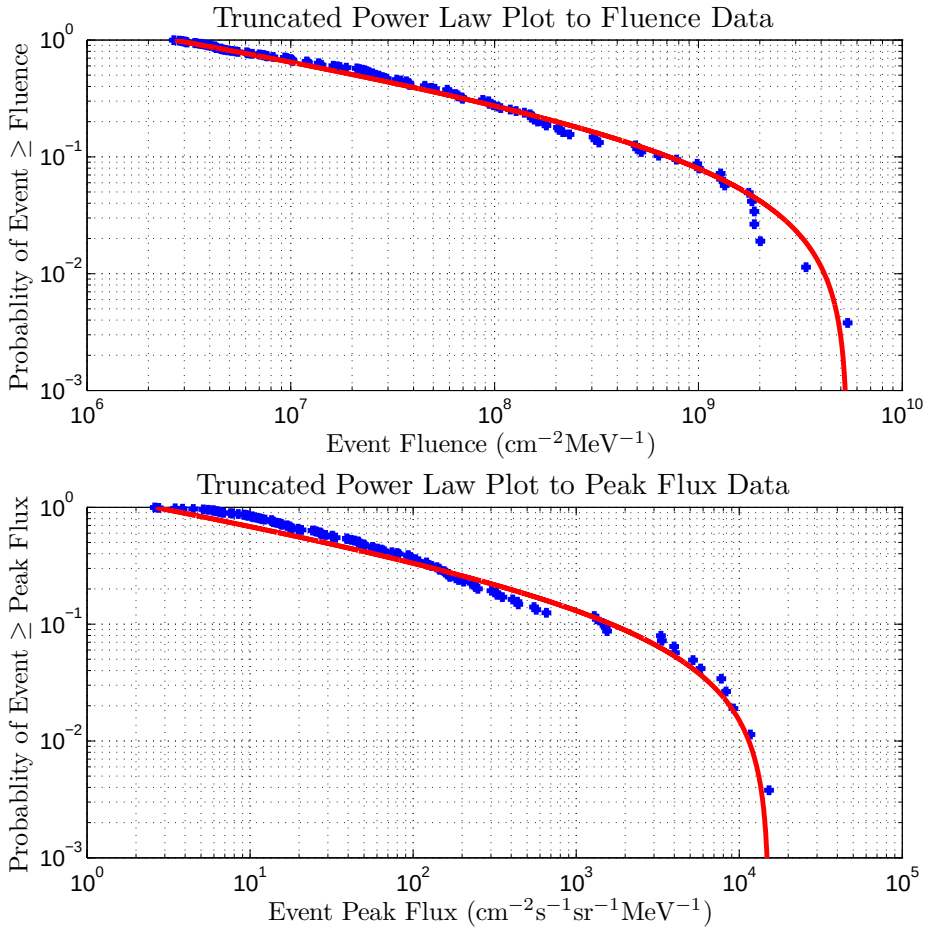

Figure C.1: Truncated Power Law Fits for Channel 1: 5.00 - 7.23 MeV.

Table C.1: Fluence and peak flux fitting parameters for Channel 1.

	b	$\phi_{\max}$	S^2	χ^2
Fluence	0.2858	5.40E+09	4.365	0.2469
Peak flux	0.2421	1.53E+04	29.3783	13.9128

Table C.2: Regression parameters for Channel 1.

Peak Flux			Duration	
Gradient	Intercept	Residual σ	Adjust	Residual σ
0.9920	-13.0666	0.7004	-0.1260	0.5305

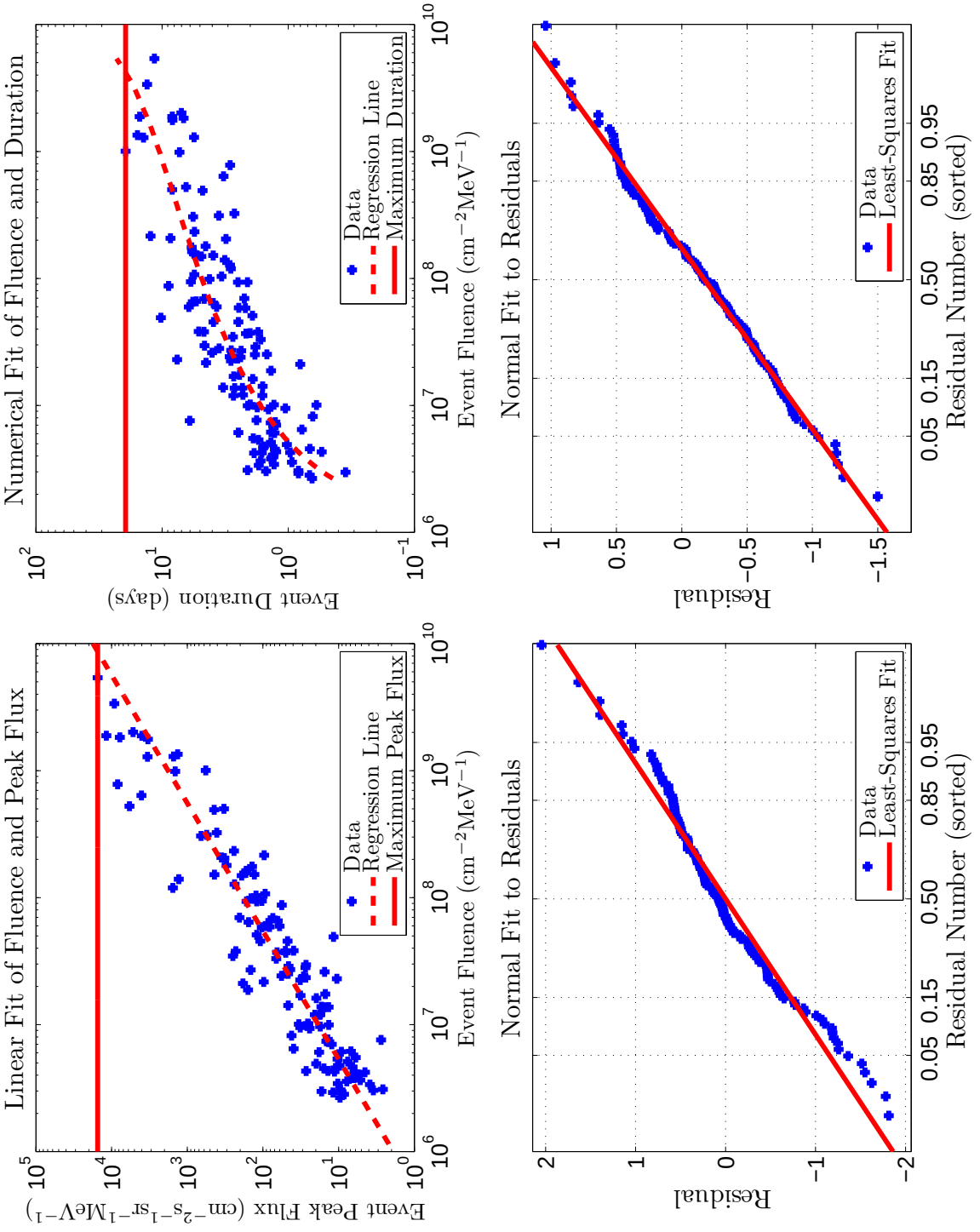

Figure C.2: Regression Fits for Channel 1: 5.00 - 7.23 MeV.

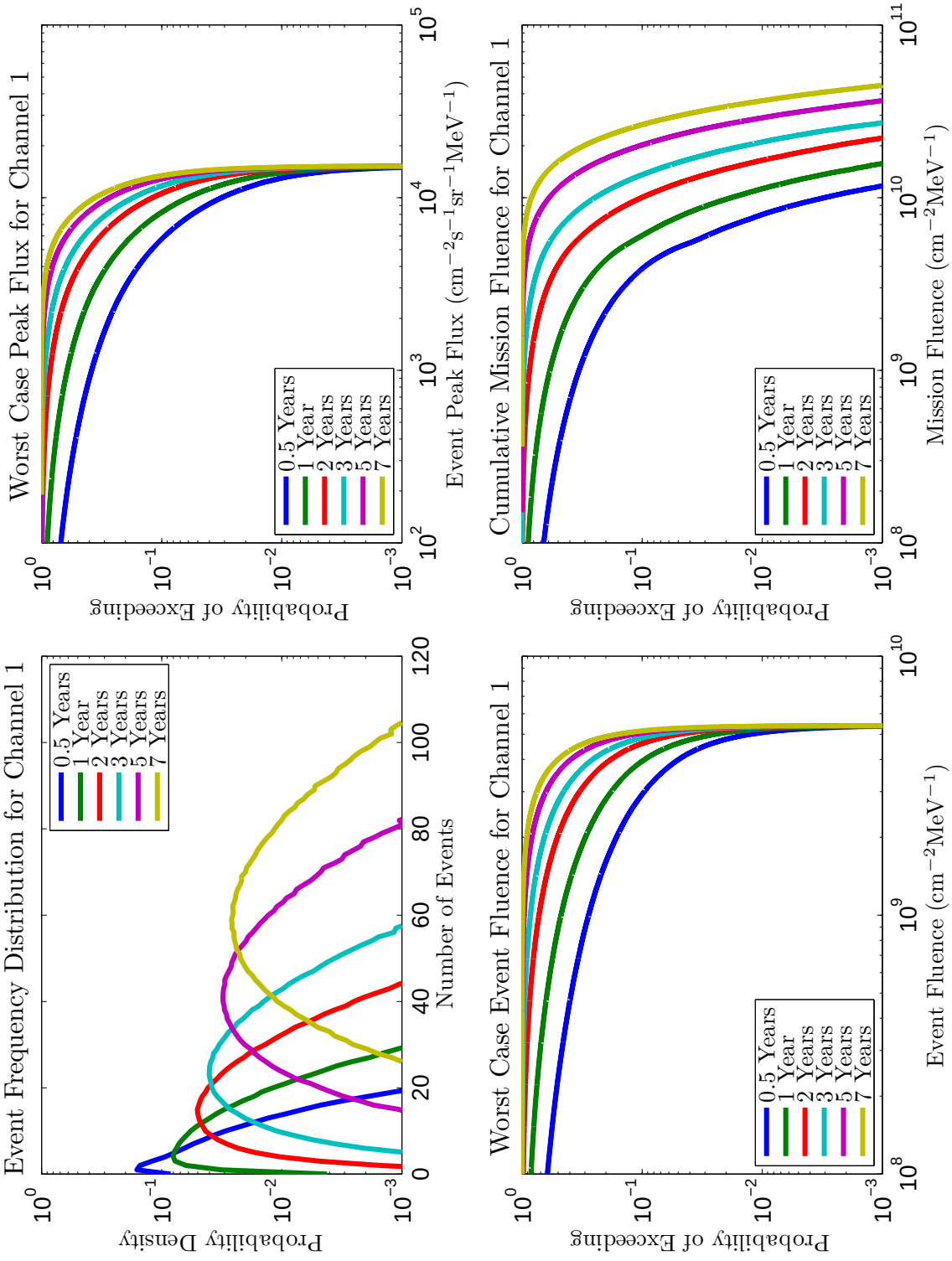

Figure C.3: Results for Channel 1: 5.00 - 7.23 MeV.

Table C.3: Table of worst-case peak flux predictions for Channel 1 ($cm^{-2}s^{-1}sr^{-1}MeV^{-1}$).

Mission	Confidence Level				
Duration	0.7	0.8	0.9	0.95	0.99
0.5 yr	1.68E+03	3.08E+03	5.76E+03	8.42E+03	1.30E+04
1 yr	3.79E+03	5.49E+03	8.23E+03	1.06E+04	1.40E+04
2 yr	6.35E+03	8.07E+03	1.06E+04	1.25E+04	1.46E+04
3 yr	7.84E+03	9.48E+03	1.17E+04	1.32E+04	1.48E+04
5 yr	9.63E+03	1.11E+04	1.29E+04	1.40E+04	1.50E+04
7 yr	1.07E+04	1.19E+04	1.34E+04	1.43E+04	1.50E+04

Table C.4: Table of worst-case event fluence predictions for Channel 1 ($cm^{-2}MeV^{-1}$).

Mission	Confidence Level				
Duration	0.7	0.8	0.9	0.95	0.99
0.5 yr	8.81E+08	1.61E+09	2.93E+09	3.99E+09	5.07E+09
1 yr	1.98E+09	2.81E+09	3.93E+09	4.61E+09	5.23E+09
2 yr	3.20E+09	3.87E+09	4.60E+09	4.99E+09	5.31E+09
3 yr	3.78E+09	4.30E+09	4.84E+09	5.12E+09	5.34E+09
5 yr	4.34E+09	4.70E+09	5.06E+09	5.23E+09	5.36E+09
7 yr	4.62E+09	4.89E+09	5.15E+09	5.28E+09	5.37E+09

Table C.5: Table of cumulative mission fluence predictions for Channel 1 ($cm^{-2}MeV^{-1}$).

Mission	Confidence Level				
Duration	0.7	0.8	0.9	0.95	0.99
0.5 yr	1.23E+09	2203000000	3880000000	5167000000	7.99E+09
1 yr	3.14E+09	4371000000	6039000000	7726000000	1.13E+10
2 yr	6.25E+09	7735000000	10043000000	12139000000	1.65E+10
3 yr	9.13E+09	10904000000	13584000000	16017000000	2.10E+10
5 yr	1.47E+10	16907000000	20209000000	23129000000	2.90E+10
7 yr	2.01E+10	22702000000	26505000000	29805000000	3.65E+10

C.2 Channel 2 Figures and Tables

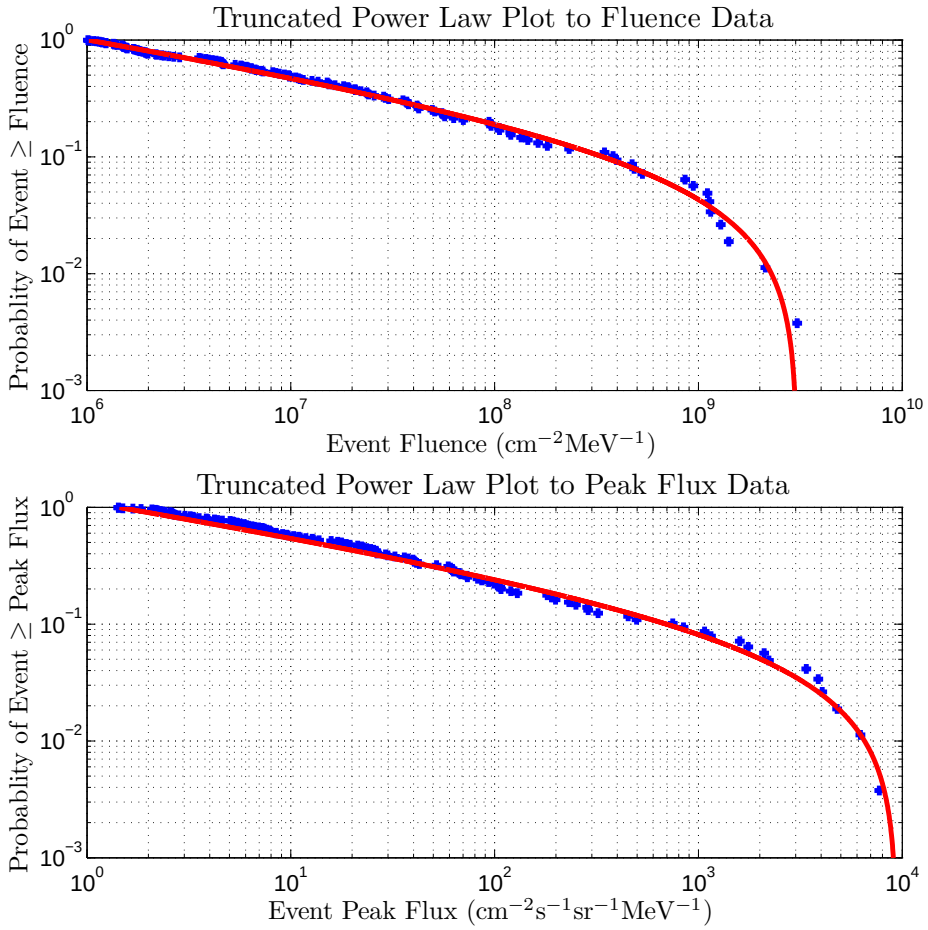

Figure C.4: Truncated Power Law Fits for Channel 2: 7.23 - 10.46 MeV.

Table C.6: Fluence and peak flux fitting parameters for Channel 2.

	b	$\phi_{\max}$	S^2	χ^2
Fluence	0.2819	3.05E+09	2.0270	0.1191
Peak flux	0.2801	9.40E+03	7.1541	4.3423

Table C.7: Regression parameters for Channel 2.

Peak Flux			Duration	
Gradient	Intercept	Residual σ	Adjust	Residual σ
0.9773	-12.8480	0.6632	-0.1918	0.5307

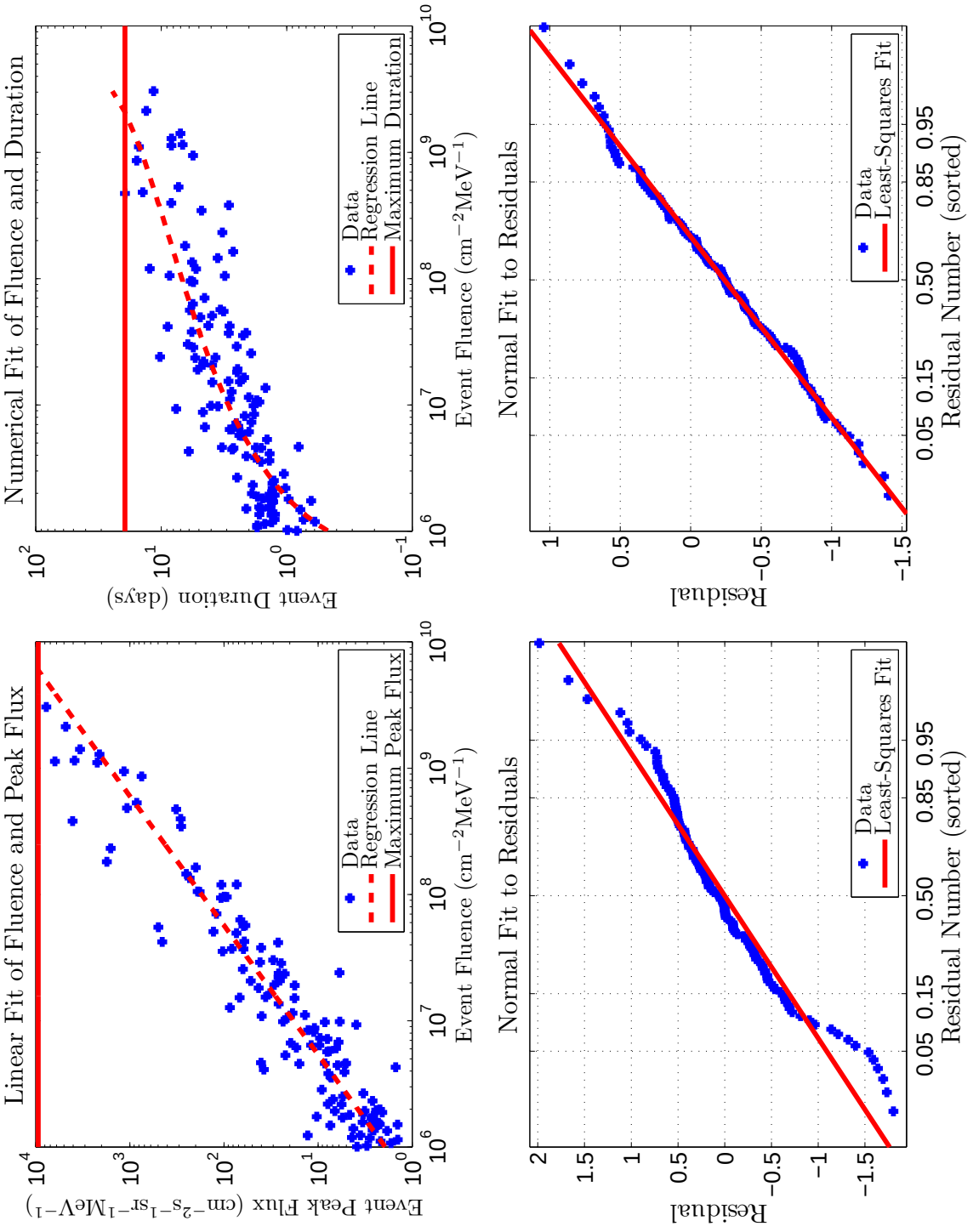

Figure C.5: Regression Fits for Channel 2: 7.23 - 10.46 MeV.

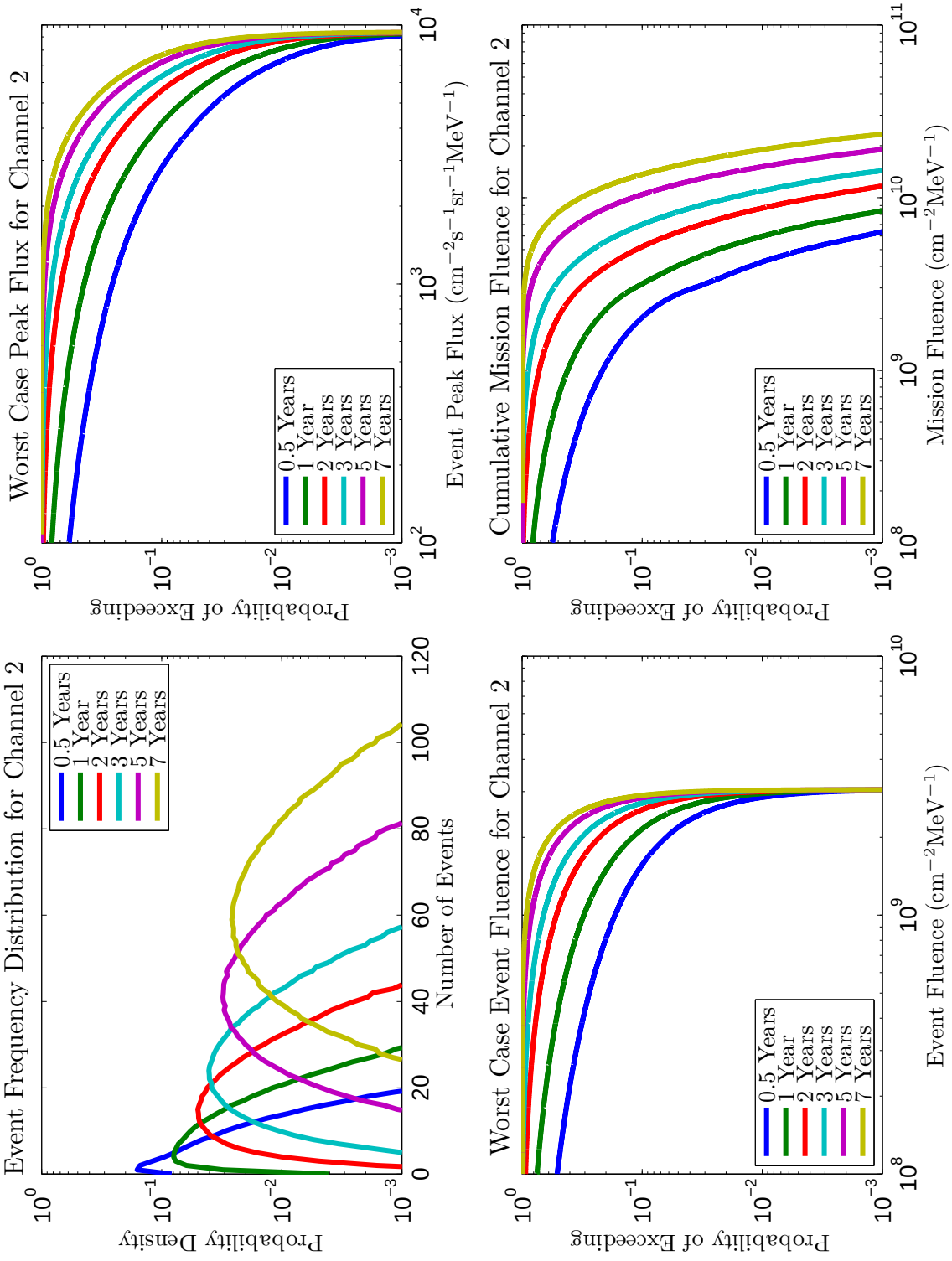

Figure C.6: Results for Channel 2: 7.23 - 10.46 MeV.

Table C.8: Table of worst-case peak flux predictions for Channel 2 ($cm^{-2}s^{-1}sr^{-1}MeV^{-1}$).

Mission	Confidence Level				
Duration	0.7	0.8	0.9	0.95	0.99
0.5 yr	7.62E+02	1.44E+03	2.81E+03	4.27E+03	7.29E+03
1 yr	1.79E+03	2.67E+03	4.20E+03	5.63E+03	8.12E+03
2 yr	3.12E+03	4.08E+03	5.59E+03	6.88E+03	8.70E+03
3 yr	3.94E+03	4.90E+03	6.34E+03	7.47E+03	8.90E+03
5 yr	5.00E+03	5.90E+03	7.18E+03	8.10E+03	9.09E+03
7 yr	5.66E+03	6.52E+03	7.66E+03	8.42E+03	9.17E+03

Table C.9: Table of worst-case event fluence predictions for Channel 2 ($cm^{-2}MeV^{-1}$).

Mission	Confidence Level				
Duration	0.7	0.8	0.9	0.95	0.99
0.5 yr	4.28E+08	8.14E+08	1.57E+09	2.19E+09	2.85E+09
1 yr	1.02E+09	1.49E+09	2.15E+09	2.57E+09	2.95E+09
2 yr	1.71E+09	2.11E+09	2.56E+09	2.80E+09	3.00E+09
3 yr	2.06E+09	2.38E+09	2.71E+09	2.88E+09	3.02E+09
5 yr	2.40E+09	2.63E+09	2.84E+09	2.95E+09	3.03E+09
7 yr	2.57E+09	2.74E+09	2.90E+09	2.98E+09	3.04E+09

Table C.10: Table of cumulative mission fluence predictions for Channel 2 ($cm^{-2}MeV^{-1}$).

Mission	Confidence Level				
Duration	0.7	0.8	0.9	0.95	0.99
0.5 yr	5.90E+08	1.09E+09	2.03E+09	2.77E+09	4.24E+09
1 yr	1.58E+09	2.25E+09	3.17E+09	4.05E+09	5.98E+09
2 yr	3.19E+09	3.97E+09	5.20E+09	6.33E+09	8.70E+09
3 yr	4.65E+09	5.59E+09	7.00E+09	8.28E+09	1.10E+10
5 yr	7.51E+09	8.69E+09	1.04E+10	1.20E+10	1.51E+10
7 yr	1.03E+10	1.16E+10	1.36E+10	1.54E+10	1.90E+10

C.3 Channel 3 Figures and Tables

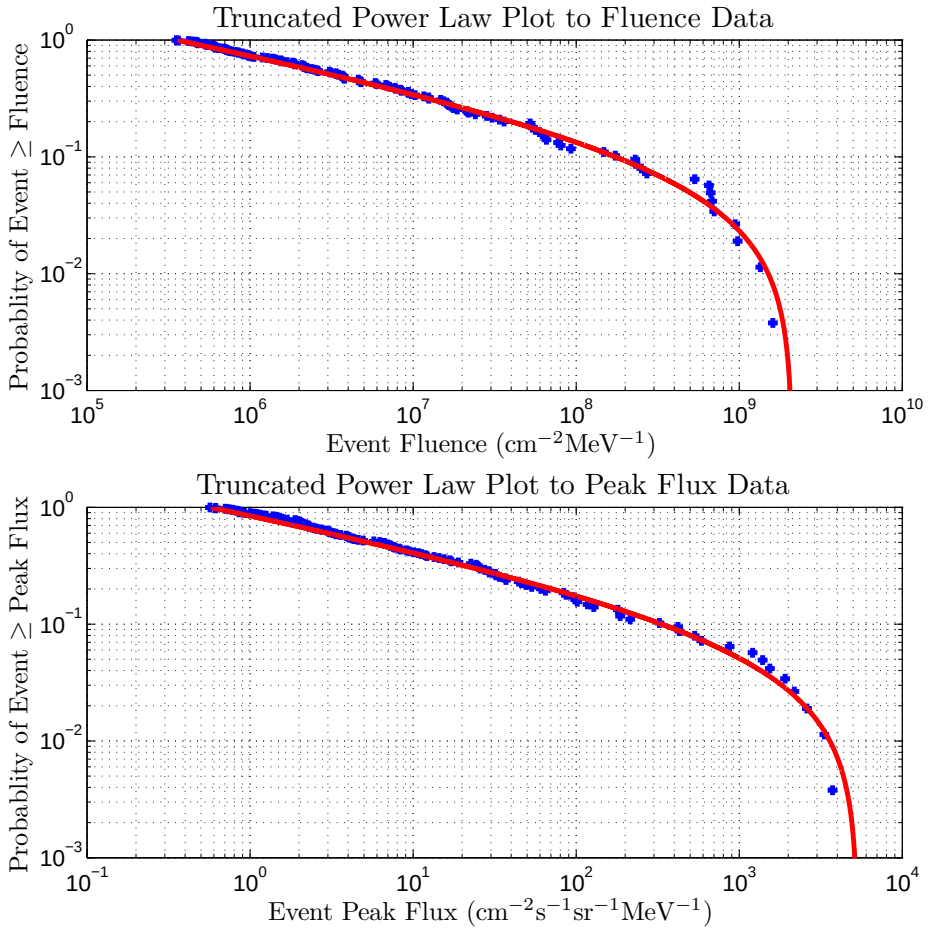

Figure C.7: Truncated Power Law Fits for Channel 3: 10.46 - 15.12 MeV.

Table C.11: Fluence and peak flux fitting parameters for Channel 3.

	b	$\phi_{\max}$	S^2	χ^2
Fluence	0.2740	2.12E+09	2.2425	0.1371
Peak flux	0.2760	5.33E+03	3.7754	1.6169

Table C.12: Regression parameters for Channel 3.

Peak Flux			Duration	
Gradient	Intercept	Residual σ	Adjust	Residual σ
0.9745	-12.8453	0.6508	-0.1712	0.4935

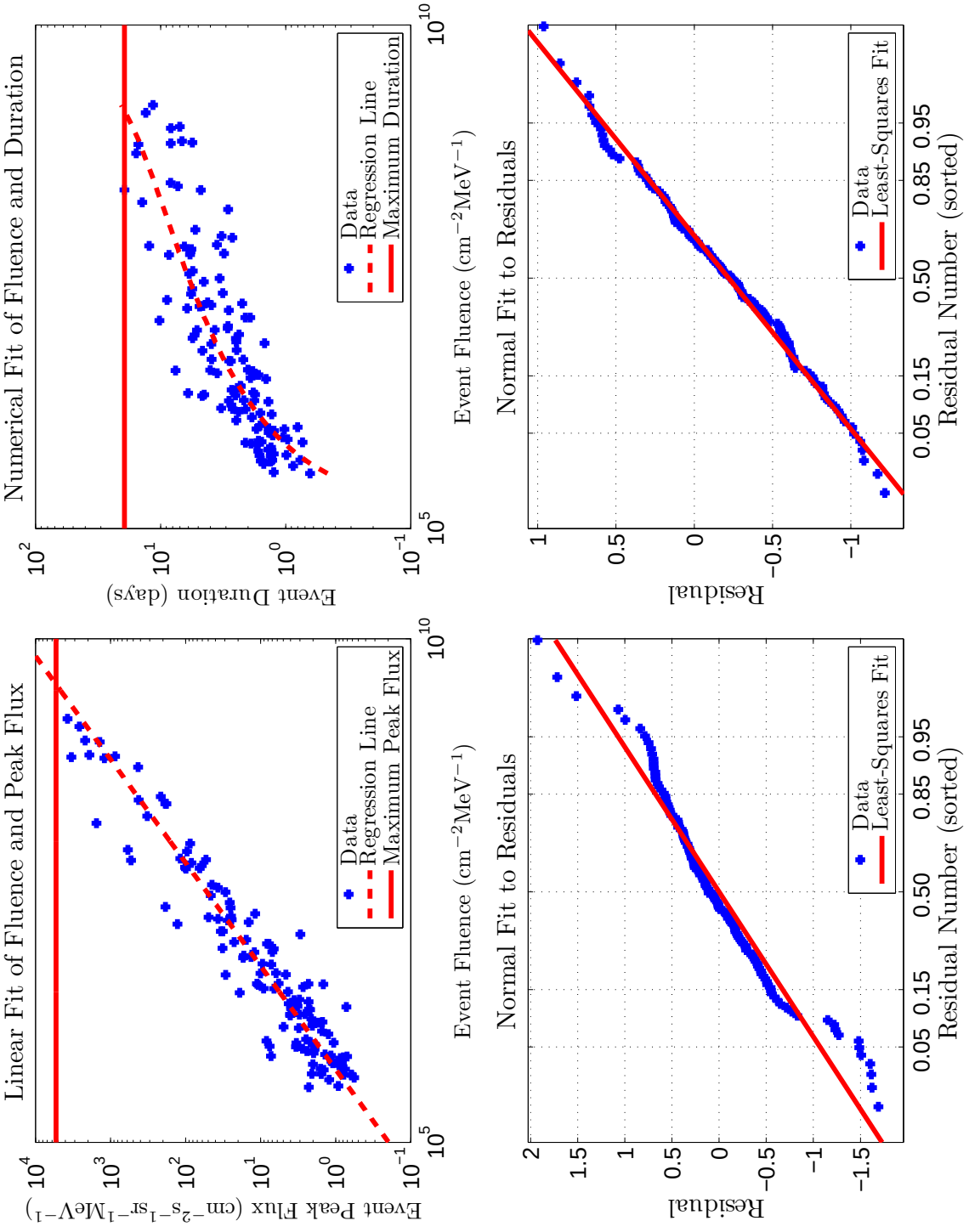

Figure C.8: Regression Fits for Channel 3: 10.46 - 15.12 MeV.

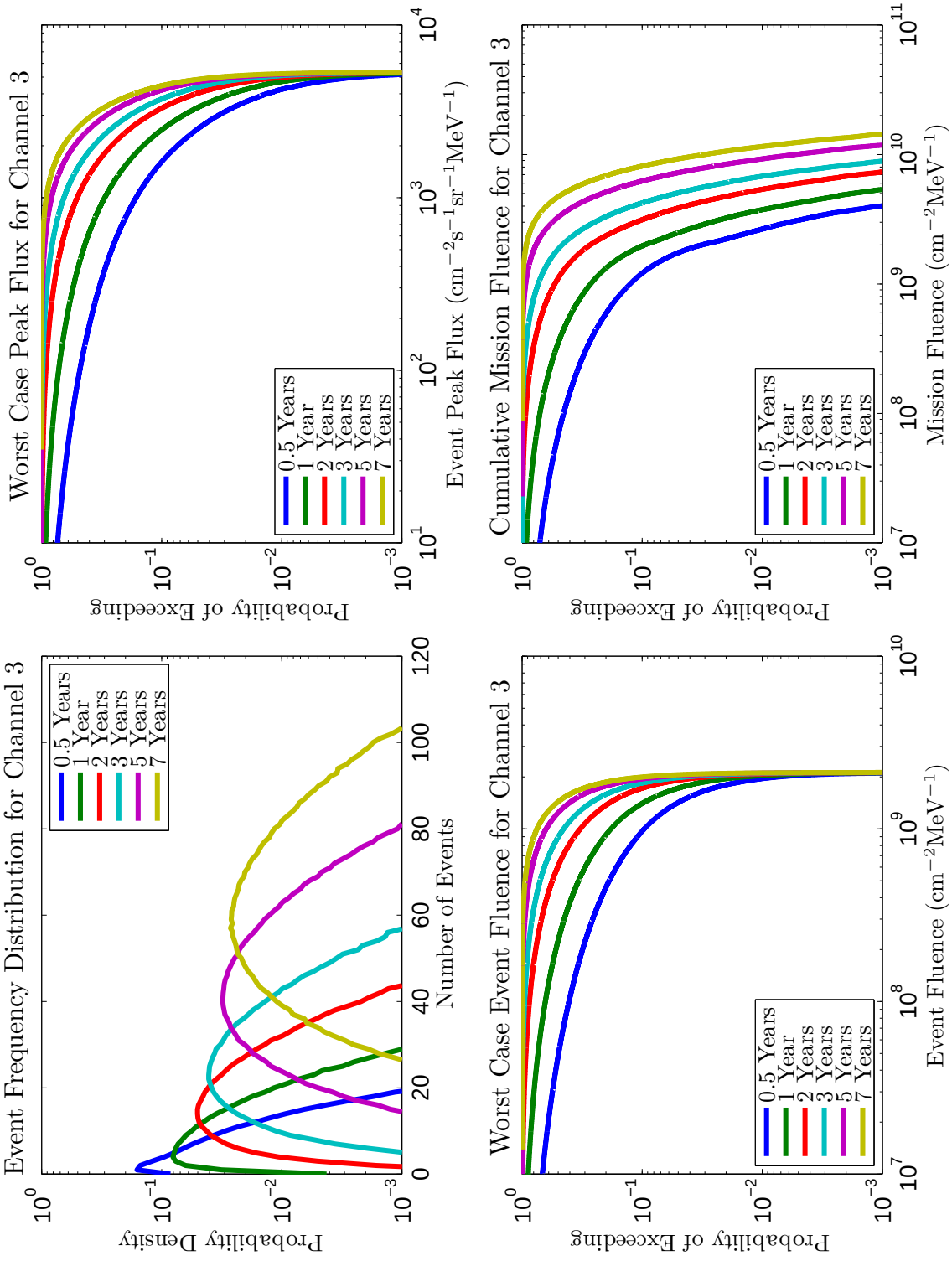

Figure C.9: Results for Channel 3: 10.46 - 15.12 MeV.

Table C.13: Table of worst-case peak flux predictions for Channel 3 ($cm^{-2}s^{-1}sr^{-1}MeV^{-1}$).

Mission	Confidence Level				
Duration	0.7	0.8	0.9	0.95	0.99
0.5 yr	3.78E+02	7.70E+02	1.61E+03	2.51E+03	4.24E+03
1 yr	9.93E+02	1.54E+03	2.47E+03	3.33E+03	4.71E+03
2 yr	1.80E+03	2.39E+03	3.30E+03	4.03E+03	4.98E+03
3 yr	2.32E+03	2.90E+03	3.73E+03	4.37E+03	5.10E+03
5 yr	2.95E+03	3.48E+03	4.20E+03	4.69E+03	5.18E+03
7 yr	3.34E+03	3.83E+03	4.46E+03	4.84E+03	5.22E+03

Table C.14: Table of worst-case event fluence predictions for Channel 3 ($cm^{-2}MeV^{-1}$).

Mission	Confidence Level				
Duration	0.7	0.8	0.9	0.95	0.99
0.5 yr	2.21E+08	4.59E+08	9.70E+08	1.42E+09	1.95E+09
1 yr	5.96E+08	9.25E+08	1.40E+09	1.72E+09	2.04E+09
2 yr	1.07E+09	1.37E+09	1.72E+09	1.91E+09	2.08E+09
3 yr	1.34E+09	1.59E+09	1.84E+09	1.98E+09	2.09E+09
5 yr	1.60E+09	1.77E+09	1.95E+09	2.04E+09	2.11E+09
7 yr	1.73E+09	1.87E+09	2.00E+09	2.06E+09	2.11E+09

Table C.15: Table of cumulative mission fluence predictions for Channel 3 ($cm^{-2}MeV^{-1}$).

Mission	Confidence Level				
Duration	0.7	0.8	0.9	0.95	0.99
0.5 yr	2.97E+08	5.93E+08	1.21E+09	1.75E+09	2.66E+09
1 yr	8.77E+08	1.33E+09	1.97E+09	2.49E+09	3.75E+09
2 yr	1.87E+09	2.36E+09	3.14E+09	3.87E+09	5.39E+09
3 yr	2.72E+09	3.32E+09	4.23E+09	5.07E+09	6.80E+09
5 yr	4.40E+09	5.14E+09	6.24E+09	7.25E+09	9.26E+09
7 yr	6.02E+09	6.87E+09	8.14E+09	9.27E+09	1.15E+10

C.4 Channel 4 Figures and Tables

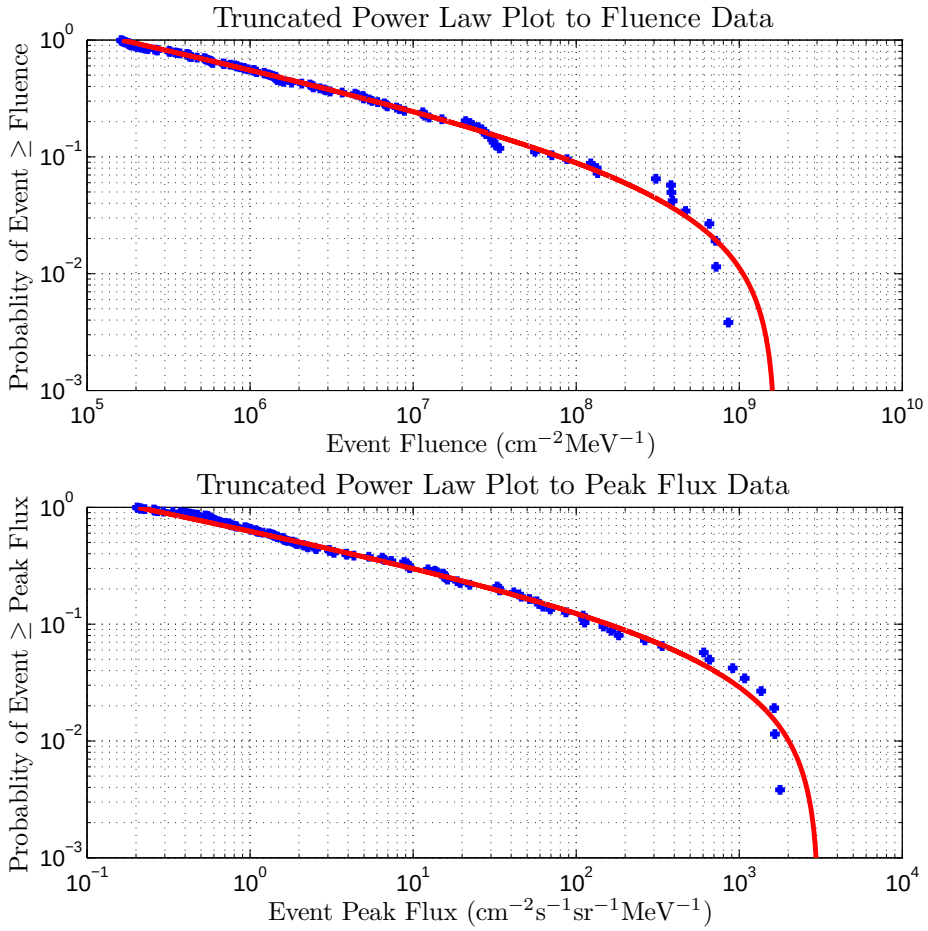

Figure C.10: Truncated Power Law Fits for Channel 4: 15.12 - 21.87 MeV.

Table C.16: Fluence and peak flux fitting parameters for Channel 4.

	b	$\phi_{\max}$	S^2	χ^2
Fluence	0.2998	1.68E+09	2.9029	0.1735
Peak flux	0.2686	3.10E+03	4.2913	-1.1592

Table C.17: Regression parameters for Channel 4.

Peak Flux			Duration	
Gradient	Intercept	Residual σ	Adjust	Residual σ
0.9803	-12.9826	0.6544	-0.2403	0.5508

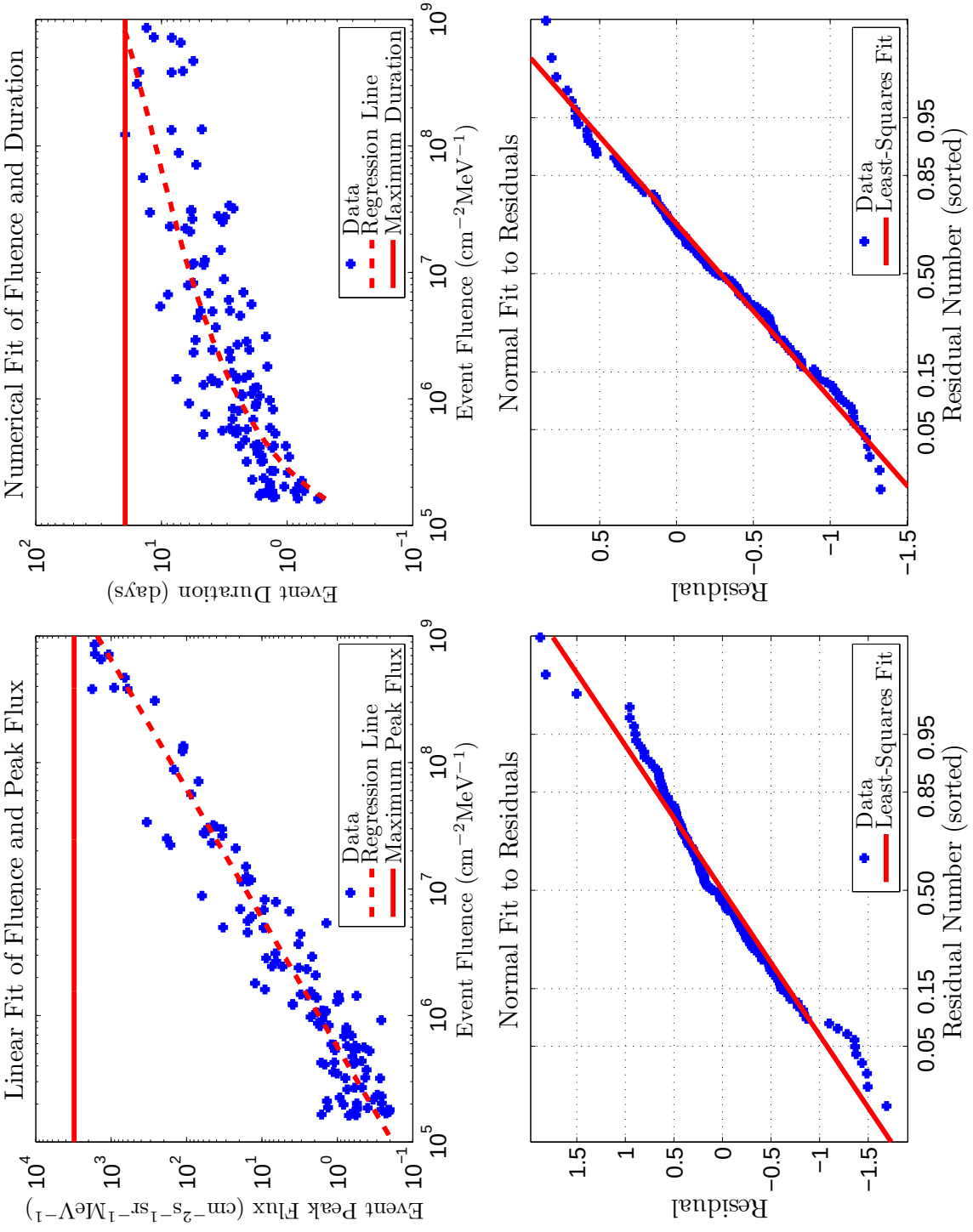

Figure C.11: Regression Fits for Channel 4: 15.12 - 21.87 MeV.

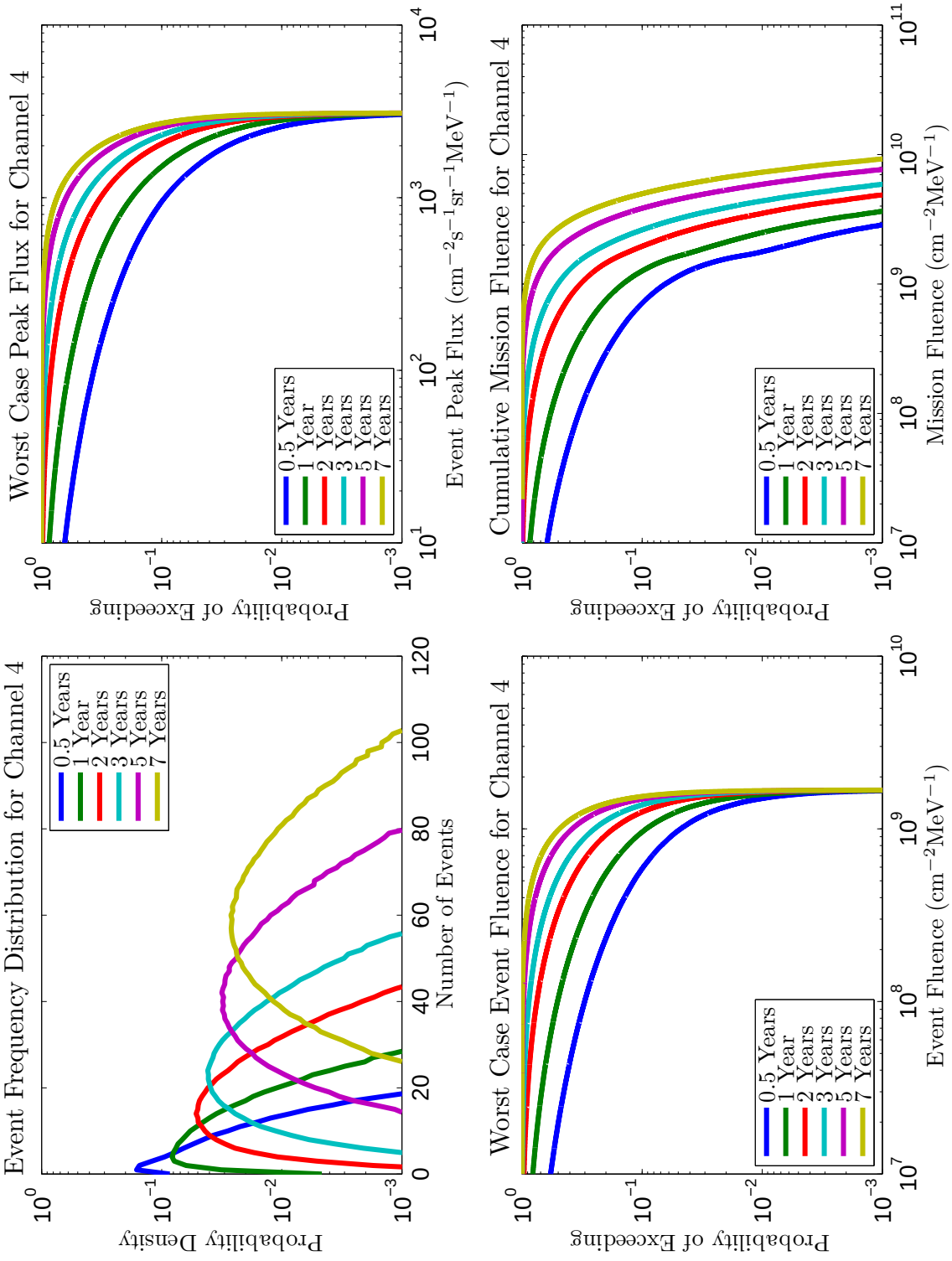

Figure C.12: Results for Channel 4: 15.12 - 21.87 MeV.

Table C.18: Table of worst-case peak flux predictions for Channel 4 ($cm^{-2}s^{-1}sr^{-1}MeV^{-1}$).

Mission	Confidence Level				
Duration	0.7	0.8	0.9	0.95	0.99
0.5 yr	1.72E+02	3.93E+02	9.50E+02	1.55E+03	2.58E+03
1 yr	5.32E+02	8.93E+02	1.52E+03	2.07E+03	2.81E+03
2 yr	1.08E+03	1.48E+03	2.05E+03	2.48E+03	2.95E+03
3 yr	1.42E+03	1.80E+03	2.31E+03	2.64E+03	2.99E+03
5 yr	1.83E+03	2.16E+03	2.56E+03	2.81E+03	3.04E+03
7 yr	2.07E+03	2.36E+03	2.70E+03	2.89E+03	3.06E+03

Table C.19: Table of worst-case event fluence predictions for Channel 4 ($cm^{-2}MeV^{-1}$).

Mission	Confidence Level				
Duration	0.7	0.8	0.9	0.95	0.99
0.5 yr	1.01E+08	2.34E+08	5.89E+08	9.77E+08	1.50E+09
1 yr	3.22E+08	5.55E+08	9.59E+08	1.27E+09	1.58E+09
2 yr	6.73E+08	9.24E+08	1.25E+09	1.45E+09	1.63E+09
3 yr	8.90E+08	1.12E+09	1.38E+09	1.52E+09	1.65E+09
5 yr	1.14E+09	1.31E+09	1.49E+09	1.58E+09	1.66E+09
7 yr	1.26E+09	1.40E+09	1.54E+09	1.61E+09	1.67E+09

Table C.20: Table of cumulative mission fluence predictions for Channel 4 ($cm^{-2}MeV^{-1}$).

Mission	Confidence Level				
Duration	0.7	0.8	0.9	0.95	0.99
0.5 yr	1.33E+08	2.95E+08	7.11E+08	1.15E+09	1.78E+09
1 yr	4.54E+08	7.57E+08	1.26E+09	1.64E+09	2.50E+09
2 yr	1.09E+09	1.45E+09	1.96E+09	2.46E+09	3.52E+09
3 yr	1.62E+09	2.01E+09	2.62E+09	3.20E+09	4.39E+09
5 yr	2.60E+09	3.09E+09	3.85E+09	4.51E+09	5.90E+09
7 yr	3.57E+09	4.13E+09	4.98E+09	5.75E+09	7.30E+09

C.5 Channel 5 Figures and Tables

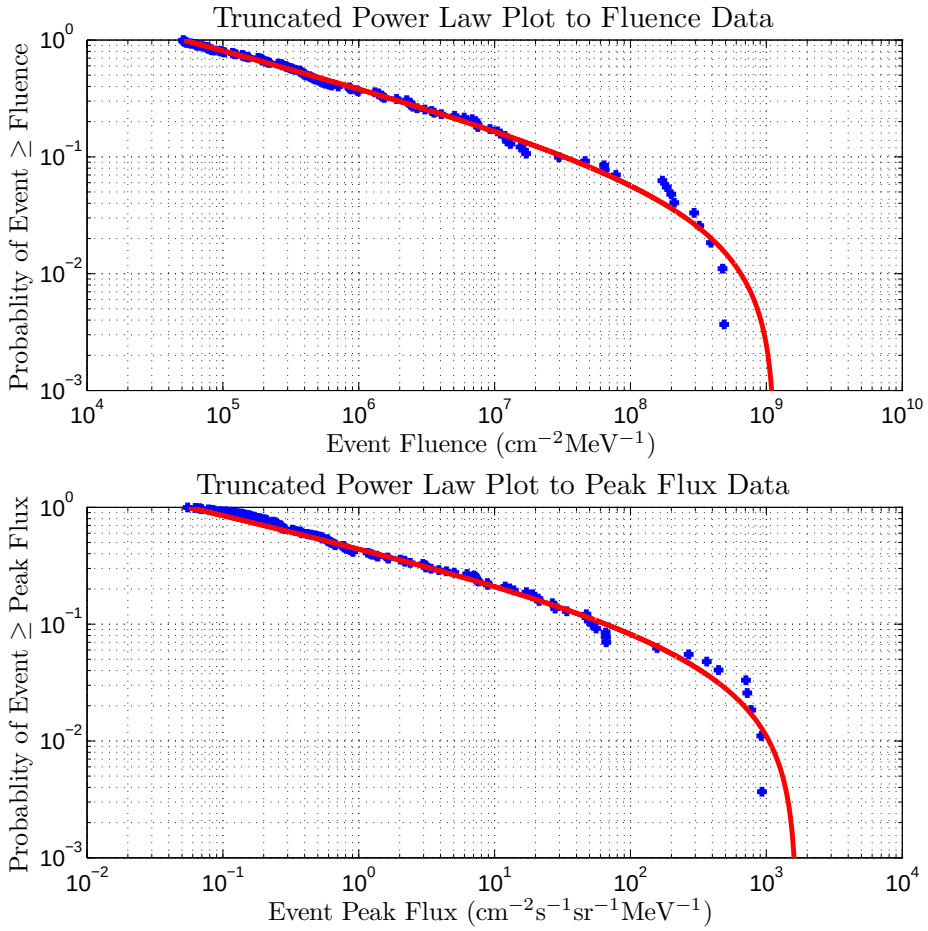

Figure C.13: Truncated Power Law Fits for Channel 5: 21.87 - 31.62 MeV.

Table C.21: Fluence and peak flux fitting parameters for Channel 5.

	b	$\phi_{\max}$	S^2	χ^2
Fluence	0.2998	1.17E+09	3.8273	0.2381
Peak flux	0.2544	1.68E+03	9.0566	42.2772

Table C.22: Regression parameters for Channel 5.

Peak Flux			Duration	
Gradient	Intercept	Residual σ	Adjust	Residual σ
0.9814	-13.0368	0.6696	-0.1591	0.5470

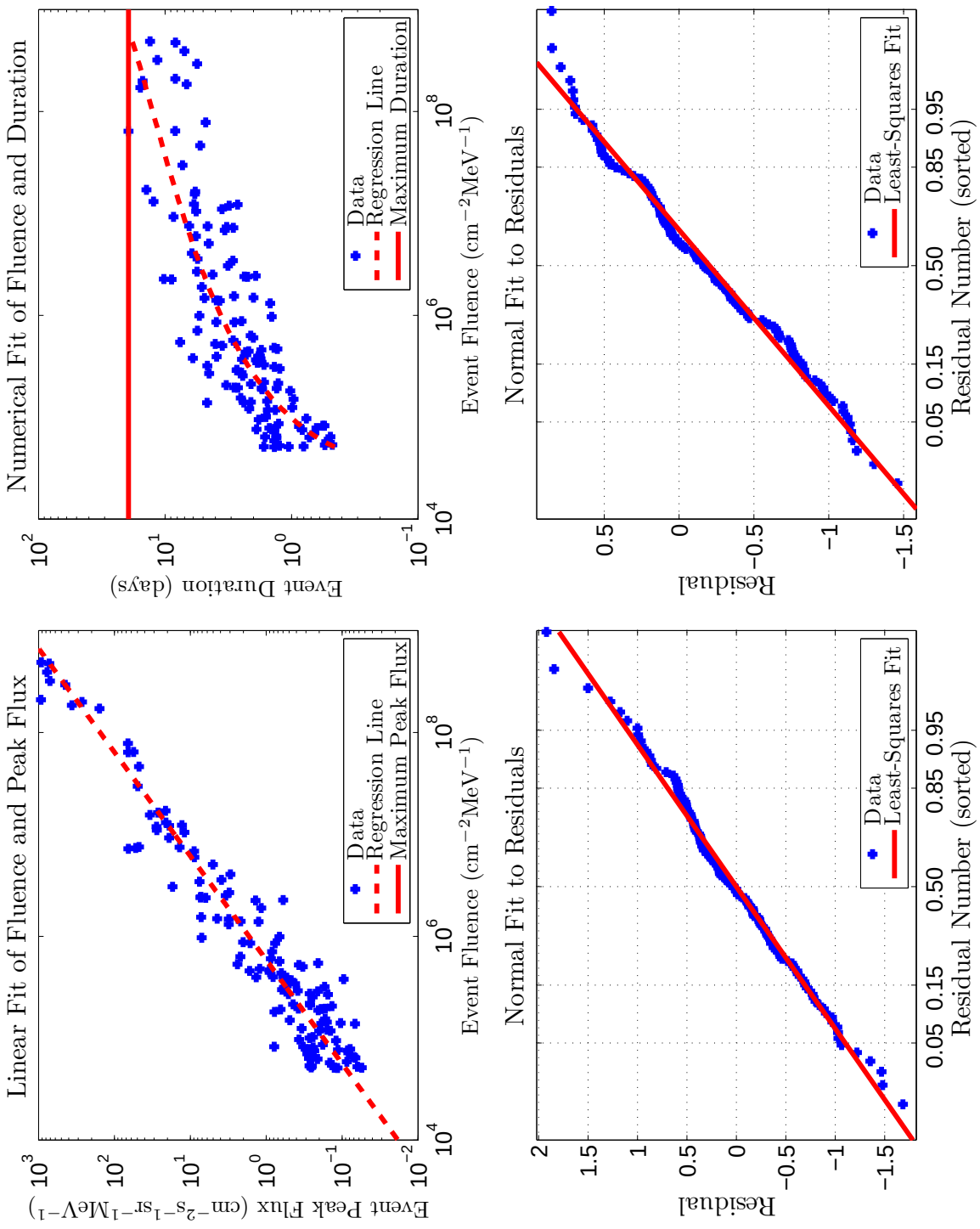

Figure C.14: Regression Fits for Channel 5: 21.87 - 31.62 MeV.

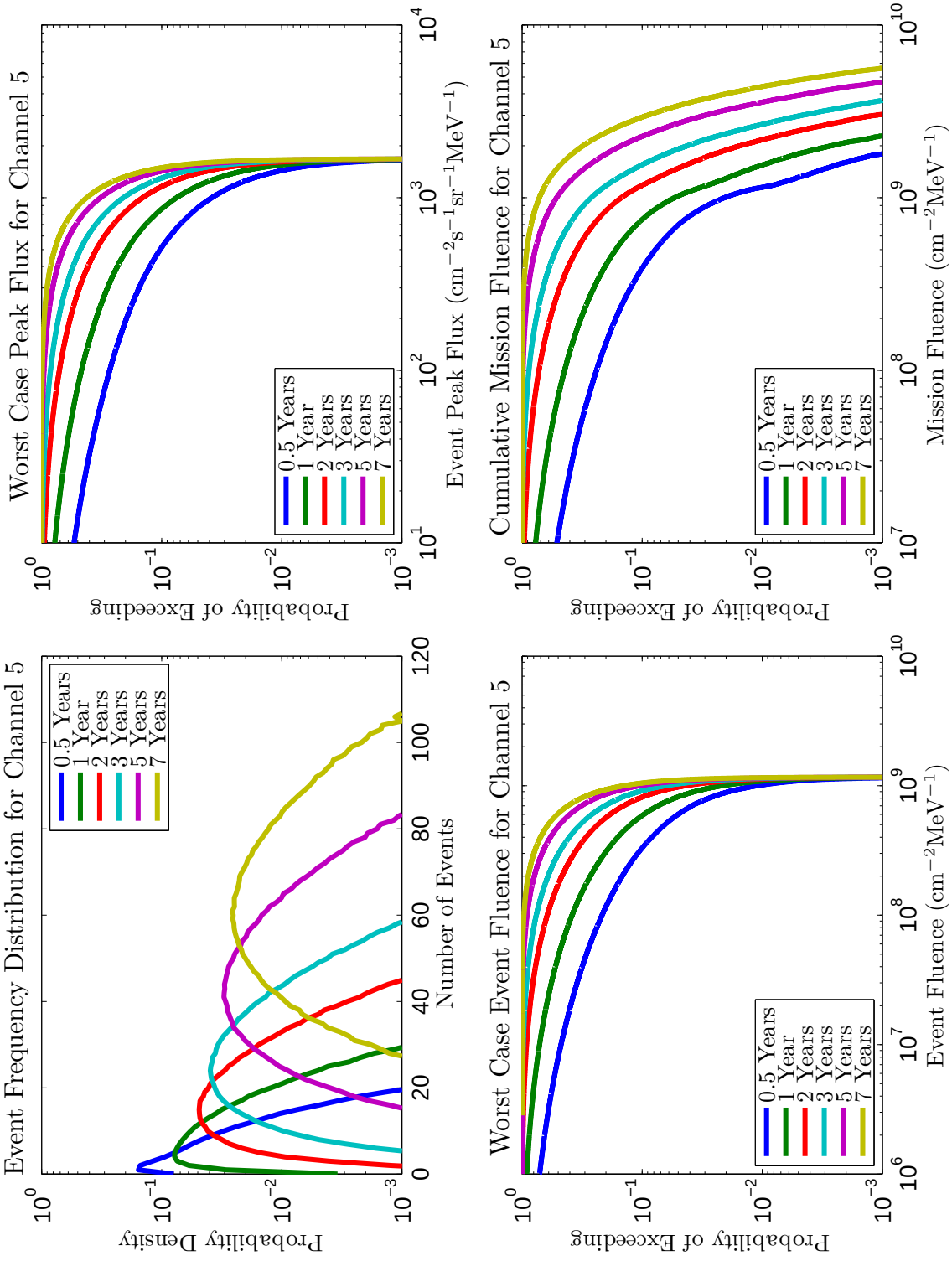

Figure C.15: Results for Channel 5: 21.87 - 31.62 MeV.

Table C.23: Table of worst-case peak flux predictions for Channel 5 ($cm^{-2}s^{-1}sr^{-1}MeV^{-1}$).

Mission	Confidence Level				
Duration	0.7	0.8	0.9	0.95	0.99
0.5 yr	7.70E+01	1.93E+02	5.16E+02	8.76E+02	1.44E+03
1 yr	2.71E+02	4.86E+02	8.61E+02	1.17E+03	1.55E+03
2 yr	5.98E+02	8.33E+02	1.16E+03	1.38E+03	1.61E+03
3 yr	8.02E+02	1.02E+03	1.30E+03	1.47E+03	1.63E+03
5 yr	1.04E+03	1.22E+03	1.43E+03	1.55E+03	1.65E+03
7 yr	1.17E+03	1.33E+03	1.49E+03	1.58E+03	1.66E+03

Table C.24: Table of worst-case event fluence predictions for Channel 5 ($cm^{-2}MeV^{-1}$).

Mission	Confidence Level				
Duration	0.7	0.8	0.9	0.95	0.99
0.5 yr	4.61E+07	1.17E+08	3.31E+08	6.02E+08	1.01E+09
1 yr	1.67E+08	3.10E+08	5.88E+08	8.21E+08	1.09E+09
2 yr	3.91E+08	5.68E+08	8.17E+08	9.77E+08	1.13E+09
3 yr	5.42E+08	7.08E+08	9.15E+08	1.03E+09	1.14E+09
5 yr	7.26E+08	8.61E+08	1.01E+09	1.09E+09	1.15E+09
7 yr	8.24E+08	9.35E+08	1.05E+09	1.11E+09	1.15E+09

Table C.25: Table of cumulative mission fluence predictions for Channel 5 ($cm^{-2}MeV^{-1}$).

Mission	Confidence Level				
Duration	0.7	0.8	0.9	0.95	0.99
0.5 yr	5.96E+07	1.44E+08	3.91E+08	6.97E+08	1.15E+09
1 yr	2.29E+08	4.09E+08	7.48E+08	1.02E+09	1.55E+09
2 yr	5.97E+08	8.41E+08	1.18E+09	1.48E+09	2.17E+09
3 yr	9.19E+08	1.17E+09	1.55E+09	1.91E+09	2.66E+09
5 yr	1.48E+09	1.79E+09	2.26E+09	2.70E+09	3.58E+09
7 yr	2.03E+09	2.39E+09	2.93E+09	3.41E+09	4.40E+09

C.6 Channel 6 Figures and Tables

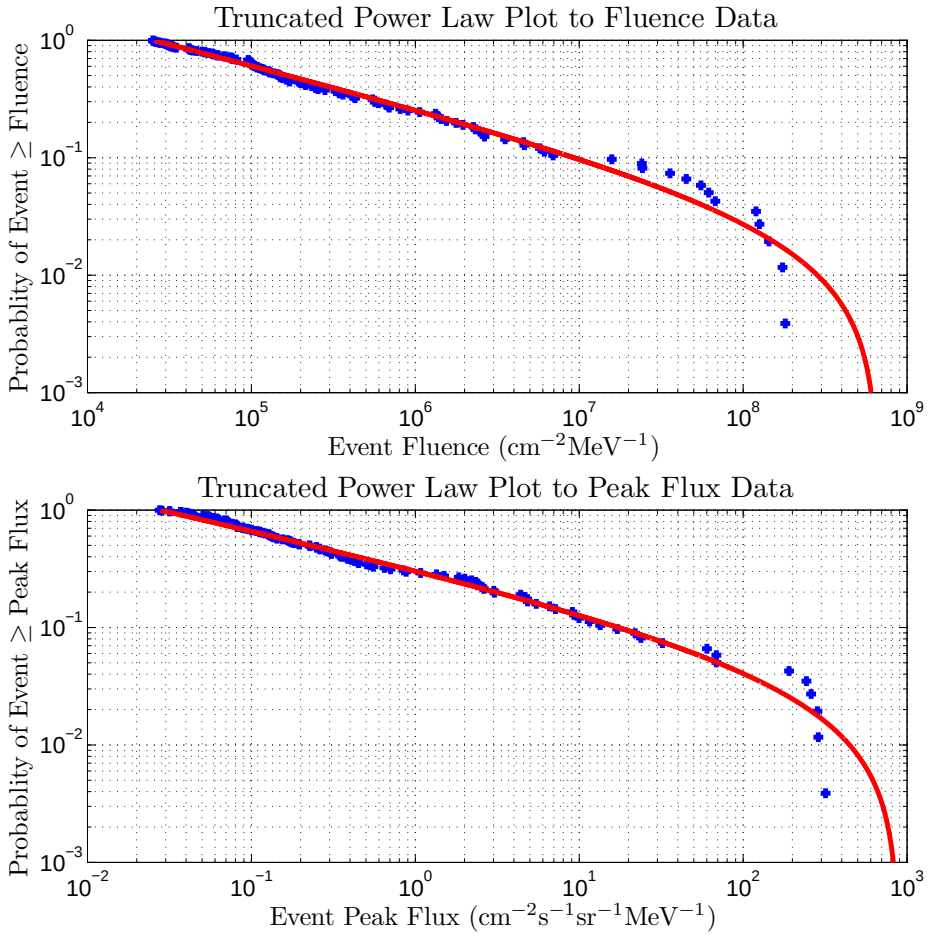

Figure C.16: Truncated Power Law Fits for Channel 6: 31.62 - 45.73 MeV.

Table C.26: Fluence and peak flux fitting parameters for Channel 6.

	b	$\phi_{\max}$	S^2	χ^2
Fluence	0.3519	6.66E+08	6.2754	0.4066
Peak flux	0.3096	8.91E+02	5.3976	-1.1076

Table C.27: Regression parameters for Channel 6.

Peak Flux			Duration	
Gradient	Intercept	Residual σ	Adjust	Residual σ
1.0003	-13.4263	0.6488	-0.1990	0.5402

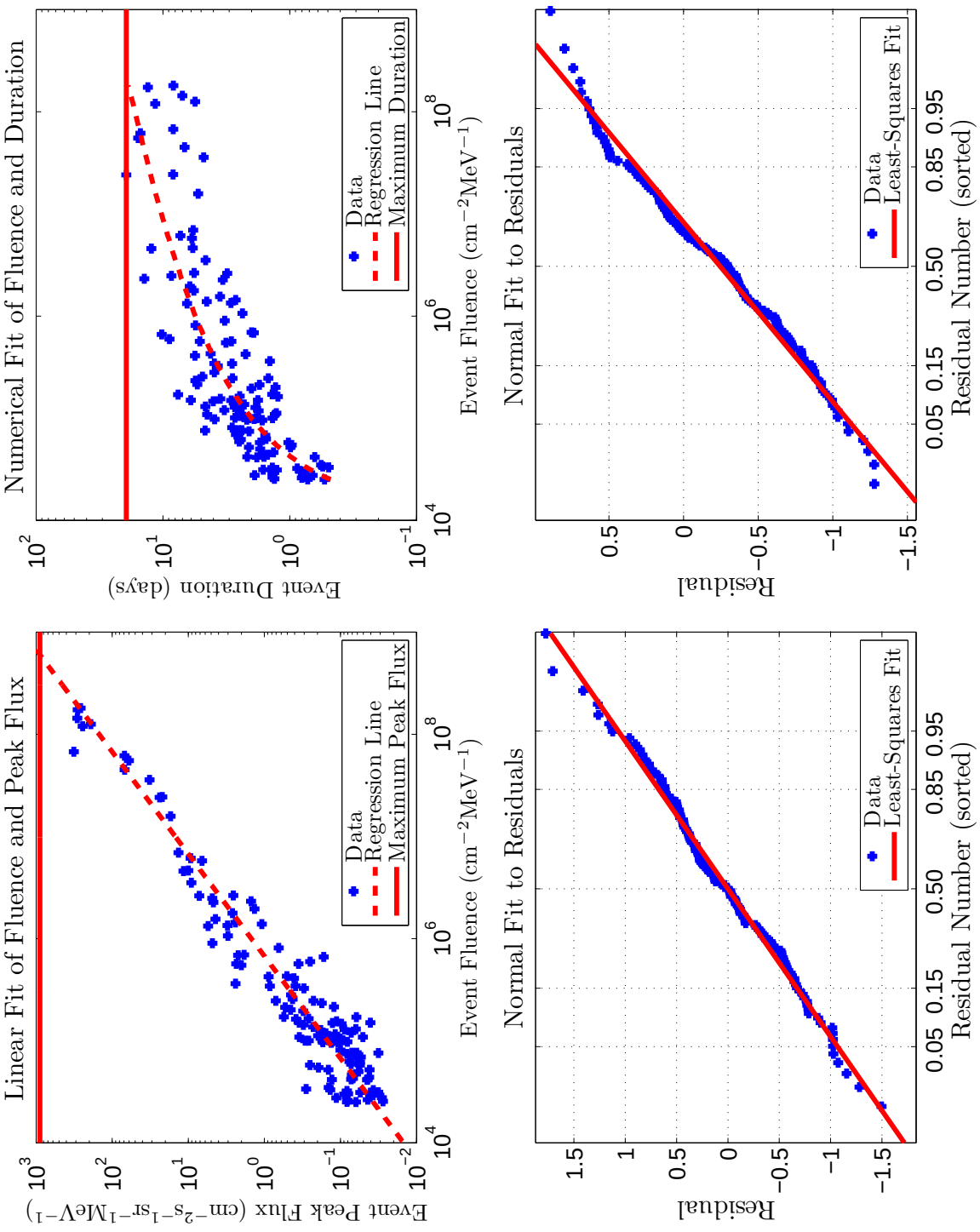

Figure C.17: Regression Fits for Channel 6: 31.62 - 45.73 MeV.

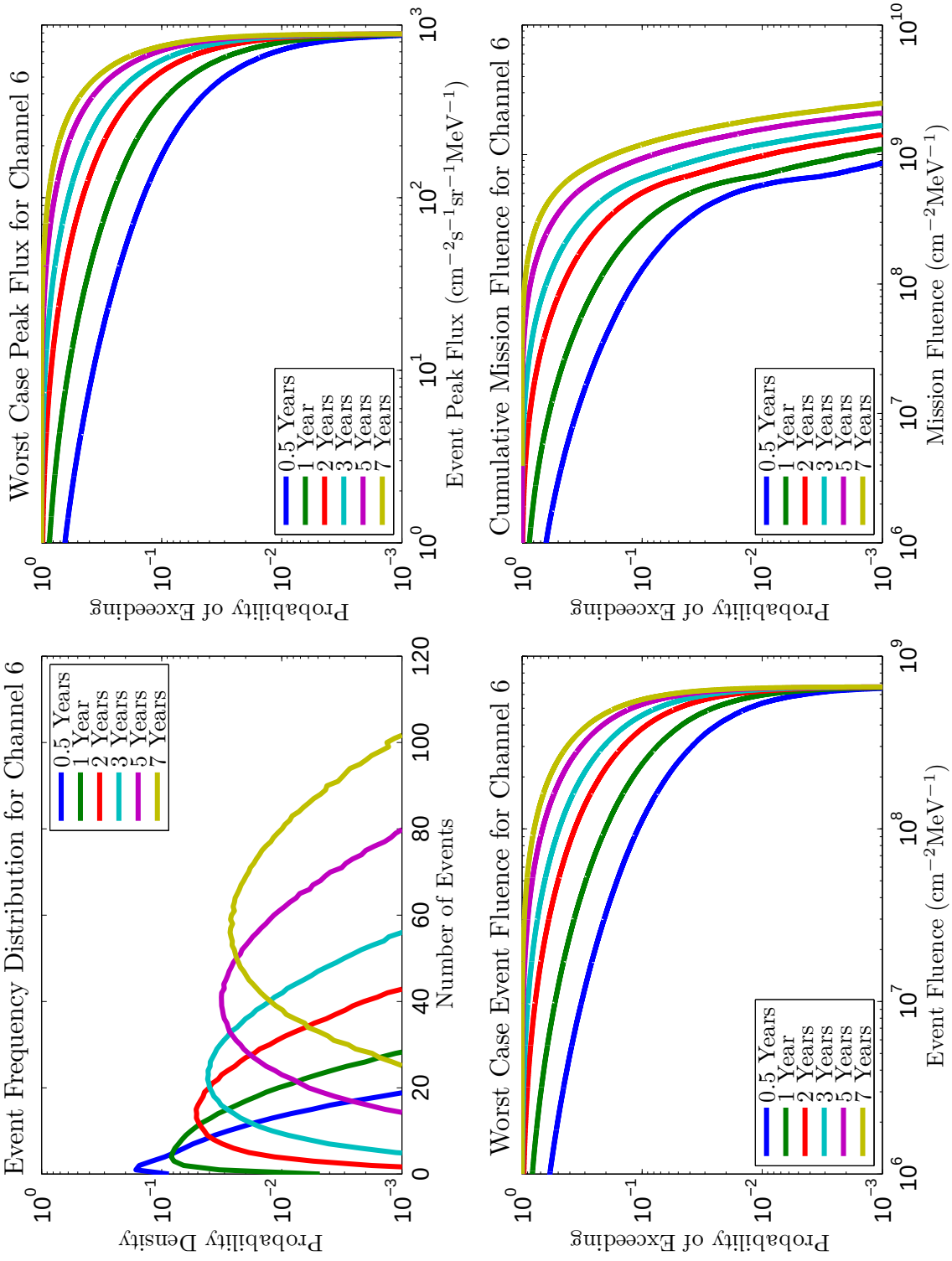

Figure C.18: Results for Channel 6: 31.62 - 45.73 MeV.

Table C.28: Table of worst-case peak flux predictions for Channel 6 ($cm^{-2}s^{-1}sr^{-1}MeV^{-1}$).

Mission	Confidence Level				
Duration	0.7	0.8	0.9	0.95	0.99
0.5 yr	1.90E+01	5.18E+01	1.76E+02	3.63E+02	7.19E+02
1 yr	7.71E+01	1.61E+02	3.57E+02	5.42E+02	7.96E+02
2 yr	2.15E+02	3.42E+02	5.37E+02	6.82E+02	8.42E+02
3 yr	3.22E+02	4.50E+02	6.26E+02	7.42E+02	8.58E+02
5 yr	4.62E+02	5.75E+02	7.13E+02	7.96E+02	8.70E+02
7 yr	5.43E+02	6.43E+02	7.56E+02	8.20E+02	8.76E+02

Table C.29: Table of worst-case event fluence predictions for Channel 6 ($cm^{-2}MeV^{-1}$).

Mission	Confidence Level				
Duration	0.7	0.8	0.9	0.95	0.99
0.5 yr	1.19E+07	3.25E+07	1.12E+08	2.45E+08	5.34E+08
1 yr	4.82E+07	1.02E+08	2.38E+08	3.86E+08	5.95E+08
2 yr	1.38E+08	2.26E+08	3.81E+08	5.01E+08	6.29E+08
3 yr	2.14E+08	3.12E+08	4.55E+08	5.51E+08	6.41E+08
5 yr	3.20E+08	4.13E+08	5.26E+08	5.93E+08	6.50E+08
7 yr	3.87E+08	4.69E+08	5.62E+08	6.12E+08	6.55E+08

Table C.30: Table of cumulative mission fluence predictions for Channel 6 ($cm^{-2}MeV^{-1}$).

Mission	Confidence Level				
Duration	0.7	0.8	0.9	0.95	0.99
0.5 yr	1.56E+07	3.99E+07	1.30E+08	2.75E+08	5.82E+08
1 yr	6.49E+07	1.30E+08	2.89E+08	4.57E+08	6.97E+08
2 yr	1.99E+08	3.14E+08	5.07E+08	6.53E+08	9.75E+08
3 yr	3.34E+08	4.69E+08	6.59E+08	8.21E+08	1.19E+09
5 yr	5.70E+08	7.14E+08	9.33E+08	1.14E+09	1.57E+09
7 yr	7.81E+08	9.43E+08	1.20E+09	1.42E+09	1.90E+09

C.7 Channel 7 Figures and Tables

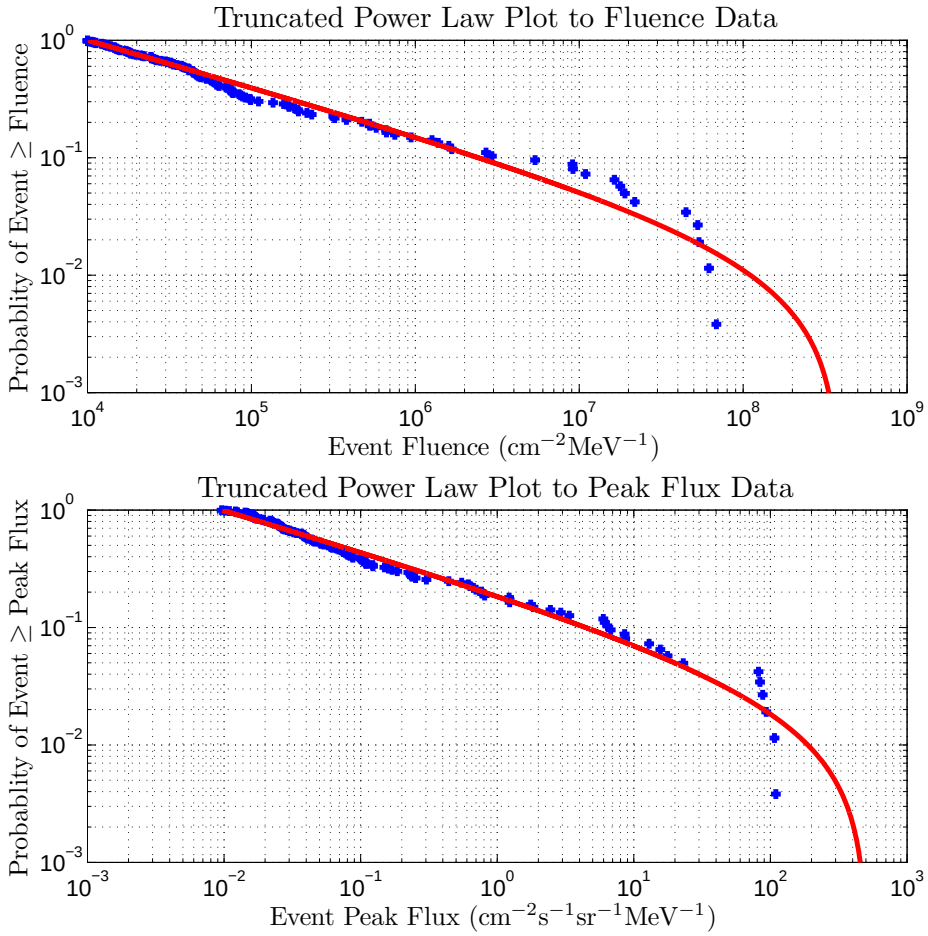

Figure C.19: Truncated Power Law Fits for Channel 7: 45.73 - 66.13 MeV.

Table C.31: Fluence and peak flux fitting parameters for Channel 7.

	b	$\phi_{\max}$	S^2	χ^2
Fluence	0.3962	3.91E+08	13.3500	0.9446
Peak flux	0.3439	5.11E+02	10.4499	-0.6630

Table C.32: Regression parameters for Channel 7.

Peak Flux			Duration	
Gradient	Intercept	Residual σ	Adjust	Residual σ
1.0173	-13.7276	0.6927	-0.2096	0.5820

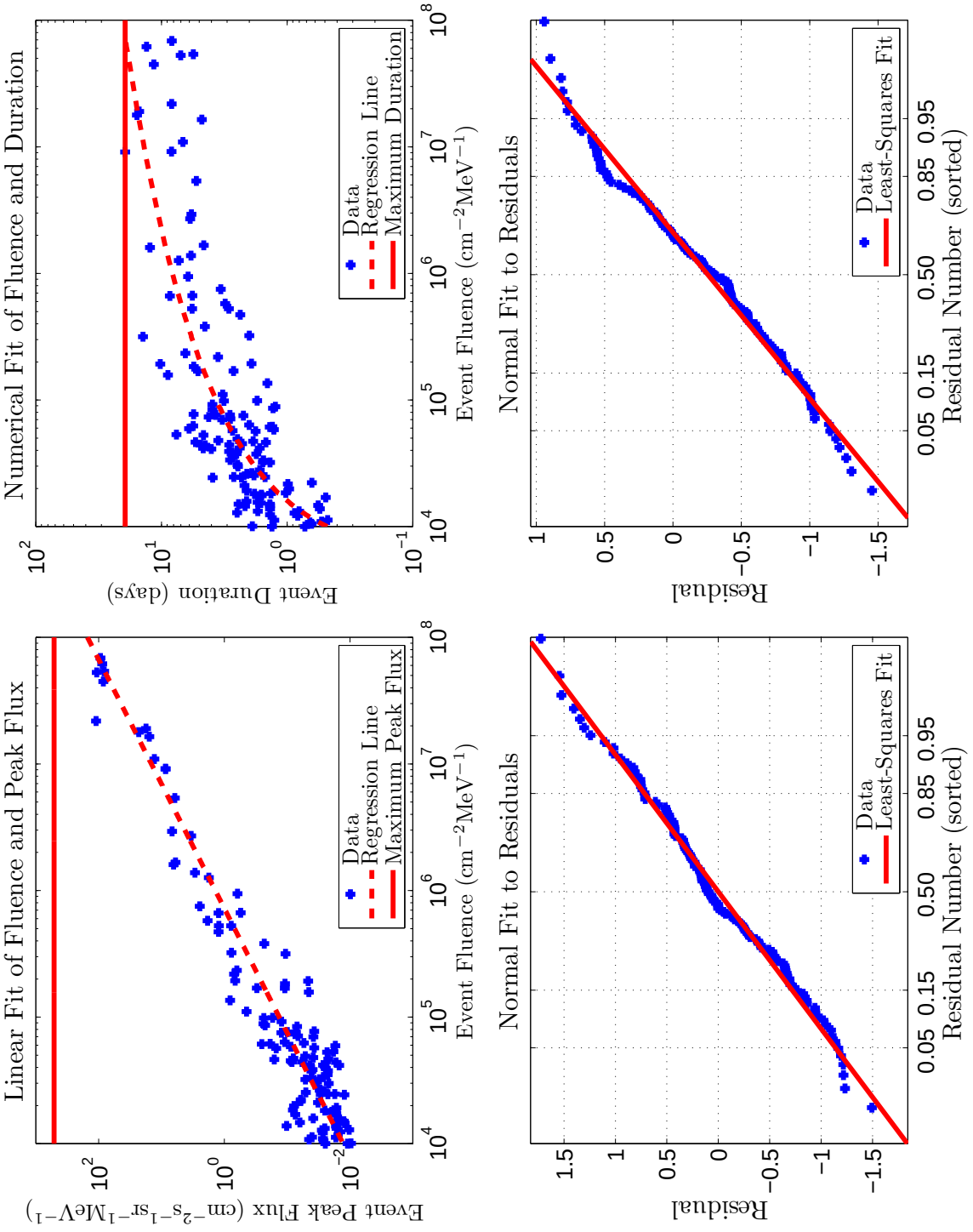

Figure C.20: Regression Fits for Channel 7: 45.73 - 66.13 MeV.

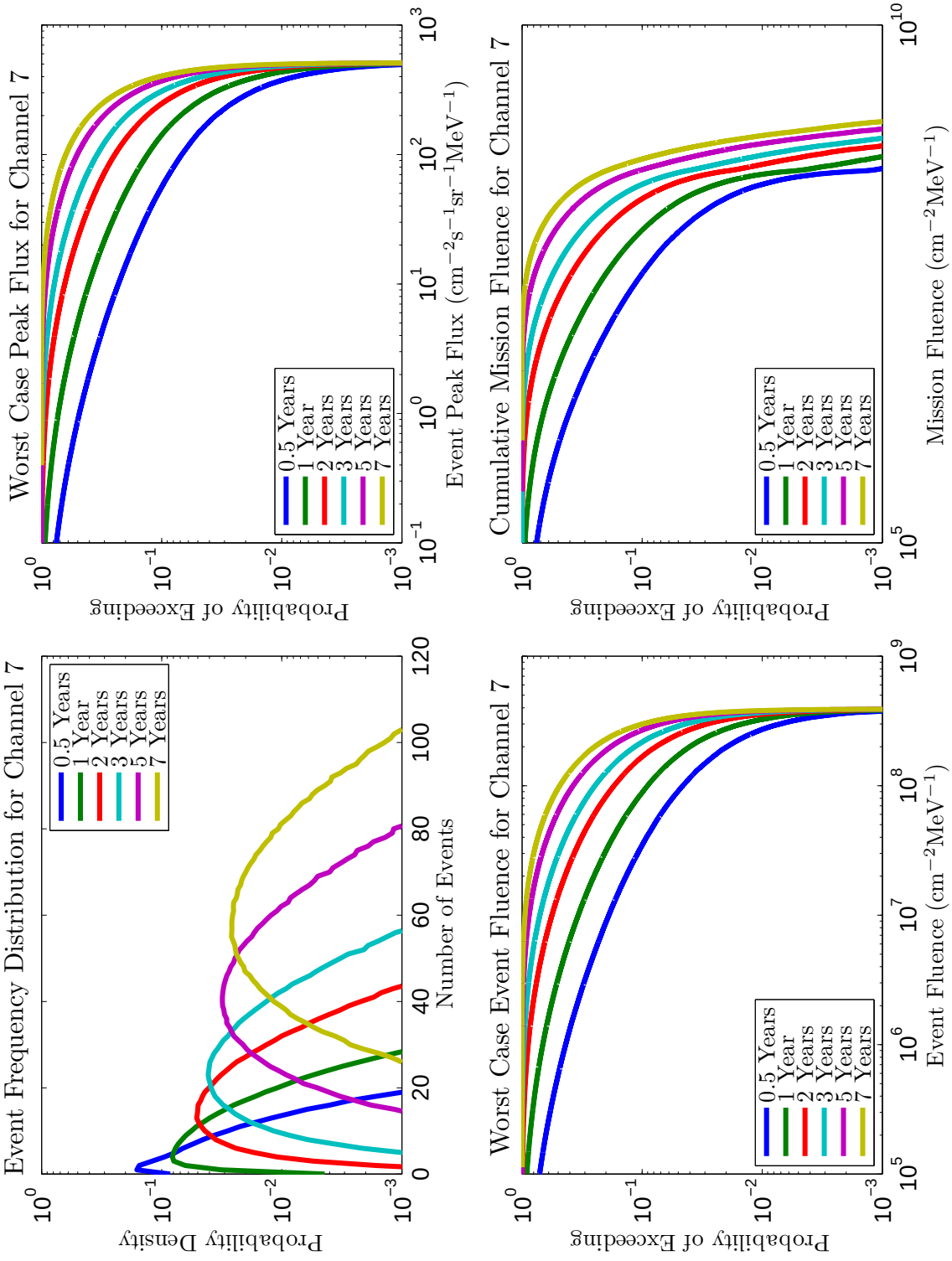

Figure C.21: Results for Channel 7: 45.73 - 66.13 MeV.

Table C.33: Table of worst-case peak flux predictions for Channel 7 ($cm^{-2}s^{-1}sr^{-1}MeV^{-1}$).

Mission	Confidence Level				
Duration	0.7	0.8	0.9	0.95	0.99
0.5 yr	4.92E+00	1.40E+01	5.61E+01	1.46E+02	3.74E+02
1 yr	2.17E+01	5.08E+01	1.42E+02	2.54E+02	4.35E+02
2 yr	7.23E+01	1.32E+02	2.47E+02	3.47E+02	4.70E+02
3 yr	1.23E+02	1.96E+02	3.09E+02	3.92E+02	4.83E+02
5 yr	2.02E+02	2.74E+02	3.71E+02	4.34E+02	4.95E+02
7 yr	2.55E+02	3.22E+02	4.04E+02	4.53E+02	4.99E+02

Table C.34: Table of worst-case event fluence predictions for Channel 7 ($cm^{-2}MeV^{-1}$).

Mission	Confidence Level				
Duration	0.7	0.8	0.9	0.95	0.99
0.5 yr	3.16E+06	8.83E+06	3.48E+07	9.10E+07	2.72E+08
1 yr	1.36E+07	3.15E+07	8.85E+07	1.72E+08	3.25E+08
2 yr	4.47E+07	8.27E+07	1.67E+08	2.49E+08	3.56E+08
3 yr	7.70E+07	1.27E+08	2.17E+08	2.89E+08	3.68E+08
5 yr	1.31E+08	1.88E+08	2.69E+08	3.24E+08	3.77E+08
7 yr	1.73E+08	2.28E+08	2.99E+08	3.42E+08	3.81E+08

Table C.35: Table of cumulative mission fluence predictions for Channel 7 ($cm^{-2}MeV^{-1}$).

Mission	Confidence Level				
Duration	0.7	0.8	0.9	0.95	0.99
0.5 yr	4.21E+06	1.09E+07	4.00E+07	1.00E+08	2.90E+08
1 yr	1.84E+07	4.00E+07	1.05E+08	1.97E+08	3.63E+08
2 yr	6.29E+07	1.11E+08	2.10E+08	3.06E+08	4.52E+08
3 yr	1.14E+08	1.79E+08	2.90E+08	3.76E+08	5.55E+08
5 yr	2.16E+08	2.93E+08	4.02E+08	4.98E+08	7.18E+08
7 yr	3.09E+08	3.91E+08	5.10E+08	6.22E+08	8.57E+08

C.8 Channel 8 Figures and Tables

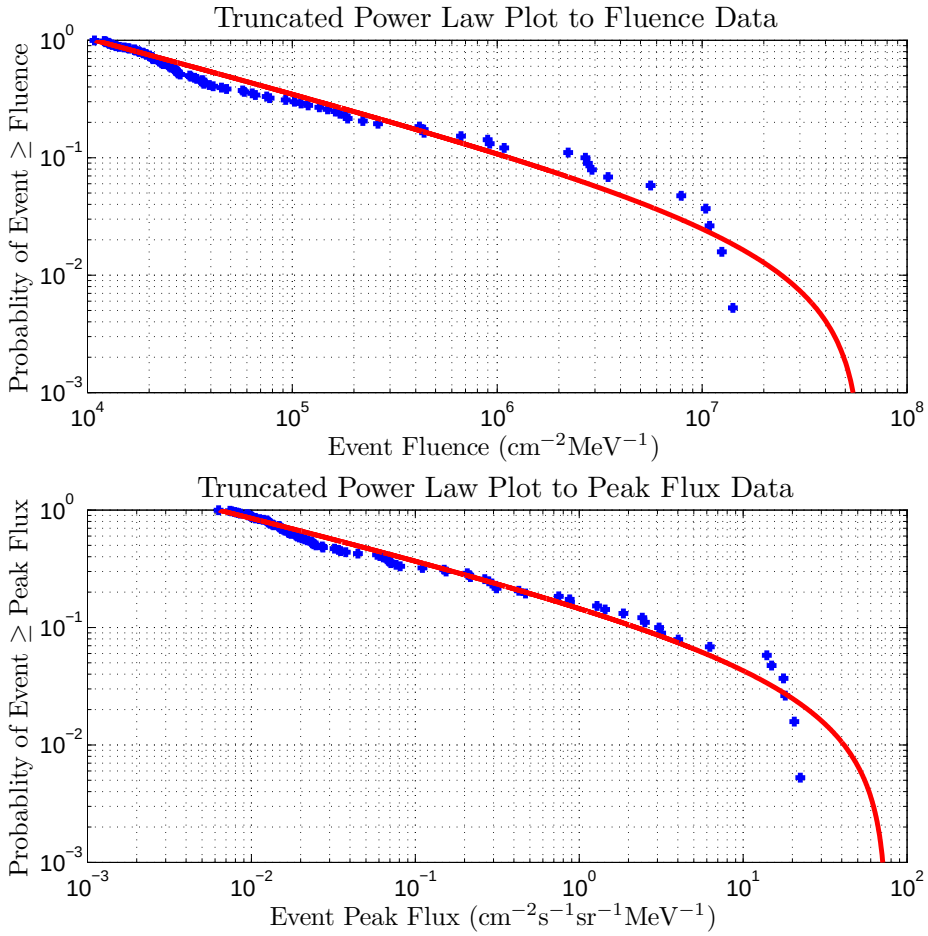

Figure C.22: Truncated Power Law Fits for Channel 8: 66.13 - 95.64 MeV.

Table C.36: Fluence and peak flux fitting parameters for Channel 8.

	b	$\phi_{\max}$	S^2	χ^2
Fluence	0.4610	6.10E+07	11.1993	0.8965
Peak flux	0.3381	7.61E+01	8.9247	1.5385

Table C.37: Regression parameters for Channel 8.

Peak Flux			Duration	
Gradient	Intercept	Residual σ	Adjust	Residual σ
1.1225	-15.1628	0.6748	-0.5740	0.6695

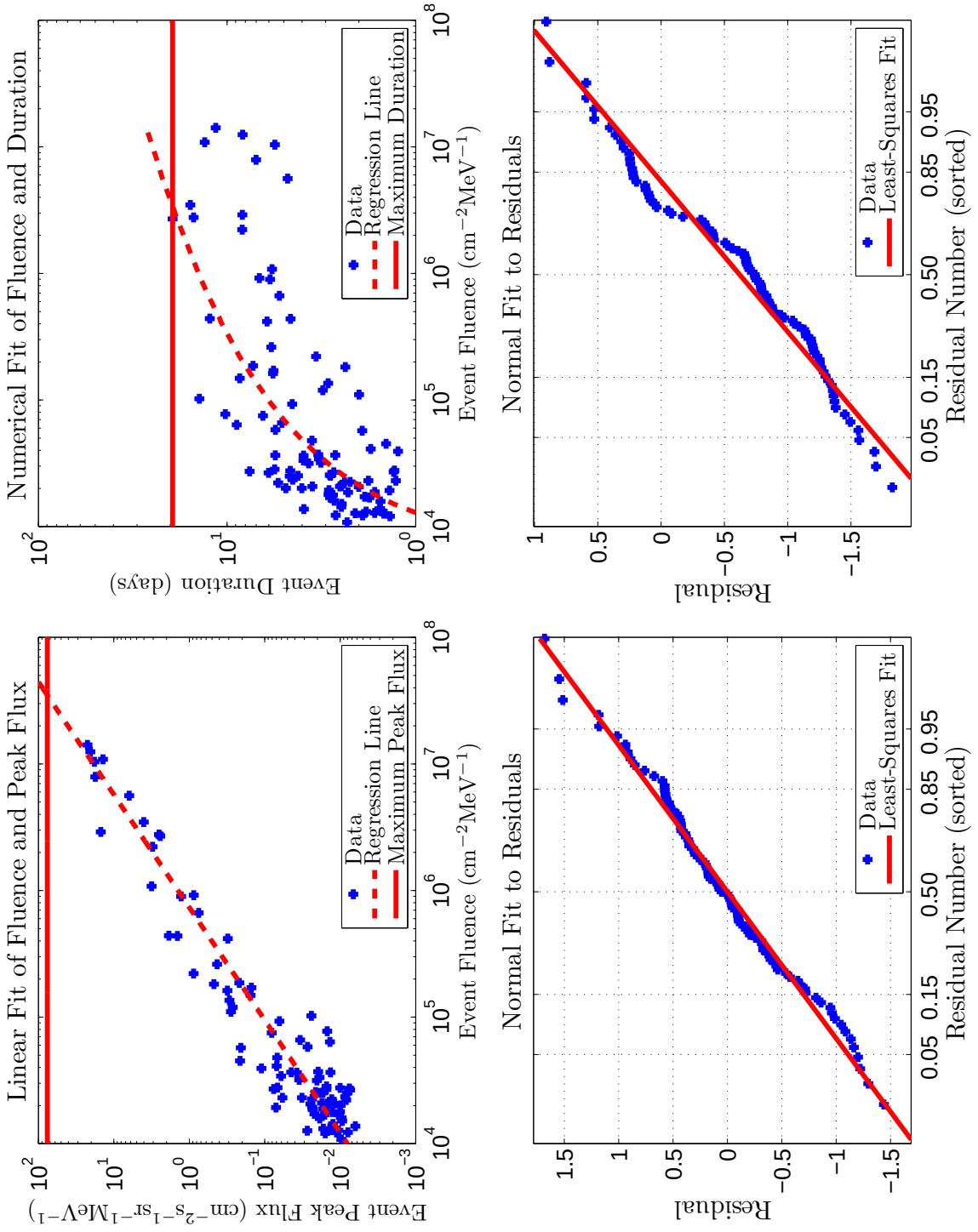

Figure C.23: Regression Fits for Channel 8: 66.13 - 95.64 MeV.

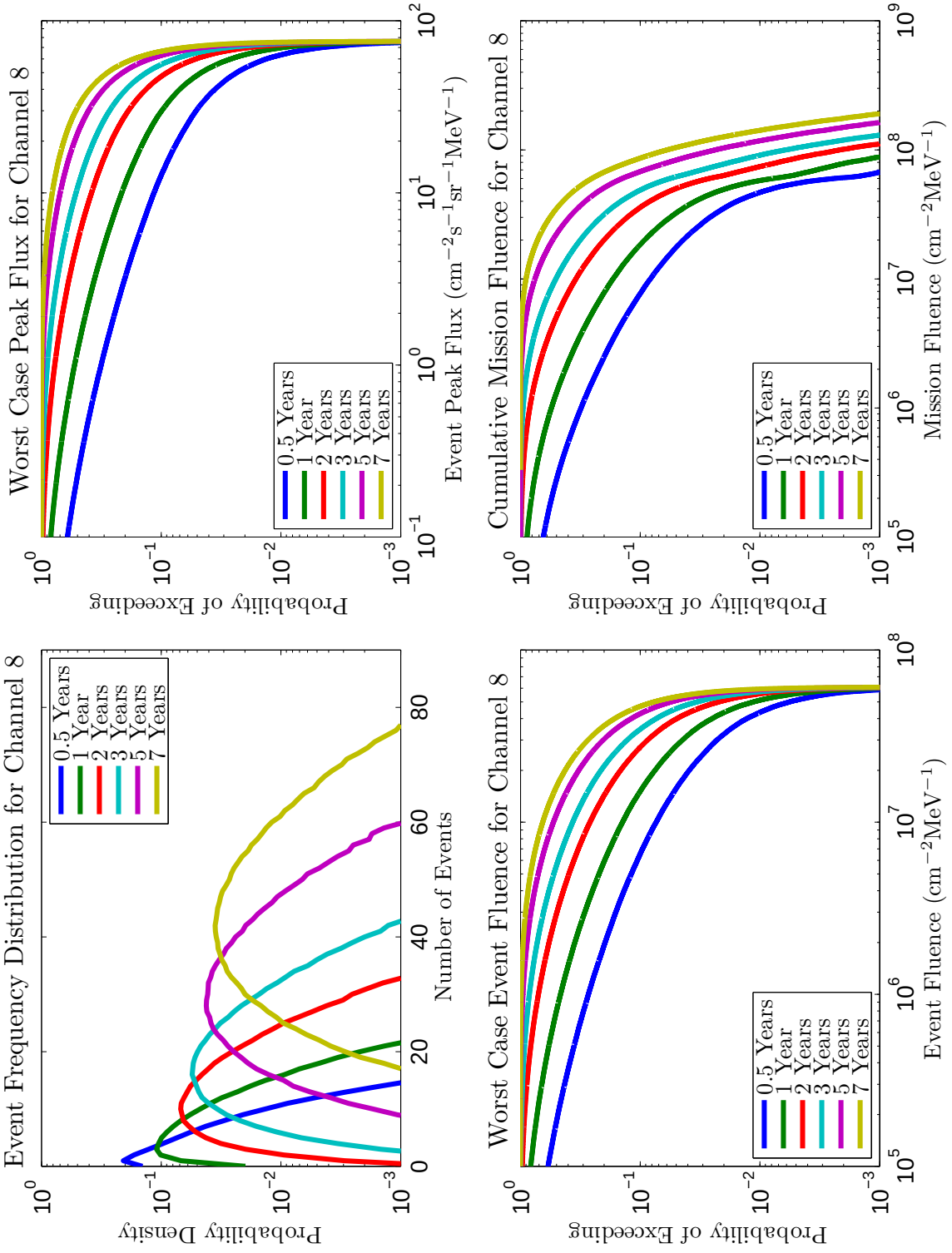

Figure C.24: Results for Channel 8: 66.13 - 95.64 MeV.

Table C.38: Table of worst-case peak flux predictions for Channel 8 ($cm^{-2}s^{-1}sr^{-1}MeV^{-1}$).

Mission	Confidence Level				
Duration	0.7	0.8	0.9	0.95	0.99
0.5 yr	1.17E+00	3.23E+00	1.27E+01	3.07E+01	6.34E+01
1 yr	4.94E+00	1.13E+01	2.97E+01	4.82E+01	6.97E+01
2 yr	1.60E+01	2.82E+01	4.75E+01	6.04E+01	7.27E+01
3 yr	2.66E+01	3.94E+01	5.57E+01	6.53E+01	7.38E+01
5 yr	4.03E+01	5.11E+01	6.29E+01	6.93E+01	7.47E+01
7 yr	4.83E+01	5.72E+01	6.65E+01	7.13E+01	7.51E+01

Table C.39: Table of worst-case event fluence predictions for Channel 8 ($cm^{-2}MeV^{-1}$).

Mission	Confidence Level				
Duration	0.7	0.8	0.9	0.95	0.99
0.5 yr	7.85E+05	1.93E+06	6.54E+06	1.57E+07	4.35E+07
1 yr	2.81E+06	5.92E+06	1.51E+07	2.78E+07	5.12E+07
2 yr	8.17E+06	1.43E+07	2.73E+07	3.98E+07	5.58E+07
3 yr	1.34E+07	2.12E+07	3.47E+07	4.57E+07	5.73E+07
5 yr	2.18E+07	3.04E+07	4.27E+07	5.10E+07	5.88E+07
7 yr	2.80E+07	3.64E+07	4.71E+07	5.36E+07	5.94E+07

Table C.40: Table of cumulative mission fluence predictions for Channel 8 ($cm^{-2}MeV^{-1}$).

Mission	Confidence Level				
Duration	0.7	0.8	0.9	0.95	0.99
0.5 yr	1.10E+06	2.50E+06	7.71E+06	1.77E+07	4.69E+07
1 yr	4.03E+06	7.85E+06	1.85E+07	3.25E+07	5.79E+07
2 yr	1.23E+07	2.01E+07	3.59E+07	5.03E+07	7.42E+07
3 yr	2.14E+07	3.17E+07	4.88E+07	6.20E+07	9.10E+07
5 yr	3.86E+07	5.09E+07	6.79E+07	8.35E+07	1.18E+08
7 yr	5.45E+07	6.73E+07	8.63E+07	1.04E+08	1.42E+08

C.9 Channel 9 Figures and Tables

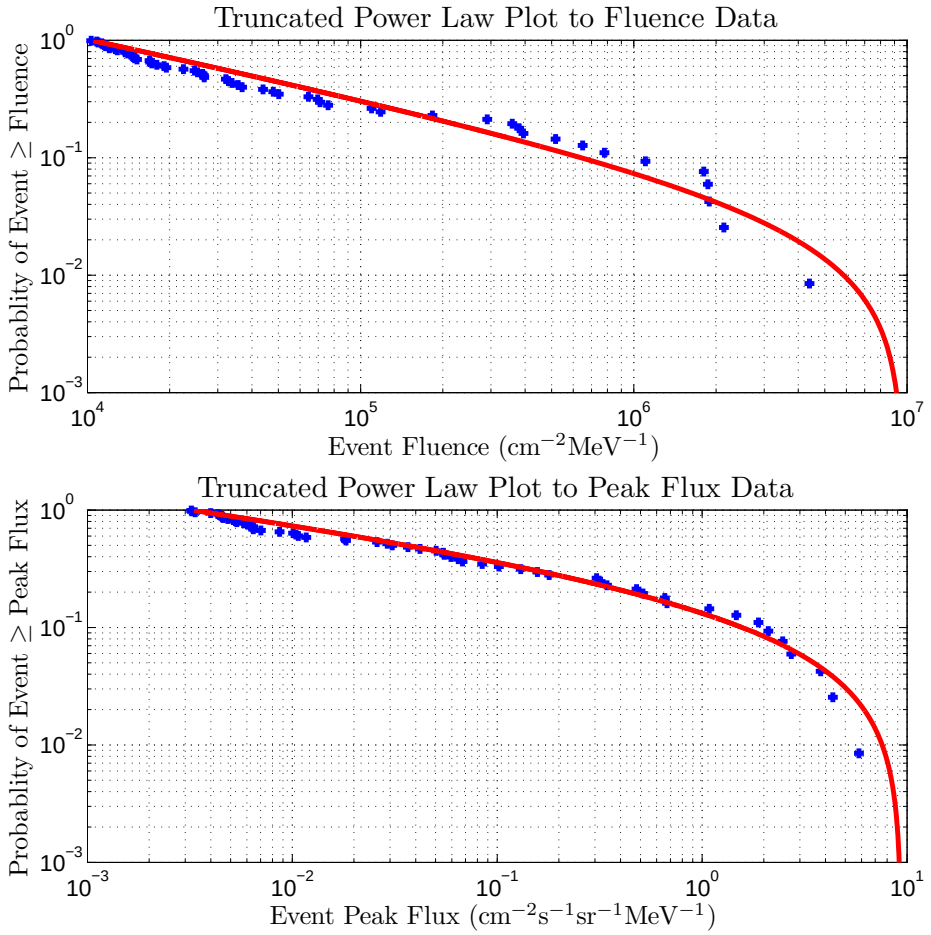

Figure C.25: Truncated Power Law Fits for Channel 9: 95.64 - 138.3 MeV.

Table C.41: Fluence and peak flux fitting parameters for Channel 9.

	b	$\phi_{\max}$	S^2	χ^2
Fluence	0.4927	9.68E+06	6.1905	0.5429
Peak flux	0.2215	9.36E+00	5.2344	0.3415

Table C.42: Regression parameters for Channel 9.

Peak Flux			Duration	
Gradient	Intercept	Residual σ	Adjust	Residual σ
1.2526	-16.6632	0.8312	-0.9719	0.8557

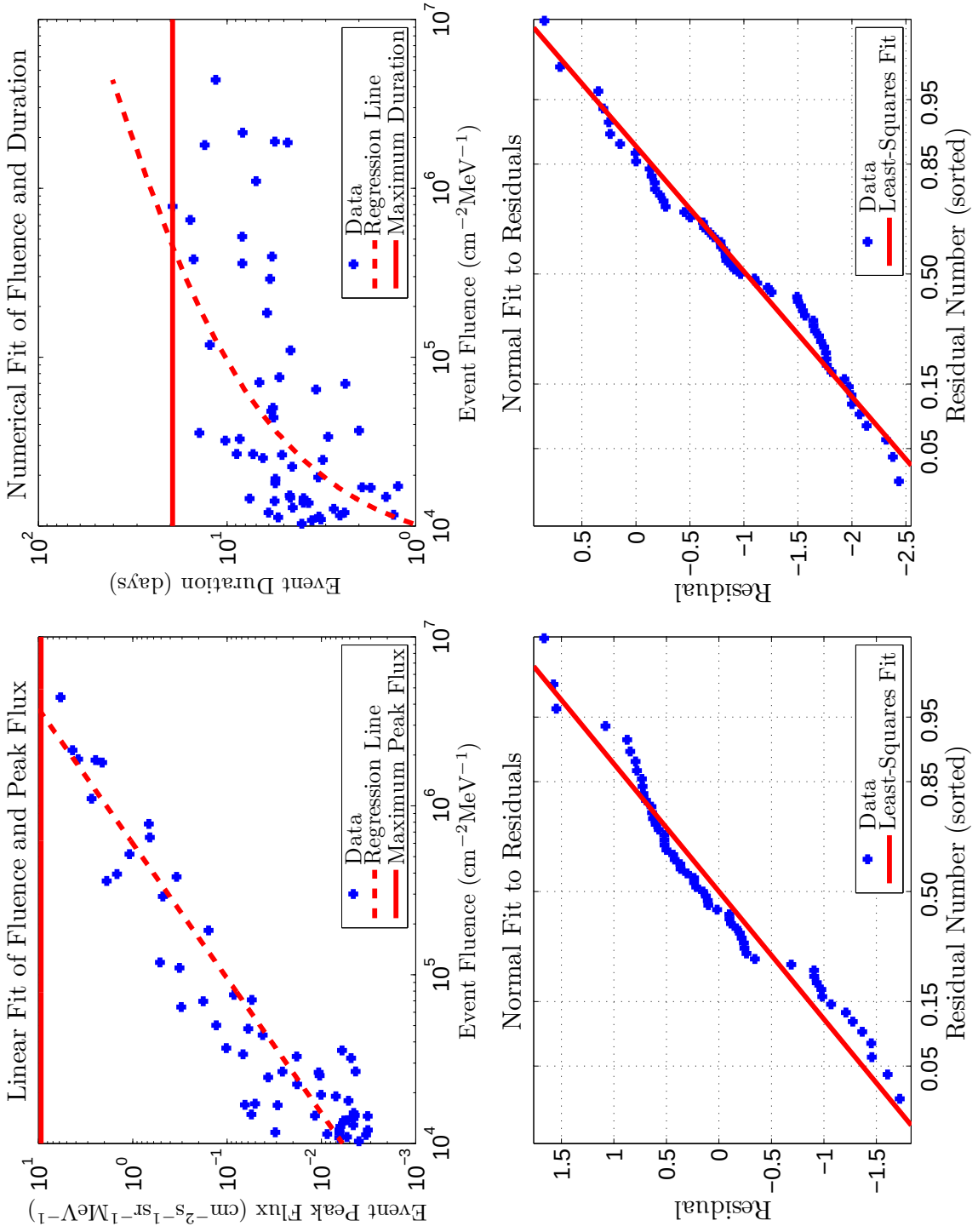

Figure C.26: Regression Fits for Channel 9: 95.64 - 138.3 MeV.

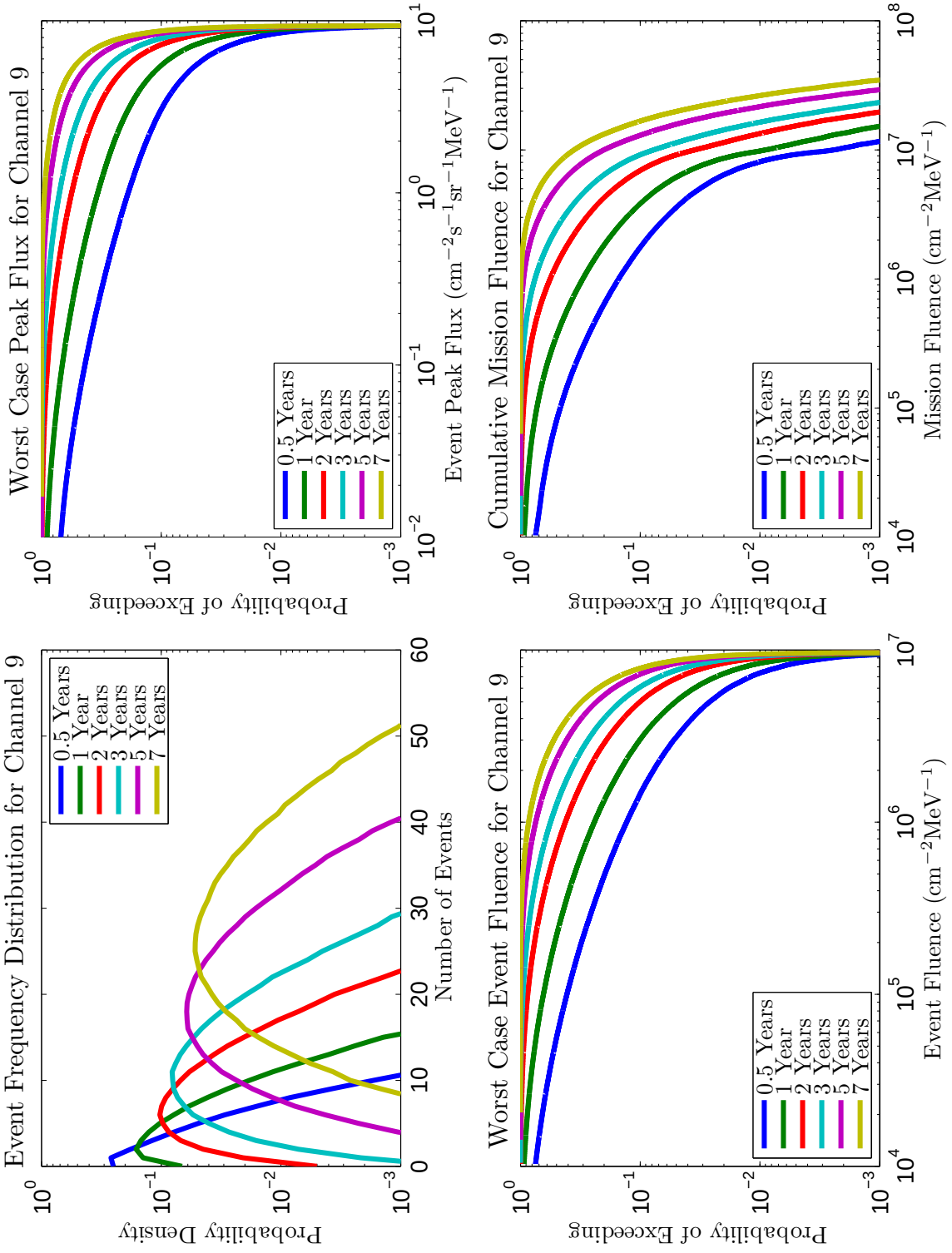

Figure C.27: Results for Channel 9: 95.64 - 138.3 MeV.

Table C.43: Table of worst-case peak flux predictions for Channel 9 ($cm^{-2}s^{-1}sr^{-1}MeV^{-1}$).

Mission	Confidence Level				
Duration	0.7	0.8	0.9	0.95	0.99
0.5 yr	3.16E-01	8.81E-01	3.06E+00	5.59E+00	8.52E+00
1 yr	1.33E+00	2.81E+00	5.50E+00	7.33E+00	8.94E+00
2 yr	3.64E+00	5.33E+00	7.27E+00	8.29E+00	9.15E+00
3 yr	5.11E+00	6.49E+00	7.91E+00	8.64E+00	9.22E+00
5 yr	6.60E+00	7.56E+00	8.48E+00	8.93E+00	9.28E+00
7 yr	7.33E+00	8.05E+00	8.73E+00	9.06E+00	9.30E+00

Table C.44: Table of worst-case event fluence predictions for Channel 9 ($cm^{-2}MeV^{-1}$).

Mission	Confidence Level				
Duration	0.7	0.8	0.9	0.95	0.99
0.5 yr	2.15E+05	4.89E+05	1.46E+06	3.12E+06	7.36E+06
1 yr	6.89E+05	1.34E+06	3.03E+06	5.05E+06	8.39E+06
2 yr	1.76E+06	2.88E+06	5.02E+06	6.85E+06	9.01E+06
3 yr	2.71E+06	4.02E+06	6.11E+06	7.63E+06	9.22E+06
5 yr	4.13E+06	5.46E+06	7.25E+06	8.38E+06	9.40E+06
7 yr	5.11E+06	6.34E+06	7.84E+06	8.71E+06	9.48E+06

Table C.45: Table of cumulative mission fluence predictions for Channel 9 ($cm^{-2}MeV^{-1}$).

Mission	Confidence Level				
Duration	0.7	0.8	0.9	0.95	0.99
0.5 yr	3.00E+05	6.42E+05	1.76E+06	3.59E+06	8.10E+06
1 yr	1.01E+06	1.84E+06	3.83E+06	6.15E+06	9.80E+06
2 yr	2.79E+06	4.28E+06	6.92E+06	9.14E+06	1.34E+07
3 yr	4.63E+06	6.43E+06	9.17E+06	1.14E+07	1.64E+07
5 yr	7.99E+06	1.00E+07	1.30E+07	1.58E+07	2.16E+07
7 yr	1.10E+07	1.33E+07	1.67E+07	1.99E+07	2.63E+07

C.10 Channel 10 Figures and Tables

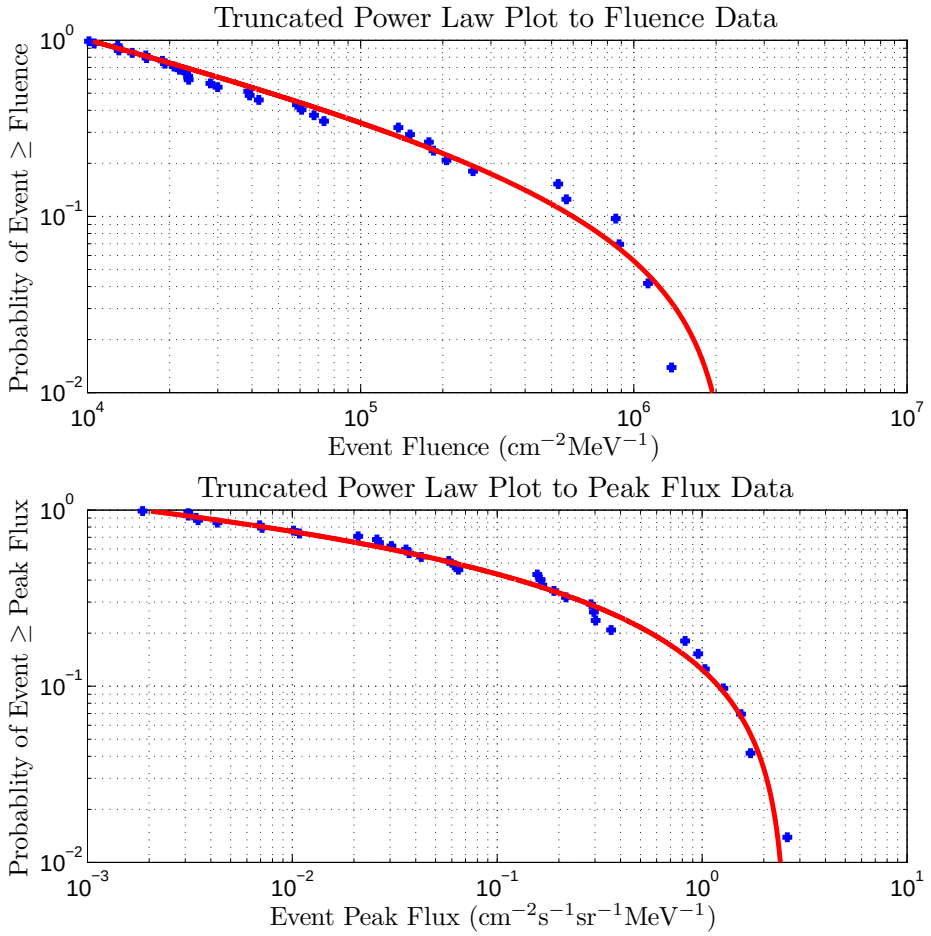

Figure C.28: Truncated Power Law Fits for Channel 10: 138.3- 200.0.

Table C.46: Fluence and peak flux fitting parameters for Channel 10.

	b	$\phi_{\max}$	S^2	χ^2
Fluence	0.3706	2.30E+06	1.1263	0.0974
Peak flux	0.0193	2.60E+00	1.4173	-1.1783

Table C.47: Regression parameters for Channel 10.

Peak Flux			Duration	
Gradient	Intercept	Residual σ	Adjust	Residual σ
1.2895	-16.9345	0.8685	-1.1108	0.9165

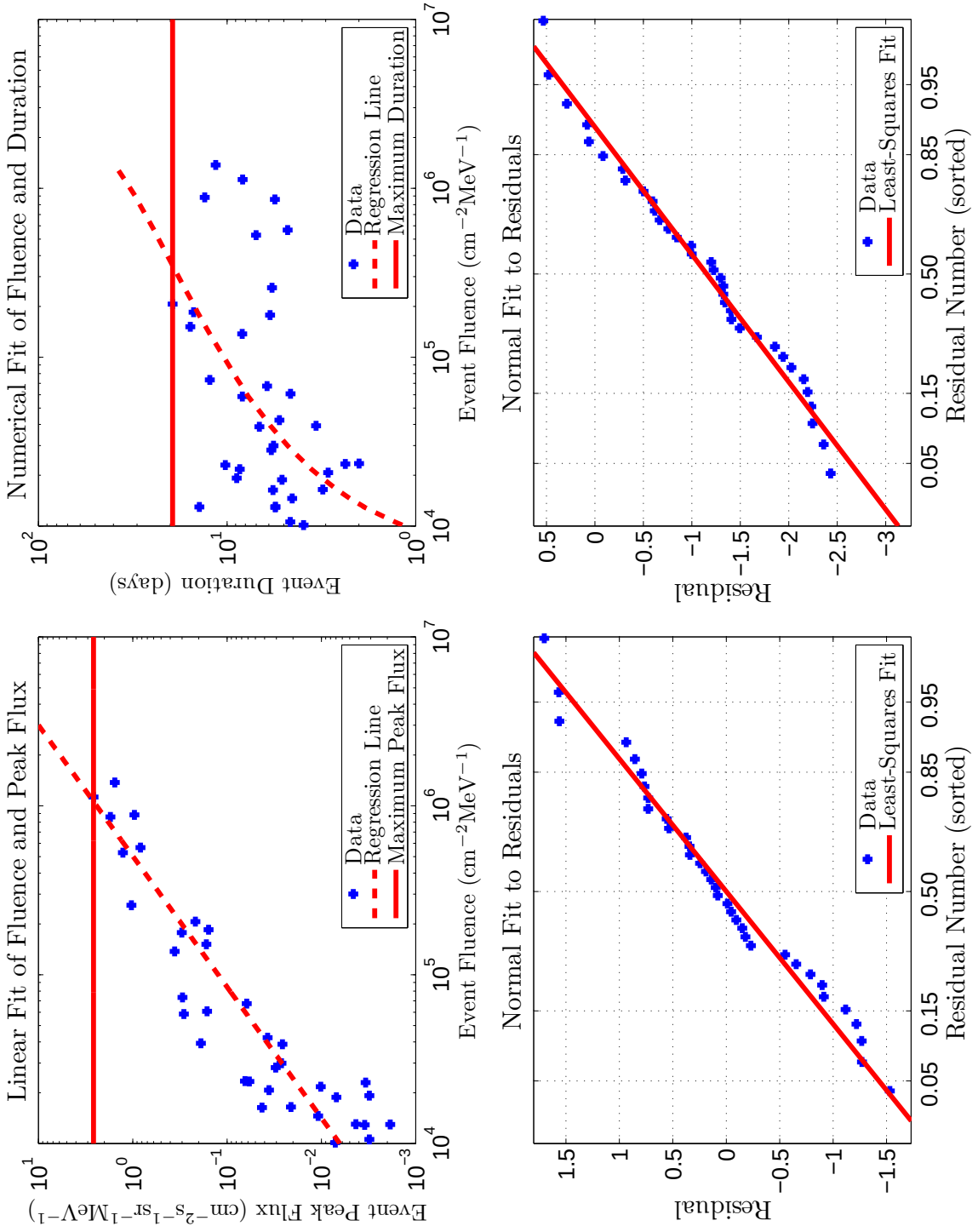

Figure C.29: Regression Fits for Channel 10: 138.3- 200.0 MeV.

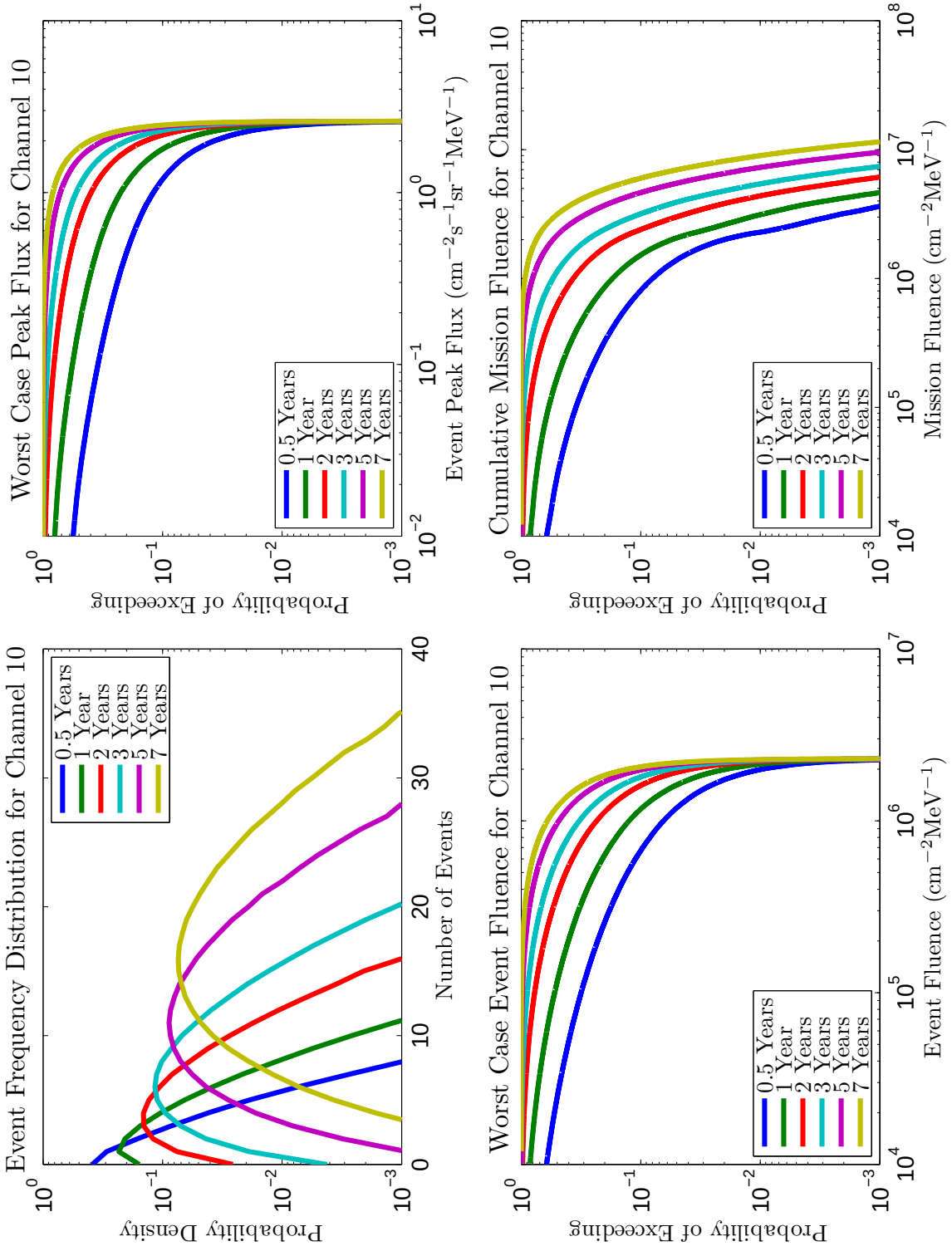

Figure C.30: Results for Channel 10: 138.3- 200.0 MeV.

Table C.48: Table of worst-case peak flux predictions for Channel 10 ($cm^{-2}s^{-1}sr^{-1}MeV^{-1}$).

Mission	Confidence Level				
Duration	0.7	0.8	0.9	0.95	0.99
0.5 yr	1.61E-01	4.50E-01	1.20E+00	1.81E+00	2.43E+00
1 yr	6.53E-01	1.14E+00	1.79E+00	2.17E+00	2.52E+00
2 yr	1.35E+00	1.75E+00	2.17E+00	2.38E+00	2.56E+00
3 yr	1.69E+00	2.00E+00	2.30E+00	2.45E+00	2.57E+00
5 yr	2.02E+00	2.23E+00	2.42E+00	2.51E+00	2.59E+00
7 yr	2.18E+00	2.33E+00	2.47E+00	2.54E+00	2.59E+00

Table C.49: Table of worst-case event fluence predictions for Channel 10 ($cm^{-2}MeV^{-1}$).

Mission	Confidence Level				
Duration	0.7	0.8	0.9	0.95	0.99
0.5 yr	1.13E+05	2.58E+05	6.71E+05	1.19E+06	1.99E+06
1 yr	3.59E+05	6.35E+05	1.17E+06	1.62E+06	2.14E+06
2 yr	7.89E+05	1.13E+06	1.61E+06	1.92E+06	2.21E+06
3 yr	1.08E+06	1.40E+06	1.80E+06	2.04E+06	2.24E+06
5 yr	1.43E+06	1.69E+06	1.98E+06	2.14E+06	2.27E+06
7 yr	1.63E+06	1.84E+06	2.06E+06	2.18E+06	2.27E+06

Table C.50: Table of cumulative mission fluence predictions for Channel 10 ($cm^{-2}MeV^{-1}$).

Mission	Confidence Level				
Duration	0.7	0.8	0.9	0.95	0.99
0.5 yr	1.46E+05	3.26E+05	8.10E+05	1.39E+06	2.29E+06
1 yr	5.02E+05	8.61E+05	1.52E+06	2.07E+06	3.13E+06
2 yr	1.26E+06	1.74E+06	2.40E+06	3.01E+06	4.38E+06
3 yr	1.91E+06	2.41E+06	3.18E+06	3.91E+06	5.43E+06
5 yr	3.08E+06	3.70E+06	4.64E+06	5.49E+06	7.28E+06
7 yr	4.22E+06	4.93E+06	6.01E+06	6.97E+06	8.99E+06

Appendix D

Plots of Energy Spectra

This appendix chapter displays the 70%, 80%, 95% and 99% confidence levels for the results of fluence plotted against energy. The same plots for the 90% confidence level are included in Chapter 5.

D.1 Differential Energy Spectra

The differential spectra are the results for a single confidence in each of the channels for each of the six mission lengths plotted on the same axes giving an impression of the number of particles arriving at each energy.

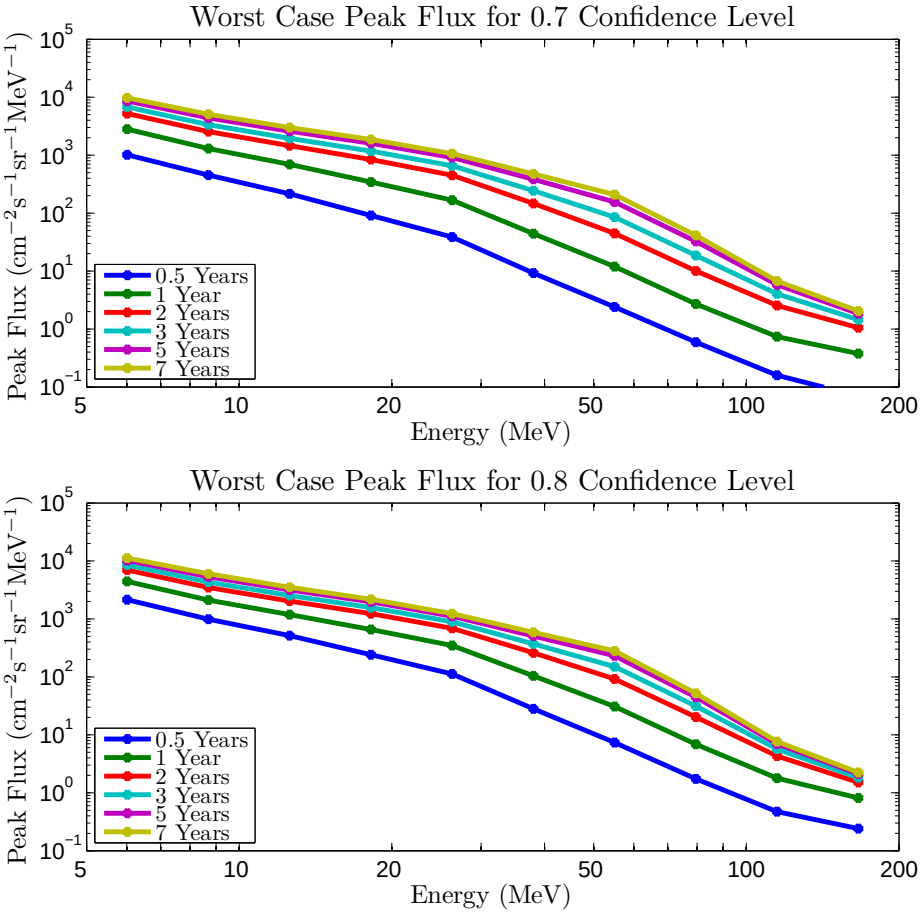

Figure D.1: Differential energy plots for worst-case peak flux at 70% confidence (top) and 80% confidence (bottom).

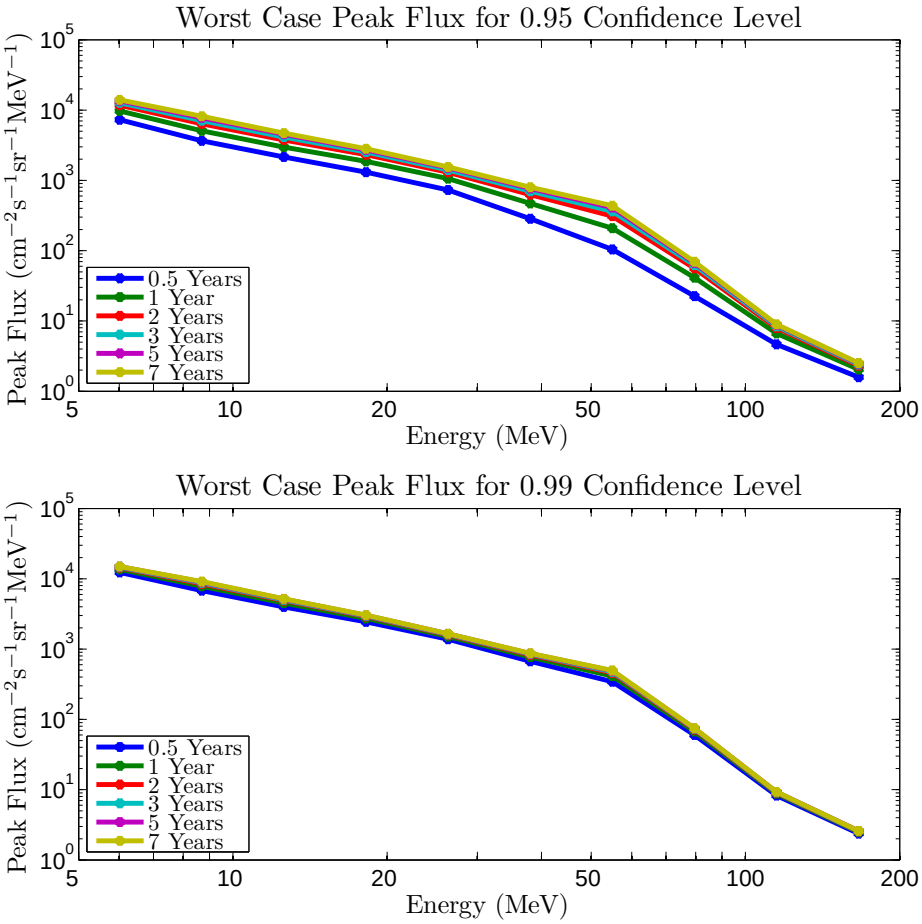

Figure D.2: Differential energy plots for worst-case peak flux at 95% confidence (top) and 99% confidence (bottom).

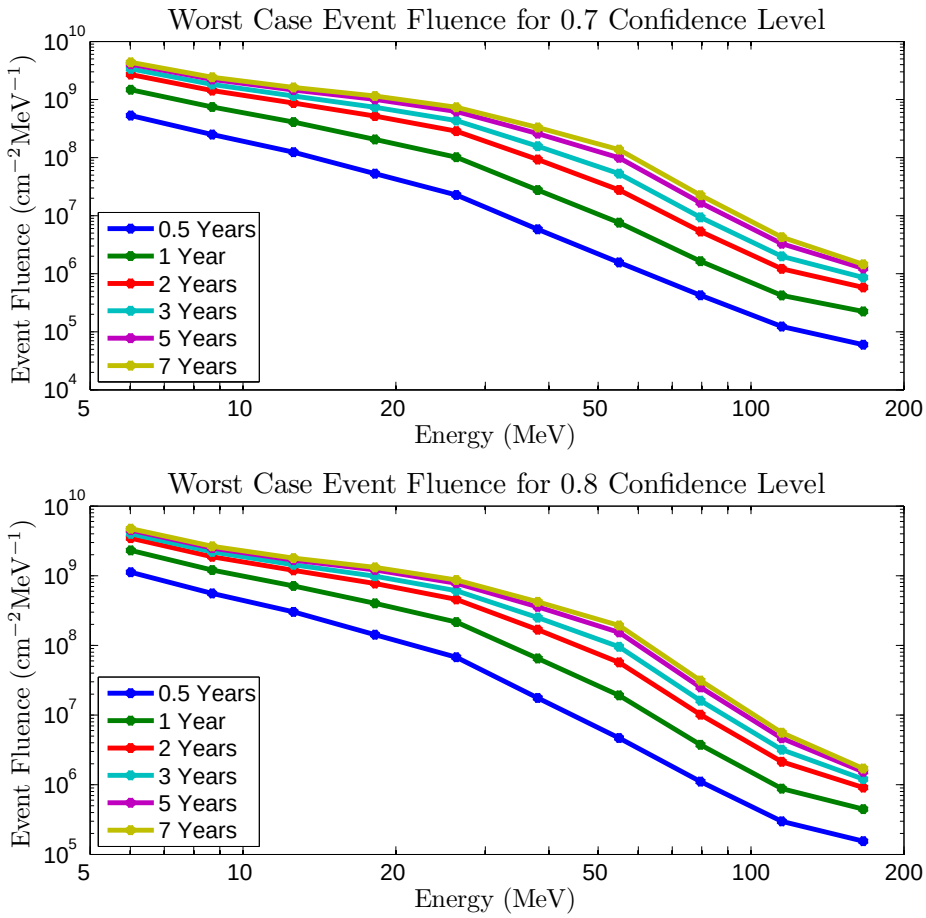

Figure D.3: Differential energy plots for worst-case event fluence at 70% confidence (top) and 80% confidence (bottom).

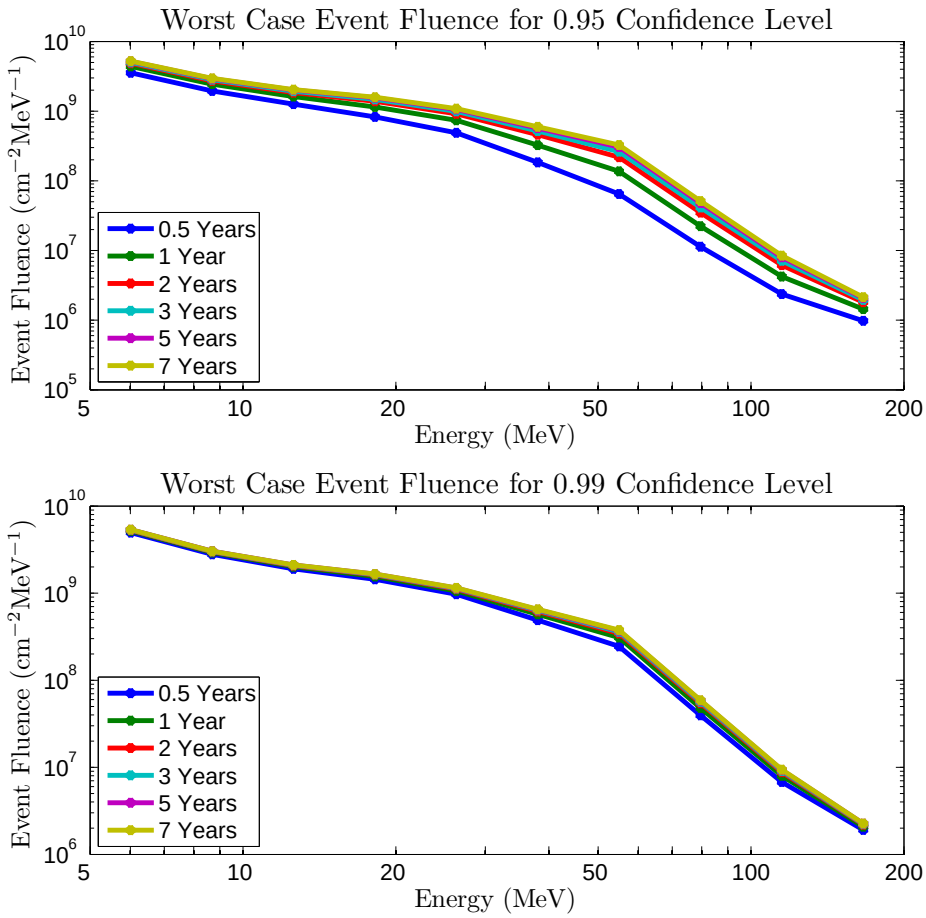

Figure D.4: Differential energy plots for worst-case event fluence at 95% confidence (top) and 99% confidence (bottom).

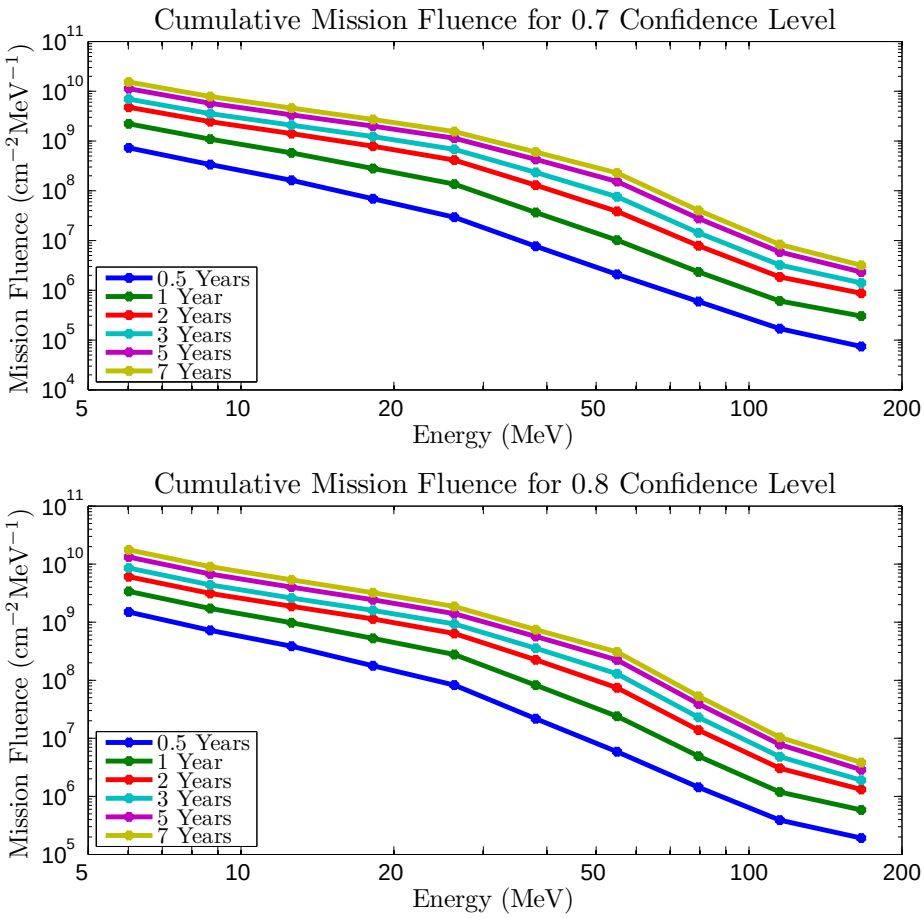

Figure D.5: Differential energy plots for cumulative mission fluence at 70% confidence (top) and 80% confidence (bottom).

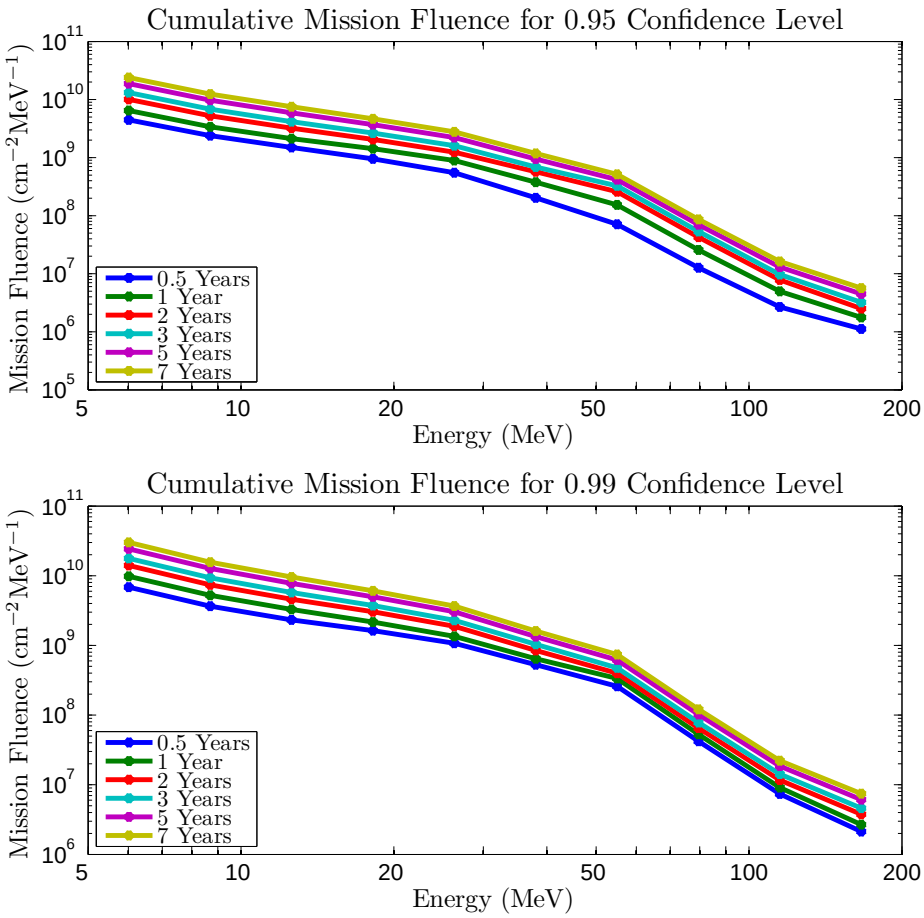

Figure D.6: Differential energy plots for cumulative mission fluence at 95% confidence (top) and 99% confidence (bottom).

D.2 Integral Energy Spectra

The integral spectra are the results for a single confidence summed over the energies from the threshold value and above. This gives a prediction of the total number of particles arriving of at least the stated threshold energy level.

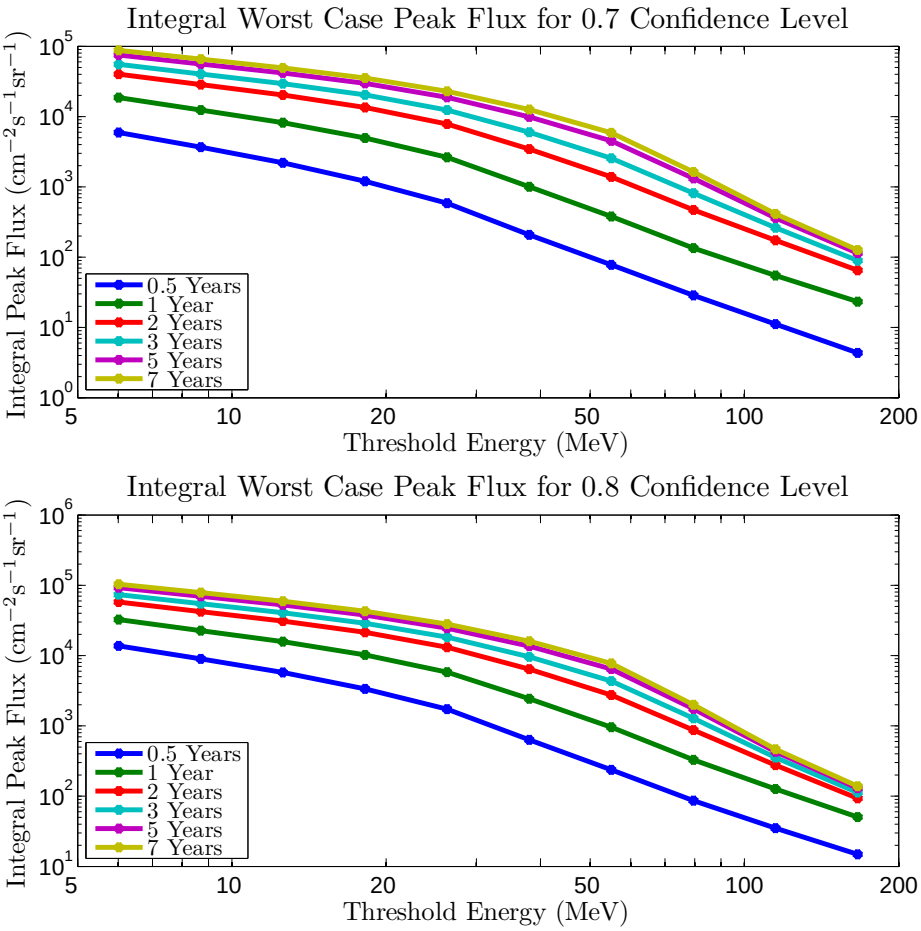

Figure D.7: Integral energy plots for worst-case peak flux at 70% confidence (top) and 80% confidence (bottom).

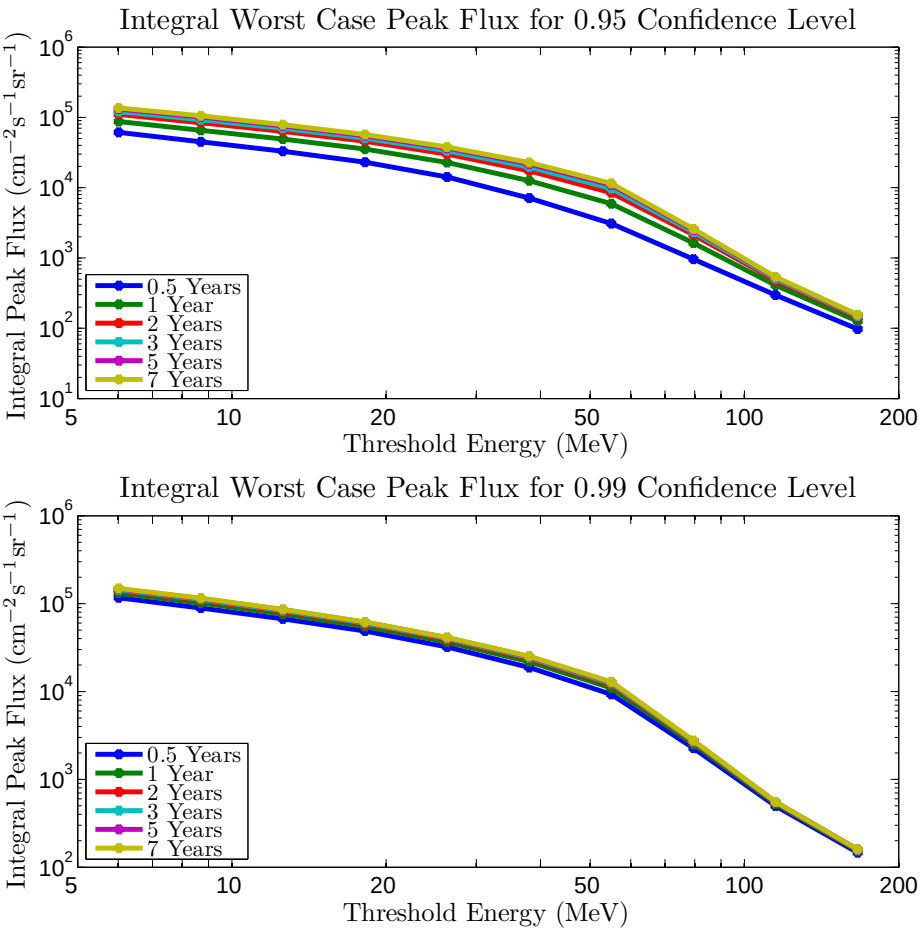

Figure D.8: Integral energy plots for worst-case peak flux at 95% confidence (top) and 99% confidence (bottom).

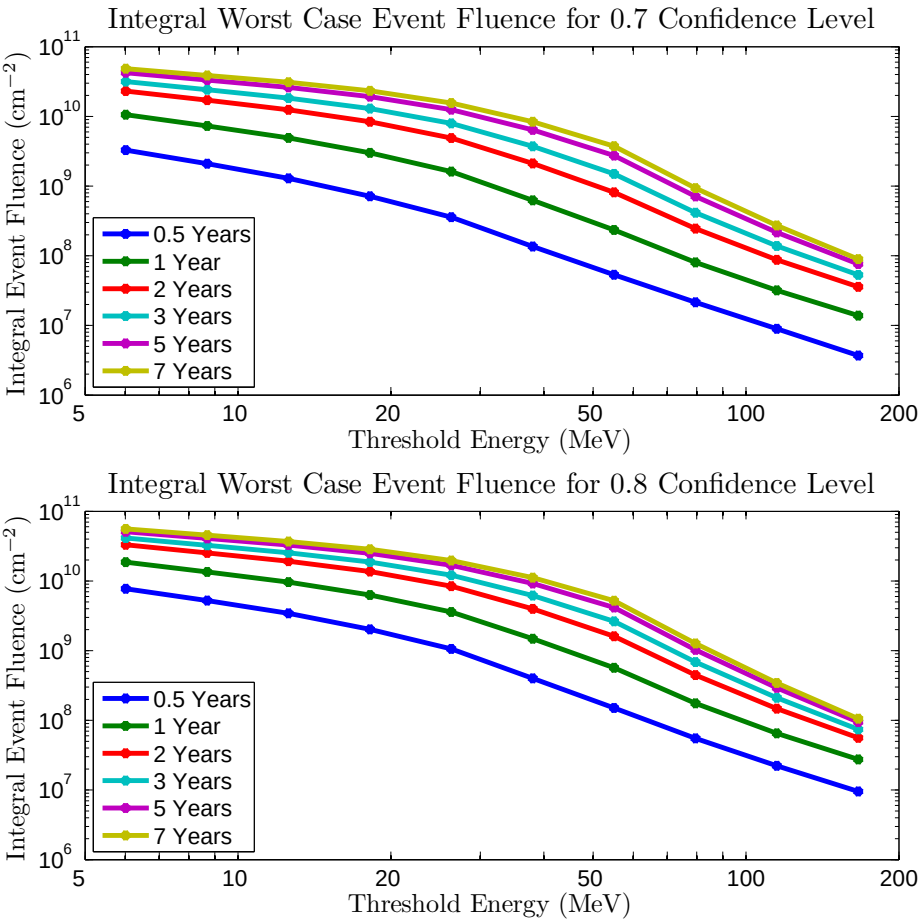

Figure D.9: Integral energy plots for worst-case event fluence at 70% confidence (top) and 80% confidence (bottom).

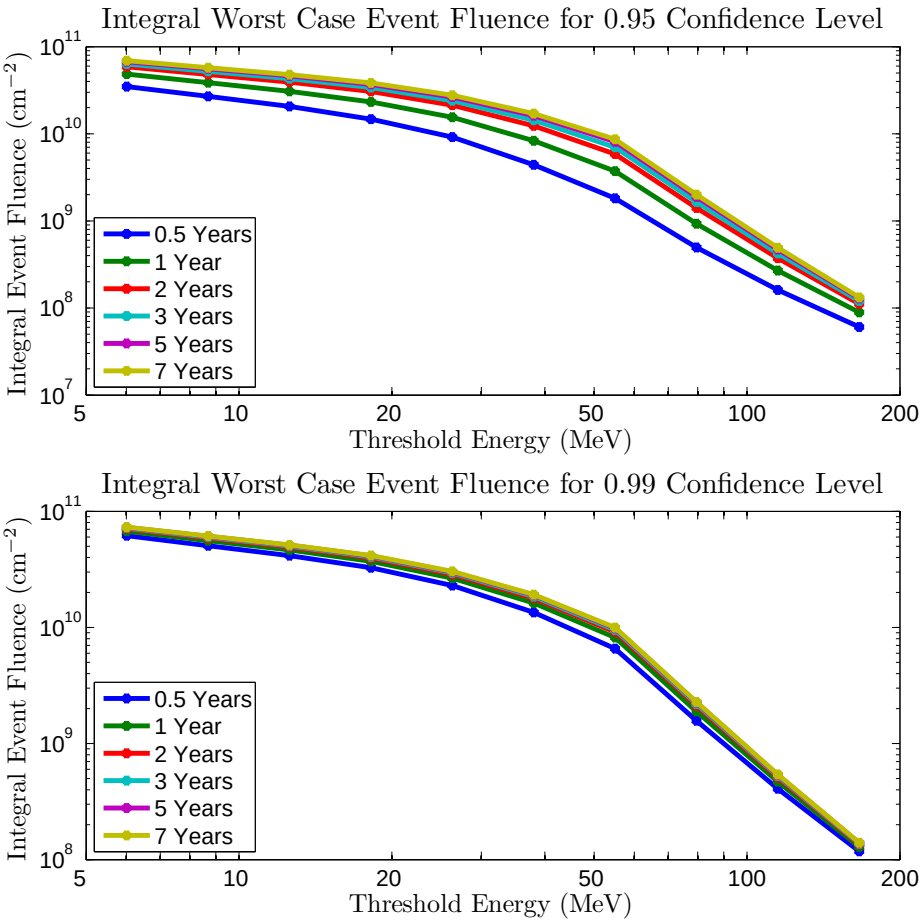

Figure D.10: Integral energy plots for worst-case event fluence at 95% confidence (top) and 99% confidence (bottom).

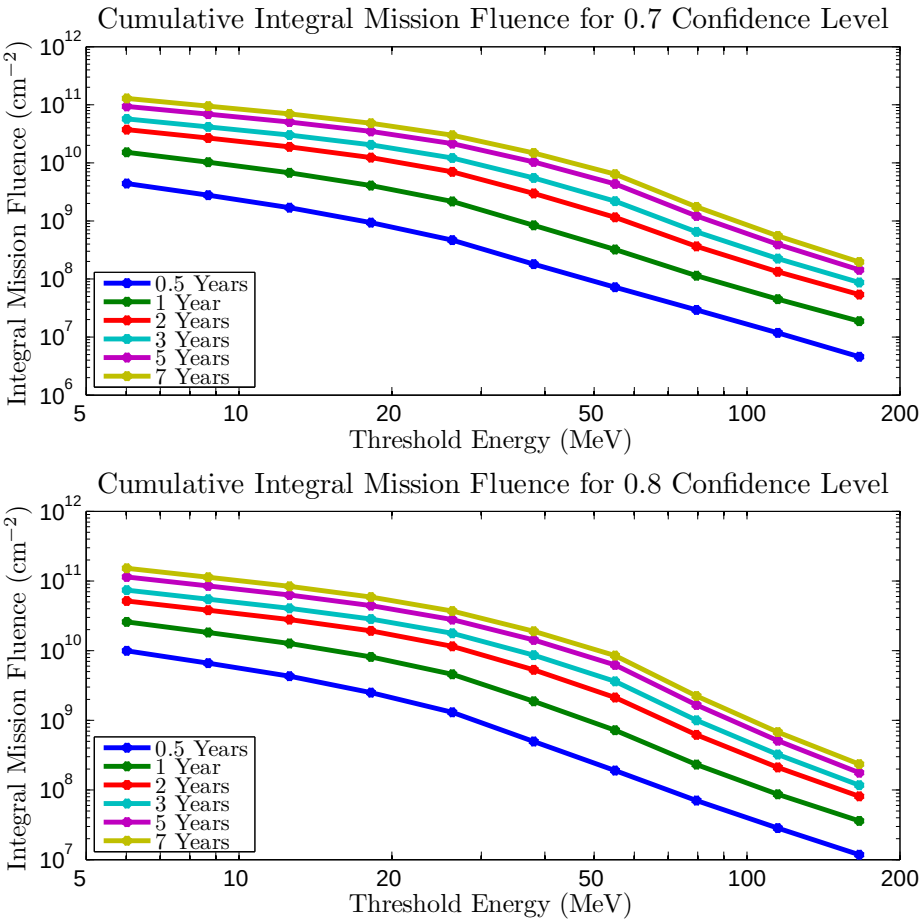

Figure D.11: Integral energy plots for cumulative mission fluence at 70% confidence (top) and 80% confidence (bottom).

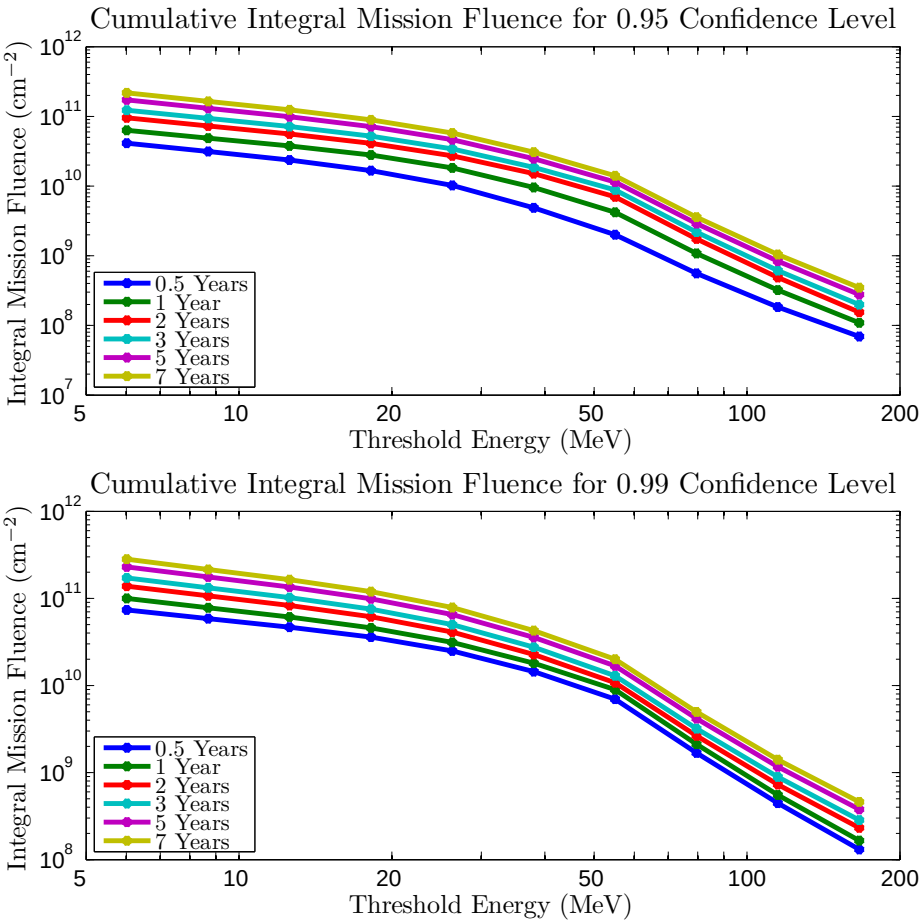

Figure D.12: Integral energy plots for cumulative mission fluence at 95% confidence (top) and 99% confidence (bottom).

Bibliography

Band, D., J. Matteson, L. Ford, B. Schaefer, D. Palmer, B. Teegarden, T. Cline, M. Briggs, W. Paciesas, G. Pendleton, G. Fishman, C. Kouveliotou, C. Meegan, R. Wilson, and P. Lestrade (1993). Batse observations of gamma-ray burst spectra. i - spectral diversity. *The Astrophysical Journal 413*(1), 281–292.

Belov, A., E. Eroshenko, H. Mavromichalaki, C. Plainaki, and V. Yanke (2005). A study of the ground level enhancement of 23 february 1956. *Solar Physics 229*(1), 135–159.

Belov, A., V. Kurt, M. Gerontidou, and H. Mavromichalaki (2001). Statistical analysis of solar proton events in different energy channels. pp. 3,465–3,468.

Bi, H., G. Börner, and Y. Chu (1989). Correlations in the absorption lines of the quasar q0420-388. *Astronomy and Astrophysics 218*, 19–23.

Boberg, P. R., A. J. Tylka, and J. H. Adams (1996). Solar energetic fe charge state measurements: Implications for acceleration by coronal mass ejection–driven shocks. *The Astrophysical Journal 471*, 165–168.

Burrell, M. O. (1972). The risk of solar proton events to space missions. *Proceedings of the 1971 National Symposium on Natural and Manmade Radiation in Space, NASA*.

Cane, H. V. (2005). Are there direct flare particles in large solar particle events? *Proceedings of the Solar Wind 11 / SOHO 16 Conference (ESA SP-592)*, 71–75.

Cane, H. V. and D. Lario (2006). An introduction to cmes and energetic particles. *Space Science Reviews 123*, 45–56.

Carrington, R. C. (1860). Description of a singular appearance seen on the sun on september 1, 1859. *Monthly Notices Royal Astronomical Society 20*, 13–15.

Cliver, E. W. (1991). Size distribution of solar energetic particle events. *3*, 25–28.

Crosby, N., M. Aschwanden, and B. Dennis (1993). Frequency distributions and correlations of solar x-ray flare parameters. *Solar Physics 143*, 275–299.

Daibog, E. I., Y. I. Logachev, S. W. Kahler, and K. Kecskemety (2003). Statistical properties of sep event flux declines. *Advances in Space Research 32*(12), 2,655–2,660.

Dikpati, M., G. de Toma, and P. A. Gilman (2006). Predicting the strength of solar cycle 24 using a flux-transport dynamo-based tool. *Geophysical Research Letters 33*(A05102).

Dyer, C. S., K. Hunter, S. Clucas, and A. Campbell (2004). Observation of the solar particle events of october and november 2003 from credo and mptb. *IEEE Transactions on Nuclear Science 51*(6), 3,388–3,393.

ECSS Standard (April 2008). ECSS E-10-04 Space Environment Standard. Technical report, ESA-ESTEC.

Feynman, J. (1989). Solar proton events during solar cycles 19, 20, and 21. *Solar Physics*.

Feynman, J., T. P. Armstrong, L. Dao-Gibner, and S. Silverman (1990). A new interplanetary fluence model. *Journal of Spacecraft and Rockets 27*(4), 403–410.

Feynman, J. and S. B. Gabriel (2000). On space weather consequences and predictions. *Journal of Geophysical Research 105*(A5), 10,543–10,564.

Feynman, J., A. Ruzmaikin, and V. Berdichevsky (2002). The jpl proton fluence model: an update. *Journal of Atmospheric and Solar-Terrestrial Physics 64*(16), 1,679–1,686.

Feynman, J., G. Spitale, J. Wang, and S. B. Gabriel (1993). Interplanetary proton fluence model: Jpl 1991. *Journal of Geophysical Research 98*(A8), 13,281–13,294.

Feynman, J., A. J. Tylka, D. B. Reames, and S. B. Gabriel (2000). Near-sun energetic particle environment of solar probe-phase1 final report. Technical report, Jet Propulsion Laboratory.

Fitzerreiter, R., J. Fainberg, and R. Bundy (1976). Directivity of low frequency solar type iii radio bursts. *Solar Physics 46*, 465–473.

Gabriel, S. B. and J. Feynman (1996). Power-law distribution for solar energetic proton events. *Solar Physics 165*(2), 337–346.

Gabriel, S. B. and G. J. Patrick (2003). Solar energetic particle events phenomenology and prediction. *Space Science Reviews 107*(1-2), 56–62.

Goh, K. I. and A. L. Barabási (2008). Burstiness and memory in complex systems. *EPL (Europhysics Letters) 81*(48002).

Gold, R. E., S. M. Krimigis, H. S. E., D. K. Haggerty, D. A. Lohr, and E. Fiore (1998). Electron, proton, and alpha monitor on the advanced composition explorer spacecraft. *Space Science Reviews*, 541–562.

Gopalswamy, N., S. Yashiro, G. Michalek, M. L. Kaiser, R. A. Howard, D. V. Reames, and R. L. T. V. Rosenvinge (2002). Interacting coronal mass ejections and solar energetic particles. *The Astrophysical Journal 572*, 103–107.

Gopalswamy, N., S. Yashiro, G. Stenborg, and R. A. Howard (2003). Coronal and interplanetary environment of large solar energetic particle events. pp. 3,549–3,552.

Gosling, J. T. (1993). The solar flare myth. *Journal of Geophysical Research 98*(A11), 18,937–18,950.

Hamilton, D. C., G. M. Mason, and F. B. McDonald (1990). The radial dependence of the peak flux and fluence in solar energetic particle events. pp. 237–240.

Hathaway, D. H., D. Nandy, R. M. Wilson, and E. J. Reichmann (2003). Evidence that a deep meridonal flow sets the sunspot cycle period. *The Astrophysical Journal 589*, 665–670.

Hathaway, D. H., R. M. Wilson, and E. J. Reichmann (1994). The shape of the sunspot cycle. *Solar Physics 151*, 177–190.

Hathaway, D. H., R. M. Wilson, and E. J. Reichmann (1999). A synthesis of solar cycle prediction techniques. *Journal of Geophysical Research 104*(A10), 22,375–22,388.

Ho, G. C., E. C. Roelef, G. M. Mason, D. Lario, R. E. Gold, J. Mazur, and J. R. Dwyer (2003). Composition variations during large solar energetic particle events. *Proceedings of the Tenth International Solar Wind Conference*, 624–627.

Jiggens, P. T. A. and S. B. Gabriel (2009). Time distributions of solar energetic particle events: Are sepes really random? *Journal of Geophysical Research 114*(A10), A10105.

Jun, I., R. T. Swimm, A. Ruzmaikin, J. Feynman, A. J. Tylka, and W. F. Dietrich (2007). Statistics of solar energetic particle events: Fluences, durations and time intervals. *Advances in Space Research 40*, 304–312.

Kahler, S. W. (2001). The correlation between solar energetic particle peak intensities and speeds of coronal mass ejections: Effects of ambient particle intensities and energy spectra. *Journal of Geophysical Research 106*, 20,947–20,955.

Kahler, S. W. (2003). Energetic particle acceleration by coronal mass ejections. *Advances in Space Research 32*(12), 2,587–2,596.

Kahler, S. W., D. V. Reames, and N. R. Sheeley (2001). Coronal mass ejections associated with impulsive solar energetic particle events. *The Astrophysical Journal 562*, 558–565.

Kallenrode, M. B. (2003). Current views on impulsive and gradual solar energetic particle events. *Journal of Physics G: Nuclear and Particle Physics 29*, 965–981.

Kallenrode, M. B. and E. W. Cliver (2001). Rogue sep events: Modeling. pp. 3,318–3,321.

Kapur, J. N. (1989). *Maximum entropy models in science and engineering*. John Wiley & Sons, Inc.

King, J. H. (1974). Solar proton fluences for 1977-1983 space missions. *Journal of Spacecraft and Rockets 11*(6), 401–408.

Krucker, S. and R. P. Lin (2000). Two classes of solar proton events derived from onset time analysis. *The Astrophysical Journal 542*, L61–L64.

Kurt, V. G. and R. A. Nymmik (1997). Distribution of solar cosmic ray events over proton fluences. *Cosmic Research 35*(6), 559–569.

Kuznetsov, N. V., R. A. Nymmik, and M. I. Panasyuk (2005). Models of solar energetic particle fluxes: The main requirements and the development prospects. *Advances in Space Research 36*(10), 2,003–2,011.

Laherrére, J. and D. Sornette (1998). Stretched exponential distributions in nature and economy: "fat tails" with characteristic scales. *The European Physical Journal 2*(4), 525–539.

Lario, D., M. B. Kallenrode, R. B. Decker, E. C. Roelof, S. M. Krimigis, A. Aran, and B. Sanahuja (2006). Radial and longitudinal dependences of solar 4-13 mev and 27-37 mev proton peak intensities and fluences: Helios and imp-8 observations. *The Astrophysical Journal 653*, 1,531–1,544.

Lepreti, F., V. Carbone, and P. Veltri (2001). Solar flare waiting time distribution: Varying rate-poisson of lévy function? *The Astrophysical Journal 555*, L113–L136.

Leske, R. A., C. M. S. Cohen, A. C. Cummings, R. A. Mewaldt, E. C. Stone, M. E. Wiedenbeck, and T. T. v. Rosenvinge (2005). Ultra-heavy elements above 10 mev/nucleon in solar energetic particle events. *00*, 101–104.

Lu, E. T., R. J. Hamilton, J. M. McTiernan, and K. R. Bromund (1993). Solar flares and valances in driven dissipative systems. *The Astrophysical Journal 412*, 841–852.

Maunder, E. W. (1922). The sun and sunspots 1820-1920. *British Astronomical Association Journal 32*, 140.

McCracken, K. G., G. A. M. Dreschhoff, E. J. Zeller, D. F. Smart, and M. A. Shea (2001). Solar cosmic ray events for the period 1561-1994 1. identification in polar ice, 1561-1950. *Journal of Geophysical Research - Space Physics 106*(A10), 21,585–21,598.

McKenna-Lawlor, S. M. P., M. Dryer, Z. Smith, K. Kecskemety, C. D. Fry, W. Sun, C. S. Deehr, D. Berdichevsky, K. Kudela, and G. Zastenker (2002). Arrival times of flare/halo cme associated shocks at the earth comparison of the predictions of three numerical models with these observations. *Annales Geophysicae 20*(7), 917–935.

Mewaldt, R. A., M. D. Looper, C. M. S. Cohen, G. M. Mason, D. K. Haggerty, M. I. Desai, A. W. Labrador, R. A. Leske, and J. E. Mazur (2005). Solar-particle energy spectra during the large events of october-november 2003 and january 2005. *00*, 101–104.

Myagkova, I. N., M. I. Panasyuk, L. L. Lazutin, E. A. Muravieva, L. I. Starostin, T. A. Ivanova, N. N. Pavlov, I. A. Rubinshtein, N. N. Vedenkin, and N. A. Vlasova (2009). December 2006 solar extreme events and their influence on the near-earth space environment: universitetskiy-tatiana satellite observations. *Advances in Space Research* (4), 489–494.

Ng, C. K. and D. V. Reames (1994). Focused interplanetary transport of approximately 1 mev solar energetic protons through self-generated alfven waves. *The Astrophysical Journal 424*, 1,032–1,048.

Nolan, J. P. (2009). *Stable Distributions - Models for Heavy Tailed Data*. Boston: Birkhäuser.

Nymmik, R. A. (1999). Probabilistic model for fluences and peak fluxes of solar energetic particles. *Radiation Measurements 30*(3), 287–296.

Parker, E. N. (1958). Dynamics of the interplanetary gas and magnetic fields. *Astrophysical Journal 128*, 664–676.

Reames, D. V. (1999). Particle acceleration at the sun and in the heliosphere. *Space Science Reviews 90*, 413–491.

Reames, D. V. (2004). Solar energetic particle variations. *Advances in Space Research 34*, 381–390.

Reames, D. V. and C. K. Ng (1998). Streaming-limited intensities of solar energetic particles. *The Astrophysical Journal 504*, 1,002–1,005.

Reames, D. V. and C. K. Ng (2004). Heavy-element abundances in solar energetic particle events. *The Astrophysical Journal 610*, 510–522.

Reedy, R. C. (1996). Constraints on solar particle events from comparisons of recent events and million year averages, in solar drivers of interplanetary and terrestrial disturbances. *95*, 429–436.

Reinard, A. A. and M. A. Andrews (2006). Comparison of cme characteristics for sep and non-sep related events. *Advances in Space Research 38*, 480–483.

Rosenqvist, L. and A. Hilgers (2003). Sensitivity of a statistical solar proton fluence model to the size of the event data set. *Geophysical Research Letters 30*(16), 1–4.

Rosenqvist, L., A. Hilgers, H. Evans, E. Daly, M. Hapgood, R. Stamper, R. Zwickl, S. Bourdarie, and D. Boscher (2005). Toolkit for updating interplanetary proton-cumulated fluence models. *Journal of Spacecraft and Rockets 42*(6), 1,077–1,090.

Shea, M. A. and D. F. Smart (1990). A summary of solar proton events. *Solar Physics 127*, 297–320.

Shea, M. A. and D. F. Smart (1995). History of solar proton event observations. *Nuclear Physics B Article Supplements 39*(A), 16–25.

Shea, M. A., D. F. Smart, K. G. McCracken, G. A. M. Dreschhoff, and H. E. Spence (2006). Solar proton events for 450 years: The carrington event in perspective. *Advances in Space Research 38*, 232–238.

Smart, D. F. and M. A. Shea (1985). A simplified model for timing the arrival of solar-flare initiated shocks. *Journal of Geophysical Research 90*, 163–190.

Stamper, R. and M. Hapgood (2001). The space environment data system (sedat).

Stassinopoulos, E. G. (1975). Solpro: A computer code to calculate probabilistic energetic solar proton fluences. Technical report.

Stone, E. C., C. M. S. Cohen, W. R. Cook, A. C. Cummings, B. Gauld, B. Kecman, R. A. Leske, R. A. Mewaldt, M. R. Thayer, B. L. Dougherty, R. L. Grumm, B. D. Milliken, R. G. Radocinski, M. E. Wiedenbeck, E. R. Christian, S. Shuman, and

T. T. von Rosenvinge (1998). The solar isotope spectrometer for the advanced composition explorer. *Space Science Reviews*.

Svalgaard, L., E. W. Cliver, and Y. Kamide (2005). Sunspot cycle 24: Smallest cycle in 100 years? *32*.

Torsti, J., L. Kocharov, D. E. Innes, J. Laivola, and T. Sahla (2001). Injection of energetic protons during solar eruption on 1999 may 9: Effect of flare and coronal mass ejection. *Astronomy & Astrophysics 365*, 198–203.

Tranquille, C. and E. J. Daly (1992). An evaluation of solar-proton event models for esa missions. *ESA Journal 16*, 275–297.

Tylka, A. J., W. F. Dietrich, and P. R. Boberg (1997). Probability distributions of high-energy solar-heavy-ion fluxes from imp-8: 1973-1996. *IEEE Transactions on Nuclear Science 44*(6), 2,140–2,149.

Wang, R. and J. Wang (2005). Coronal mass ejections and the largest solar energetic particle events. *Proceedings from International Astronomical Union Symposium 226*, 379–380.

Weron, R. (1996). On the chambers-mallows-stuck method for simulating skewed stable random variables. *statistics and Probability Letters 28*, 165–171.

Wheatland, M. S. (2000). The origin of the solar flare waiting-time distribution. *The Astrophysical Journal 536*, L109–L112.

Wheatland, M. S. (2003). The coronal mass ejection waiting-time distribution. *Solar Physics 214*, 361–373.

Wolf, R. (1852). Sunspot epochs since a.d. 1610: The periodic return of sunspot minima. *Acad. Sci. Comptes Rendus 35*, 704–705.

Xapsos, M. A., C. Stauffer, J. L. Barth, and E. A. Burke (2006). Solar particle events and self-organized criticality: Are deterministic predictions of events possible? *IEEE Transactions on Nuclear Science 53*(4), 1,839–1,843.

Xapsos, M. A., C. Stauffer, G. B. Gee, J. L. Barth, E. G. Stassinopoulos, and R. E. GcGuire (2004). Model for solar proton risk assessment. *IEEE Transactions on Nuclear Science 51*(6), 3,394–3,398.

Xapsos, M. A., C. Stauffer, T. Jordan, J. L. Barth, and R. A. Mewaldt (2007). Model for cumulative solar heavy ion energy and linear energy transfer spectra. *IEEE Transactions on Nuclear Science 54*(6), 1,985–1.989.

Xapsos, M. A., G. P. Summers, J. L. Barth, E. G. Stassinopoulos, and E. A. Burke (1999). Probability model for worst case solar proton event fluences. *IEEE Transactions on Nuclear Science 46*(6), 1,481–1,485.

Xapsos, M. A., G. P. Summers, J. L. Barth, E. G. Stassinopoulos, and E. A. Burke (2000). Probability model for cumulative solar proton event fluences. *IEEE Transactions on Nuclear Science 47*(3), 486–490.

Xapsos, M. A., G. P. Summers, and E. A. Burke (1998a). Extreme value analysis of solar energetic proton peak fluxes. *Solar Physics 183*, 157–164.

Xapsos, M. A., G. P. Summers, and E. A. Burke (1998b). Probability model for peak fluxes of solar proton events. *IEEE Transactions on Nuclear Science 45*(6), 2,948–2,953.

Zurbuchen, T. H. and I. G. Richardson (2006). In-situ solar wind and magnetic field signatures of interplanetary coronal mass ejections. *Space Science Reviews 123*, 31–43.